Deformation Styles in Accretionary Wedges at 3D Seismic to Microstructural Scales

Marco Cantido Azevedo

A thesis submitted for the degree of

Doctor of Philosophy

Cardiff University

April 2025

Abstract

This thesis uses high quality 3D post-stack migrated seismic data from the NanTroSEIZE transect, which images the outer wedge of the NAP (from the MSFZ to the deformation front) in SE Japan. It investigates the strain distribution and deformation styles experienced in the NAP at different scales of observation in order to bring new insights on how deformation within accretionary prisms is influenced by the roughness of their respective incoming subducting plate. In parallel, it investigates how deformation of accretionary prisms adapts and changes to allow the inclusion of asperities within the subduction channel.

The first part of the thesis focuses on the holistic mapping and characterisation of the structural framework of the NAP, gathered from a detailed interpretation of the seismic data. The interpreted seismic data show a much higher structural complexity than previously described by other authors - a wide range of new and previously found structures evolve together in the wider context of the accretionary prism but also changed their nature throughout the different evolutionary stages of the NAP, on a smaller scale. Structures identified in the outer wedge of the NAP and their relationships point towards an alternation between deformation styles during distinct seismic and aseismic periods. The overall structural framework provides evidence for a complex transpressional deformation regime in the NAP.

Following up on the first part, this thesis focuses on studying the roughness of the subducting Philippines Plate and its influence in the overlying NAP. This section provides a new detailed 3D mapping of the subducting PSP and estimates horizontal shortening across the outer wedge of the NAP within the NanTroSEIZE transect, an approach never attempted for the study area. The subducting oceanic plate and overlying décollement are significantly rougher than previously described and includes important features such as a 1.5 km high seamount and elongated major ridges with heights of up to 950 m. These deep structures influence the erosive – accretional behaviour of the NAP with important outcomes in the shortening and deformation experienced by the overlying accreted sediment.

The last part of this thesis explains the results of two sandbox analogue experiments, completed to better understand the interference of individual and combined asperities in the overall strain distribution and deformation within accretionary prisms. The sandbox experiments simulated a simplified, but still similar in the larger scale, asperity/roughness context of the study area, providing further evidence to understand the behaviour and evolutionary stages of the low-velocity unit within the NAP and its influence in the strain distribution along this latter. The new data provided new insights on how accretionary prisms adapt and accommodate deformation in their interior when including asperities, such as seamounts, into the subduction zone to allow the subsequent, and continuous, growth of the accretionary prism's front.

Main results of this thesis are as follows: 1) accretionary prisms document complex structural frameworks where deformation styles may change at different scales as a response to factors such as roughness of the subducting oceanic plate, characteristics of the asperities being subducted, and kinematic relationships between pre-existing and newly-formed structures within the accreted sediments; 2) the roughness of the subducting oceanic plate can be one of the most significant factors in the deformation and structural framework of accretionary prisms, having strong implications on their shortening, fluid migration, pore–fluid pressure distribution, and stress distribution; 3) seismic attributes are a key tool to help imaging structural features and the roughness of accretionary prisms and subducting oceanic plates, all this in order to assist the development of tectonic models in evolving subduction zones; 4) sandbox analogue experiments are key tools for both a quantitative and qualitative analysis of active deformation in accretionary prisms. This allows for a more complete interpretation of processes that lead to modern and future seismic events.

Author notes and status of publications

The chapters and results presented in this thesis have been prepared as scientific papers for publication in international journals. The present status of publications at the time of the submission of the thesis is as follows:

Chapter 4 has been published as: Azevedo, M. C., Alves, T. M., Fonseca, P. E., Moore, G. F. (2018). Strike-slip deformation reflects complex partitioning of strain in the Nankai Accretionary Prism (SE Japan). Tectonophysics, 723, 81-94, https://doi.org/10.1016/j.tecto.2017.11.023

Chapter 5 and 6 to be submitted shortly after the completion of this thesis.

Although the articles are jointly co-authored with the project supervisor and other authors, the work presented in the publications is that of the lead author, Marco Azevedo. Editorial work was provided by the supervisory team in accordance with a normal thesis chapter.

Acknowledgements

I would like to express my appreciation to every individual who have directly and indirectly contributed to the work presented in the thesis. Out of everyone, I would like to thank Tiago Alves the most for making this long-life dream of doing research and completing a Ph.D. possible and for his ever-present support and mentorship provided throughout this journey. I would also like to show my appreciation to Paulo Fonseca for being my structural geology mentor and friend who has always showed patience and availability to discuss any issues in relation to topics of this thesis. Gwen Pettigrew has always been a great asset in my time at the 3D Seismic Lab, not only for her IT expertise and for providing the software and support needed for some of the work carried out in this thesis but also for her companionship. João Duarte was an important contribution and support in this thesis, especially in coordinating and providing all the resources during my time at the LATEX Lab and for his expertise in the subduction zones and analogue modelling.

On a different note, I would also like to show great gratitude to my family and friends that for different reasons allowed the work of this thesis to be completed. I would like to start by thanking my parents and parent-in-law for being supportive with childcare in times of need, so I could 'just sit and work on my Ph.D. and for being great role models and setting me into the right mindset, without which I would have not pursued a Ph.D. To all my friends and staff at

Farnham Rugby Club, thank you for providing me the relaxation pathway needed to tackle the daily frustrations while doing the research and writing the chapters and thesis of this Ph.D. Ultimately, I want show my deepest appreciation to my wife, Catarina Azevedo, that during COVID kept me going despite not being able to visit Cardiff University for a while and for providing me the emotional support needed to be cope with the psychological and emotional challenges throughout the entire Ph.D. journey.

Thank you everyone!

Table of contents

List of Figures

List of Tables

List of Nomenclatures

ECD – Extension-Compression Depth

FTZ – Frontal thrust zone

IBA – Izu-Bonin Arc

IODP – International Ocean Drilling Programme

ITZ – Imbricated thrust zone

LVZ – Low velocity zone

KPR – Kyushu-Palau Ridge

KSC – Kinan Seamount Chain

MBSF – metres below sea floor

MORB – Mid-oceanic ridge basalt

MSF – Mega splay fault

MSFZ – Mega splay fault zone

NAP – Nankai Accretionary Prism

OOSZ – Out-of-sequence zone

PSDM – Pre-stack depth migration

PSP – Philippines Sea Plate

PTZ – Proto thrust zone

SIR – Shichito-Iwojima Ridge

SSE(s) – Slow-slip event(s)

VLFE(s) – Very low frequency earthquake(s)

σ_{Hmax} – Horizontal maximum stress

σ_{hmin} – Horizontal minimum stress

σ_1 – maximum stress

σ_3 – minimum stress

σ_v – vertical stress

CHAPTER 1

Introduction and literature review

1.1. Rationale and aims of this research

1.1.1. Rationale

Subduction zones are well-known areas in terms of their seismic activity, which is mainly associated with megathrust earthquakes. Such earthquakes, usually of magnitude 7.5 or greater, are responsible for 90 – 95 % of all tsunamis recorded on Earth (Keim, 2006). Over the years, several authors have worked extensively to define the seismogenic zone of multiple accretionary prisms around the world in an attempt to predict overall seismicity in such regions (e.g. Ruff and Tichelaar, 1996; Hyndman et al., 1997; Moore et al., 2007; Smith et al., 2013; Gao and Wang, 2017). From these studies it has been inferred that their overall seismicity is mainly affected by the temperature profile of subduction zones, which directly and indirectly controls the processes of consolidation, hydration – dehydration, weakening-strengthening and the rigidity of sediment and rocks within and below accretionary prisms, thus dictating where the transition between aseismic and seismogenic zones occurs, as well as where the updip and downdip limits of these two zones lie. A similar approach can be applied to the Nankai Through (e.g. Hyndman et al., 1997; Moore and Saffer, 2001; Bangs et al., 2007 Gao and Hang, 2017) (Figure 1.1).

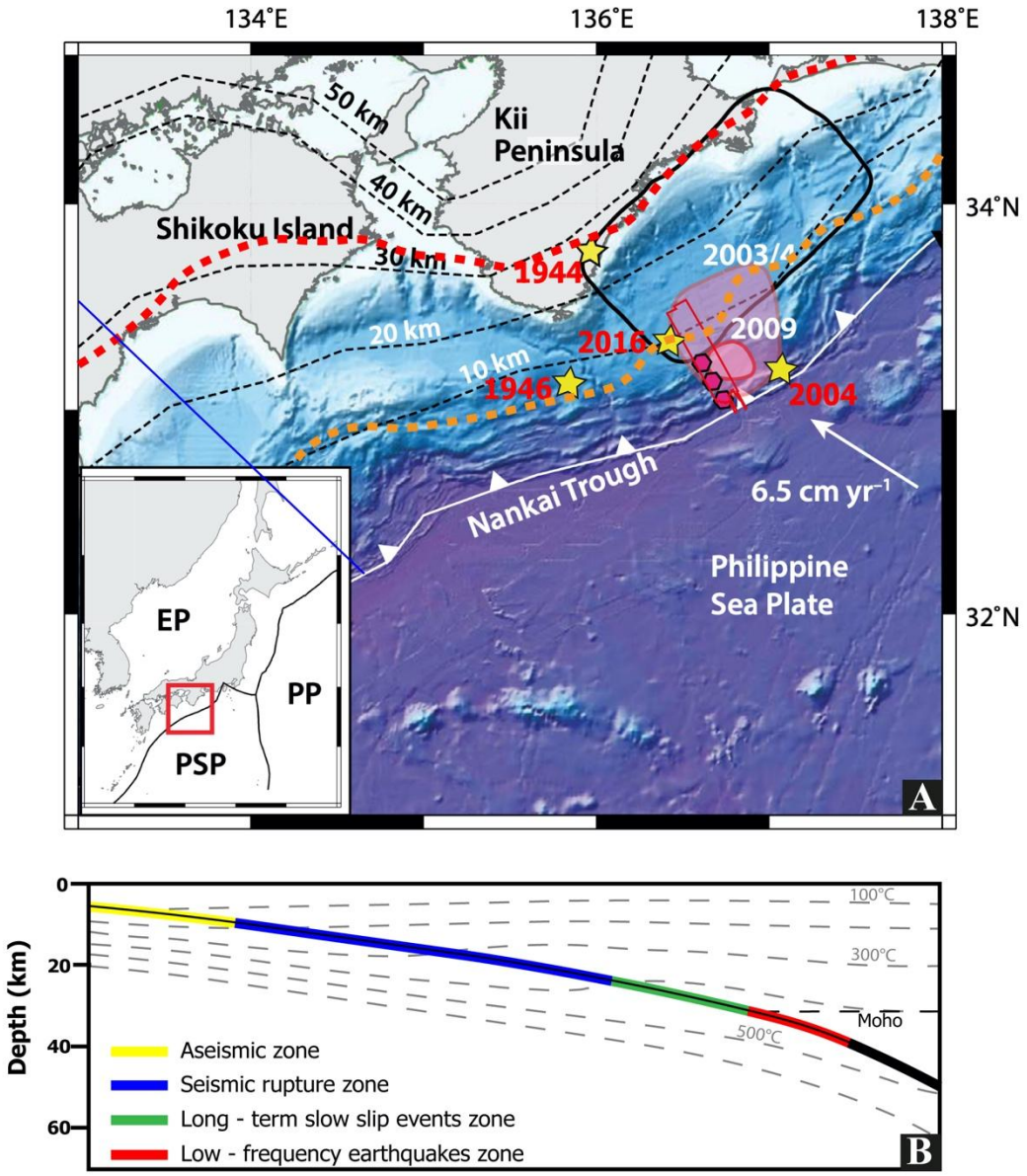

Figure 1.1 – A) Modified bathymetric map from Wallace et al. (2019) of a section of the Nankai Trough, south of Shikoku Island and Kii Peninsula, with depth of the interplate interface (black contours with depth in kilometres), location of SSEs and VLFEs (pink shaded areas), slip area from the 1944 megathrust earthquake (black solid contour) and the location of epicentres for major earthquakes (magnitude 6 or above) in the area (yellow stars with year of earthquake in red). The map includes the updip limit of the back stop (orange dashed contour) and the downdip limit of the seismogenic zone (red dashed contour) as per Basset et al. (2022). Blue line represents direction of subduction profile represent in Figure 1.1 B. B) Model from Gao and Wang (2017) of megathrust temperatures (grey dashed contours), interplate interface geometry (black solid line) and observed fault slip phenomena (colour coded as shown).

Despite the higher likelihood of megathrust earthquakes with tsunamigenic potential initiating from downdip seismogenic zones, they have also been reported at or near the outer wedge of accretionary prisms in a zone supposedly classified as aseismic and free of slip, especially in areas where slip occurs in the shallow parts of the accretionary prism (Polet and Kanamori, 2000; Hananto et al., 2020).

According to Tobin and Kinoshita (2007) the conditions of consolidation state, normal stress magnitude, pore-fluid pressure, and strain rate along the Nankai Trough should be known in order to unveil the mechanisms responsible for the transition between stable (aseismic) and unstable (seismic) sliding at the frontal parts of the NAP. Similar conditions have been inferred (Huene and Culotta, 1989; Huene and Lallemand, 1990) to be determinant to the setting of erosive vs. accretional behaviours of subduction zones at both their toes and the base of their upper plates (Figure 1.2).

1.1.1. Aims of this research

This thesis addresses the triggers and mechanisms responsible for variations in strain accumulation and related deformation styles in accretionary prisms with the aim of providing new approaches to forecasting fluid pathways and seismic initiation in their outer wedge zones. Hence, this thesis developed the detailed study of a section of the NAP, offshore southwest Japan, through

the analysis and mapping of a high-quality 3D seismic dataset (using Schlumberger's Petrel®), the quantitative analysis of horizontal shortening (using Petroleum Experts Move®) and sandbox analogue experiments. The aim was to fully characterise and understand the structural framework and evolution of the NAP and reveal the most influential factors in the distribution of stress and strain within this prism.

This thesis specifically focuses on understanding temporal and spatial relationships between different structures in the outer wedge of the NAP as well as appreciating the influence of the subducting Philippines Sea Plate on the shortening and frontal growth of the NAP and on the distribution of fluid and potential seismic initiation. Therefore, this thesis proposes the following hypotheses to be addressed both jointly and individually:

1. **Stress and strain distribution in the NAP accretionary prism are partitioned.** If correct, one should expect to discover a complex structural framework in the study area, and one that changes either spatially or temporally with clear difference in the deformation styles. If incorrect, then the NAP behaves as a typical, structurally homogeneous accretionary prism – *see Chapters 4, 5 and 6*.

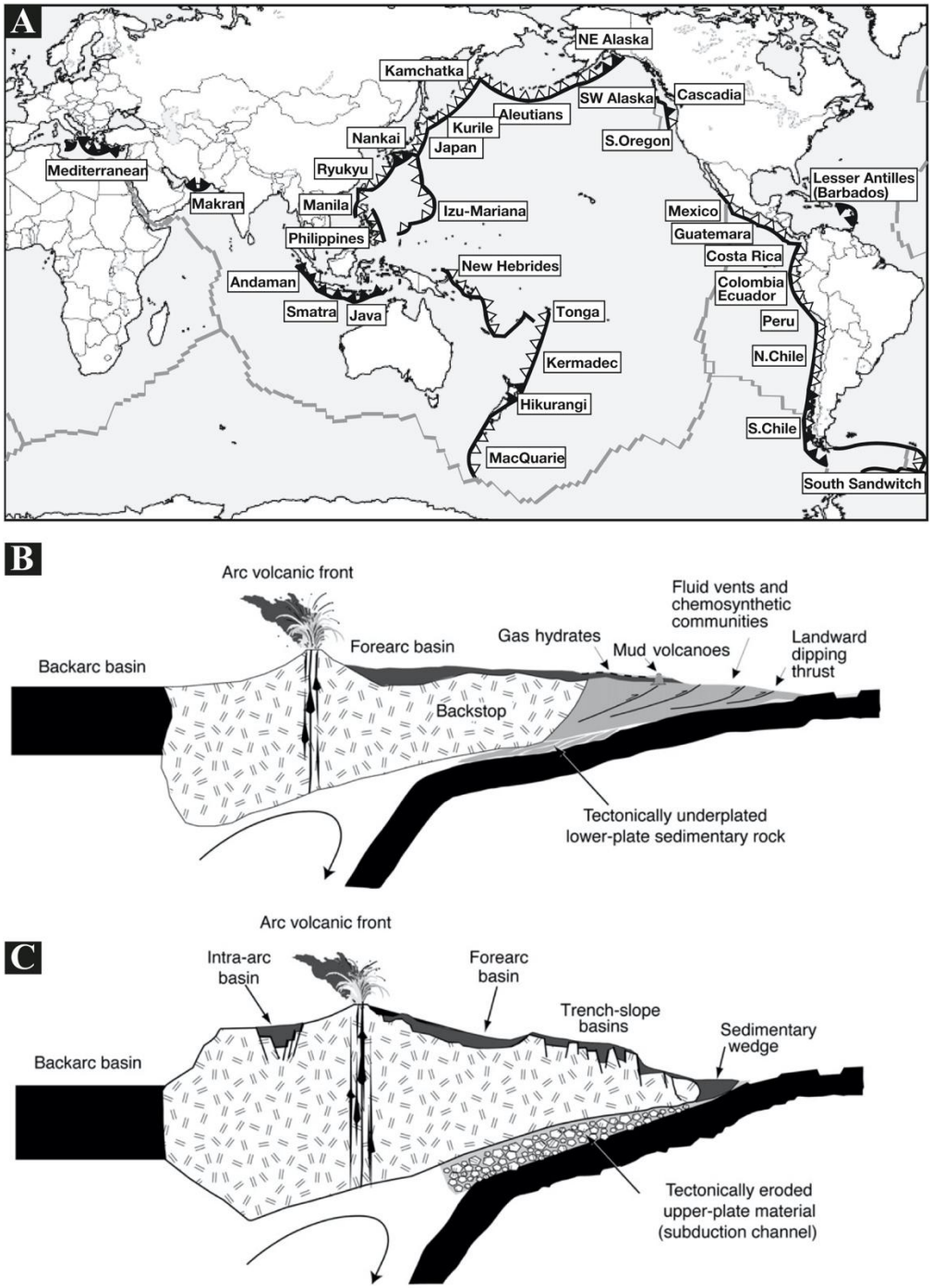

Figure 1.2 – A) World map showing the distribution of erosive (open triangles) and accretionary (black solid triangles) margins in subduction zones (from Azuma et al., 2017). B) Schematic cartoon showing a typical non-erosive or accretional (from Draut and Clift, 2013). (B) Schematic cartoon showing a typical erosive margin (from Draut and Clift, 2013).

2. **The roughness of the subducting Philippines Plate is greater than previously described.** If correct, detailed 3D seismic mapping will show evidence of asperities within the incoming subducting plate. If incorrect, the subducting plate will be smooth and tendentially flat – *see Chapter 5*.
3. **Horizontal shortening and frontal growth of the NAP are affected by the roughness of the subducting Philippines Plate.** If correct, estimations of horizontal shortening, the length of the accretionary prism, and structures in the overlying NAP will all show evidence for some sort of physical or structural relationship. If incorrect, no correlation will be found – *see Chapters 5 and 6*.
4. **The roughness of the subducting Philippines Plate will affect interplate coupling and initiate earthquakes.** If correct, there will be evidence in both the 3D seismic dataset and sandbox analogue models for asperities affecting stress and strain distribution, as well as fluid pathways within the NAP. If incorrect, then any asperities on the subducting plate will not show sign of interference with the overlying NAP – *see Chapters 4, 5 and 6*.

The section ahead includes a literature review of the background geology of the NAP. The literature review section will detail the tectonic framework of accretionary prisms and will the describe the structures and processes operating within each tectonic sector. It will also focus on the current classifications of

subduction margins, their characteristics, and known influence of asperities in the subduction process per se.

1.2 Convergent Margins

Huene and Scholl (1991) summarise convergent margins as being dynamic plate boundaries characterised: a) geomorphologically by deep ocean trenches; b) seismically by landward dipping zones of earthquakes; c) tectonically by regional-scale crustal faulting and terrane movements; and d) magmatically by linear belts of volcanic arcs. Zheng et al. (2022) describe convergent margins as narrow-belt structures in the rigid outer layer of Earth, corresponding to subduction zones at lithospheric mantle depths and orogenic belts at crustal depths. Stern (2002) alluded to the interchangeability of the terms convergent margin, subduction zone and island arc as they are all related but with different meanings. The same author defined convergent margins as the superficial manifestations of downwelling while subduction zones as the three-dimensional manifestation of convective downwelling. In such a setting, arc-trench complexes are the superficial and crustal manifestations of a subduction zone that is operating beneath them.

As this thesis focuses more on subduction zones than convergent margins, it is important to note that the geometric rules of plate tectonics in terms of movement of rigid spherical shells around the Euler pole of rotation does not

apply to the behaviour of the lithosphere once it descends below the surface. This makes subduction zones intrinsically different from convergent margins. Therefore, subduction zones tend to be defined as an inclined array of earthquakes, also known in the literature as the "Wadati-Benioff Zone" (Stern, 2002).

1.2.1 Classification based on type of tectonic plate

Convergent margins can be divided into subduction zones, where a subducting plate sinks under the overriding plate, or collision zones, normally related to collision between two continental plates. However, such a division is not always clear due to the large variability in the structure of both subduction zones and collision zones; some subduction zones showcase typical characteristics of collision zones whereas collision zones can contain features typical of those observed in subduction zones (Schellart and Rawlinson, 2009). Categorisation of convergent margins can be interpreted as transitional, both in space and time, as active convergent margins are normally initiated as subduction zones and, in their final phase of existence, may become a collision zone once the entire ocean basin has been consumed (Dewey and Bird, 1970; Zheng et al., 2022).

In summary, subduction zones can be classified into three categories (Figure 1.3), depending on the properties of their subducting and overriding tectonic plates:

- one oceanic plate subducting underneath another oceanic plate (Figure 1.3A), resulting in the formation of an oceanic volcanic arc above such as the Mariana subduction zone at the western Pacific margin.
- one oceanic plate subducting below a continental plate (Figure 1.3B), resulting in the formation of a continental volcanic arc as exemplified by Andean subduction zone at the eastern Pacific margin.
- one continental plate sliding under another continental plate following collision (Figure 1.3C) such as the Himalayan orogen formed by the collision between the Indian and Eurasian plates.

1.2.2 Classification based on nature of the back arc

Convergent margins can also be classified based on the nature of their back-arc regions with the two end members being the Chilean-type (Figure 1.4 A) characterised by active compressional regimes, and the Mariana-type (Figure 1.4B) experiencing active extensional regimes. Such differences in subduction behaviour relate also to the age of the subducting plate and relative buoyancy, whereby older and denser lithospheric plates are more likely to sink in contrast to younger lithosphere, which is more buoyant and, therefore, resists subduction (Uyeda, 1982; Stern, 2002; Zheng et al., 2017).

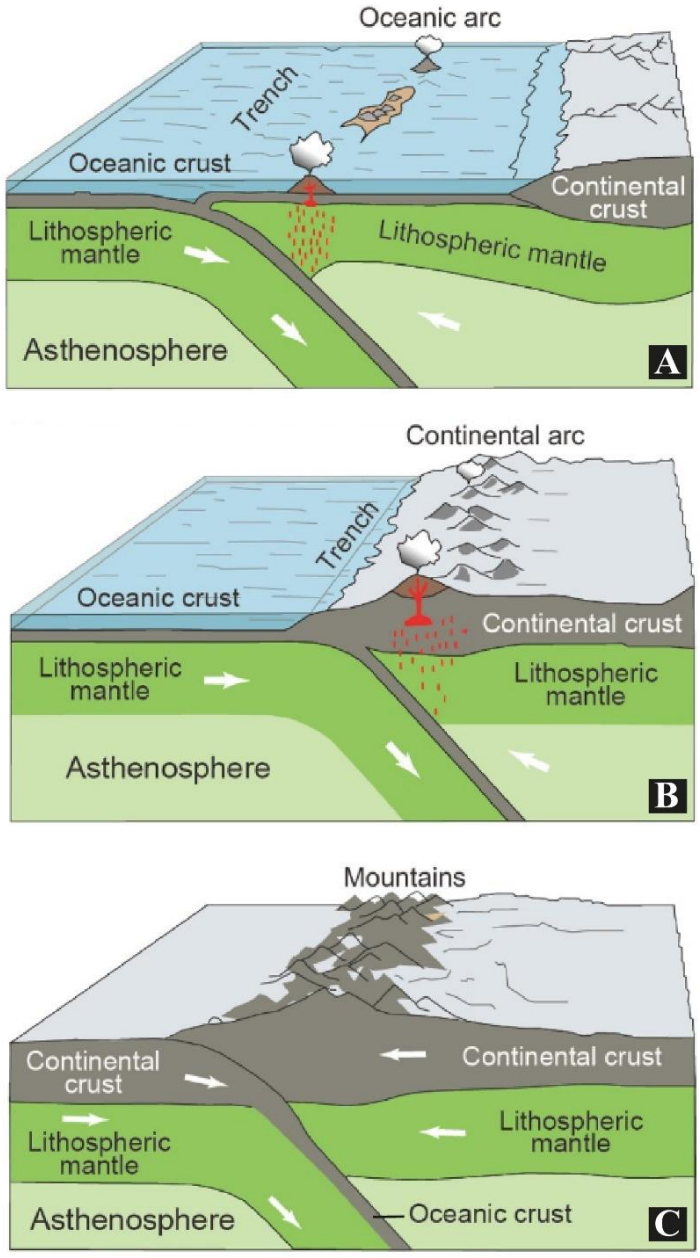

Figure 1.3 - Schematic diagram of the different types of subduction zones (from Zheng et al., 2022). A) Oceanic plate-oceanic plate subduction zone along the trench. The subducting slab undergoes metamorphic dehydration and partial melting at sub arc depths, where the released fluids metasomatize the overlying mantle wedge to form the source of subduction zone magmas that originate the volcanic oceanic arc. B) Oceanic plate-continental plate subduction zone along the trench. The subducting slab undergoes metamorphic dehydration and partial melting at sub arc depths, where the released fluids metasomatize the overlying mantle wedge to form the source of subduction zone magmas that originate the volcanic continental arc. C) Continental collision subduction zone along the forming a mountain belt. One continental plate may subduct to lithospheric mantle depths.

On Chilean-type margins, the resistance to subduction from a younger and buoyant subducting plate causes the colliding plates to become strongly coupled, thus creating conditions for earthquakes of higher magnitudes (8+). The low dip angle of the subduction, typical from this type of margin, also restricts the flow of the asthenosphere mantle wedge, inducing folding and thrusting in the back arc. In contrast, on Mariana-type margins, the older, colder, and denser subducting plate enhances subduction, making plates virtually decoupled. This facilitates the predominance of extension in the back arc, where rifting or seafloor spreading are seen (Uyeda, 1982; Stern, 2002; Zheng et al., 2017).

De Franco et al. (2008) adds that Chilean-type margins typically have thick trench fills with a subduction channel thinning arc-wards, where seamounts get entirely subducted, becoming seismogenic asperities. Conversely, Mariana-type margins have a thin or non-existent accretionary prism, and the subduction channel thickens with depth. In this case, seamounts entering the trench tend to get truncated, which combined with the thick subduction channel impedes subducted seamounts from developing into seismogenic asperities.

Intermediate subduction scenarios are probably far more common that the Chilean-type and Mariana-type end members. Uyeda (1987) also suggested that changes in the roll-back of a subducting plate, together with motion and distance changes between the overriding plate and the trench, are determinant factors as they can change the coupling between plates and, therefore, the class of subduction zones in time.

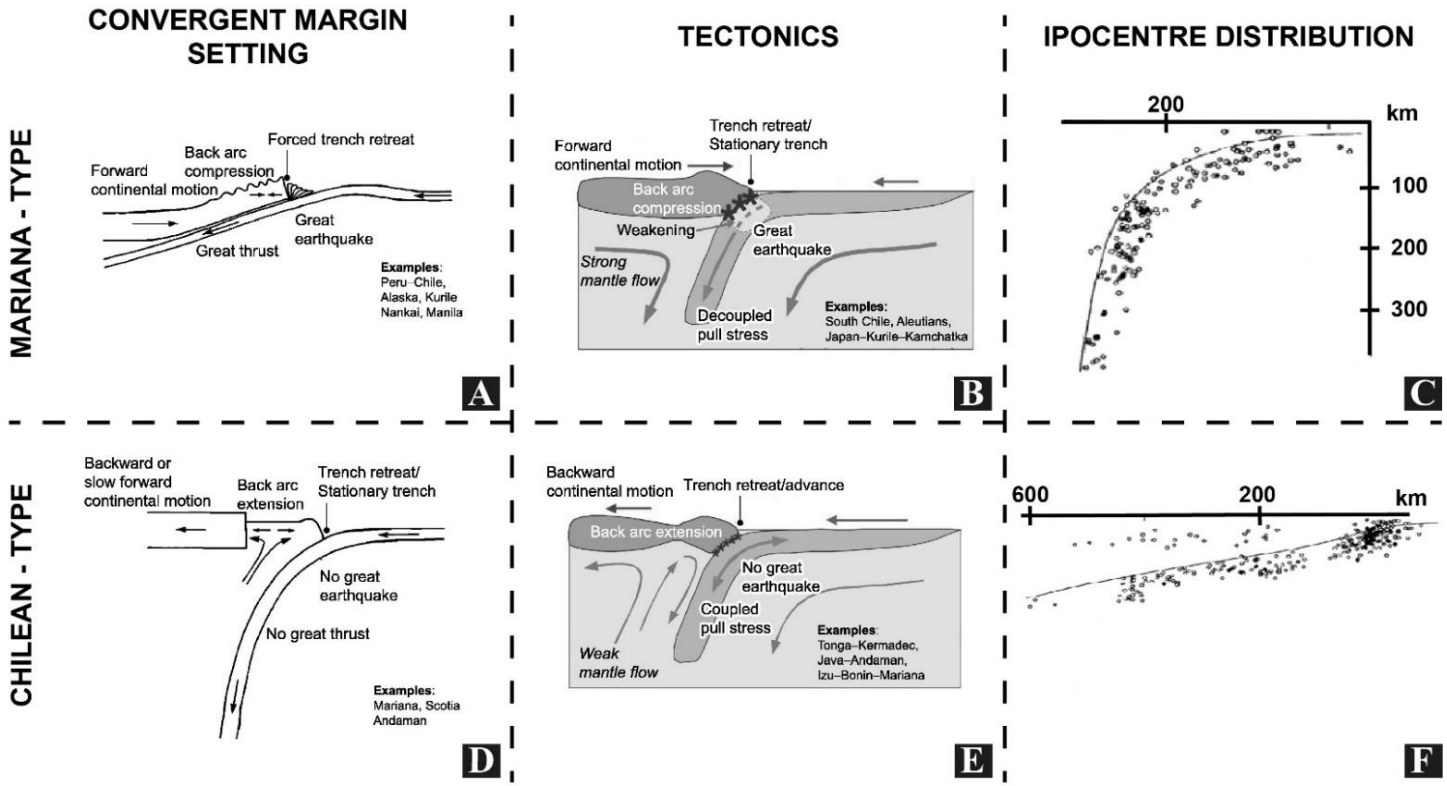

Figure 1.4 – Comparison amongst convergent margin types and their tectonics and distribution of hypocentres as taken from Yoshida (2017) (A, B, D and E) and Arjamandzadeh et al. (2011) (C and F). A) Chilean-type convergent margin with gentle subduction angle dominated by back arc compression and great seismicity. B) Crust and mantle tectonics typical of compressional subduction. C) Distribution of hypocentres of earthquakes following the steep angle of subduction. D) Mariana-type convergent margin with steep angle of subduction leading to back arc extension and great seismicity. E) Crust and mantle tectonics typical of extensional subduction. C) Distribution of hypocentres of earthquakes following a gentle angle of subduction.

1.2.3 Classification based on tectonic regime

Convergent margins can be equally classified into two distinct categories - erosive or accretional - based on subduction behaviour (Figure 1.2). Accretional margins are dominated by oceanic and trench-filled sediment that have been scrapped and frontally accreted from the incoming oceanic plate. In turn, erosive margins are described by the actual subduction of oceanic and trench sediments together with inclusions of crystalline crustal rocks that are tectonically removed from the overring plate (Von Huelle and Scholl, 1991; Clift and Vannucchi, 2004; Munoz-Montecinos et al., 2023). Similarly to other classifications, intermediate systems are recognised where both accretional and erosive behaviours can occur, either alternating through time or simultaneously in different parts of a vast region of tectonic convergence (Clift and Vannucchi, 2004).

Although it is still not yet fully understood, there is a wider variety of factors that seem to influence the shear stresses and coupling between the overriding and subduction plates and, therefore, the tectonic regime of convergent margins (Munoz-Montecinos et al., 2023). One determinant factor is the high-friction abrasion experienced between the two interacting plates, normally triggered by the topography of subducting plates and characterised by the existence of bathymetric features, such as seamounts and ridges. This is also often referred to as the *roughness* or *asperity* of the subducting oceanic plate.

Another important factor is the impact of fluid in the subduction process per se. According to Gerya and Meilik (2011), fluids expelled from high-porosity rocks being accreted or subducted cause rheological weakening; this fluid-related weakening causes plate decoupling and a lowering of the friction experienced in the subduction drag, thus promoting an accretional regime. A relatively weaker fluid effect leads to a strong interplate coupling promoting an erosive regime. Additionally higher pore-fluid pressures, especially in the sediments above the interplate surface, tend to decrease the shear stresses and favour the development of an accretional regime (Loreto et al., 2007).

Sediment availability is another factor influencing the tectonic regime of convergent margins, whereby accretional margins tend to be associated with areas of rapid sediment delivery from the trench, continental interior and pelagic areas above the incoming subducting oceanic plate. Therefore, accretion is favoured when the sedimentary cover is over 1 km thick. Nevertheless, it has also been suggested that the rate of sedimentation is influenced by the speed of convergence and related subduction, with faster convergence rates (normally below 76 mm / year) leading to more effective accretion (Huene and Scholl, 1991; Le Pichon et al., 1994; Clift and Vannucchi, 2004).

1.2.4 Structure of subduction zones

Stern (2002) describes subduction zones as geodynamic systems in which sediments, oceanic crust and mantle lithosphere return to and re-balance themselves relative to the Earth's mantle. Therefore, several components exist within subduction zones that need to be taken into consideration when studying any geological processes operating on convergent margins. Such components can be separated in crustal and upper mantle components and include the incoming plate, downgoing plate, mantle wedge, arc-trench complex, and the subduction channel, amongst others (Figure 1.5A).

1.2.3.1 Incoming and downgoing plates

Oceanic lithosphere usually collides with a continental lithosphere composed of uppermost oceanic crust and upper mantle. Mantle lithosphere, crust and overlying sediments are the most important sub-components of the incoming plate and record a significant influence on subduction behaviour. Fischer et al. (2020) describes oceanic lithosphere as formed at mid-ocean ridges, areas where two lithospheric plates diverge, and where the underlying mantle rises to replace it. The lithosphere then cools and thickens with time, and moves away from the ridge, until it returns into the mantle via subduction when it meets a more buoyant tectonic plate.

While the thickness of the oceanic crust is virtually constant, the thickness of the mantle lithosphere is age-dependent, a characteristic that determines the readiness and angle of subduction observed between the extremes of Mariana- and Chilean-type convergent margins (Stein and Stein, 1992; Stern, 2002). According to Stern (2002), oceanic crust is ca. 6 km thick and mainly composed of MORB and diabase underlain by gabbroic equivalents, where formation of amphibolite and serpentinisation are important mechanisms of water inclusion in the crust and water recycling into the mantle.

A key aspect is that the sediment carried by the incoming plate can be a determinant factor in the type of great shallow earthquakes, but with much greater variability than the composition of the mantle lithosphere and crust. Some subduction zones are dominated, or strongly influenced by, carbonate strata (e.g. Peru-Chile, Central America, and the Aegean), while others are dominated by terrigenous (e.g. the Aleutians, Cascades, and Nankai) or siliceous sediments (e.g. Kamchatka) (Stern, 2002). The thickness of the sediment also influences the seawards growth of the accretionary prism, and the processes behind trench retreat, whereby thicker incoming plate sediments enhance the development of a shallower dipping megathrusts within a wider seismogenic zone. Sediment-rich subduction segments are often characterised by a shallower interface dip and a larger seismogenic zone width when compared with sediment-starved ones (Brizzi et al., 2020). Behr and Becker (2018) also suggest

that sediment subducted at depth significantly influences the speed of subduction whereby the abundance of sediments at depth contributes to lower viscosities than asthenospheric mantle, a factor leading to faster plate velocities.

The characters of the mantle lithosphere, crust and overlying sediments have a crucial role in the processes occurring when the oceanic plate changes its configuration from an incoming to a downgoing plate. The age and speed of the downgoing plate will determine interplate coupling at shallower depths, with the faster subduction of younger plates causing an increased tendency for coupling and a larger likelihood for higher magnitude seismicity. Similarly, deeper earthquake activity is also controlled by the age and speed of the downgoing plate as they control the thermal state of the subducted plate. The faster the convergence velocity and the older the plate, the lower the temperature is at the slab surface, therefore, increasing the depth of significant earthquakes (Stern, 2002; Leng and Mao, 2015).

During the subduction process, the downgoing slab experiences varying levels of metamorphism, from greenschist- or sub-greenschist-facies, through blueschist-facies to eclogite-facies assemblages, accompanied by profound dehydration, also known as *slab devolatilisation*. Fluid escape from the subducted plate to the overlying mantle wedge continuously occurs down to a maximum depth of 70 km, for young and hot plates, and to a maximum depth of 300 km for old and cold plates (Stern, 2002; Spandler and Pirard, 2013).

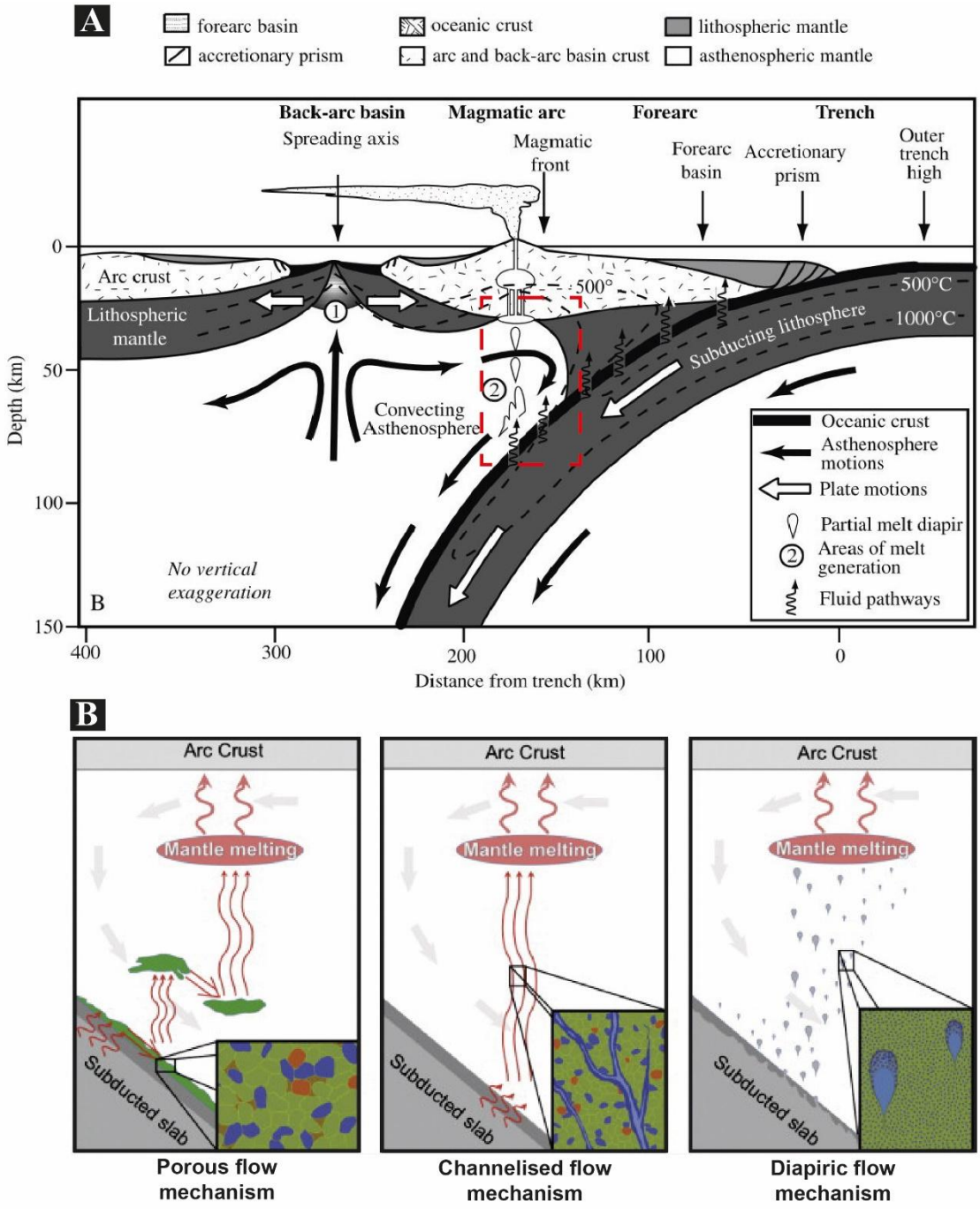

Figure 1.5 – A) Schematic diagram from Stern (2002) showing the different components of subduction zones. Red dashed box delineates the area represented in Figure 1.5B. B) Schematic diagrams from Spandler and Pirard (2013) showing the path of fluids in the mantle wedge via mechanisms as varied as porous flow, channelised flow and diapiric flow (from left to right).

1.2.3.2 Mantle wedge

According to Stern (2002), the mantle wedge is that part of the mantle immediately above the downgoing plate, where fluids dehydrated from the downgoing plate mix with asthenospheric mantle to form the arc magmas also typical of convergent margins.

Fluids tend to move out of the subducting plate to the mantle above via three distinct mechanisms (Figure 1.5B). The first is known as *porous flow*, during which a succession of melting and metasomatism events eventually transfers slab components to the principal site of mantle wedge melting. The second is known as *channelised or focused flow*, characterised by a direct transfer of slab melt from the top of the slab to the loci of partial melting of the mantle wedge using veins and faults. The last process is known as *diapiric flow* and is caused by the detachment of slab sediments or mélanges due to buoyancy (Stern, 2002; Spandler and Pirard, 2013).

The addition of fluids to the asthenospheric mantle wedge leads to a decrease in its melting point, resulting in the formation of melts that will eventually rise to feed the arc volcanoes, a configuration similar to the *diapiric model* suggested for the rise of fluids from the subducting slab (Van Keken, 2003).

1.2.3.3 Arc-trench complex

Stern (2002) describe arc-trench complexes as the magmatic and tectonic manifestations of a subduction zone in the overlying lithospheric plate, with this latter separated into forearc, magmatic arc and back-arc sub-components (Figure 1.5A). The forearc is the area of the arc-trench complex located between the trench and the magmatic front (Dickinson and Seely, 1979), It includes:

- a bathymetric trench in its seaward-most limit, which is the superficial tracing of the subduction thrust. The trench is a dynamic feature that migrates seawards as the accretionary wedge or prism grows.
- The lower trench slope, which comprises the sedimentary or accretionary wedge depending on the nature of the convergent margin – accretional or erosive. This component of the forearc is characterised by a relative seafloor high extending from the trench to the forearc high. The structure of accretionary prisms is further reviewed in Chapter 1.3.
- Landwards of the forearc high lies a shallow topographic basin, known as the forearc basin. This forearc basin can lie above older oceanic plate remnants from an older subduction zone, above older accreted material, or the intramassif, where magmatic front and arc is formed.
- in its landwards limit, the forearc is bordered by the intramassif.

Stern (2002) considers the magmatic front as marking the boundary between low heat-flow in the forearc and high heat-flow beneath the magmatic arc and the back-arc region, with this heat being caused by igneous activity related to the melting of the mantle wedge below. Magmatic activity is concentrated in the magmatic front and diminishes landwards.

Further landwards lies the back-arc region, which is characterised by a wide range of magmatic and tectonics styles between low strain and active extension, typical of Mariana-type convergent margins, and high-strain and compressional regimes common in Chilean-type convergent margins (Figures 1.4A, 1.4B, 1.4D, 1.4E).

1.3 Accretionary prisms

Moore and Silver (1987) describe an accretionary prism as a parallelogram with a wedge shape formed by the tectonic underscraping and accretion of sediments and rocks from deep oceans. This process happens through thin-skinned deformation during lithospheric convergence at a subduction zone.

Commonly, accretionary prisms start with sediment and rocks being accreted near the front of the prism. At a later stage, sediments and rocks begin to underthrust together with the subducting plate, where they are included in

the subduction megathrust, sometimes also mentioned as the *subduction channel* or *décollement* (Davis et al., 1983; Dahlen et al., 1984). Subducting sediments and rocks can then be transferred to the overring plate. This process of progressive addition of material to the upper plate is known as *underplating* and is responsible for the upwards flow and growth of the accretionary prism as its underthrusting continues in time (Cowan and Silling, 1978). Subduction thrusts exhume deeper and older sediments and rocks to become structurally higher in the inner parts of the accretionary prism. Accretionary prisms are then cut by later faults, or out-of-sequence thrusts, which tend to individualise rocks of similar sedimentary, deformational, and metamorphic history (Moore et al., 2007).

An alternative model is discussed by Hamilton (1977) whereby material is added to the toe of a wedge by off scraping, causing the lateral spreading of the wedge due to gravity. This process generates internal imbricate thrusts that are responsible for the tectonic mixing of sediments deposited on the wedge with underlying, and previously accreted, materials.

1.3.1 Critical-wedge theory

The mechanics behind the formation of accretionary prism have been widely discussed via mechanical models that compare them with a wedge of soil or snow in front of a moving bulldozer (Figure 1.6A). In these models, the material deforms until reaching a so-called *critical taper* (θ), which is the shape

under which the accretionary wedge will be at the brink of failure everywhere when under horizontal compression. The critical taper is defined by the sum of the upper surface slope (α), towards the foreland, and the dip of the décollement or basal slope (β). When a critical taper is achieved, the wedge will slide, maintaining its shape (taper), thus promoting the growth of the accretionary prism. If the wedge becomes under critical in its state, it will stop sliding to deform internally and increase its slope angle - until it achieves a new taper angle to resume it sliding and growth (Figure 1.6B). As critical taper behaviour can be empirically predicted by the Coulomb failure criterion, accretionary wedges are also known as Coulomb wedges (Davis et al., 1983; Dahlen et al., 1984).

Willett (1992) suggested that changes in the geometry, boundary conditions and internal strength of a Coulomb wedge causes variations in the style of deformation experienced by it, thus causing the whole accretionary prism to deform through multiple phases, rather than one as suggested by previous authors (Davis et al., 1983; Dahlen et al., 1984). According to the same author if a critical Coulomb wedge becomes sub-critical, the accretionary prism will enter a transitional phase of no deformation in the inner wedge and no displacement along the décollement. However, due the continuing convergence against the rigid backstop, the wedge continues to deform internally to increase its taper angle from the back to the toe of the accretionary prism. As the critical taper angle of the wedge is a function of the internal strength of the material and the coefficient of friction on the basal detachment (décollement) of the wedge,

when the taper angle is larger than the basal strength, the wedge transitions to a stable phase.

During the stable phase, the Coulomb wedge slides along the décollement with no internal deformation while the toe of the accretionary prism continues to accrete material as a way of increasing its shallower taper to form against the now older (and rigid) wedge, which will eventually become the backstop of the newer and frontal accretionary prism. Equally, if the basal strength cannot support a larger taper angle, then extension may occur as a new mechanism to reduce the wedge taper angle, while accretion is still happening at the toe of the accretionary prism. The result of all these competing processes is that out-of-sequence faulting and tectonic uplift of high-pressure terranes in the inner parts of the accretionary prisms can be justified (and effectively occur) during the transitional phases in which the wedge is in a non-critical stage of deformation (Figure 1.6C and 1.6D).

Wang and Hu (2006) introduced the concept of dynamic Coulomb wedge, a wedge that also evolves through transitional phases related to the subduction fault - alternating between interseismic locking and coseismic slip stages that vary along the subduction fault (3D) as well as varying through time (4D). In this dynamic model it is important to consider that the seismogenic section of the subduction fault (Figure 1.1B) presents a velocity-weakening behaviour (frictional resistance against slip decreases as slip rate increases) while most of the

updip segment (Figure 1.1B) records a velocity-strengthening behaviour (frictional resistance against slip increases as slip rate increases). Therefore, during interseismic periods, the seismogenic section can be locked and the updip section exhibits little to no slip. When shear stress builds up to cause failure, stress immediately drops, and seismic rupture occurs in the seismogenic sections forcing the updip sections to slip aseismically while increasing their strength to resist such slip. Due to the spatial and time variations in the basal strength and stress, the outer wedge reaches a critical state during coseismic events, during which sediment accretion and basal erosion occur, and relaxes during inter-seismic phases. Conversely, the inner wedge of accretionary prisms remains mostly in a stable regime throughout distinct seismic phases (Figure 1.7).

Noda et al. (2023) also showed that both the inner and outer wedges experience strengthening/weakening and decoupling/coupling during an accretion cycle, whereby the wedge strength is dependent on variations in internal friction angles, causing strain hardening and softening. Therefore, when an accretionary prism is in the process of forming a new frontal thrust due to accretion in its frontal zone, both the inner and outer wedges are strengthened and progress to a critical taper state. The newly formed frontal thrust causes the outer wedge to become stronger and decoupled from the décollement, while the accompanying reduction in the strength of the décollement below the inner wedge causes it to creep. Coupling with the décollement is slowly re-established as the outer wedge gradually weakens and/or the décollement strengthens (Figure 1.7B and 1.7C).

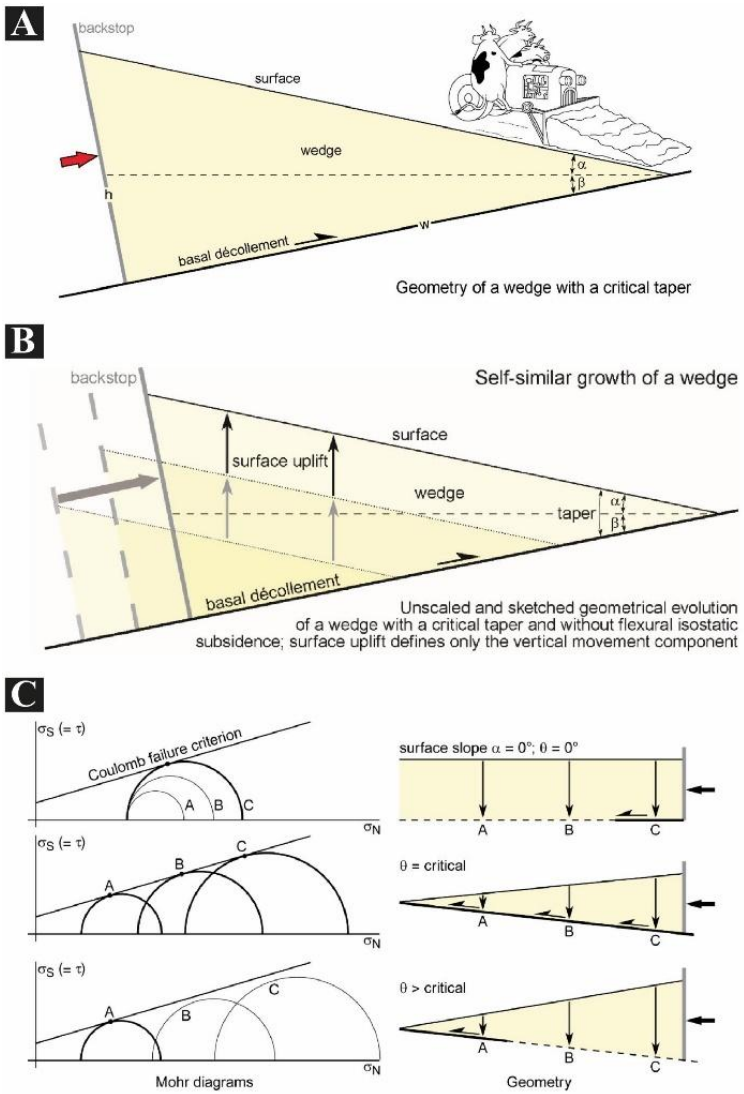
A
backstop
surface
wedge
α
β
h
w
basal décollement
Geometry of a wedge with a critical taper
B
Self-similar growth of a wedge
backstop
surface
surface uplift
wedge
taper
α
β
basal décollement
Unscaled and sketched geometrical evolution
of a wedge with a critical taper and without flexural isostatic
subsidence; surface uplift defines only the vertical movement component
C
σS (= τ)
Coulomb failure criterion
A B C
σN
surface slope α = 0°; θ = 0°
θ = critical
θ > critical
Mohr diagrams
Geometry

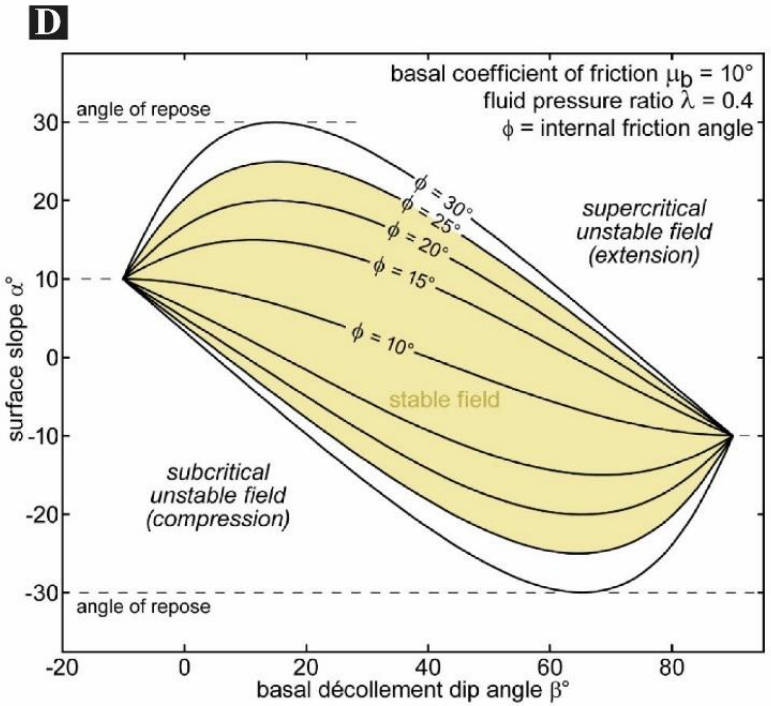
D
basal coefficient of friction μb = 10°
fluid pressure ratio λ = 0.4
ϕ = internal friction angle
angle of repose
ϕ = 30°
ϕ = 25°
ϕ = 20°
ϕ = 15°
ϕ = 10°
supercritical
unstable field
(extension)
stable field
subcritical
unstable field
(compression)
angle of repose
surface slope α°
basal décollement dip angle β°
30
20
10
0
-10
-20
-30
-20
0
20
40
60
80

Figure 1.6 – Collection of diagrams on Critical Wedge Theory and the Coulomb Failure Criterion from https://www.files.ethz.ch/structurgeology/jpb/files/Theoretical/mecthrusts.pdf. A) Adaptation from Dahlen et al. (1984) on the formation of accretionary prisms being analogous to a bulldozer pushing sand or snow uphill, growing a wedge until the critical taper (θ) is achieved. B) Diagram illustrating how the wedge maintains it shape by incorporating and uplifting the landward part of the accretionary prism to maintain or re-achieve the critical taper. C) Mohr-Coulomb scenarios for three different wedge shapes. When taper angle is 0, the depth to the décollement and vertical stress are constant, therefore the minimum stress for all Mohr circles is the same, but pressure is the highest at the back due to the sliding backstop and smallest in front. Therefore, the back of the wedge thickens by thrusting while the front remains undeformed, increasing taper angle. When critical taper is achieved, the back Mohr circle (C) is larger but shifted to the right of the frontal one because it is deeper (higher pressure). As all Mohr circles touch the Coulomb Failure Criterion, the whole décollement can slip. When the taper angle is larger than the critical value, pressure increases from back to front and the back Mohr circle no longer meet the Coulomb Failure Criterion, thus only causing the front part of the décollement to fail, stretching the wedge, and lowering the taper angle. D) Equilibrium conditions of a tapered wedge as a product of adjustment to variation in both surface slope (α) and basal slope (β) angle during the evolution and growth of an accretionary prism. The stable condition of a wedge is dependent on the combination of surface slope and basal slope angles as well as the internal friction angle. Above the stability domain, the wedge is considered supercritical due to excessive thickness and the basal plane no longer can support the load, leading to wedge thinning and gravitational collapse aided by normal faulting. Under the stability domain, the wedge is considered subcritical, lacking the gravitational load to cause shear stress and activation of the décollement, which causes the accretionary prism to build up through internal deformation via folding and thrusting.

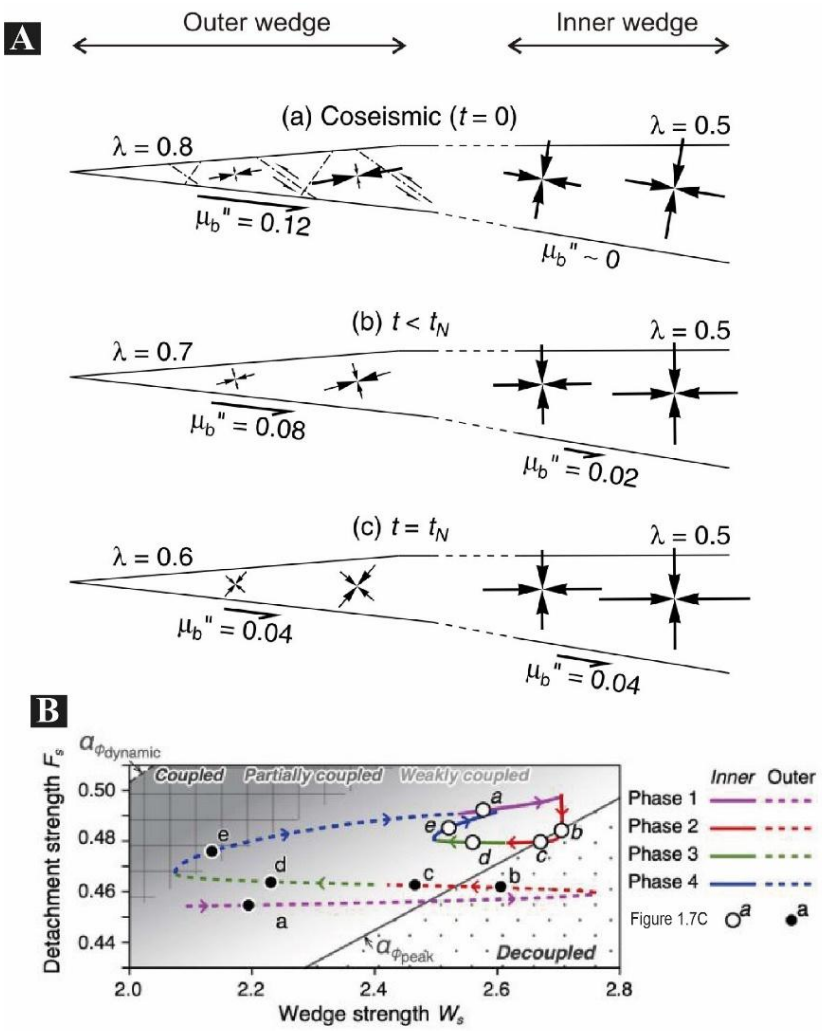
A
Outer wedge
Inner wedge
(a) Coseismic (t = 0)
λ = 0.8
λ = 0.5
μb" = 0.12
μb" ~ 0
(b) t < tN
λ = 0.7
λ = 0.5
μb" = 0.08
μb" = 0.02
(c) t = tN
λ = 0.6
λ = 0.5
μb" = 0.04
μb" = 0.04
B
Coupled
Partially coupled
Weakly coupled
Decoupled
Detachment strength Fs
Wedge strength Ws
Inner Outer
Phase 1
Phase 2
Phase 3
Phase 4
Figure 1.7C

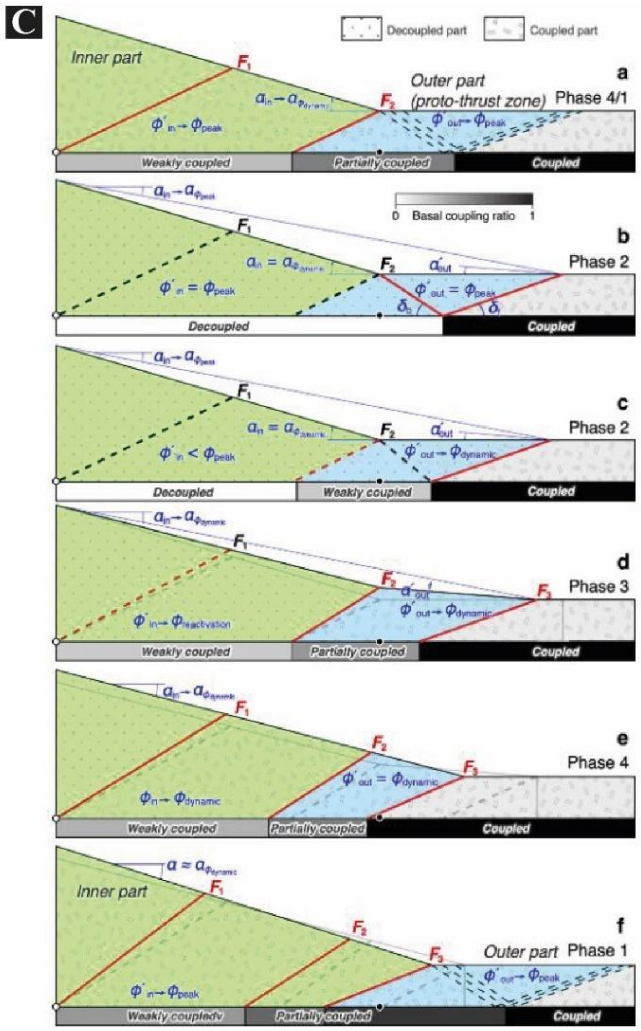
C
Decoupled part
Coupled part
Inner part
Outer part
(proto-thrust zone)
Phase 4/1
Phase 2
Phase 2
Phase 3
Phase 4
Outer part Phase 1
Basal coupling ratio
Weakly coupled
Partially coupled
Coupled
Decoupled

Figure 1.7 – A) Illustration of a stress cycle using the geometry of the Nankai prism offshore the Kii Peninsula from Wang and Hu (2006), where λ values represents pore fluid pressures in response to the stress cycle; dashed lines represent the transitional segments between the outer and inner wedges, where the state of stress could not be modelled; and μ_b'' is the basal friction. (a) During a coseismic event (t = 0)., the outer wedge is in a critical state, where μ_b'' peaks beneath the outer wedge and reaches minimum value beneath the inner wedge. (b) After the seismic event ($t < t_N$)., the outer wedge begins to relax while the inner wedge experiences locking of the seismogenic zone, leading to changes in the basal friction. (c) In between seismic events ($t = t_N$), the outer wedge reaches a neutral state and shear stress in the seismogenic zone under the inner wedge approaches fault strength, so the stress cycle restarts. B) Variations in the wedge and décollement strengths in the inner and outer wedges of an accretionary prism. Open and filled circles represent the stages in inner and outer wedges respectively, represented in Figure 1.7C. C) Conceptual models of an accretion cycle in the frontal proto – thrust zone at different stages showing the changing in coupling between the inner and outer wedges and underlying décollement. Stage 1 – deformation propagation or reactivation; Phase 2 – Newly formed frontal thrust; Phase 3 - Accretion of a new thrust nappe into the accretionary prism to the wedge and reactivation of the previous frontal thrust; Phase 4 – Landward propagation of coupling between the accretionary prism and the decollement, uplift of the inner wedge accompanied by reactivation of pre-existing thrusts.

1.3.2 Fluid migration in accretionary prisms

Fluids in accretionary prisms are mainly sourced from compaction induced expelling of seawater in pore spaces of sediments and rocks being accreted at the toe of accretionary prisms - and from dewatering induced by mineral dehydration and hydrocarbon generation at depth (Langseth and Moore, 1990; Moore and Vrolijk, 1992; Carson and Screaton, 1998; Teichert et al., 2005).

The lithostatic pressure exerted by the accretionary prism will force the fluid to migrate upwards from the subduction zone and return to the ocean. Such a migration can be *focused* or *dispersed*, and the rate at which fluids migrate within the accretionary prism depends on the balance between pressure inputs, sedimentation rates (which control effective pressures), tectonic accretion, and the rate of mineral dehydration, and the ability of the prism to 'lose' or store such fluids, such as its primary and secondary permeabilities. If the permeability between the grains of the sediment or within the rocks of accretionary prism - intergranular permeability - is high enough, then it may be sufficient for fluid to be expelled via stratigraphic boundaries or dispersed within the accretionary prism. If intergranular permeability is low, then fluid escape is normally accommodated by fault networks or diapiric structures, and also by pathways created by the frontal thrusts in both the inner and outer wedge areas.

It is possible both pathways for fluid escape to coexist, with intergranular permeability being significantly slower and secondary permeability much more dispersed (Carson and Screaton, 1998; Teichert et al., 2005) (Figure 1.8A).

Carson and Screaton (1998) discuss that fault permeability as an escape pathway for fluids in accretionary prisms can be important, but dependent on multiple factors:

- Pore pressure needs to overcome hydrostatic pressure to cause the dilation of existing faults.
- Faults need to alternate their behaviour between fluid accumulation when faults present lower pressure than the surrounding higher-pressure rocks, and fluid transport when pore pressure in the faults is at, or near, lithostatic pressure (Figure 1.8B).

Saffer and Bekins (2006) identify the décollement as another significant source of fluids, presenting the highest pore pressures within accretionary prisms and causing the base of the wedge to be weaker than the surrounding sediment. The subducting hydrated oceanic crust provides an important source of fluids that can be expelled in the décollement, and potentially within the overlying accretionary prism, by subduction-related heating (Moore et al., 1989). Similarly to the mechanism suggested for fault permeability, fluid migrating along and out of the décollement involves (Moore et al, 1989) (Figure 1.8B):

1. A period of strain accumulation that allows fluid flow from surrounding rocks to dilate any fractures developed along the décollement.

2. The resulting increase in fluid pressure leads to the merging of dilated fractures within the décollement, which reduces its strength and leads to its failure and slip. During décollement slip, fluid moves along it and, in some cases, moves to the overlying accreted sediment, if intergranular permeability is sufficiently high. However, it does not migrate back to its origin due to the lower intergranular permeability of the source sediment.
3. A recovery period, during which the source sediment will resume the accumulation of strain because of intraplate locking, increases pore pressure again and leads to a new phase of décollement dilation.

1.3.2.1 Impact on critical wedge theory

The taper angle conditions of accretionary prisms are closely influenced by the presence of fluid as the critical taper theory suggests the total taper angle to be also a function of the pore pressure ratio (λ = fluid pressure/lithostatic pressure) along the décollement and within the wedge per se. The densities of the water and bulk sediment, not just the coefficient of friction of décollement and wedge, are also important. Accretionary wedges with low-permeability or thick incoming sediment normally present small critical-taper angles (Davis et al., 1983; Saffer and Bekins, 2006).

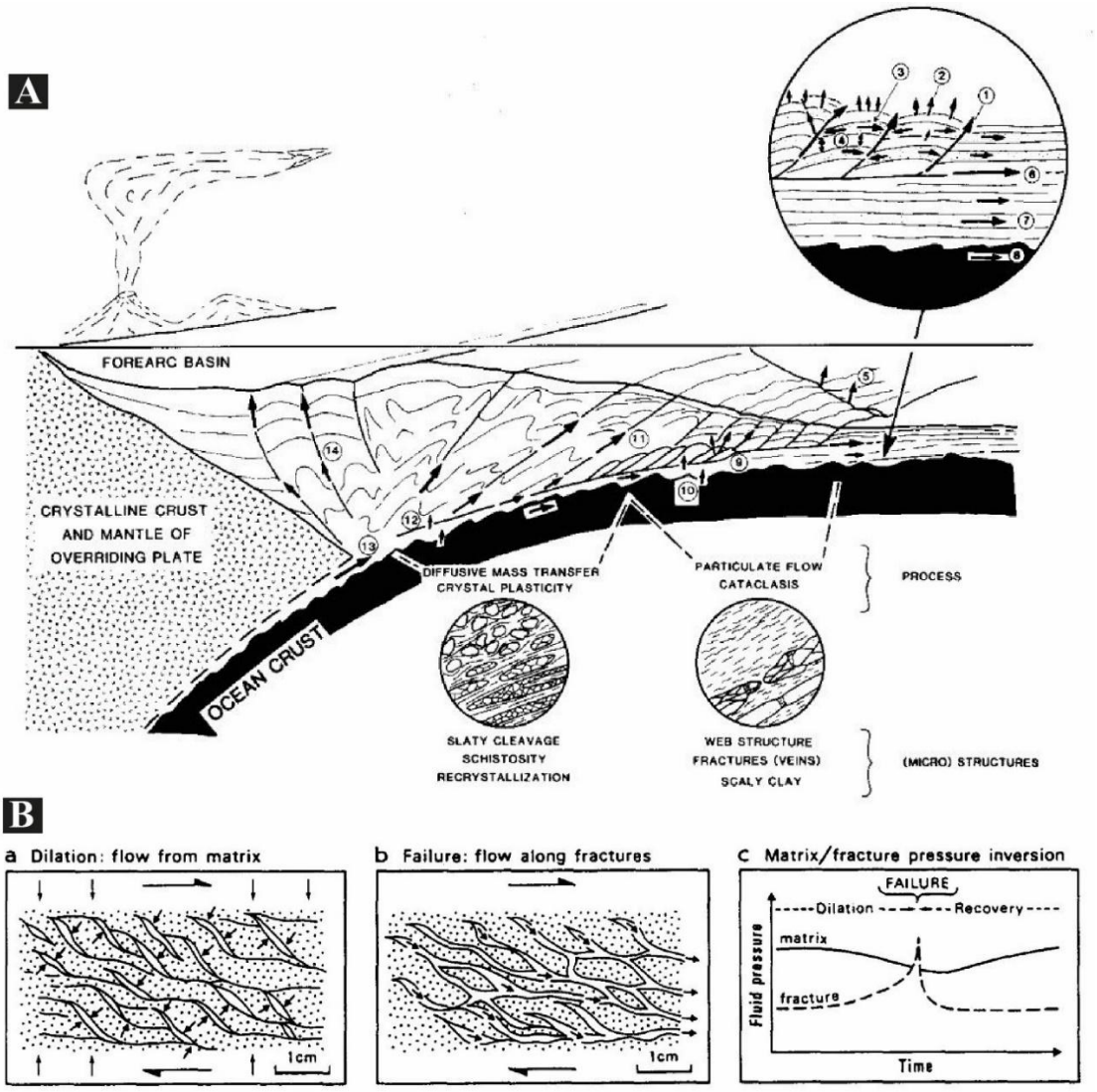

Figure 1.8 – A) Diagram from Langseth and Moore (1990) showing the different fluid pathways within an accretionary prism, as identified by the numbered circles. B) Diagram from Moore (1989) illustrating the main stages of dilation (a) and failure (b) where fluid is collected and expelled respectively from faults and décollement, as well as variations in fluid pressure vs time during the stages of dilation, failure, and recovery.

1.3.3 Domains

According to Raimbourg et al. (2009), accretionary prisms are internally structured into: 1) a seawards domain, known as the outer wedge, characterised by a steeper slope and compressional deformation in which folding and thrusting dominate, and 2) a landwards domain known as the inner wedge, characterised by a gentler slope, relatively less deformation and sometimes overlaying forearc basins. The process of dewatering and compaction experienced by the inner wedge, when compared to the more recently formed outer wedge, is responsible for the contrast in the strength often observed between such domains. Both inner and outer wedges of accretionary prisms often showcase large thrust faults. However, in the inner wedges the spacing between thrusts tends to be narrower and the slope angle of thrusts steeper (Noda et al., 2023).

The outer wedge of accretionary prisms is often recognised as a fold-and-thrust domain characterised by a well-defined imbricated system of thrust faults that is occasionally intersected by some out-of-sequence faults behind the frontal thrust. Studying these fault systems in the outer wedge helps our understanding of the evolution and deformation of accretionary prisms, as well as the recognition of episodes of wedge widening, thickening, and shortening (Ito and Moore, 2021).

High-resolution seismic data reveals the seaward-most part of accretionary prisms to be distinct from the outer wedge. This seawards 'toe' is characterised by several cross-cutting faults developed in newly accreted sediment, offsetting the seafloor but not quite intersecting the décollement. This domain has been referred to as the protothrust zone (Weiss et al., 2018; Noda et al., 2023). Karig (1986) define the protothrust zone as a domain landwards of the most recently frontal thrust with diffuse shortening and thickening. It is accompanied by significant porosity reduction prior to the formation of a new frontal thrust (Figure 1.9).

Another key domain to consider is the structure immediately underlying the accretionary prism, known as the décollement or basal detachment. Moore (1989) defined the décollement as a surface or zone of structural disharmony that marks the boundary between the two converging plates. This boundary is maintained by high fluid pressure, and acts as a major conduit for fluid expulsion – therefore, it has significant influence on the structural development of accretionary prisms. Décollements can display various geometries across different accretionary prisms and have profound influence in the accretion cycle, development of fault networks, and the strength of accretionary prisms (Couzens and Wiltschko, 1996; Noda et., 2023) (Figure 1.9). They are usually classified as:

- Type 1, known as continuous single décollements, where episodic frontal accretion occurs within the constant accretion cycle. Their development depends on the relative coupling between the wedge and the décollement and therefore, their strengths (Figure 1.7B and 1.7C).
- Type 2, known as continuous double décollement layers or interbedded décollement layers, is where wedge partitioning occurring in tandem with a reorganisation of the internal faulting network weakens the wedge. Interbedding is caused by lithological changes, or unconformities, which facilitate underplating of the underthrusted sediment below the inner wedge. Such a setting forms a very gentle, long, deeply rooted thrust, from which multiple cycles of frontal accretion nucleate at a deformation front through shallowly rooted, short-lived fore thrusts.
- Types 3 and 4, comprising different forms of discontinuous décollement, occur when the existence of ridges, seamounts or deeply rooted out-of- sequence thrusts can disrupt the updip continuity of the décollement.

Additionally, it is possible to identify an extension of the décollement seawards of the deformation front and through the incoming undeformed sediment, known as the proto décollement, which suggests that stratigraphic weaknesses within the incoming plate may be key in the formation of the décollement even before subduction takes place (Yamada et al., 2006).

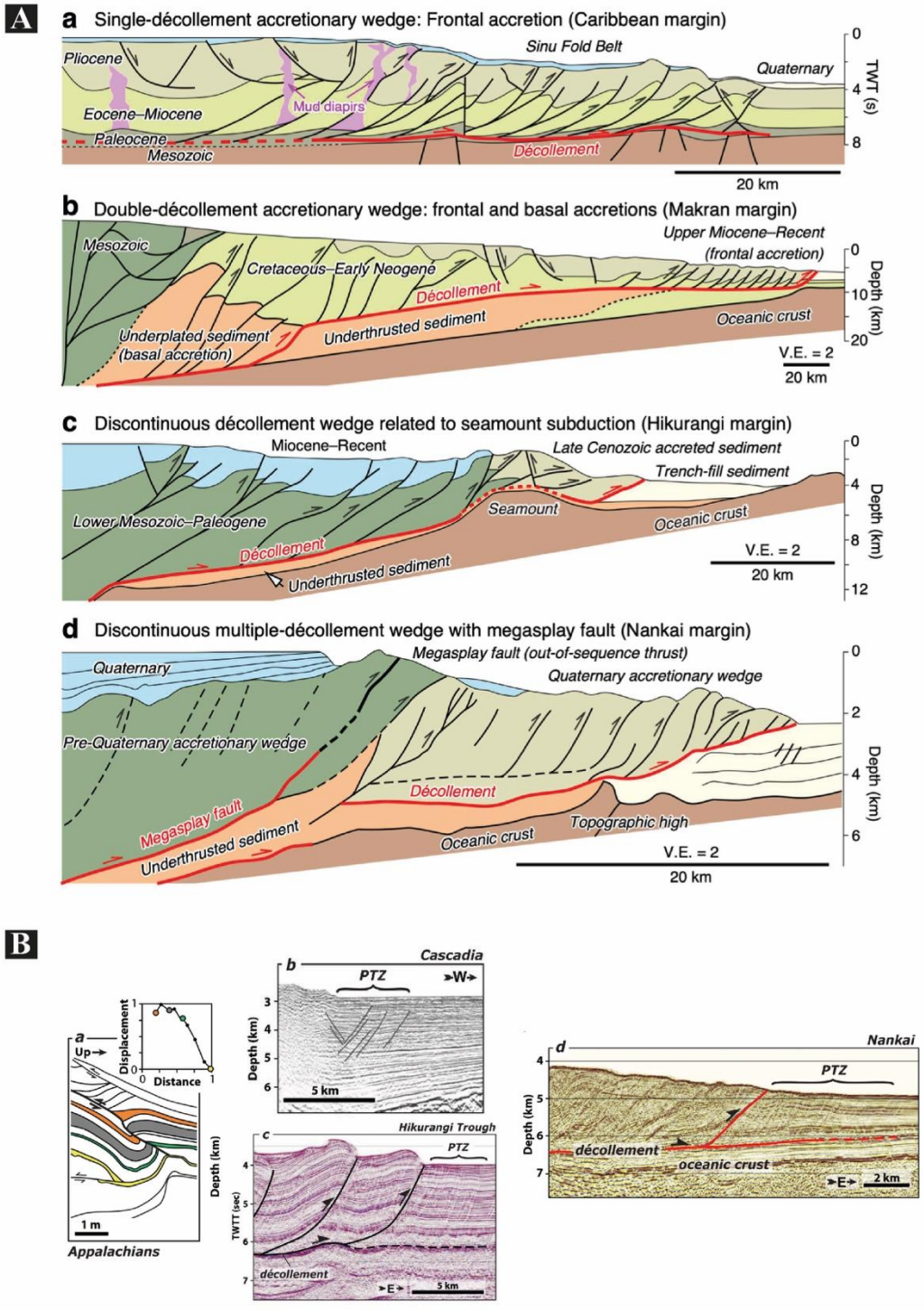

Figure 1.9 – A) Illustrations from Noda et al. (2023) showing different accretionary prisms (a-Caribbean margin; b-Makran margin; c-Hikurangi margin; d-Nankai margin) and their types of décollements and corresponding morpho-tectonic deformation of the overlying accretionary prism. B) Illustrations from Weiss et al., (2018) showing proto-thrust zones from different accretionary prisms (a-Appalachians; b-Cascadia; c-Hikurangi; d-Nankai).

1.4 Subduction of seamounts and asperities

Subduction of seamounts, ridges, and other bathymetric features have been extensively documented and discussed, as in the case of the Muroto seamount (Kodaira et al. 2000), the Mediterranean Ridge (von Huene et al., 1997) and the Marianas Trench (Oakley et al., 2008). Subducting seamounts have a significant impact on both the upper surface and internal sections of accretionary prisms (Figure 1.11A). Near the seafloor it can generate scars, embayments, slumps, bulges, and slides, whereas in the internal part of the accretionary prism will cause changes in the deformation experienced by the overlying plate, in the frontal growth of the wedge, in fluid and pore pressure distribution, in local uplift and subsidence history, as well as imposing variations in the accretional vs erosive behaviour of the accretionary prism (Watts et al., 2010; Ruh et al, 2016).

1.4.1 Influencing factors

The way asperities are included in either the accretionary prism or the subduction channel depends on several factors (Watts et al., 2010):

1. **The thickness of the subduction channel or décollement**. When the thickness of the décollement is greater relative to the asperity it can then engulf the asperity while subduction is occurring.

This will cause the asperity to subduct within the subduction channel. However, if the asperity is relatively high, there is a greater chance of resisting being subducted – instead, it will be truncated. This is a typical characteristic of Mariana-type margins (Ruh et al., 2016) (Figure 1.10B). In the former scenario where the asperity is included within the subduction channel, the asperities could still be truncated at the depths where the friction with the upper part of the décollement, or lower part of the accretionary prism, increases (Cloos, 1992; Cloos and Shreve, 1996). This is a setting typical of Chilean-type margins (Ruh et al., 2016) (Figure 1.10A).

2. **Relative strength of the subducting and overriding plates**. Softer and weaker accretionary prisms tend to offer little resistance, flexing elastically while sliding over the asperities. This allows basal asperities to intrude without suffering much deformation, leading only to a local increase in normal stresses on the subduction interface, which enhances seismic coupling. This is particularly observed in Barbados (Zhao et al., 1998; Ruh et al., 2016) (Figure 1.10C). Otherwise, harder crystalline forearcs are stronger and, therefore, offer more resistance to the inclusion of asperities causing them to jam and break. In the latter scenario, asperities can be subducted but cause the overring plate and accretionary prism to suffer permanent brittle defor-

mation, generating complex heterogeneous stress fields that are favourable to aseismic creep. Such a setting is observed in Cascadia (Ruh et al, 2016; Morton et al., 2018) (Figure 1.10D).

3. **Internal structure of the asperities**: asperities with complex internal structures that are dense and compact tend to be harder to include within the subduction channel when compared to asperities with a layered structure. Hence, layered asperities may help the propagation of the décollement through them causing it to become a seismic asperity (Wang and Bilek, 2011). Equally, such asperities tend to also be more prone to truncation as nucleation of rupture is facilitated by their layered structure.

4. **Buoyancy of the asperity**: an asperity formed on a strong plate that is more regionally supported will be less buoyant and, therefore, less likely to lift the forearc. If the asperity is formed on a weak plate, and more locally compensated, it will be relatively buoyant and more likely to jam a subduction zone.

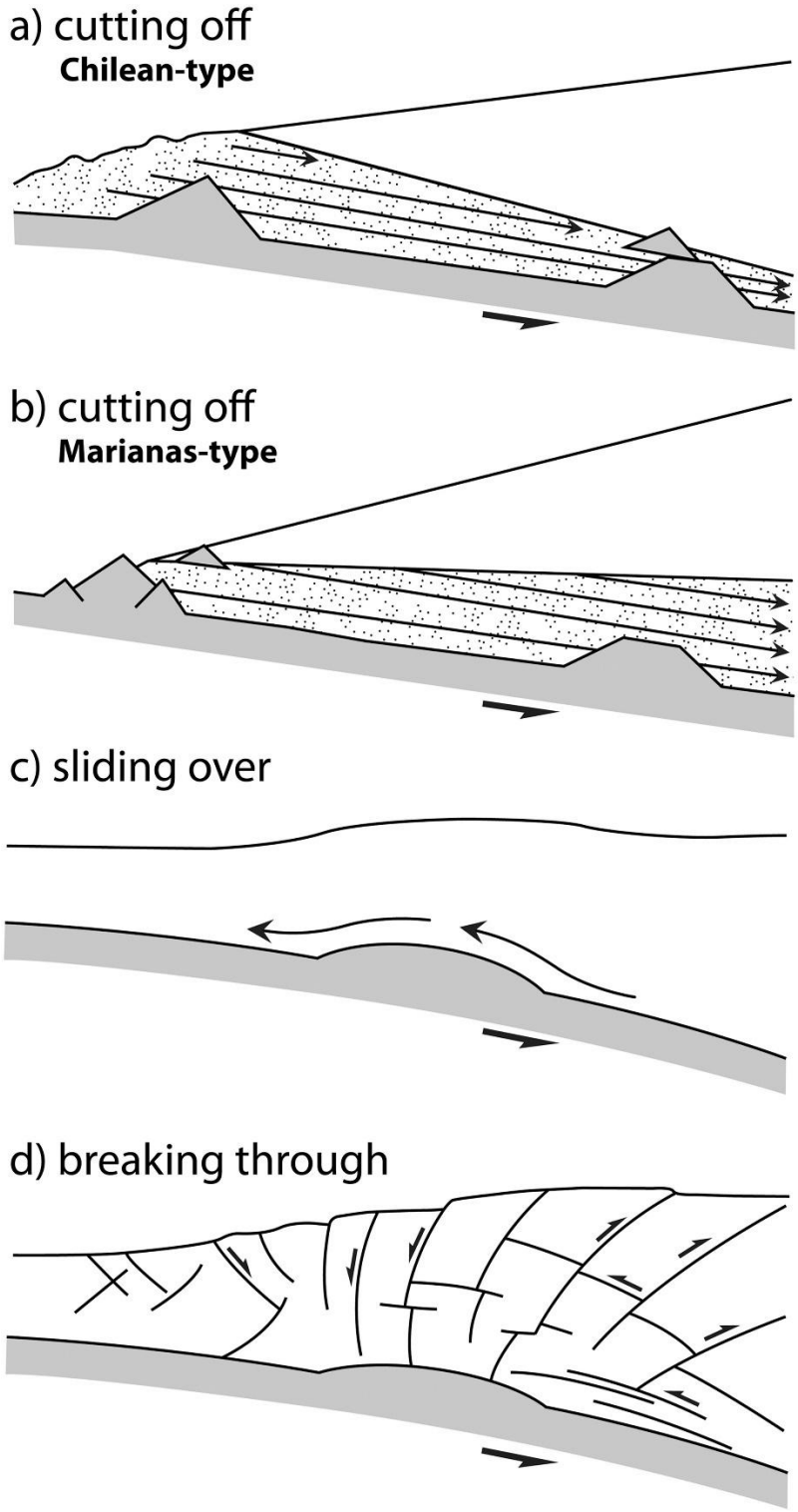

Figure 1.10 - Suggested scenarios for overriding plate response to subduction of a seamount (Modified from Ruh et al., 2016). a) Large earthquakes occur due to seamount decapitation at high confining pressures. b) Absence of large earthquakes due to very shallow seamount decapitation. c) The upper plate slides over subducting seamounts without internal deformation. d) Subducting seamount severely breaks (i.e. fractures) the overriding plate.

1.4.2 Controls on the deformation and growth of accretionary prisms

According to Dominguez et al. (1998), the subduction of asperities can shortly interrupt frontal accretion while causing significant loss of material from the accretionary prism into the subduction. Equally, sediment within the accretionary prism becomes laterally trapped while the subduction creates a trail of weak zones as it subducts. These weak zones start as a dense network of vertical faults showcasing a mixture of forward thrusting, back thrusting and strike-slip movements that are later reactivated as normal faults, after the passage of the subducted asperity. The décollement tends to mould and engulf around the seamount (Figure 1.11B and 1.11C). However, this mainly happens when the asperities can underplate the overriding accretionary prism, causing the accretionary prism to temporarily hold its frontal (seawards) growth. Other scenarios that equally affect the growth of the accretionary prisms have been proposed, such as those in Yang et al (2022):

- The incorporation of the asperities into the accretionary prism, where asperities are actively contributing to the growth of the wedge.
- The obduction of the asperities over the overriding plate, which can change the critical taper angle and cause the accretionary prism to adjust its growth to re-achieve critical taper angle.
- The collision with the accretionary prism causing it to stop growing, thus becoming a backstop together with the asperity.

Bangs et al. (2006) showed that seamount subduction also causes stepping up of the décollement into the accretionary wedge as a key mechanism to continue the subduction process.

1.4.3 Impact of fluids and pore pressure

The fracturing of the accretionary prism caused by subducting seamounts can affect the distribution of fluids and pore pressure (Dominguez et al., 1998; Sun et al., 2020), generating several permeable pathways for deeply sourced fluids (Saffer and Tobin, 2011). It can also influence the shear deformation in front of subducting seamounts, allowing for the accumulation of a fluid-rich sediment (Wang and Bilek, 2011).

Sun et al. (2020) describes the accretionary prism immediately in front of a subducting seamount as being under significant tectonic compression and drainage, causing sediment to be over-consolidated at depth greater that the seamount height, and subsequent porosity values to be reduced. In contrast, above and behind the seamount there is a stress shadow where the sediment is underconsolidated and porosity values remain anomalously high (Figure 1.11C and 1.11D).

Seismic reflection data provide critical insights into fluid migration pathways and accumulation zones and there several key seismic indicators identified and used across several studies (e.g. Baba and Yamada, 2008; Moore et al., 2009; Cartwright and Santamarina, 2015; Rass et al., 2018, Li et al., 2024):

- High-amplitude reflectors, also commonly known as bright spots, normally interpreted as localized gas/fluid accumulations, often linked to over pressured zones.
- Low-amplitude zones, also referred to as dim spots, consist of fluid-saturated or pervasive fluid migration, fractured sediments with reduced acoustic impedance.
- chaotic/disrupted reflectors which are normally associated fluid expulsion features along fracture networks or shear deformation.
- Vertical fluid pathways, sometimes referred to as acoustic pipes or chimneys, which tend represent more focused fluid flow along faults or fractures.
- Bottom-simulating reflectors (BSRs) that mark the base of gas hydrate stability, with free gas accumulation beneath.

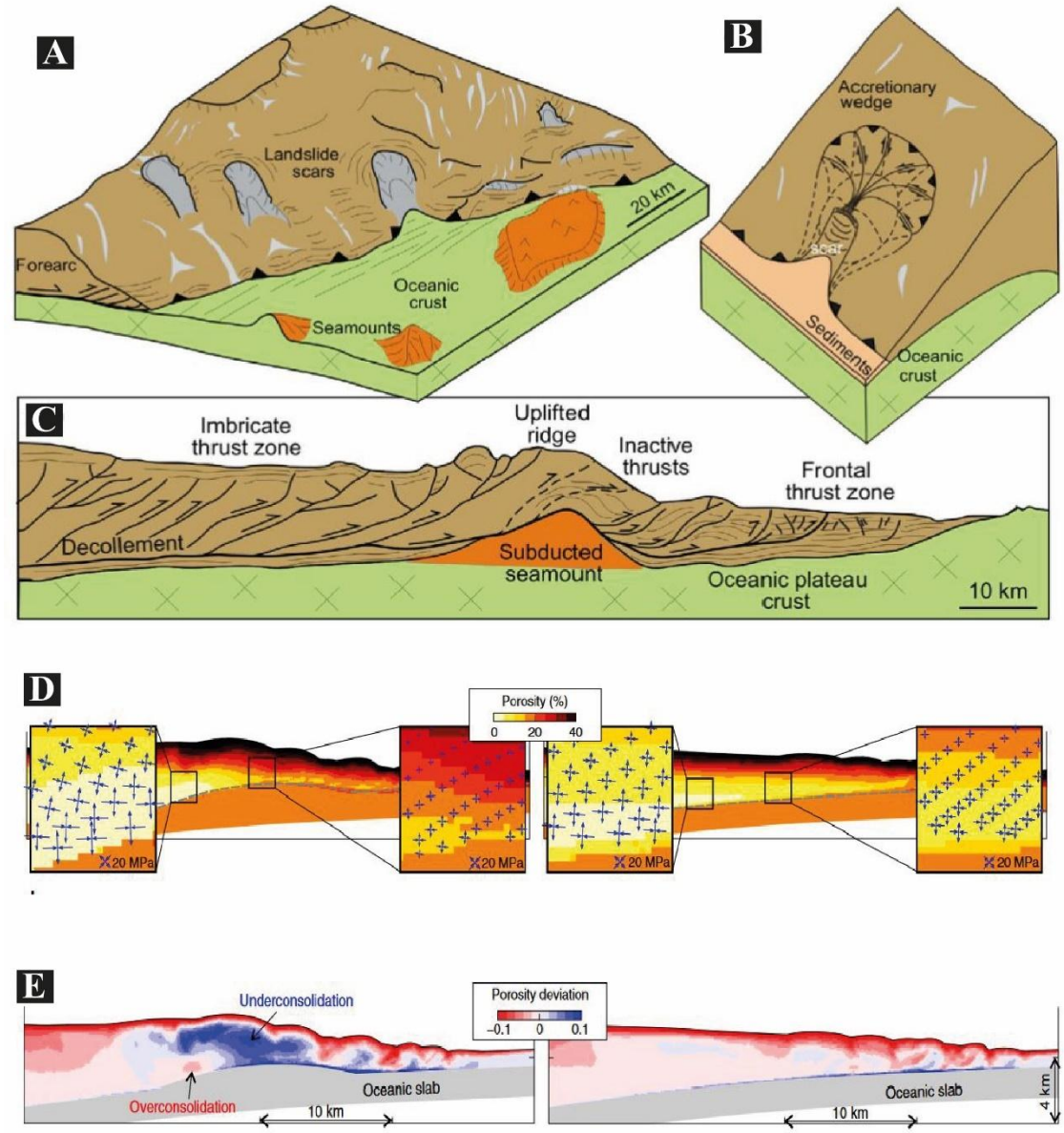

Figure 1.11 – Illustrations from Yang et al. (2022) (A-C) and models (from Sun et al., 2020) (D-E) showing the deformation, tectonic response, and porosity and consolidation changes in the overriding accretionary prism because of the introduction of a seamount into the subduction zone. A) Landslide scars, embayments and associated normal faults as a near-surface response to the internal deformation observed in C). B) Geometry of the fault planes in the landward part of the subducting seamount C) Uplifted ridges and fault distribution in a section of the accretionary prism. D) Porosity distribution in the accretionary prism when of the subduction of a seamount (left) within a smooth décollement (right). Blue arrows in insets show deviatoric stress in the upper plate. E) Porosity deviation in accretionary prism with the subduction of seamount (left) in a smooth décollement (right). Zones of enhanced loading and stress shadows are shown above the leading and trailing flanks of the seamount, respectively.

1.4.4 Impact on accretional vs erosive behaviour

The impact of subducting asperities, such as seamounts and ridges, on subduction behaviour seems to vary in both time and space. However, it is generally accepted that the subduction of basal asperities promotes an erosive behaviour.

Clarke et al. (2018) defend that the subduction of seamounts leads to spatial variations in accretional vs. erosive behaviour along the trench, with the seamount itself favouring an erosive behaviour. In contrast, the sediment moats around the seamount will favour an accretional behaviour.

Bangs et al. (2006) stated that the main effect of ridge collision is tectonic erosion from the base of the accretionary wedge as a mechanism to include the seamount under the accretionary prism and for the seamount to be able to move down the subduction zone. Similarly, Wang and Bilek (2011) showed that the fracture network generated by the seamount when ploughing through the accretionary prism is able to loosen up the overlying rocks and sediments, thus helping the underscrapping process of the seamount. Therefore, such tectonic erosion is unavoidable unless seamounts are accreted into the accretionary prism.

1.4.5 Impacts on seismicity

Scholz and Small (1997) observed that seamount subduction results in the local increase in seismic coupling between the subducting and overriding plates because of the increase in the normal stresses caused by the larger mass and buoyancy of these asperities. However, they also stated that coupling conditions are only significantly changed if a seamount is of considerable size as structural coupling can still result in aseismic subduction. In contrast, Wang and Bilek (2011) state that the intensive fracturing and faulting of rocks and sediments within the accretionary prism, around a subducting seamount, causes heterogenous stress and strain transfer in different parts, and at different times, as the seamount pushes itself through. While some faults are locked, others are slipping, allowing the accretionary prism to deform and the seamount to aseismically creep. Occasionally, earthquakes can occur, but they tend to be small due to the limited rupture slip caused by an intense crosscutting between fractures and faults in the accretionary prism. Wang and Bilek (2011) do not discard the possibility of seamounts influencing or causing great earthquakes but consider this to be a rare event. One such occasion can occur when a smooth locked portion of the interplate boundary is in the vicinity of a seamount, with the seamount incrementing stress on the locked area by creeping forwards and stopping rupture propagation when the locked area finally slips. Another possible great earthquake scenario could occur when the complex fracturing and

faulting network in the accretionary prism, around the seamount, joins to form a large structure and therefore a composite seismic event. This seems to in agreement with Kelleher and McCann (1976), who argued that the size and frequency of large earthquakes were lower in the areas of thick oceanic crust containing asperities about to enter a subduction zone.

Recently, Menichelli et al. (2023) stated that the presence of a seamount reduces recurrence time, interseismic coupling, and fault strength, therefore acting as a barrier as 80% of the ruptures concentrate in neighbouring flat regions and only smaller magnitude earthquakes nucleate above it. Additionally, the subduction of fluid-rich sediments tends to promote overpressure conditions that decrease friction, thus also decreasing the likelihood of great earthquakes in such conditions.

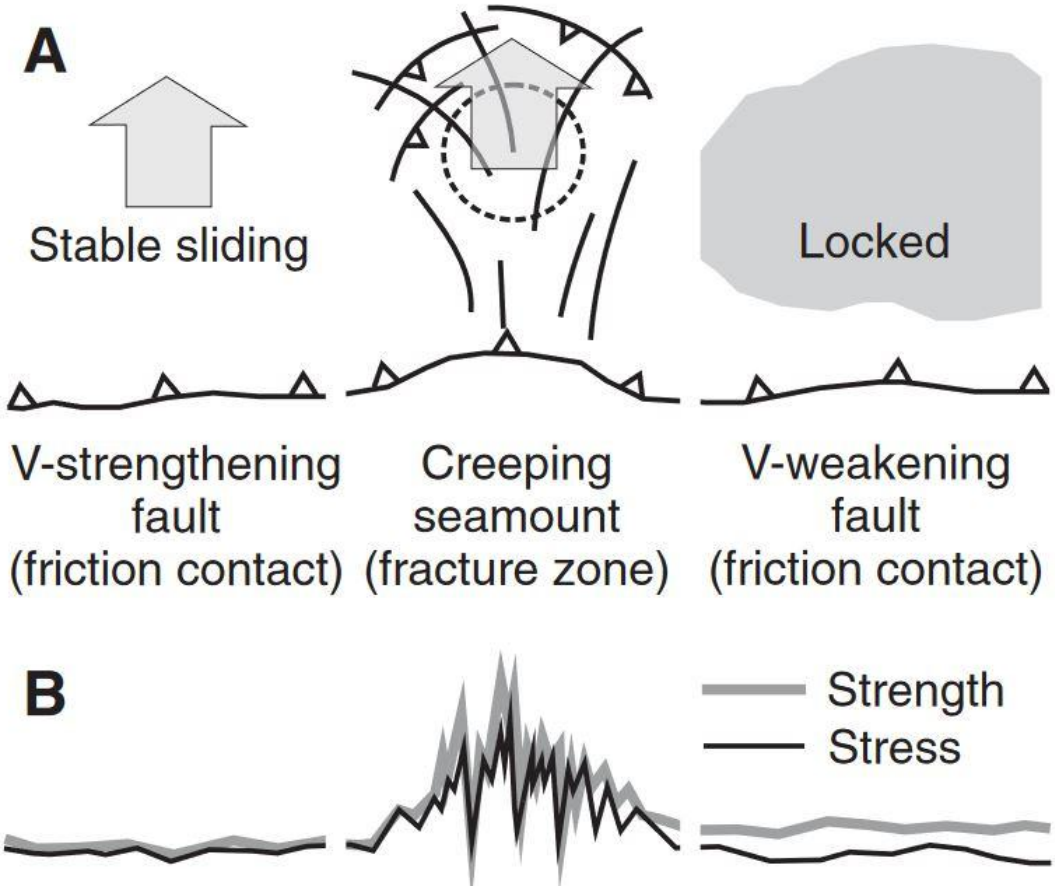

Figure 1.12 – A) Slip or creep behaviour of subducting seamount (dashed circle) and smooth faults. B) Strength and stress for the three different types of fault zone shown in A. Fracture zone deformation around a seamount leads to creep and numerous small earthquakes. A velocity-strengthening fault may remain at failure (stress = strength) and slide stably (left). A velocity-weakening fault alternates between locking and earthquake rupture; when locked, stress < strength (right). (from Wang and Bilek, 2011).

CHAPTER 2

Geological Setting

2.1 Introduction

This chapter outlines the geological setting of the Nankai Trough with particular focus on the study area relevant to this thesis. It includes an overview of the main domains along the Nankai Trough as it is important to understand the placement and scale of our study area within the wider trench. Furthermore, this chapter explores the bathymetric features of the incoming and overriding plates, followed by a thorough review of the morpho-tectonic features and of the tectono-stratigraphic characteristics of the NAP.

2.2 The study area

The Deep Sea Drilling Program (DSDP), the Ocean drilling Program (ODP), the Integrated Ocean Drilling Program (IODP) and the International Ocean drilling Program (IODP) have all carried several expeditions along the Nankai Trough and focused their efforts, in last few decades, on three drilling/seismic transects (Ashizuri, Muroto and Kumano). The Kumano transect, the most recent one, was drilled during a multistage project called Nankai Trough Seismogenic Zone Experiment (NanTroSEIZE). The study area is in the south-east coast of Japan, just off the Kii Pen-insula, within the Kumano Transect (Figure 2.1). In this transect, a 3D PSDM seismic volume was acquired across the Nankai continental slope as part of the NanTroSEIZE (Figure 2.1B and 2.1C).

The study area comprises the southern half of the acquired 3D PSDM seismic block, imaging the ITZ and FTZ just seawards of the MSFZ (Moore et al., 2001; Park et al., 2002; Tobin and Kinoshita, 2006) (Figure 2.1B-C). This region is also known as the outer wedge of the NAP.

2.3 The Nankai Trough

The Nankai Trough is located off the coast of south Japan (Figure 2.1 and 2.2) and is one of the most studied subduction zones in the world, delineating an active and seismogenic convergent margin where the PSP is being subducted under the Amur Plate at a variable rate of 2 to 6.5 cm/year (Miyazaki and Heki, 2001; Tsuji et al., 2014). This is an accretionary margin that is actively off scraping and accreting sediment, resulting in the formation of the NAP, a ca. 100 km wide accretionary prism (Moore et al., 2009).

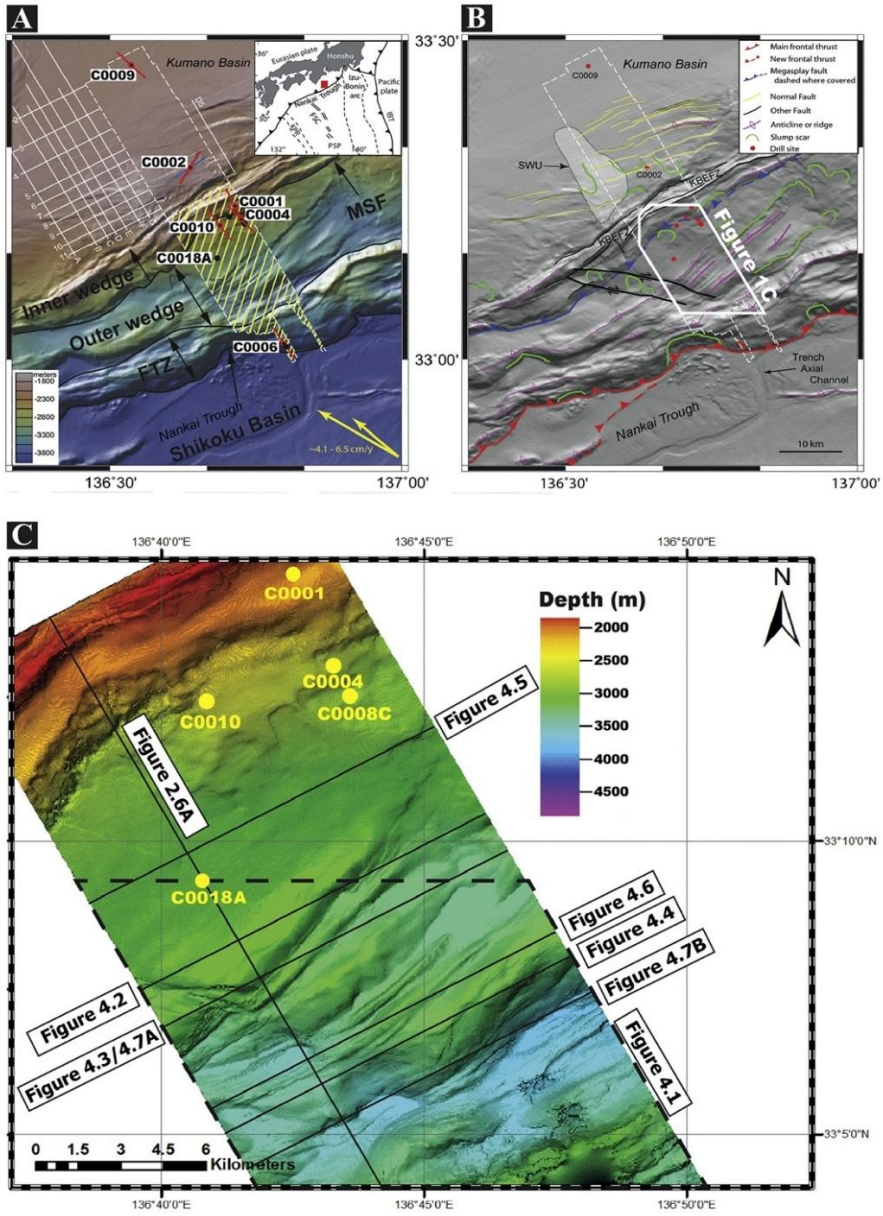

Figure 2.1 - A) Relief map of the Kumano Basin region of the Nankai Trough as modified from Moore et al. (2013). The figure shows the location of the 3D PSDM volume (white dashed box), maximum horizontal stress directions (red lines and blue line), the location of JAMSTEC 2-D seismic lines (white lines) and convergence vectors between the Philippine Sea Plate and Japan (yellow arrows). Also highlighted in the figure are the study area (yellow lines) and distinct tectonic regions in the NAP as shown in Kimura et al. (2011). The inset shows a regional tectonic map with the present-day configuration of the Nankai Trough. Red box shows the location of the study area in SE Japan. B) Tectonic interpretation from Moore et al. (2013) showing the area interpreted in Figure 2.1C. KBEFZ = Kumano Basin Edge Fault Zone; SWU = southwestern uplift. C) Bathymetric map derived from the Kumano 3D PSDM volume showing the direction of seismic profiles in Chapter 4 and IODP Sites C0001, C0004, C0008C, C0010 and C0018A. The study area comprises the southern limit of the Kumano Transect, up to the MSFZ.

The Nankai Trough is an area well known for the occurrence of great earthquakes of magnitude 8 or above (and related tsunamis) with return intervals between 50 and 150 years (Ando, 1975), which contributes to the multitude of studies done in this margin. Such studies cover a wide range of scientific fields, including structural geology and seismicity (e.g. Moore et al., 2001; 2007; Kamei et al., 2012), scientific ocean drilling expeditions (e.g., Karig et al., 1986; Moore et al., 2001; Tobin et al., 2006), seismic reflection and gravity (e.g. Kimura et al., 2018), pore pressure and fluid pressure (Saffer and Benkins, 2006; Saffer and Tobin, 2011), sedimentary properties (Karig, 1986), amongst others. The extensive study of the Nankai Trough provided several key data about the structure, properties, hydrogeology, deformation, and seismicity of this forearc region.

As the most recent great seismic events happened in 1946 (Nankaido, M 8.4), 1944 (Tonankai, M 8.1), and 1854 (Ansei-Nankai), there is a significant imminent threat of another great earthquake and related tsunami in the region as we are within the recurrence interval of 50 -150 years (Ando, 1975). Thus, continuing to research the Nankai Trough is of paramount importance.

2.3.1 Along – strike domains

The Nankai Trough is one of the most studied, yet complex, subduction zones from the collision between the overlying Amur Plate and underlying PSP

since ca. 15 Ma and is isolated from other adjacent subduction zones by the KPR and the IBA. This margin is commonly divided into three parts based on past and predicted seismic activity: the western part, also known as the Nankai region, located just off Shikoku; the central part, also known as Tonankai region, located off the Kii Peninsula; and the eastern part, addressed as Tokai region, just off Ise Bay (Liu et al., 2013; Zhang et al., 2020; Saito and Noda, 2022) (Figure 2.2).

Kawamura et al. (2009) interpret the bathymetric expression of the Nankai Trough, in its Eastern part, as a sequence of 'thrust-cored anticlines' characterised by asymmetric ridges and valleys parallel to the thrusts, presenting to be steeper seaward slopes and gentler landward slopes. However, spatial bathymetric variations divide the NAP into four distinct structural sectors: the Frontal Thrust; the Prism Toe; the Imbricate Thrust; and the Tokai Thrust zones, and the boundaries between them are generally thrust faults dipping towards the island arc. Studies in the central part of the Nankai Trough (Bangs et al., 2009; Ikari and Saffer, 2012; Shiraishi et al, 2019) also point for distinct structural sectors within the NAP, including a Frontal Thrust Zone, Imbricated Thrust Zone and a large out-of-sequence thrust fault, known as the MSF, that branches from the subducting oceanic plate. Similarly, in its western counterparts, the NAP is also divided into the Proto-thrust zone, the Imbricated Thrust zone and Frontal Out-of-sequence thrust zone (Moore et al., 2001; Ikari and Saffer, 2012).

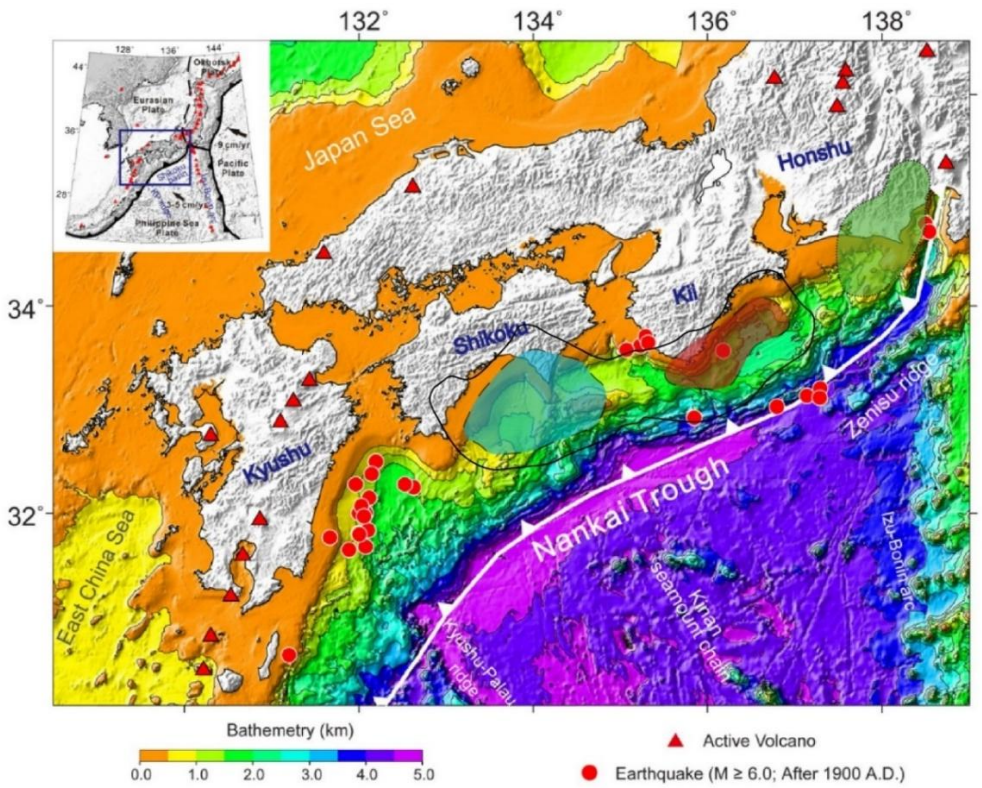

Figure 2.2 - Tectonic background of the Nankai subduction zone from Liu et al. 2013. The white bold sawtooth line denotes the Nankai trough. The inset map shows the simplified tectonic background within the wide region (blue box). The black and dashed bold lines on the inset map denote the plate boundaries. The topography data are derived from the GEBCO_08 Grid, version 20100927, http://www.gebco.net. (For interpretation of the references to colour in this figure legend, the reader is referred to the web version of this article.). Dotted line delineates a region supposed to be sources of the anticipated Tokai earthquake (green area). Solid and dashed lines denote the regions of estimated large slips (>2 and 4 m, respectively) resulting from the 1946 Nankai (blue area) and 1944 Tonankai (red area) earthquakes.

2.4 The subducting plate

The subducting PSP is a narrow NS-trending rhombic-shaped plate, surrounded by several convergent plate boundaries. The Nankai Trough, the Ryukyu Trench, and the Philippine Trench border the PSP at its western and southwestern parts, while the Izu-Bonin Trench and Mariana Trench are bordering the PSP at its easternmost limit. At the southern limit, the PSP is bordered by the Yap Trench and the Palau Trench part (Zhang et al., 2020; Zhang et al., 2022) (Figure 2.3).

Yinxia et al. (2011) suggested that the PSP is not uniform in thickness and that the plate can be separated into a West Philippine Sea Plate, dominated by approximately E-W tectonic structures, and an East Philippine Sea Plate, dominated by N-S structures. The East PSP is characterised by some important geologic and bathymetric heights that are worth mentioning (Figure 2.3), such as:

- the Kyushu-Palau Ridge: a discontinuous bathymetric ridge that borders the Nankai Trough at its westernmost limit. The Kyushu-Palau Ridge extends from the Palau Island in the south until the Kyushu Island, in Japan, where it subducts. This ridge is described as a remnant arc associated with back arc spreading of the Shikoku Basin at about 30–15 Ma (Okino et al, 1994; Park et al., 2009 Zhang et al., 2020).

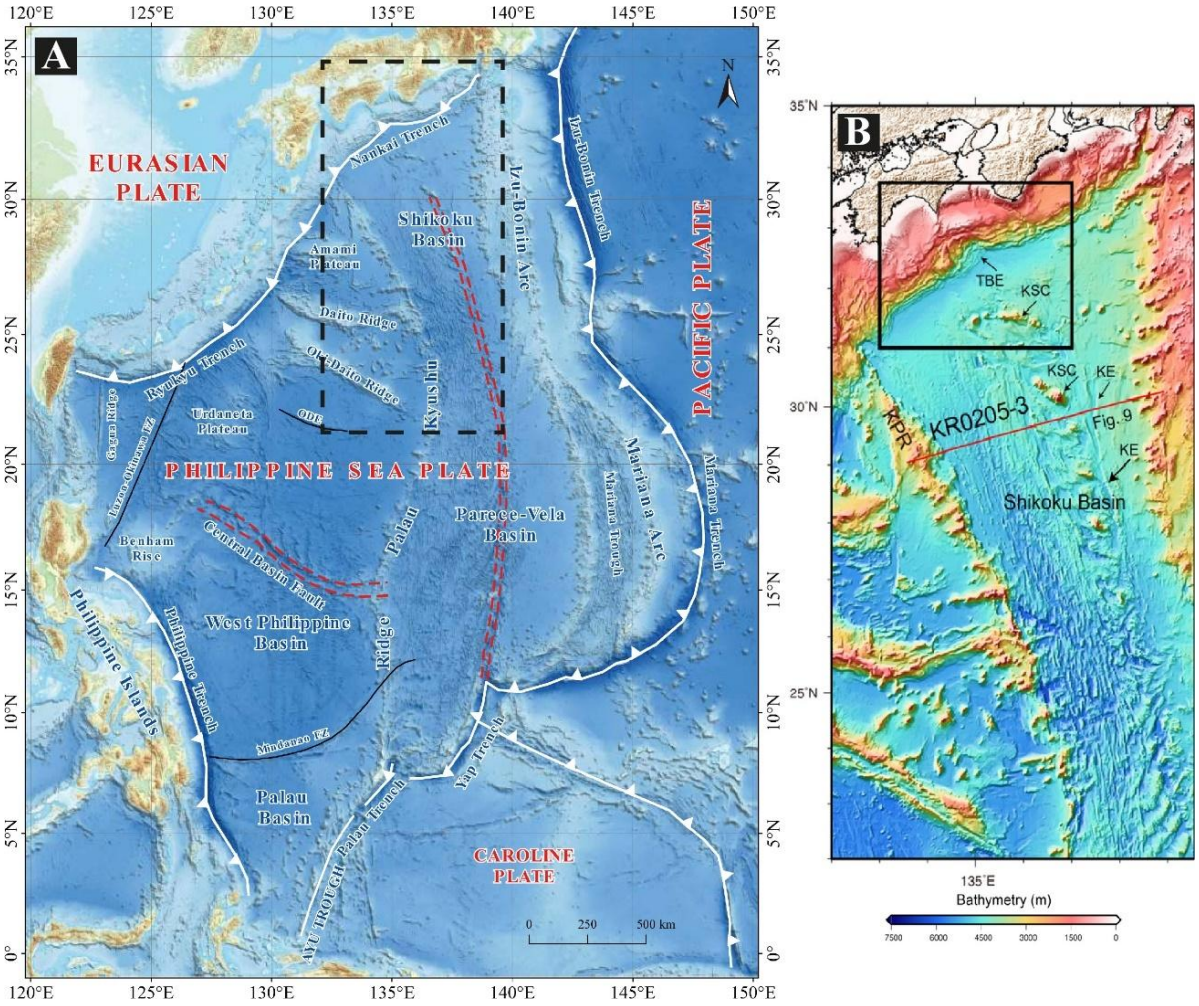

Figure 2.3 – A) Geotectonic location map of the Philippine Sea Plate from Zhang et al., 2022. The red double-dashed lines represent ancient spreading centres, and the black dashed box represent the area of Figure 1.4B. B) Bathymetric map of the Shikoku Basin just south of the Nankai Trough. KE, Kinan escarpment; KSC, Kinan seamount chain; TBE, Tosa bae embayment.

- the Shikoku Basin: the back arc basin that rifted from ca. 30 to 15 Ma in two distinct spreading periods related to the clockwise rotation of the PSP; an initial ENE-WSW spreading direction followed by a NE-SW spreading direction (Okino et al., 1994; Yan et al., 2022).
- the Kinan Seamount Chain: an alignment of seamounts and bathymetric heights generated during the last stage or even after the cessation of the Shikoku Basin spreading, related to post-spreading magmatism from deeper parts of the mantle (Kobayashi et al., 1995, Sato et al., 2002).
- the Zenisu Ridge: a double NE-striking thrust system interpreted to result from N-S intraoceanic shortening, consisting of three distinct segments with a gradual decrease of deformation from NW to SE, due to the kinematic discontinuity between the diffuse shortening present in the colliding Izu-Bonin Arc and the concentrated shortening along the subducting Nankai Trough (Le Pichon et al., 1987; Mazzotti et al., 2002).
- the Izu-Bonin Arch: an intraoceanic volcanic arc bordering the Nankai Trough at it easternmost part. The Izu-Bonin Arc is related to the subduction initiation of the Pacific plate and separated from the Kyushu-Palau Ridge at 25 Ma, forming the Shikoku back arc basin (Okino et al, 1999; Arai et al, 2013).

Since 50 Ma, the PSP moved from its near equator position to its current subduction under the Amur Plate along the Nankai Trough and Ryukyu Trench

between 6 and 2 Ma. During 50 – 42 Ma, the westward movement of the Pacific Plate converted the N – S transform fault in the PSP into a subduction zone, forming the paleo Izu-Bonin Arc. The consequent back arc spreading formed the Parece Vela and Shikoku Basins and separated the Kyushu-Palau Ridge separated from the paleo-IBA.

2.5 The Nankai Accretionary Prism (NAP)

Submarine accretionary prisms and associated structures are usually described by the classical critical-wedge and dynamic Coulomb-wedge theories (Davis et al., 1983; Dahlen et al., 1984), with the NAP being no exception (Wang and Hu, 2006). These two theories suggest a transition between a highly compressional outer wedge and a less compressional and moderately seismogenic inner wedge. Moore et al. (2009) divides the NAP into six distinct domains: the PTZ, the FTZ, the ITZ, the MFSZ or OOSZ, the Kumano Basin Edge and the Kumano forearc basin and underlying inner wedge (Figure 2.4). The ca. 100 km wide accretionary prism can be simplistically divided into inner and outer wedges separated by the MSF, which is a large out-of-sequence thrust branching from the décollement. The outer wedge of the NAP comprises a series of imbricated thrust faults (i.e. reflecting a zone of low shear strength) and is the result of accreted trench turbidites and Shikoku Basin sediment from the incoming PSP while the inner wedge forms a zone of accreted sediment, mainly composed of

mudstone, acting as a backstop, and is characterised by the absence of active compressional structures (Wang and Hu, 2006; Moore et al., 2009).

2.5.1 The Megasplay Fault Zone (MSFZ)

The MSFZ defines the landwards (and northern) boundary of this thesis study area (Figure 2.1). This area is described as the dominantly compressional zone of the accretionary prism, controlled by a large MSF, on the upper continental slope of the Nankai Trough (Moore et al., 2007; Kimura et al., 2011; Moore et al., 2015). In published literature, the MSFZ is associated with a WNW-directed (~ N120°–N125°) convergence vector that is deviated ca. 15°-45° counter-clockwise from a direction orthogonal to the trench (e.g. DeMets et al., 2010; Tsuji et al., 2014).

Reference to important strike-slip movements in the landward part of the MSFZ was made by Martin et al. (2010) and Tsuji et al. (2014), who justified these movements as reflecting a transtensional tectonic regime. Such a regime allowed the formation of local to regional scale trench-parallel and right-lateral strike-slip faults with associated normal offsets. The same authors stated that present-day transtension is associated with oblique subduction at obliquity values as little as 15°. However, Byrne et al. (1993) also stated that a detailed picture of an underlying backstop could not be determined from surface information alone.

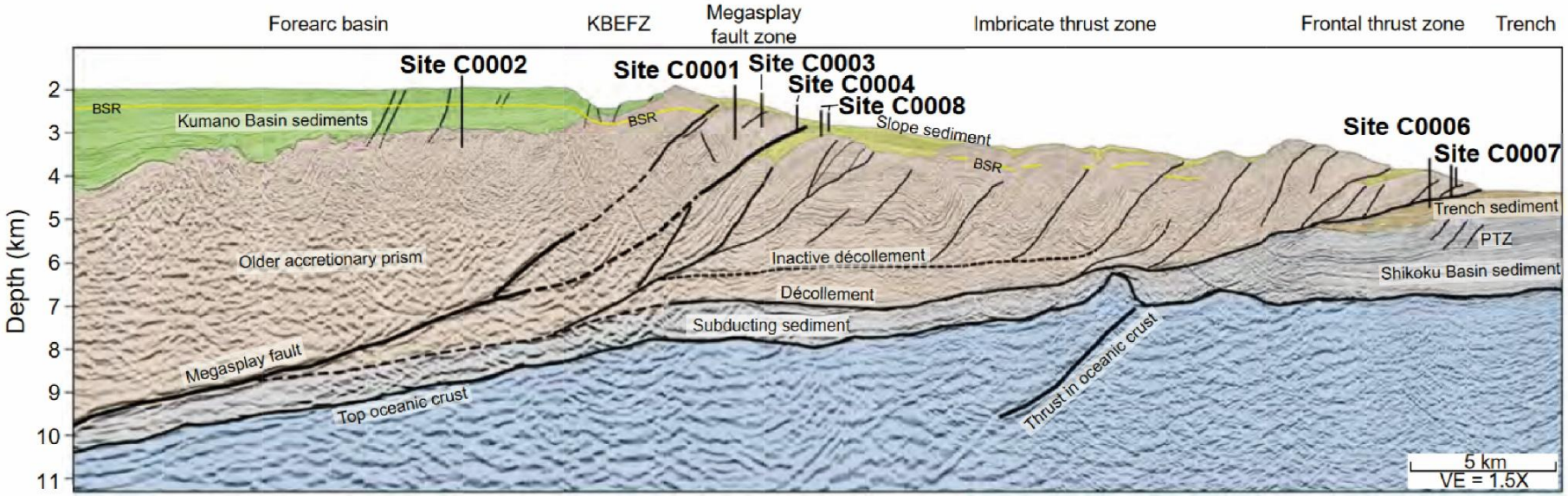

Figure 2.4 – Interpreted seismic line by Moore et al. (2009) from the Kumano Transect 3D seismic volume. The interpreted seismic line illustrates the main morpho-tectonic domains within the NAP, with interpreted imbricated and out-of-sequence thrust faults and décollement. It also includes the location of drilling/coring sites from NanTroSEIZE also seen in Figure 2.1. KBEFZ = Kumano Basin edge fault zone, PTZ = protothrust zone. BSR = bottom-simulating reflector. VE = vertical exaggeration

The slipping of MSF lead to the uplift of the seaward part of the inner wedge in relation to the landward part of the outer wedge causing the formation of the Kumano Basin Edge and consequently the landward tilting Kumano Basin, overlying the inner wedge of the NAP (Park et al., 2002). According to Egawa et al. (2013), the sediment filling the Kumano Basin derives from the Kii Peninsula and from east Honshu (Figure 2.4). The Kumano Basin is also showcasing different venting systems, such as seeps and mud volcanoes related to dewatering of underlying sediments. While 13 mud volcanoes have been identified in the Kumano Basin, most seepage occurs at the frontal part of the NAP (Toki et al., 2014).

2.5.2 The outer wedge

The NAP results from the subduction of the Philippine Sea Plate under the Amur Plate along the Nankai Trough (Miyazaki and Heki, 2001; Tsuji et al., 2014). The seaward edge of the forearc Kumano Basin, known as the Forearc High, divides the NAP into an inner wedge at its landward side (with the Kumano Basin), and the outer wedge at its seaward part. The outer wedge recorded a rapid growth ca. 1.95–2.0 M, being mainly composed of previous trench-filling turbidites and Shikoku Basin sediments of the PSP, that do not only get accreted into the NAP but also underplated, thus promoting an even quicker growth of the lower section of the outer wedge (Kimura et al., 2018).

The outer wedge of the NAP is structurally divided into three main sections (Figure 2.4):

- **Frontal Thrust Zone (FTZ)**, bordered by the deformation front at its seaward edge and by the first frontal thrusts rooting from the basal décollement at its landward edge.
- **Imbricated Thrust Zone (ITZ)**, characterised by in-sequence folds and thrusts bordered by the FTZ at its seaward end and by the MSFZ at its landward edge.
- **MSFZ or Out-of-Sequence Zone (OOSTZ)** characterised by a large-scale fault zone that extends from the basal décollement until the surface (Moore et al., 1990; Gulick et al., 2004; Moore et al., 2007; Kimura et al., 2011; Strasser et al., 2011; Moore et al., 2015) (Figure 4).

Recent studies (Azevedo et al., 2018; Shiraishi et al., 2019) show that the outer edge near the ITZ is intersected by a younger family of strike-slip conjugate faults, particularly at the top of thrust anticlines, occasionally rooting down into the décollement. The same authors suggested that the superficial deformation of the NAP is partitioned by the presence of an important regional a right-lateral strike-slip fault, which divides the outer wedge into two structural domains as discussed in further detail in Chapter 4.

2.5.3 Stress field and deformations styles

Knowledge on the stress state(s) at accretionary prisms is of paramount importance to assess how strain is accommodated inside them and, subsequently, to determine their deformation style(s). Considering that the NAP is divided into inner and outer wedges with a transitional area that is mainly controlled by the MSFZ (Wang and Hu, 2006; Kimura et al., 2011), this thesis opts to follow the dynamic wedge theory of Wang and Hu (2006) to individualise the stress states in the NAP, instead of the classic wedge concepts in Davis et al. (1983), as the latter is known to generalise the stress states for the study area.

According to Wang and Hu (2006), the mechanics of the inner and outer wedges of the NAP are different due to the distinct behaviour of their décollement. In the inner part of the wedge, the décollement has a velocity weakening behaviour (downdip zone) that locks it, allowing stress to accumulate until a critical point, leading to its rupture. It thus comprises a seismogenic zone. However, the inner wedge rarely ruptures compressively due to its relatively low basal friction, a character allowing for significant slip along its décollement. This means the décollement does not lock in the entire section of the NAP. In the outer wedge of the NAP (updip zone), the décollement has a velocity strengthening behaviour that does allow stress to build up to a critical state and generates a highly compressional region at the toe of the continental slope.

Wang and Hu (2006) argue that wedge mechanics also varies with the seismic cycle due to changes in the stress state during and after an earthquake. During an earthquake, σ_1 is sub horizontal and the décollement slips, pressurising the outer wedge into elastic or permanent compressive deformation. In contrast, the inner wedge is in a stable extensional state, as shear stress is null due to slip in the décollement. After an earthquake, the outer wedge records interseismic relaxation that is accompanied by a decrease in shear stress, seaward movement of this part of the NAP, and an increase in the dip of σ_1, whereas the inner wedge starts to become more compressional as shear stresses start to build up again (Figure 1.7A).

Several methods have been applied to IODP data to define the stress field and deformation style(s) currently operating across the NAP, and on the incoming PSP (Shikoku Basin) (Wu et al., 2013; Lin et al., 2015; Huffman and Saffer, 2016; Chang and Song, 2016). These papers not only show important changes in the stress field and deformation style(s) across the NAP, and between the NAP and Shikoku Basin; they also show results that are not consistent for the same IODP sites. This is because different methods have been applied to define these stress field(s) and associated deformation regime(s), and that measurements were taken at different depths and scales of observation.

Wu et al. (2013) used a compilation of Formation Micro Imager (FMI), Logging While Drilling (LWD) and core data to calculate the magnitudes of maximum (σ_{Hmax}) and minimum (σ_{hmin}) horizontal stresses. The magnitudes were constrained in stress polygons to derive the field stress in different areas of the NAP and Shikoku Basin. At IODP Site C0009, in the inner wedge of the NAP and at ca. 1540 mbsf, Wu et al. (2013) showed that σ_{Hmax} and σ_{hmin} correspond to σ_1 and σ_3, respectively. Here, σ_1 is perpendicular to the trench direction (which is NE-trending), and the deformation style is concordant with that of strike-slip faulting. However, at IODP Site C0002, in the seaward part of the inner wedge (at ca. 1000 mbsf), the same authors estimated a NE-trending σ_{Hmax} where $\sigma_v > \sigma_{Hmax}$, a configuration that reflects a normal faulting regime. At IODP Site C0006, in the Frontal Thrust Zone (ca. 476 mbsf), Wu et al. (2013) interpreted a normal faulting regime with a vertical σ_1 ($=\sigma_v$), but close to strike-slip faulting due to σ_{Hmax} being NW-trending and only 0.5 MPa lower than σ_v. In the Shikoku Basin, at IODP Site C0011 (ca. 610 mbsf), the stress field and deformation styles are parallel to those at IODP Site C0002, but again very close to strike-slip faulting regime due to the minor difference in magnitude between σ_v and σ_{Hmax}. Despite these results, Wu et al. (2013) state that their stress analysis was limited by the total drilling depth, borehole conditions and deviations in the slip deficit method, thus returning less reliable results at relevant depths.

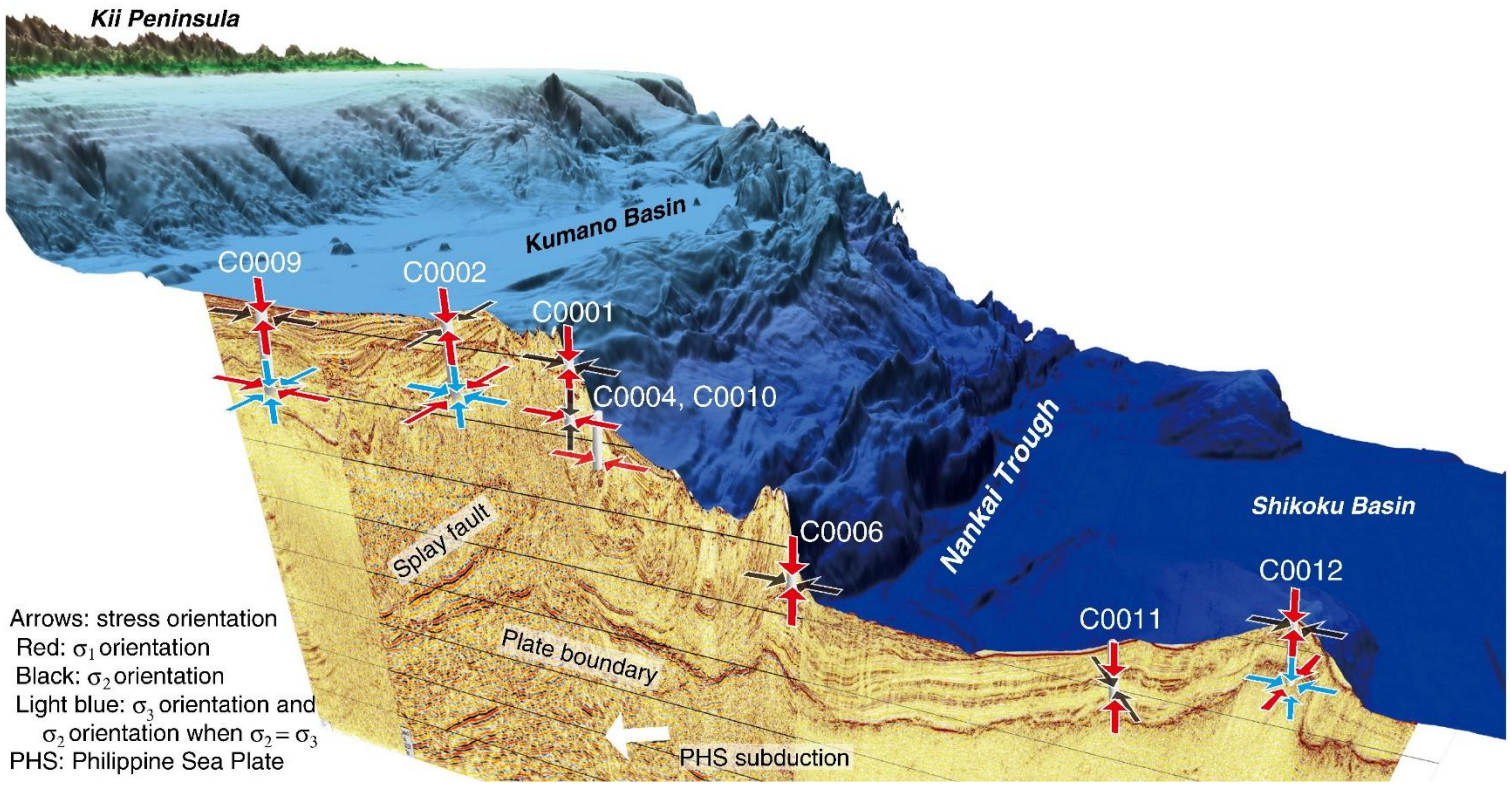

Figure 2.5 - Distributions of three-dimensional stress state in NanTroSEIZE transect drilling sites (C0009, C0002, C0001, C0004, C0010, C0006, C0011, C0012) from Lin et al (2015). Red, black, and light blue arrows are the orientations of the maximum, intermediate and minimum principal stresses, respectively. Two pair arrows in the same light blue colour in the deeper part of C0009, C0002 and C0012 mean that the intermediate and minimum principal stresses are nearly equal each other, or the intermediate and minimum principal stresses are highly variable.

Lin et al. (2015) used a similar approach to Wu et al. (2013) in a larger number of IODP Sites across the NAP and Shikoku Basin, together with hydraulic fracturing experiments and anelastic strain recovery (ASR) measurements on retrieved cores. This approach allowed a detailed investigation of stress states across the NAP and Shikoku Basin, in three dimensions, leading to the conclusion that, overall, the NAP is currently undergoing an (interseismic) extensional regime.

According to Lin et al. (2015), the sediment cover overlying the inner wedge of the NAP (Kumano Basin) has a vertical σ_1 and expresses a normal faulting regime. However, the strikes of σ_{Hmax} at IODP Sites C0009 and C0002 agree with the results in Wu et al. (2013). The transition from the Kumano Basin strata to the inner wedge of the NAP is accompanied by a change in σ_1 from vertical to sub-horizontal, where $\sigma_{Hmax} = \sigma_1$, and by a change from normal to strike-slip and thrust faulting. At the MSFZ, IODP Site C0001 shows a similar stress distribution (and deformation style) to that of IODP Site C0009 with depth, with the change occurring at ca. 500 mbsf. However, at IODP Sites C0004 and C0010, where the hanging-wall of the MSFZ was drilled, σ_1 is interpreted to be sub-horizontal and parallel to the plate convergence vector, reflecting thrust and strike-slip faulting regimes. In the shallower part of the hanging wall of the Frontal Thrust Zone, drilled at IODP Sites C0006 and C0007, Lin et al. (2015) interpreted a similar stress field and deformation style to the shallow part of IODP Site C0001. Finally, in the Shikoku Basin, the interpretation of IODP Site C0011 coincides with the results in Wu et al. (2013), while at IODP Site C0012

ASR analyses show evidence for strike-slip and reverse faulting with a NE-trending σ_{Hmax}. In such a setting, Lin et al. (2015) state that, at present, the overall NAP is dominated by a shallow extensional regime and a relatively deep strike-slip to reverse faulting regime, mainly due to stress field reorganization in the areas where σ_1 becomes σ_{Hmax}. This transition between different tectonic regimes at depth is often referred to as ECD and there is consistent data suggesting that the ECD is highly variable along the entire NAP, in both the inner and outer wedges, depending on the thickness of the overlying sediment cover (Lewis et al., 2013; Van Tuyl et al., 2015; Lin et al., 2015). Lin et al. (2015) refer that principal stresses permute in the deeper levels of the NAP, but that sediment cores have yet to be recovered at such depths.

More recently, Chang and Song (2016) integrated borehole breakouts, drilling-induced tensile fractures, and leak-off tests at IODP Site C0002 to interpret tectonic stresses (up to a depth of ca. 2000 mbsf) at the seaward limit of the inner wedge of the NAP. They concluded that deformation in this latter region varies between strike-slip and normal faulting because of σ_{Hmax} and σ_v having similar magnitudes. They stress that σ_{Hmax} is NE-trending above the MSFZ. The same authors postulate that strike-slip and extensional structures are found in both core and regional seismic data.

In the Muroto Transect, outside the study area of this thesis but still in the NAP, Huffman and Saffer (2016) showed comparable results and interpretations to the authors previously mentioned. Stress states at the toe of NAP are

likely associated with strike-slip or thrust faults across the active Frontal Thrust Zone down to a depth of ca. 800 mbsf. The uppermost 300 mbsf are near thrust failure, where $\sigma_{Hmax} > \sigma_v$. However, Huffman and Saffer (2016) conclude that the stress state in the upper 300 mbsf changes into a normal faulting regime at depth, where $\sigma_v > \sigma_{Hmax}$. These authors recognise the large uncertainties associated with the parameters used in their stress analysis.

It is important to highlight that depth and location of the boreholes, and conditions in which data were acquired are limiting factors in the analysis of regional stress states. Nevertheless, there seems to be a consensus that the NAP is a compressional structure currently dominated by shallow normal (Wu et al., 2013; Lin et al., 2015; Chang and Song, 2016) and strike-slip (Huffman and Saffer, 2016; Chang and Song, 2016) faulting regimes. Borehole data are clear that shallower stress conditions differ from those affecting deeper strata, but the lack of deep measurements does not allow definite conclusions about the stress field and deformation styles operating at depth, and on the relationship between the shallow and deep settings of the NAP. Furthermore, strike-slip is an important deformation style within the NAP that is yet to be characterised in detail.

Against this backdrop, three-dimensional interpretations of stress magnitudes and tensors along the NAP are not unequivocal at some drilling sites. Furthermore, stress field studies have not been performed in the outer wedge of the NAP due to the lack of borehole data in this region, and at higher depths

within the inner wedge (below the sediment cover of the Kumano Basin). This means that extrapolations based on few localised wells in the MSFZ, and inner wedge are not fully reliable.

2.5.4 Tectono-stratigraphy

Most of the lithologic information acquired in the NAP derives from core and well-log data gathered by the NanTroSeize Project. IODP Sites C0018A and C0006 (Figure 2.1), which are respectively located seaward of the MSFZ (in the outer wedge of the NAP) and in the Frontal Thrust Zone, provide valuable lithologic and stratigraphic information on the shallow sedimentary cover, uppermost part of the accretionary prism, and underthrusted sediments from the PSP. Multiple IODP campaigns reached strata within the outer wedge of the NAP and collected stratigraphic evidence to show that the study area is mainly composed of a relatively thin Unit I (Expedition 315 Scientists, 2009; Expedition 316 Scientists, 2009; Kimura et al., 2011; Strasser et al., 2014). Slope sediments were accumulated above an angular unconformity separating them from an underlying Unit II, this latter comprising strata belonging to the upper part of the accretionary prism (Kimura et al., 2011) (Figure 2.6D). In addition, cores collected at IODP Site C0006 drilled through a deep Unit III composed of underthrust deep-marine sediment from the subducting Shikoku Basin.

Unit I can be up to 2.4 Ma old and comprises slope-apron fine-grained turbidite facies spanning the latest Pliocene-Holocene. Data from IODP Sites C0008 and C0018A (Expedition 315 Scientists, 2009; Expedition 316 Scientists, 2009; Expedition 333 Scientists, 2012) divided Unit I into Units Ia, Ib and Ic, which mark a gradual transition from upper-slope apron facies to base of slope apron facies. Unit Ia comprises hemipelagic mud and silty-clay sequences intercalated with multiple ash layers. Unit Ib is composed of hemipelagic mud, silty clay and silty turbidites with ash layers. Finally, Unit Ic reflects sediment deposited above Unit II and it is characterised by turbiditic sand and sandy silt intercalated with mud and ash layers (Expedition 315 Scientists, 2009; Kimura et al., 2011; Alves et al., 2013; Strasser et al., 2014).

IODP Sites C0006, C0008 and C0018 (Expedition 315 Scientists, 2009; Expedition 316 Scientists, 2009) define Unit II as reflecting the uppermost part of the accretionary prism. This unit is of Pliocene age or older (Expedition 315 Scientists, 2009; Expedition 316 Scientists, 2009; Alves et al., 2013). It comprises accreted sediments with mudstone- to sand-dominated lithologies (Expedition 315 Scientists, 2009; Kimura et al., 2011; Alves et al., 2013; Strasser et al., 2014).

Unit III was identified below Unit II in the Frontal Thrust Zone, at IODP Sites C0006 and C0007 (Expedition 316 Scientists, 2009) and comprises hemipelagic mud interbedded with volcanic ash and tuffs. Unit III is deformed by

thrust faults and transitions at depth into Unit IV, which represents underthrusted Shikoku Basin sediment (Expedition 316 Scientists, 2009).

In the inner wedge of the NAP, the presence of an overlying forearc basin (Kumano Basin), and underlying thrust-and-fold accretionary prism, agrees with the stratigraphic units defined by IODP Expeditions 315 and 316. However, slope sediments are relatively thin and discontinuous in the outer wedge of the NAP, having been removed by erosion at places (Van Tuyl et al., 2015). This means that Unit I may not exist in most of the outer wedge. Furthermore, it is difficult to characterise the strata inside the outer wedge of the NAP due to the lack of borehole data crossing the complex, folded sequences that form this same accretionary prism. In the study area, 3D seismic data show that the accretionary prism should be divided in several tectono-stratigraphic units instead of being classified as Unit II and Unit III (Figure 2.6B).

As this thesis focus on the structural interpretation of the outer wedge of the NAP, published information on Unit I is used (due to the extensive core/log data acquired in this latter) to propose an adaptation of the tectono-stratigraphic division of the outer wedge of the NAP from Park et al. (2010) (Figure 2.6):

- **Unit I:** this uppermost unit comprises slope sediment overlying the NAP. Strata is up to 2.45 Ma old and composed of slope-apron fine-grained turbidites accumulated in a slope apron (Expedition 315 Scientists, 2009; Expedition 316 Scientists, 2009; Expedition 333 Scientists, 2012; Lackey et al., 2020).

- **Unit A:** comprises the uppermost internal part of the over-thrusting accretionary prism that includes Unit II. Unit A is formed by turbiditic sand and sandy silt intercalated with Pliocene (or older) mud and ash layers (Expedition 315 Scientists, 2009; Kimura et al., 2011; Alves et al., 2013; Strasser et al.,2014; Expedition 358 Scientists, 2019).
- **Unit B**: also known as the low velocity zone (LVZ), a fluid-rich and high pore pressure zone at the upper portion of the underthrust sediment, composed of mud intercalated with ash and tuff (Bangs et al., 2009, Park et al., 2010; Kamei et al., 2012; Akuhara et al., 2020).
- **Unit C:** the deepest unit of the outer wedge of the NAP comprises the material underthrusting the accretionary prism and is, therefore, of similar composition to Unit B. This unit is separated from the overlying Unit B by a high-amplitude seismic reflector - the décollement. Unit C comprises strata between the basal décollement at the top and the subducted oceanic crust at the bottom (Bangs et al., 2009, Park et al., 2010; Kamei et al., 2012). Park et al. (2010), Unit C is crucial for the NAP to maintain critical taper, where its geometry allows the seaward growth of Unit A to produce the LVZ and associated Unit B. In contrast, Kamei et al. (2012) propose a thicker LVZ that includes both Units B and C from Park et al. (2010), with a décollement on top of Unit C.

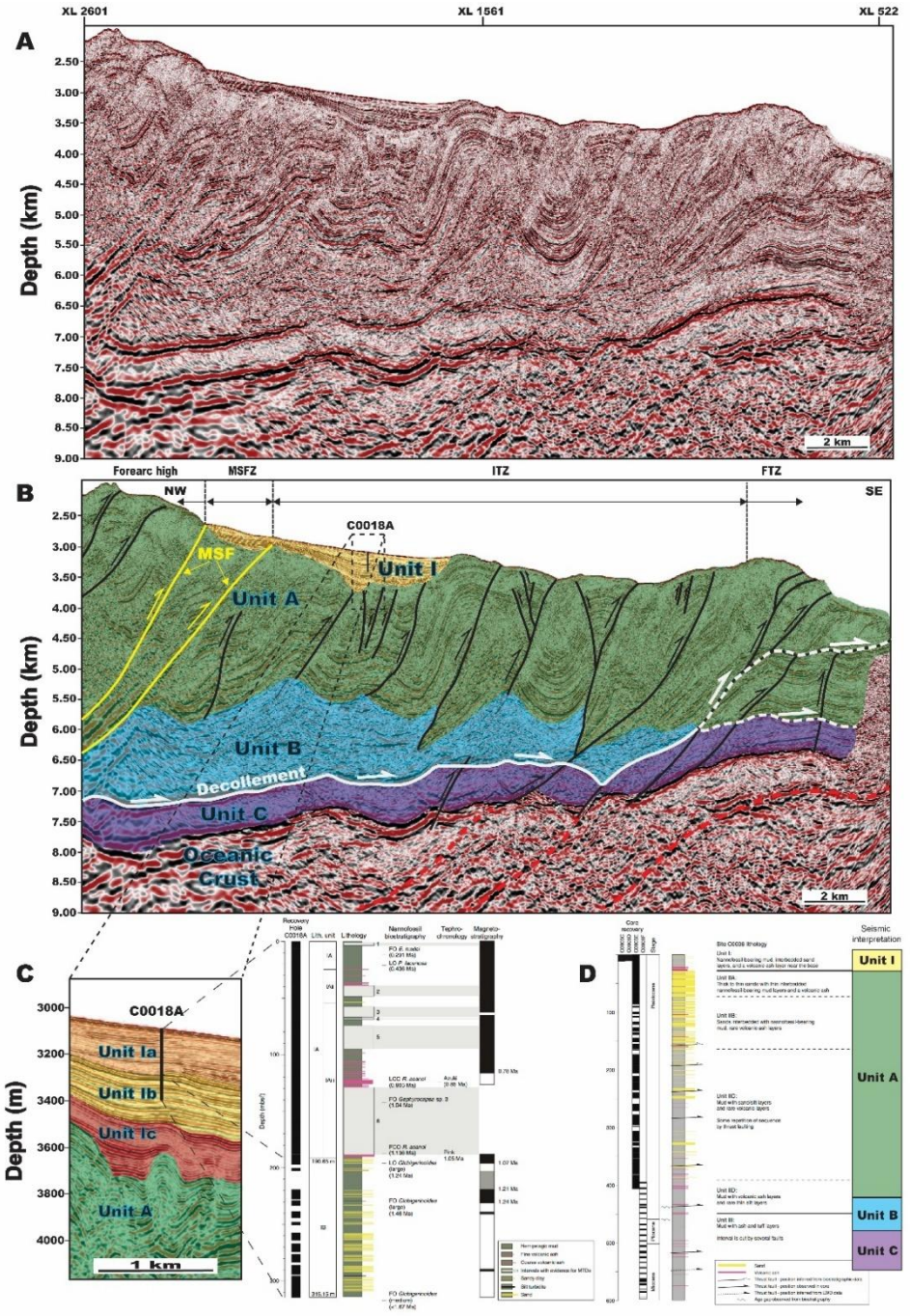

Figure 2.6 – Illustration from Azevedo et al. (2018). A & B) Depth-migrated seismic profile (Inline 2315) across the thrust-and-fold framework (black lines – major thrust and back-thrust faults; arrows – vergence of anticlines and thrusting) of the NAP showing the interpreted (coloured and shaded) tectono-stratigraphic units and the location of IODP well C0018A. Unit I (yellow) is slope sediment cover (Expedition 315 Scientists 2009; Kimura et al., 2011; Alves et al., 2013; Strasser et al., 2014) and Units A1 (green), A2 (blue), B (purple) and C (colourless) are adapted from the Park et al. (2010) and the equivalent of Unit II described by the previous authors. C) Close-up of well C0018A with subdivision of Unit I in Units Ia, Ib and Ic based on the well logging from Strasser et al. (2014). D) Compiled well log of site C0001 from Expedition 315 Scientists (2009) with correlation to our interpreted units.

The seismic data used in this thesis show clear evidence for two units of low reflectivity separated by a strong seismic reflection (décollement), strengthening the idea that Units B and C represent similar lithologies, i.e. Unit B originating from the underthrusting or underplating of Unit C (Bangs et al., 2009; Park et al., 2010; Kamei et al., 2012). Bangs et al. (2009) discussed the possibility of the décollement being initially at the top of the LZV (Unit B), changing later to its present-day position. Such a character suggests a similar lithology across Units B and C, but with both units reflecting distinct tectonic and rheological behaviours.

2.5.5 Décollement

The basal décollement delineates the boundary between tectono-stratigraphic units B and C and comprises homogeneous Lower Shikoku Basin facies, i.e., hemipelagic clay-rich sediments with an approximate age of 7.0 Ma (Moore et al., 2001; Morgan and Karig, 1995). The latter authors observed a lack of well-developed shear fabrics and expressive penetrative mineral alignments in borehole cores, usually expected in a décollement zone, and suggest that the décollement of the NAP is probably formed as a sub-horizontal tension fracture induced by locally high pore-fluid pressures. These conditions can effectively decouple the tectonic stress in the overlying accreting material from the subducting sediments (Morgan and Karig, 1995).

Differences in the frictional strength of the plate has led to the interpretation that the basal décollement is formed as a mechanical boundary, rather than a diagenetic one. Strata below the décollement is recognised as being stronger than the sediments in the overlying NAP, where there is a mixture of ductile and fragile deformation (Le Pichon and Henry, 1992; Morgan and Ask, 2004; Hamada et al., 2018). Contrasts in the strength of the rocks below and above the décollement are responsible for promoting slip along this surface/zone and for driving tectonic deformation upwards into the NAP, further strengthening the strata below the décollement. Evidence also suggests that the décollement preferably incorporates deformed strata from the overlying NAP, rather than undeformed strata from below, contributing to the landward growth of Unit B in the NAP.

Rowe et al. (2012) argued that the progressive landward increase in loading from the overlying sediments of the NAP, and subsequent increase in friction, are responsible for raising pore pressures. This leads to a décollement driven by pure shear slip, as well as its down-stepping and underplating, especially in the transition between the ITZ and the MSFZ. Micro-structural analyses of core samples show that décollement propagation is driven by the coexistence of tectonic compaction and brittle fracturing, where fracture porosity amounts between 1.8% and 8.5%. This could have a significant effect on the permeability of the décollement, thus affecting the distribution of pore pressure, seismic slip, décollement propagation and ultimately, tectonic deformation in the NAP (Bourlange et al., 2003).

2.5.6 Shikoku Basin

The subducting oceanic crust is overlain by a wider range of lithologies, including aeolian dust from Asia and volcanic ash from the Japanese volcanic arc, both transported by wind, as well as erosional material and ash from subaquatic eruptions, transported by water currents (Scudder et al., 2018). These sources of sediment feed the Shikoku Basin, east of the NAP, which is essentially composed of six units (Figure 2.7): (1) Unit I with ash-rich, fine-grained hemipelagic-pyroclastic material; (2) Unit II marked by the abrupt appearance of volcano-clastic and tuffaceous sandstone turbidites interbedded with dark grey clayey siltstone; (3) Unit III composed of bioturbated hemipelagic claystone; (4) Unit IV with bioturbated mudstone interbedded with siltstone and fine-grained sandstone; (5) Unit V with tuffaceous sandy mudstone and sandstone; and (6) Unit VI with thin pelagic claystone facies (Expedition 333 Scientists, 2012; Scudder et al., 2018).

Kobayashi and Nakada (1978) and Kobayashi (1984) describe the Shikoku Basin as a N-S back arc basin situated in the northern part of the Philippine Sea Plate, bordered by the KPR, to the West, the SIR, to the East, the Nankai Trough, to the North, and the Parece Vela Basin (another back arc basin) to the South. According to the same authors, the evolution of the Shikoku Basin recorded three different stages: (1) rifting between the KPR and SIR, (2) parallel

spreading of the Shikoku Basin, (3) more irregular opening, formation of seamounts and post-spreading intrusions. Other authors, such as Okino et al. (1995) and Okino et al. (1999) propose five stages for the formation of the Shikoku Basin:

1. Rifting (47.5 – 28 Ma).
2. NNW-SSE opening (30 – 23 Ma).
3. N-S opening (23 - 19 Ma).
4. NW-SE opening (19 – 15 Ma).
5. Volcanism and deformation after opening (amagmatic extension).

Bathymetric and gravimetric data show that the Shikoku basin comprises a clear lineation of NNE-striking structural highs that are parallel to the Kyushu-Palau Ridge (azimuth: 160° - 170°). Some of these highs have a relief of up to 1.5 km. De-spite the non-active horst and graben structures observed in seismic data from Shikoku Basin, it is possible to observe a chain of seamounts in its central area, known as the Kinan and Kinin Seamount Chains (Figure 2.3). This chain of seamounts is believed to have been formed because of the spreading of the Shikoku Basin (Kobayashi and Nakada, 1978; Kobayashi, 1984). The Shichito-Iwojima Ridge comprises en-echelon chains of seamounts resulting from Tertiary and Quaternary volcanism, all striking NE-SW (Okino et al, 1995; Okino et al., 2009).

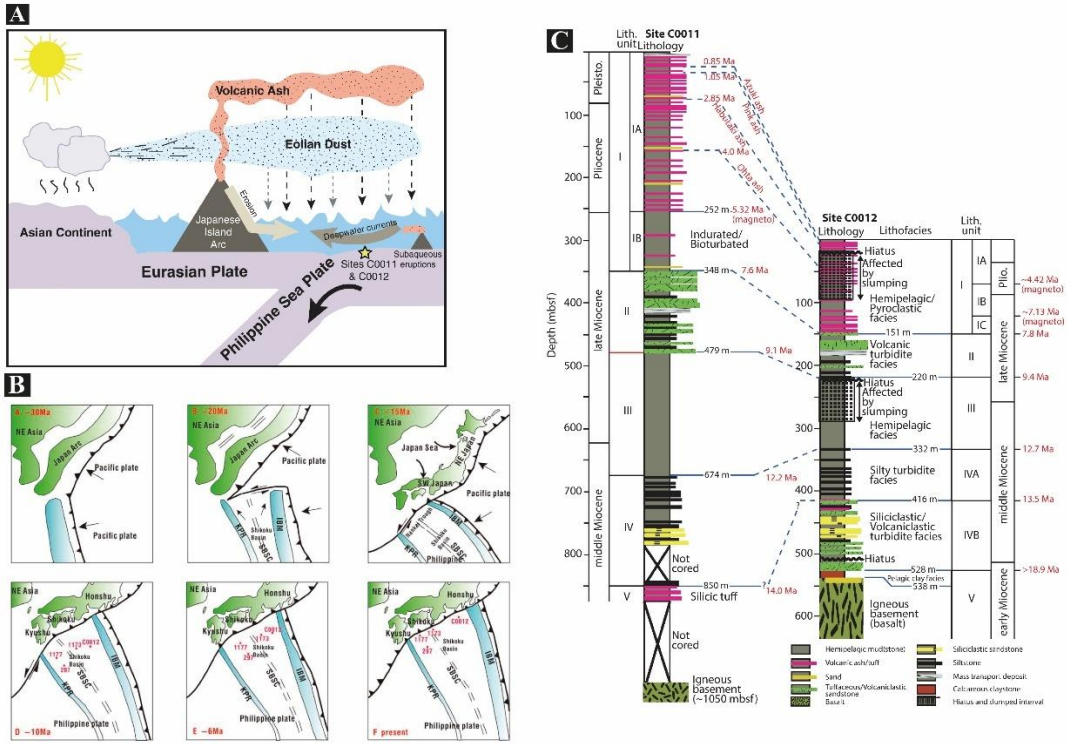

Figure 2.7 – A) Summary diagram of potential transport mechanisms of the sources to the bulk sediment at Sites C0011 and C0012, Nankai Trough from Scrudden et al (2018), indicating four main different: Asian Dust, which is more likely to have been transported by wind rather than by erosion from the nearby terrestrial sources; "Rhyolitic Ash" dispersed ash component is the result of ash that was transported through the atmosphere; "Dacitic Ash" and "intermediate Kyushyu Ash" components do not appear in the measured discrete layers, therefore we interpret that their most recent source is more likely to be erosional with a portion potentially being transported through the atmosphere. B) Schematic map of the opening of the Shikoku Basin from Cheng et al. (2020). C) Lithologic columns for Sites C0011 and C0012 based on results from Expeditions 322 and 333 from Scudder et al. (2018).

Landwards of the study area, the incoming Shikoku Basin contains several scattered bathymetric highs striking NE-SW similar to those observed in the SIR, known as the Kinin seamounts, (Nishizawa et al., 2011; Doo et al., 2014) (Figure 2.3). It is expected that these bathymetric highs are and will eventually subduct at the Nankai Trough, under the Amur Plate.

CHAPTER 3

Data and Methods

3.1 Introduction

This thesis mainly uses the section of the Kumano Transect 3D seismic volume that covers the outer wedge of the NAP, which is stored in Cardiff University and being used by the Seismic Lab for research purposes. This 3D seismic volume set covers an area ca. 12 km × 56 km, extending from the Kumano Basin, at landward limit, to the frontal thrust, at seaward limit. It extends along strike ca. 4 km northeast and ca. 8 km southwest of the NanTroSEIZE drilling transect (Figure 2.1). The inline seismic profiles correspond to the long axis of the survey which is oriented at 330.1° while the crossline seismic profiles are parallel to the short axis, at 60.1° (Moore et al., 2009). The 3D seismic volume provides a high-resolution imaging of the internal structural of the NAP that provided the basis of the structural interpretation and analysis presented throughout this thesis.

This chapter provides an overview of the process of seismic acquisition, processing, and interpretation as well as any additional technical details relevant to the structural interpretation done throughout this thesis. Chapters 4, 5 and 6 will include an additional section on specific methodologies which will entail relevant information on the specific methods and data used in each of these specific chapters.

3.2 Seismic data

Although the 3D seismic data acquisition is mainly motivated by oil and gas exploration, seismic data applications in the academic research have been widely expanded and proved to be an invaluable source of information to study and understand subsurface structures. Seismic data was initially applied in rift basins and continental margins. However, seismic data is increasingly being used in a wider variety of geological settings with complex geological structures, including convergent margins and their accretionary prisms (Alei, 2012).

According to Cartwright and Huuse (2005), the application of 3D seismic interpretation is immense, especially for description and analysis of fault system geometry and kinematics. The advancement from 2D to 3D seismic data allowed a higher resolution in terms of being able to visualise greater geometrical complexity.

The next three sub-chapters will summarise the seismic acquisition, processing and resolution of the seismic data used in the thesis as described by Moore et al. (2009)

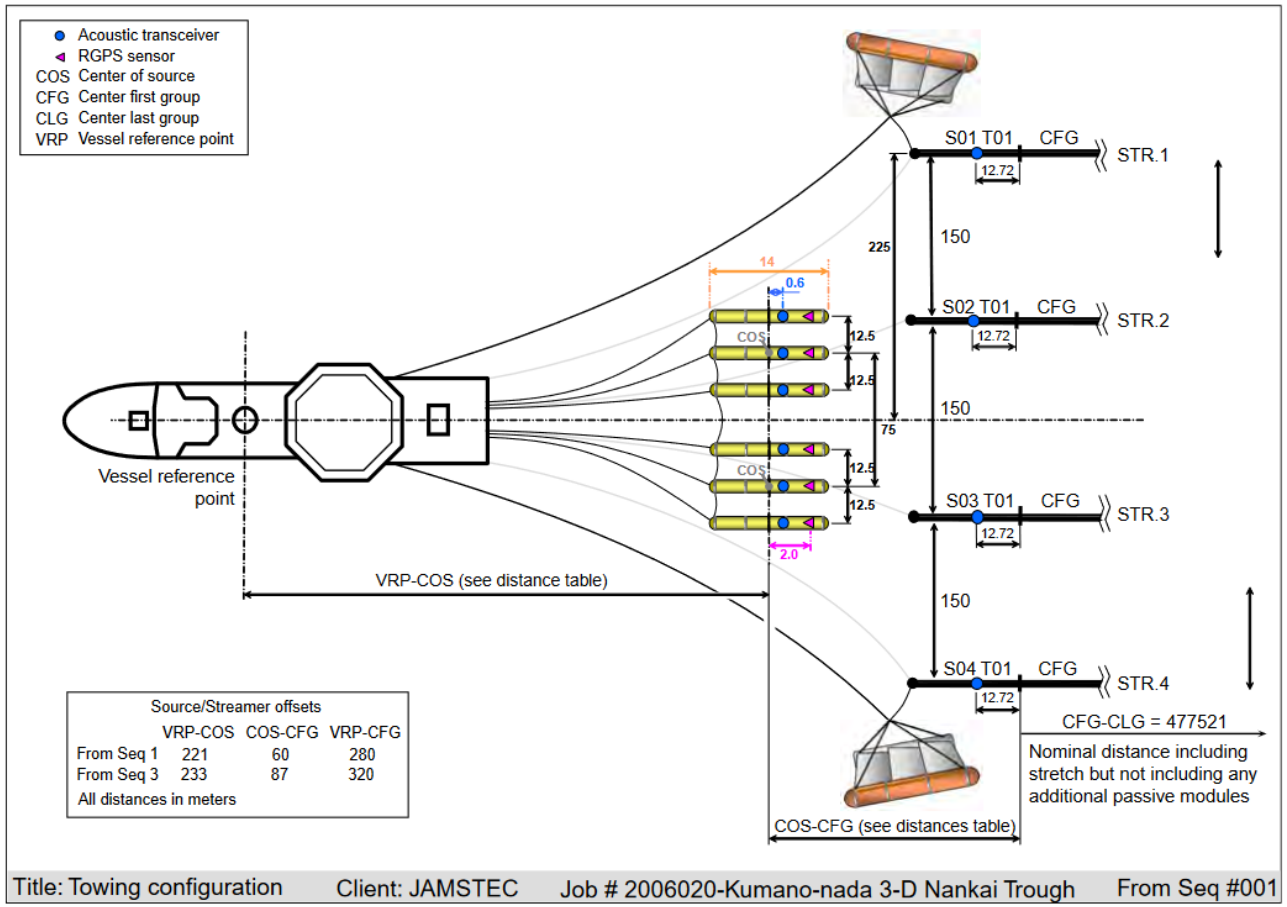

Figure 3.1 - Acquisition geometry for Kumano 3-D seismic survey from Moore et al. (2009). STR = streamer.

3.2.1 Seismic acquisition

The 3D seismic volume of the Kumano Transect (Figure 2.1) was surveyed by Petroleum Geo-Services with the M/V Nordic Explorer from April 2006 to May 2006. Two arrays of 28 Sodera G-guns totalling 51 L (3090 in^3) each were fired alternately at 37.5 m shot intervals to generate the sound. Four 4500m long receiver cables spaced 150m apart were used with 360 receiver groups spaced 12.5m apart. This 4-streamer/2-source array geometry yielded 8 source-receiver common midpoint lines per sail line at a spacing of 37.5 m and nominal 30-fold data. Additionally, the M/V Nordic Explorer and each G-gun array were equipped with GPS received and a Sonardyne SIPS2 acoustic transponder array was used on the G-guns and streamers in order to accurately record the location of each receiver at the end of every shot. The relative accuracy of the shot and receiver is estimated to be ca. 5m (Figure 3.1). The resulting 3D volume covers an area of approximately 62.5 km × 12 km with irregular boundaries around the trench because of difficulties experienced during acquisition due to the high-speed Kuroshio current. As both the current's direction and intensity were inconsistent, the feather angle of the streamers varied accordingly, making it impossible to perfectly match the offsets on adjacent passes, meaning that most of the common midpoint lines did not reach the trench axis, which explain the not uniform southern boundary of the Kumano Transect 3D seismic volume (Moore et al., 2009).

3.2.2 Seismic processing

Similarly to other seismic acquisitions, the raw seismic data of the Kumano Transect was just not suitable for interpretation as artefacts and noise interference will hide and overlap subsurface features (Bacon et al., 2007). Therefore, the Kumano Transect 3D seismic volume was processed so that it could be used for interpretation. The processing of the seismic data was comprised of three stages (Moore et al., 2009):

- **Stage 1:** 3D stack and post-stack migration processed by Petroleum Geo-Services for quick check on 3D data volume and on regional seismic reflection characteristics that served as baseline for the parameters chosen on later stage of seismic processing.
- **Stage 2:** 3D pre-stack time migration (PSTM) processed by Compagnie Générale de Géophysique. Due to the variable streamer feathering, several processing steps were necessary to fill all the bins.
- **Stage 3:** 3D pre-stack depth migration (PSDM) processed at Japan Agency for Marine Earth Science and Technology and Institute for Research on Earth Evolution. Data processing included pre-stack multiple removal and data conditioning (e.g., amplitude recovery, time-variant filtering, and predictive deconvolution). The final 3D PSDM clearly images details of faults and small-scale structures that were not easily recognized in the previously processed data set (Figure 3.2).

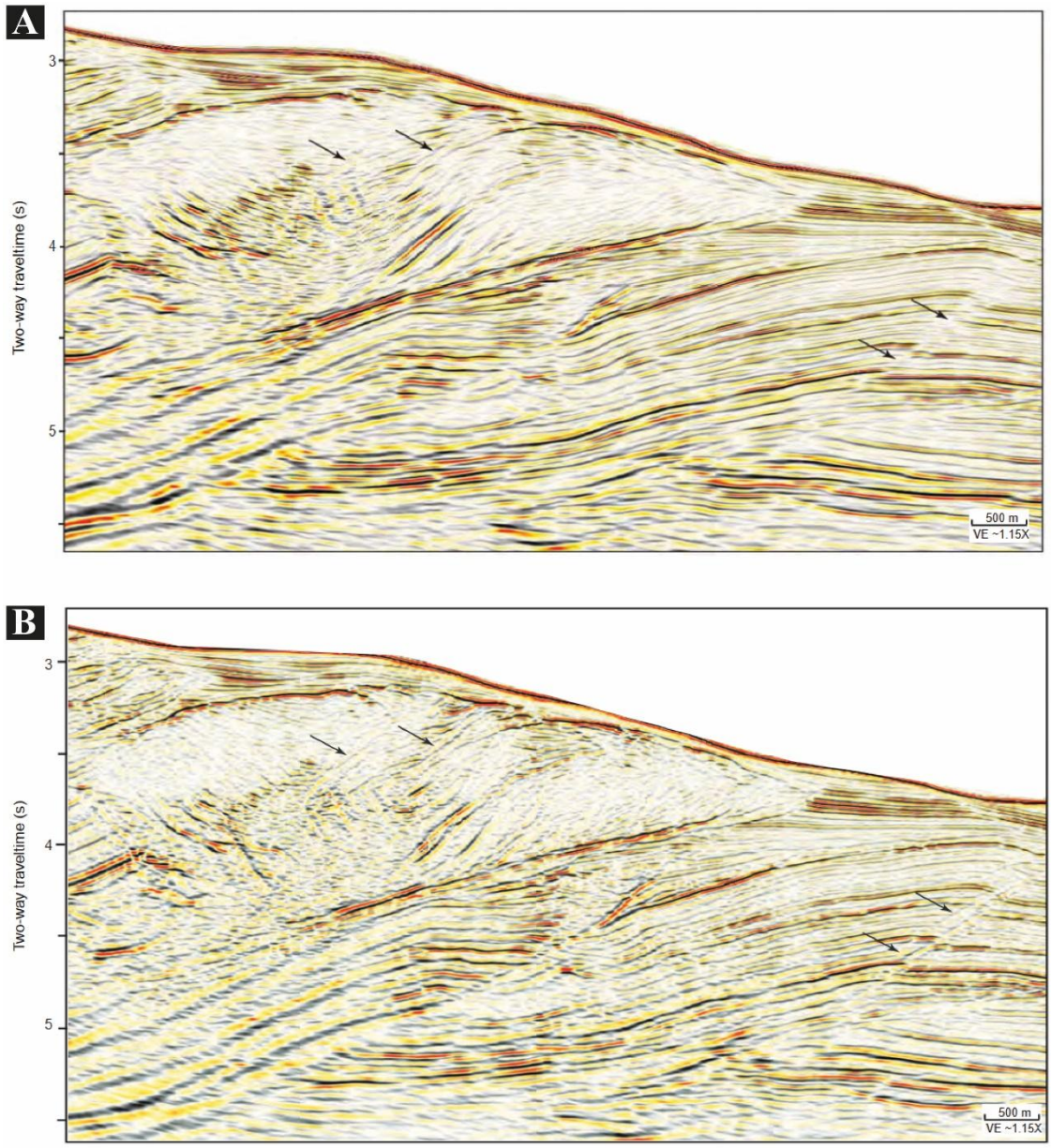

Figure 3.2 – Comparison of 3D seismic Inline 2675 from Moore et al. (2009). A) Pre-stack time migrated seismic. B) Pre-stack depth migrated converted to time for comparison purposes. Arrows = specific examples of reflections that are clarified in the depth migration

However, due to the length of the streamers (4500 m) and the strong feathering, velocity resolution deeper than ca. 4500–5000 m becomes less accurate. Therefore, although imaging of the deeper section (i.e., the top of oceanic crust) is quite good, the deeper landward parts of the NAP are less accurate than in the shallower seawards region.

3.2.3 Seismic resolution

According to Bacon et al. (2007), both vertical and horizontal resolutions are limiting factors on the recognition of the subsurface geological features. Vertical resolution is mainly affected by the seismic source signal and how it is filtered by the earth, while horizontal resolution is affected by several factors, with migration processing being amongst the most impactful.

The seismic resolution reduces with depth because of the increase in seismic velocity with depth due to mechanical and chemical compaction and decrease in frequency due to higher frequencies attenuating more significantly than lower ones (Faleide et al, 2021). Therefore, resolution of high-quality 3D seismic tends to be defined in terms of the wavelength of the data. The limit of resolution is one quarter of the wavelength (λ/4), which can be expressed as a function of velocity and frequency as V/4f, where λ = wavelength, V = velocity, and f = frequency (Bacon et al., 2007).

Moore et al., (2009) used the expression above to estimate the resolution limitations of the Kumano Transect 3D seismic:

1. **For the near-surface sediments:** P-wave velocity is generally <1600–1800 m/s and frequency content is ~60–80 Hz, so λ/4 = (1600–1900 m/s)/4 × (80–60 Hz) which resolves to ~5–7 m.
2. **At our maximum drilling depths of ~1400 m:** velocities are ~2400 m/s and frequencies are ~40 Hz, thus λ/4 = (2000–2400 m/s)/4 × (50–30 Hz), resolving into ~10–20 m.
3. **For the deepest regions imaged by our data set:** velocities increase to >4000 m/s and frequency decreases to ~8 Hz, where λ/4 = (3600-4000 m/s)/4 × (10–8 Hz) and a resolution of ~90–125 m for the oceanic crust region.

Seismic resolution can reach <5 m at the depth of the shallower faults, for a range of 6–10 m in the deeper strata based on the dominant wavelength of ~24 m observed on synthetic logs and seismic profiles. The main limitation of this method results from the fact that it is only possible to observe, map and interpret structures that are within this latter range in seismic resolution.

3.3 Seismic interpretation

Seismic interpretation constitutes a considerable part of the thesis, which has been done with using the software Schlumberger's Petrel® in the 3D Seismic Lab, at Cardiff University.

3.3.1 Horizon and fault mapping

According to Cartwright and Huuse (2005), 3D high-quality resolution also opens opportunities to define fault networks with greater accuracy and therefore perform structural analysis of fault systems beyond traditional out-crop-based methods.

As mapping structural features was one of the main priorities of this thesis, especially in areas of higher structural complexity, the auto-tracking feature from Schlumberger's Petrel® was not used while interpreting seismic data along 2D seismic profiles. Instead, manual picking of seismic reflections was used by tracking similar seismic amplitudes as this presented to be the most accurate procedure to map seismic horizons. The manual picking was done along seismic inline profiles, every 10, and complemented with seismic crossline profiles, every 20. In areas of structural complexity, the spacing was reduced to 1 for inline seismic profiles and 5 for crossline seismic profiles. Consequently, a grid of inline

and crossline seismic profiles is created that will then allow the use of Petrel's automated horizon tracking tool to then interpolate the empty areas in between the interpreted inline and crossline seismic profiles. The produced horizon is then analysed for inconsistencies and mismatches in local areas of the study area that have not been initially interpreted. These errors are then corrected by going through several cycles of manual picking until a smooth surface is obtained (Figure 3.3).

Similarly, fault interpretation was carried out by manually picking and mapping displacements observed at seismic resolution along seismic reflectors that are linear, crosscut, and offset packages of seismic reflections. A conservative approach was taken where faults were only fully mapped where offset is observable at seismic resolution (Figure 3.4). Lateral continuation of faults was acquired by mapping the same fault surface every 5 seismic line profiles and every 1 in high complexity areas.

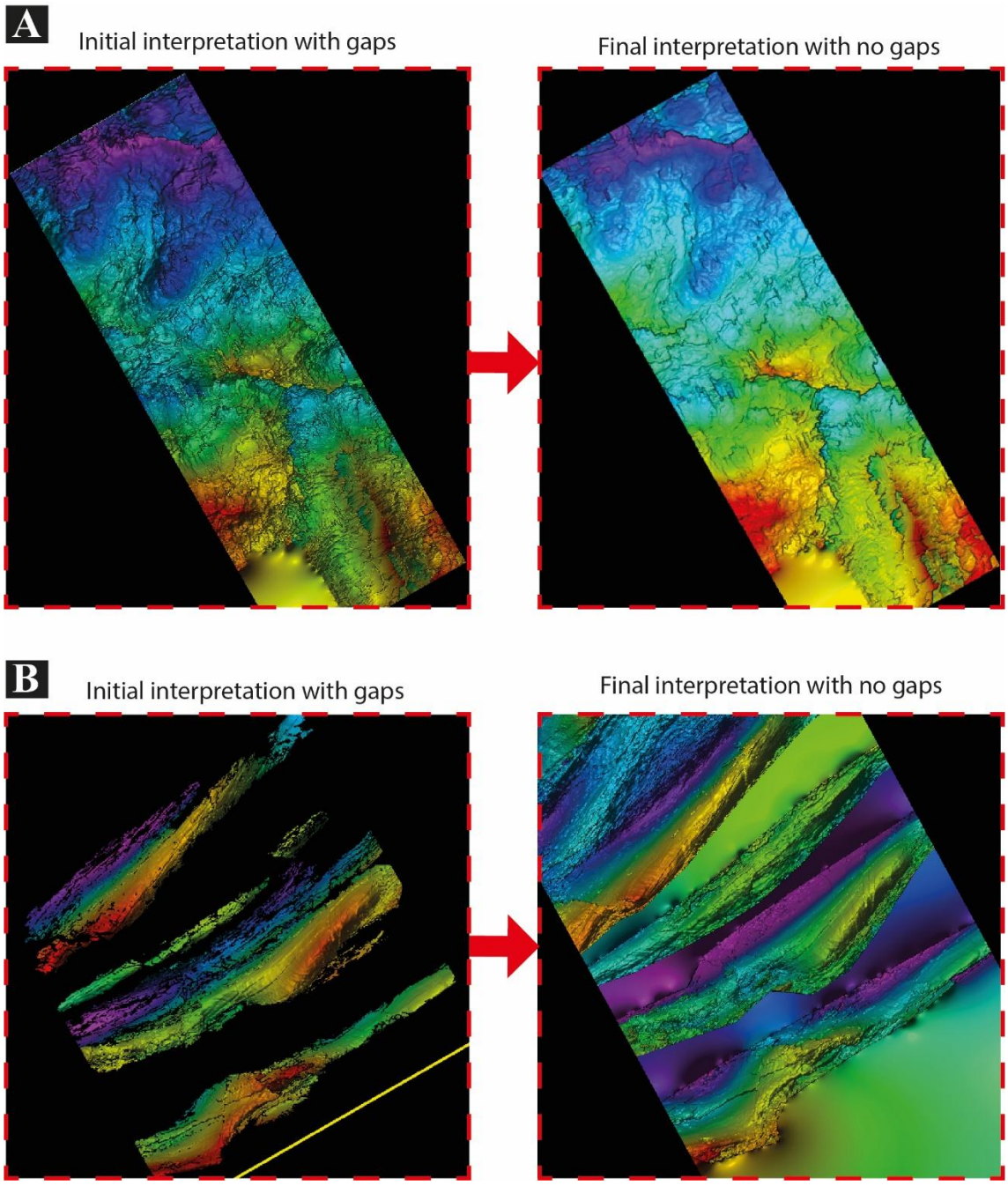

Figure 3.3 – Examples of seismic horizons manually picked and auto-tracked before quality control and after quality control. A) seismic mapping of the décollement used in Chapter 5. B) seismic mapping of the main fold-and-thrust nappes within the morpho-tectonic Unit A of the NAP.

3.3.2 Seismic attributes

According to Roberts (2001) and Chopra and Marfurt (2005, 2007a, 2007b), attribute data such as coherence and maximum curvature have crucial importance to the 3D interpretation of seismic data. Both attributes are particularly helpful in structural analysis, as they enhance faults that are often not recognised on vertical seismic profiles or time-structure maps alone. Volumetric curvature is a property that measures lateral changes in dip-magnitude and dip-azimuth waveforms (Mai et al., 2009). The presence of fractures and small faults is closely related to reflection curvature. In this thesis, maximum curvature is used to visualise small-scale faults and to later obtain measurements of maximum horizontal displacements from them. In addition, coherence comprises a technique of cross-correlating seismic amplitudes in adjacent traces and has a proven record of efficiently portraying faults by measuring lateral changes in waveform (Chopra and Marfurt, 2005; Mai et al., 2009).

These attributes are automatically extracted from specialised seismic interpretation software, such as Schlumberger's Petrel®, but it is necessary to choose a horizontal time- or depth-specific slice that is deep enough to intersect a wide range of well-resolved structures (Figure 3.4).

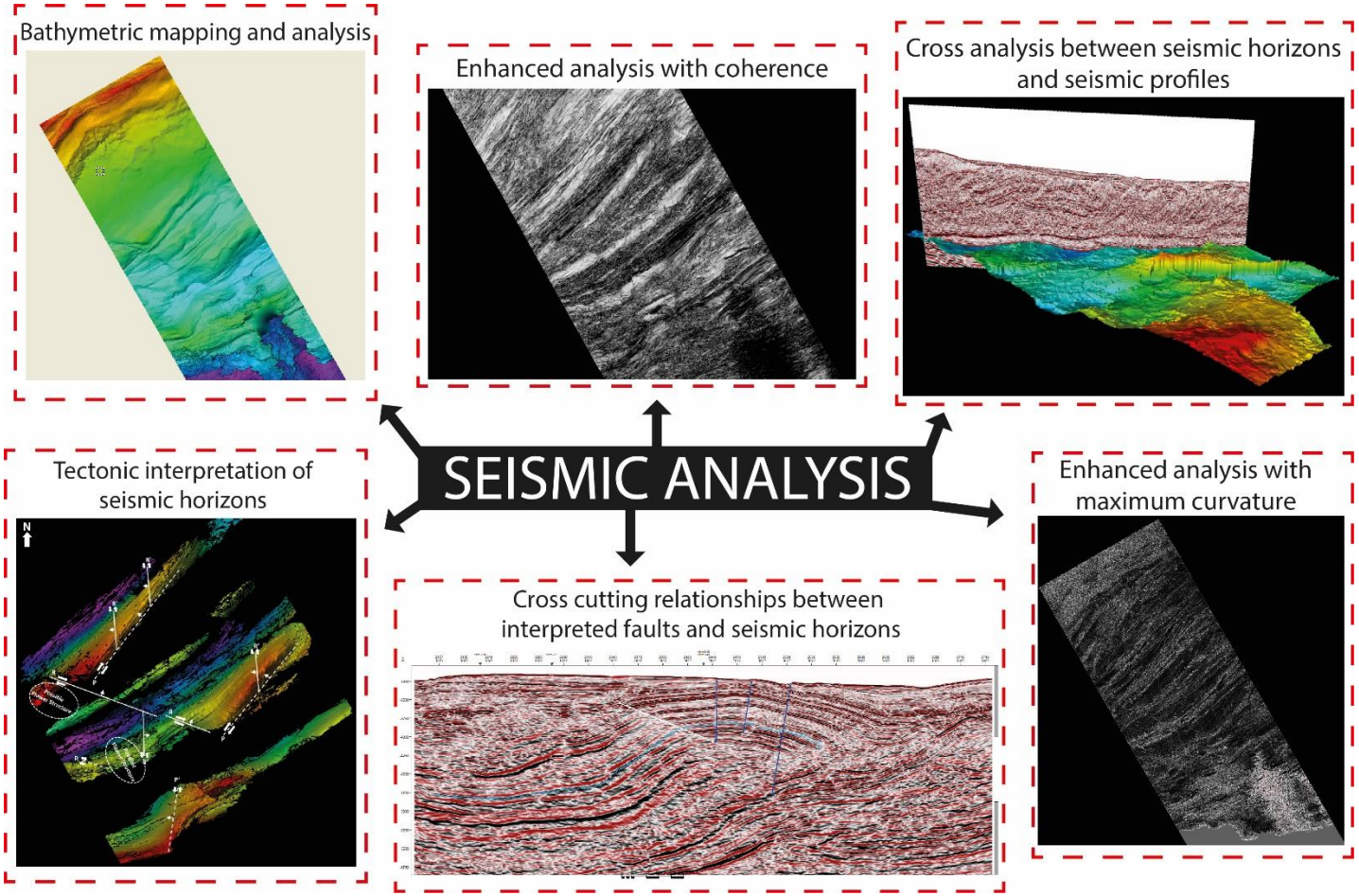

Figure 3.4 – Different methods used for structural and tectonic analysis of the 3D seismic data in this thesis.

CHAPTER 4

Structural features and complex partitioning of strain in the Nankai Accretionary Prism (SE Japan)

An abridged version of this chapter has been published as:

Azevedo, M. C., Alves, T. M., Fonseca, P. E., & Moore, G. F. (2018). Strike-slip deformation reflects complex partitioning of strain in the Nankai Accretionary Prism (SE Japan). Tectonophysics, 723, 81-94.

4.1 Abstract

Previous studies suggest predominant extensional tectonics acting, at present, on the Nankai Accretionary Prism (NAP), and following a parallel direction to the convergence vector between the Philippine Sea and Amur Plates. However, a complex set of thrusts, pop-up structures, thrust anticlines and strike-slip faults is recorded on seismic data of the outer wedge of the NAP, hinting at a complex strain distribution across SE Japan. Three-dimensional (3D) seismic data reveal three main families of faults: (1) NE-trending thrusts and back-thrusts; (2) NNW- to N-trending left-lateral strike-slip faults; and (3) WNW-trending to E-W right-lateral strike-slip faults. Such a fault pattern suggests that lateral slip, together with thrusting, are the two major styles of deformation operating in the outer wedge of the NAP. Both styles of deformation reflect a transpressional tectonic regime in which the maximum horizontal stress is geometrically close to the convergence vector. This chapter reveals evidence in favour of a progressive change from faults trending perpendicularly to the convergence vector, to a broader partitioning of strain in the form of thrusts and conjugated strike-slip faults. Similar families of faults potentially also exist within the inner wedge of the NAP, below the Kumano Basin, and controlled stress accumulation and strain accommodation in this region during its prior accretion phase.

4.2 Introduction

The theoretical interpretation of a predominantly compressional accretionary prism offshore Nankai was developed by Byrne et al. (2009), Moore et al. (2013) and Lin et al. (2015), who also confirmed the existence of a component of extension acting near the sea floor. In fact, extensional tectonics accounts for most of the modern deformation recorded in the forearc basin that overlies the inner wedge of the Nankai Accretionary Prism (NAP). According to Wang and Hu (2006), Byrne et al. (2009) and Lin et al. (2015), this extensional regime is particularly active during interseismic cycles. Nevertheless, Lin et al. (2015) show evidence for compression at Integrated Ocean Drilling Program (IODP) Sites C0004 and C0010, seawards from the Megasplay Fault Zone (MSFZ), with a σ_1 parallel to the convergence vector. Alternative interpretations consider stress decoupling between a shallow regime of normal faulting and a deeper regime of strike-slip faulting and thrusting in both the inner and outer wedges of the NAP (Moore et al., 2013; Van Tuyl et al., 2015).

Previous reference to strike-slip faulting and flower structures in the outer wedge of the northeast NAP (Zenisu area) was made by Le Pichon et al. (1992; 1996). In the Nankai Trough region, flower structures and associated strike-slip faults were identified by Takahashi et al. (2002). In parallel, micro seismicity studies documented the rupture of a major NW-trending, right-lateral strike-slip fault crossing the outer wedge of the NAP during the aftershocks of the 2004

earthquake off the Kii Peninsula (M = 7.4) (Obana et al., 2005). Obana et al. (2005) proved the existence of several N- to NE-trending strike-slip fault systems operating within the Shikoku Basin. Similar strike-slip faults in the seawards part of the MSFZ, and outer wedge of NAP, have been interpreted as inherited structures from the subducted crust (Shikoku Basin) (Kodaira et al., 2006). Moore et al. (2013, 2015) focused on the Kumano Basin, which overlies the inner wedge of the NAP, to interpret two major WNW-trending strike-slip faults offsetting both the outer wedge of the NAP and its MSFZ. Furthermore, most of recent research has been focused on the landward (Kumano Basin) and most seaward (Frontal Thrust Zone) parts of the NAP, where in-situ stresses measured at several IODP Sites have demonstrated that extension predominates at present (Lin et al., 2015).

To understand the structural evolution of the outer wedge of the NAP and, ultimately, of the NAP itself, it is necessary to assess: (1) where and how tectonic stresses accumulate in the prism, and (2) how shallow and deep structures relate across distinct sub-surface units. Strike-slip faulting that is not associated with the MSFZ, and within the outer wedge of the NAP, has been mentioned but never fully characterised or studied, resulting in a relative under representation of such tectonic regime in published literature. The outer wedge is the zone most actively deforming in accretionary prisms, and where the response to tectonic stresses is better expressed (MacKay et al., 1992; Park et al., 1999). Several questions remain to be addressed, some of which will have a

large impact on the present understanding of the tectono-stratigraphic evolution of the NAP. Hence, the key aims of this chapter are:

1. To describe the structural framework of the outer wedge of the NAP.
2. To investigate the tectonic regime operating in the outer wedge of the NAP, as well as its related stress field(s), based on structural analysis of the 3D PSDM seismic data.
3. To compare and discuss our interpretations with published information on the inner wedge of the NAP and older accretionary prisms.

4.3 Chapter-specific methodology

Interpreted faults, following the methodology delineated in Chapter 3.3, are here classified based on their strikes as there is a direct relationship between their geometry and the observed deformation styles in the outer wedge of the NAP.

Strike measurements are automatically undertaken by the seismic interpretation software, Schlumberger's Petrel®, after faults are mapped. For curved faults and fractures one measurement is taken as the average strike, which coincides with the best fitting straight line to the curve. Taking into consideration that several authors agree with the interpretation of distinct deformation regimes at shallow and deep levels of the NAP (e.g. Lin et al., 2015; Van Tuyl et

al., 2015; Chang and Song, 2016), a classification based on the length of imaged faults, and their depth, can also be used. However, such a classification will bear no relation to either the geometry or the deformation styles of such structures, as the boundary between shallow and deep structures occurs at a variable depth.

Van Tuyl et al. (2015) explained that the depth of the Extensional-Compressional Decoupling (ECD) surface in the study area is markedly variable, being shallower in the outer wedge than in the inner wedge and clearly related to the thickness of overlying slope sediment (Unit I) and tectonic uplift caused by adjacent active faults. Therefore, to classify the different families of faults in terms of length and depth they reach, focus was given to those structures affecting Units A to C and classified as:

- **Shallow structures**: those affecting the uppermost Unit A and Unit B of the NAP.
- **Deep structures**: those propagating from the décollement, intersecting the décollement, or offsetting Unit C and/or the subducting oceanic crust.

Seismic attribute mapping, such as coherence and maximum curvature, provided the basis for statistical analysis of geometry, kinematics, and dynamics of the main faults in this chapter (Figures 3.4 and 4.1). The depth of 3840m was chosen for both seismic attributes map as it presents the best compromise between seismic resolution and representation of structures impacting the NAP.

The strikes, dip azimuths and dips of faults were measured prior to the estimate of stress and/or paleo stress fields as well as coefficients and angle of internal friction from Andersonian analysis and dihedral angles, using Stereonet 11® (Hancock, 1985; Fossen, 2016). This estimation provided the basis for our structural analysis, allowing the 3D mapping of small- and large- scale faults and fractures, and detailed descriptions of their geometry, kinematics, and dynamics. The approach includes the quantitative characterisation of the strike of faults and their throws and horizontal (strike-slip) displacements, together with quantitative analysis of fault dips.

4.4 Structural analysis

The Imbricated Thrust Zone (ITZ) and the Frontal Thrust Zone (FTZ) chiefly comprise NE-striking thrusts formed by horizontal shortening, dipping to the NW (in-sequence) or SE (out-of-sequence and back thrusts) (see Moore et al., 2001; Gulick et al., 2004; Strasser et al., 2011). Nevertheless, seismic attribute maps coupled with 3D seismic analysis reveal the existence of at least three sets of faults with varied geometry (Figure 4.1 and 4.2): NE-trending, WNW-trending and NNW-trending. Other more local structures have also been identified and will presented and discussed in separate later sub-sections.

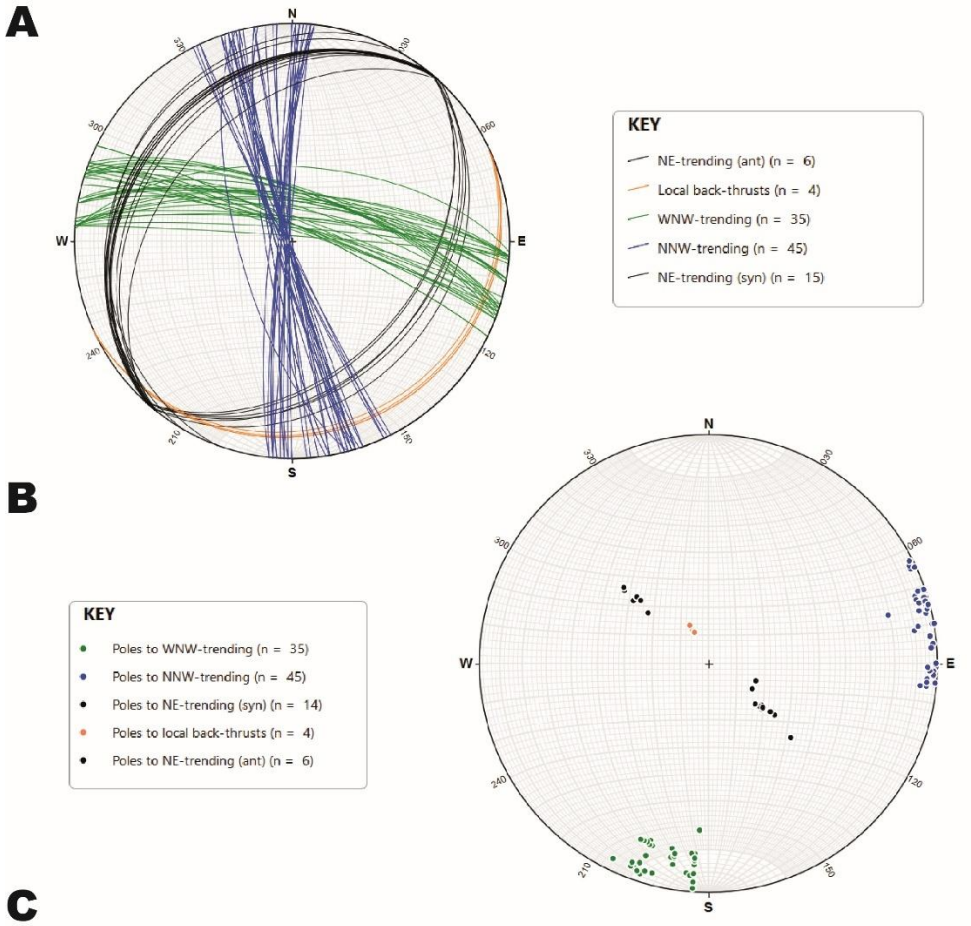

Fault Type	Range of azimuth	Average azimuth	Range of dip	Average dip	Comparison with published data (azimuth / dip)
NE-trending	290–312°	**307.8±5.7**	18–40°	**24.6±5.3**	290–320° / 15–45° (thrust) Bangs et al. (2009), Strasser et al. (2009)
WNW-trending	3–26°	**12.9±7.1**	62–88°	**77.5±6.1**	5–30° / 70–90° (strike-slip) Seno et al. (1993), Kobayashi et al. (2011)
NNW-trending	243–276°	**260.8±9.9**	70–90°	**86.4±3.4**	240–280° / 80–90° (strike-slip) Park et al. (2002), Tsuji et al. (2014)
Back thrusts	154–156°	**155.2±0.8**	12–15°	**13±1.2**	150–160° / 10–20° Kimura et al. (2007), Moore et al. (2009)

Figure 4.1 - A & B) Lower hemisphere Schmidt Stereonet projections of fault planes (A) and poles (B) identified and mapped from coherence and maximum curvature seismic attribute map (Figure 4.2). Data suggest three distinct geometries: NE-, WNW- and NNW-trending. A local cluster of seawards verging thrusts (here referred to as back-thrusts) have also been recognised and are here presented for later discussion in this and later chapters. C) Summary table presenting the range and average of dip azimuth and dip for each family of faults identified and comparison with other similar geometrical trends identified in literature referring to the Nankai Trough.

Structures of similar geometries have been previously identified (see Figure 4.1C), in particular two major NW-trending faults by Moore et al. (2013) as displacing surface ridges within the ITZ and are here also identified as major faults F1 and F6 (Figure 4.2).

4.4.1 NE-trending faults (shallow and deep)

Main structures within the NAP comprise curved NE-trending (azimuth: 40° to 70°) thrusts and back thrusts dipping towards the NW and SE, respectively (Moore et al., 2001; Bangs et al. 2009; Strasser et al., 2009) (Figures 2.6A–B, 4.1, 4.2, 4.3 and 4.4). Thrust faults are clearly associated with the formation of SE-verging anticlines with bathymetric expression on the sea floor (Figures 2.6A–B, 4.2, 4.3, 4.3 and 4.5). Other interesting but less common features have also been observed on either the 3D seismic or the coherence and maximum curvature attributes that could prove useful for the discussion:

1. only a small number of antithetic thrusts have been observed but they tend to be more commonly found towards the NE end of larger anticlines.
2. possible horse-tail splay terminations of thrusts occurring at their NE tips (Figures 4.2A–B, 4.3 and 4.5).
3. slight vergence of hanging-wall anticlines towards the NE (Figure 4.5).

Most of the shallow and shorter NE-trending thrusts are clearly early tectonic structures, as they are intersected by or offset by other faults with different trends (Figure 4.3). Yet, the deep and large-scale thrusts do not seem to be affected by the same structures (Figure 4.3 and 4.5). Whether the deep thrusts are older structures displaced by younger faults with different trends, or these younger faults propagate from deeper thrusts, is a crucial discussion topic as it is not possible to ascertain clear cross-cutting relationships among all interpreted structures, mainly due to lack of seismic resolution (see Chapter 3.2.2). Either way, the observed geometries may suggest that faults are diachronous; the larger, deeper thrusts moved before and after the time of formation of the remaining faults with different trends.

The deep thrust faults root in (or start from) the décollement, usually at a depth between 6.5 and 8 km, only intersecting the NAP in its the frontal part (Figure 2.6A–B). In addition, the deep thrusts usually show synthetic motion and with no recognisable antithetic thrusts (Figures 2.6A–B, 4.3 and 4.5) as they follow the vergence of the décollement.

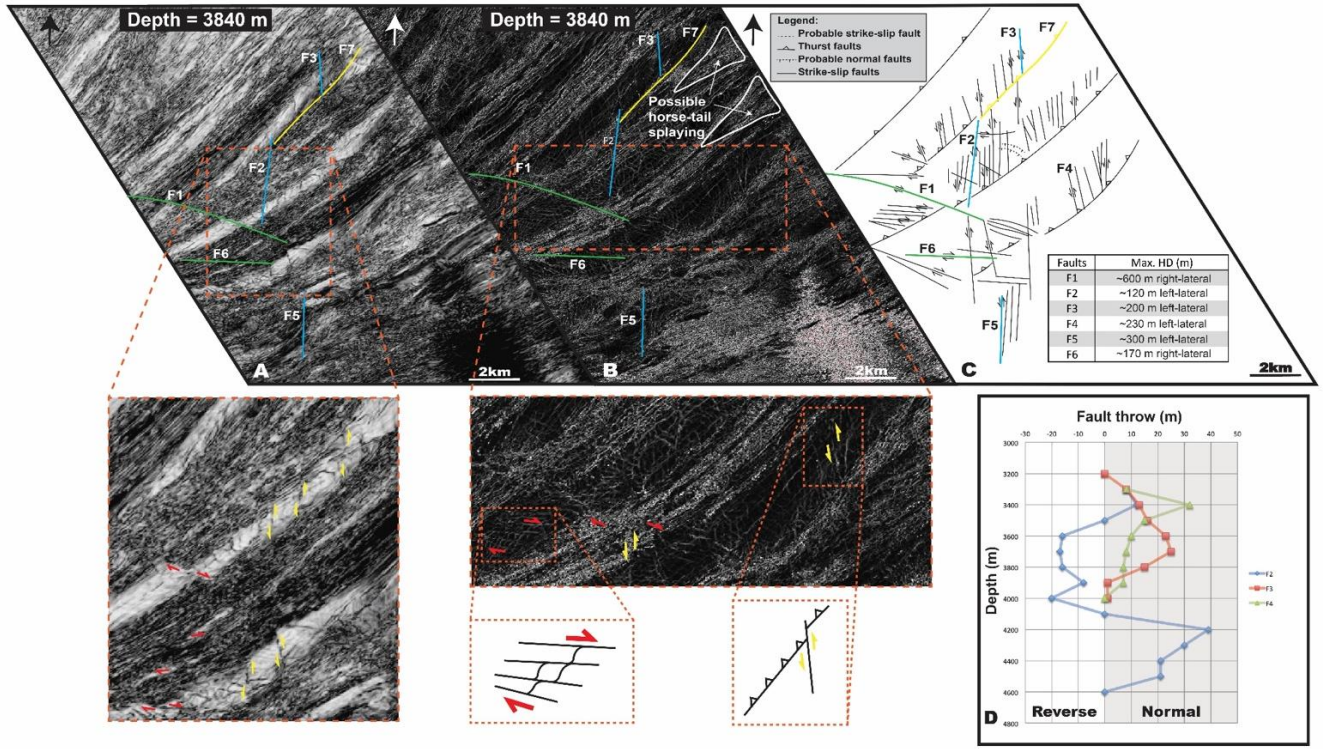

Figure 4.2 - A & B) Coherence and maximum curvature maps (at depth 3840m) with close ups showing main structural lineaments and interpreted faults. Red half-arrows – relative right-lateral movement; yellow half-arrows – relative left-lateral movement C) Schematic interpretation of the geometry and kinematics of main faults. Lower right-hand corner: table showing the maximum horizontal displacement (max. HD) and the type of horizontal displacement of faults F1 to F6. Three families of faults have been identified: NE-trending thrusts (yellow), NNW- to N-trending left-lateral strike-slip faults (blue) and WNW- to E-W right-lateral strike-slip faults (green). D) Graph showing the amount of displacement and the nature of vertical displacement in three NNW- to N-trending faults (F2 to F4). This shows a variation in the throw of the faults as well as the type of vertical movement along dip-slip direction, which is evidence for horizontal movement in these faults. In most faults, lateral-slip is much larger than dip-slip.

4.4.2 WNW-trending faults (predominantly shallow)

One of the most striking features in the NAP is the very steep (sub-vertical at times) WNW-trending F1 fault (azimuth: 110° - 115°), a structure ca. 8 km long and ca. 3km high, at places intersecting the basal décollement (Figures 4.2A–C, 4.4 and 4.5). The geometry and dip direction of F1 are not constant along strike, therefore F1 could perfectly be an alignment of several closely spaced WNW-trending faults that seismic does not possess enough resolution to distinguish.

Fault F1 displaces most thrust anticlines imaged on the 3D seismic data and exhibits a right-lateral strike-slip kinematics in map view (Figures 2.1 and 4.2A–C). In contrast, vertical seismic profiles reveal normal throws for this same fault (Figures 4.4 and 4.5). Its NW tip shows multiple faults with similar trends and slips (Figures 4.2A–C and 4.4). It is not possible to define if these minor faults are branching out from a deeper fault, or if they reflect a highly deformed zone near the sea floor as revealed by the presence of several minor faults (Figure 4.4). Nevertheless, the SE tip of F1 splays out in several branching faults that join or stop against other thrusts (Figure 4.2A–C). Similar fault geometries to F1 have been described as negative flower structures in which the horizontal component is dominant (Harding, 1985).

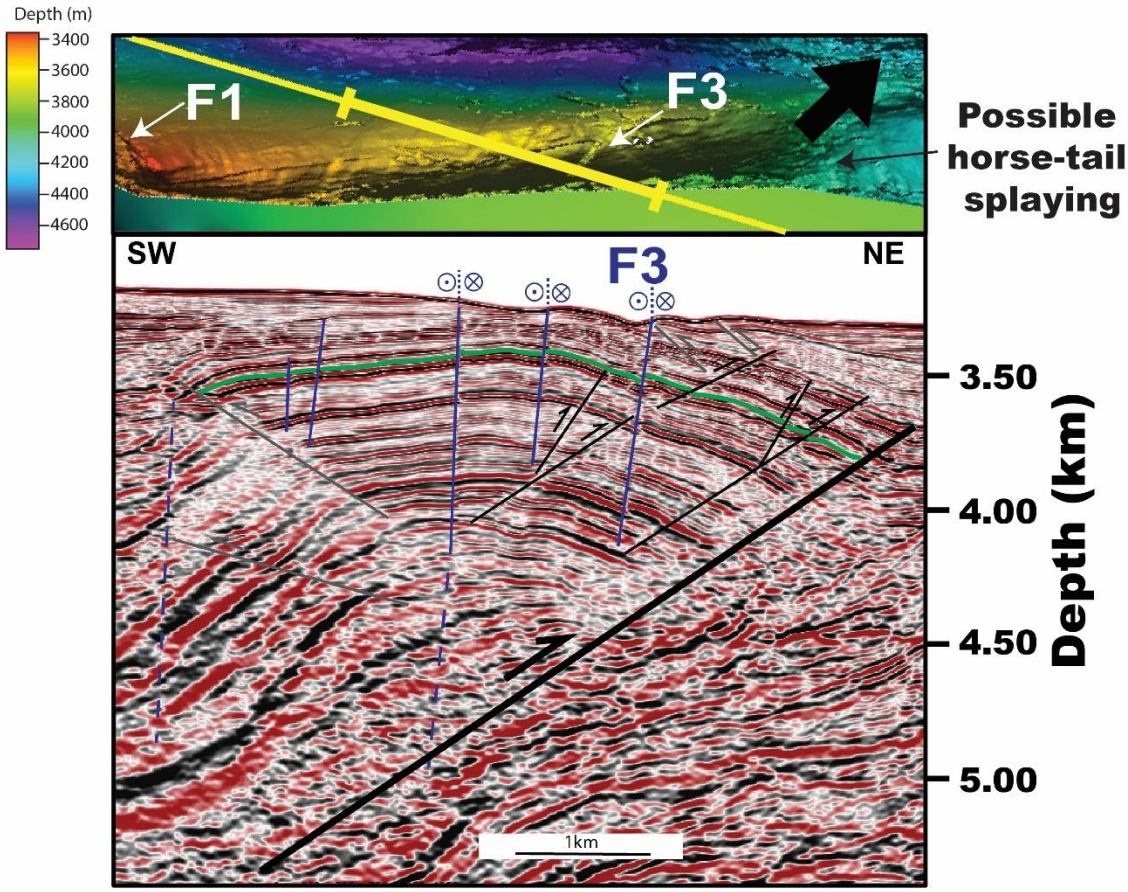

Figure 4.3 - Seismic crossline XL1671 showing strike-slip faults intersecting and displacing primary thrust faults, whereas larger scale thrusts do not seem to be affected. Upper figure is a highly detailed seismic horizon following the main thrust anticlines identified in Figure 4.2. Lower figure is a seismic profile intersecting the main thrust anticlines and highlighting the geometry of interpreted faults and their kinematics within Unit A. Yellow line - trend of the seismic profile below; Green line – seismic horizon of map view above; Blue – strike-slip fault; Black – thrust fault; Grey – antithetic thrust fault. Dashed line – probable fault.

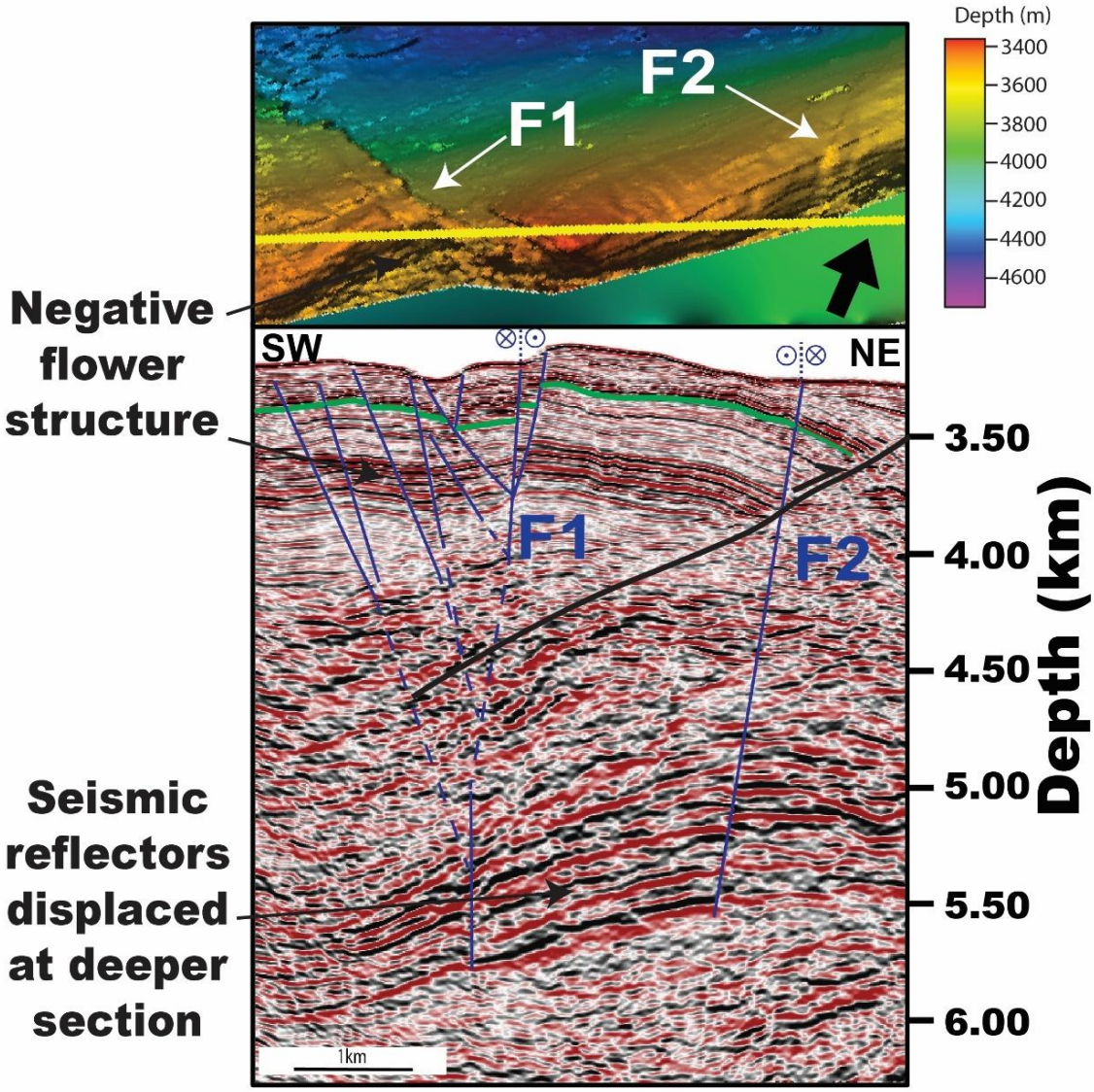

Figure 4.4 - Seismic crossline profile XL1571 illustrating a negative flower structure, likely associated with local transtensional regime. Upper figure is a highly detailed seismic horizon following the main thrust anticlines identified in Figure 4.2. Lower figure is a seismic profile intersecting the main thrust anticlines and highlighting the geometry of interpreted faults and their kinematics within Unit A. Yellow line - trend of the seismic profile below; Green line – seismic horizon of map view above; Blue – strike-slip fault; Black – thrust fault; Dashed line – probable fault.

The F1 fault separates two geometrically distinct structural sectors: (1) a sector to the N where NNW-trending faults are more common and related, both geometrically and kinematically, to F2 (analysed in the next section of this chapter), and (2) a sector to the S where WNW-trending structures are more prevalent and related, both geometrically and kinematically, to F1 (Figure 4.2C). At a smaller scale, there are structures with similar kinematics to F1, trending WNW-ESE to close to E-W (azimuth: 85°–115°), with variable lengths (Figure 4.2A–C). For those where 3D seismic resolves their throw and heave, it is possible to infer a mixture between pure strike-slip to oblique-slip faults. Their dip slip component (Figures 4.2, 4.3, 4.4, 4.5) can result from normal movement or comprise an apparent displacement associated with strike-slip motion, which is not possible to distinguish due to limitations in the seismic resolution. However, the variable throw values recorded, usually increasing towards the surface, together with contrasts between total offset and its bathymetric expression (Figure 4.2D) indicate that the observed normal slip can be an apparent slip from slipping along strike. Kinematically, the strike-slip motion of these structures is consistently of right-lateral nature and these faults intersect the shallower inherited NE-trending fold-and-thrust sheets analysed in the previous section of this chapter (Figure 4.5). Furthermore, trend-parallel horizontal offsets are much larger than fault throws, up to a factor of 2 to 3 (Figure 4.2C–D). It is important to highlight that not all WNW-trending structures show lateral movement, suggesting that strike-slip motion along some of these structures is recent or have not slip enough to be resolved in seismic. Similar fault patterns have been found on

other convergent margins, but at larger scales of observation (Lewis et al., 1988; Platt et al., 1988), and in the Nankai Trough, where they have been described as strike-slip faults (Seno et al., 1993; Kobayashi et al., 2011).

Except for F1 fault being a deep structure that reaches, and seemingly intersects, the décollement, most WNW-trending faults do not propagate beyond a depth of 1 km below the sea floor and seem to be stopping at the NE-trending synthetic main thrusts (Figure 4.3, 4.4, 4.5). As most of these NE-trending thrusts are close to the transition between Units A and B, limitations in the seismic resolution do not allow cross cutting relationships to be analysed with certainty.

4.4.3 NNW-trending faults (predominantly shallow)

In the outer wedge of the NAP there are several NNW- and N-trending structures (azimuth: 345°–10°) dipping towards W or sub-vertical, rarely reaching the sea floor (Figure 4.2A–C, 4.3, 4.4, 4.5). These faults normally exhibit a left-lateral strike-slip motion, and a variable normal dip slip throw (Figure 4.2C). These faults show variable lengths but usually occur within thrust anticlines, rarely extending into their adjacent synclines, very similarly to most of the WNW-trending structures analysed in the previous section of this chapter. Their vertical extension is also variable, from a few meters to hundreds of meters, seldom affecting the sea floor. The exceptions are F2, F3 and F4 faults that

resolve both dip-slip and strike-slip motions in the seismic data, with F2 and F4 being the most relevant NNW-trending structures in the study area due to their propagation to deeper sections of the NAP and their clear left-lateral motion. Park et al. (2002) and Tsuji et al. (2014) have reported strike-slip faults of similar trend in the Nankai Trough.

In some cases, similar structures are observed on both the hanging-wall and footwall of major thrust faults, intersecting some of the deeper thrusts in the NAP (Figure 4.3 and 4.5).

4.4.4 Normal faults

Minor normal faults on the scale of tens of meters have been observed and are normally confined to the uppermost part of the sediment cover (Unit I, as previously described by Strasser et al. (2011) and Van Tuyl et al. (2015). These minor faults tend to follow the trends of strike-slip and thrust faults previously identified (Figure 4.6) and have been classified as normal mainly due to showing minor throws without any evidence for horizontal movement. However, they can comprise oblique-slip faults in which their horizontal displacement is below the horizontal seismic resolution to be recognisable on the 3D PSDM volume.

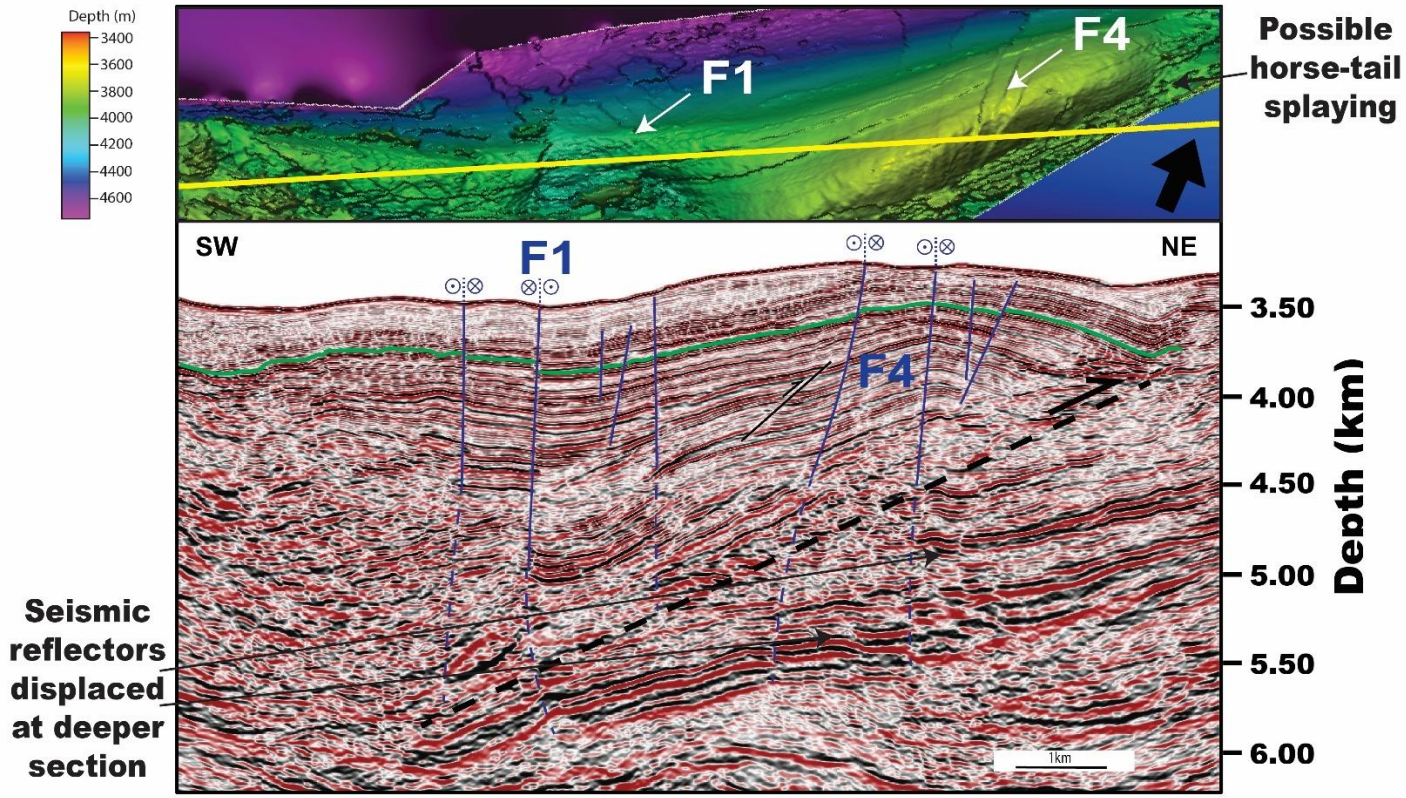

Figure 4.5 - Seismic crossline profile XL1251 showing right-lateral and left-lateral strike-slip faults with variable vertical throw. Some faults are observed in both the hanging-wall and footwall of thrust anticlines. Upper figure is a highly detailed seismic horizon following the main thrust anticlines identified in Figure 4.2. Lower figure is a seismic profile intersecting the main thrust anticlines and highlighting the geometry of interpreted faults and their kinematics within Unit A. Yellow line - trend of the seismic profile below; Green line – seismic horizon of map view above; Blue – strike-slip fault; Black – thrust fault; Dashed line – probable fault.

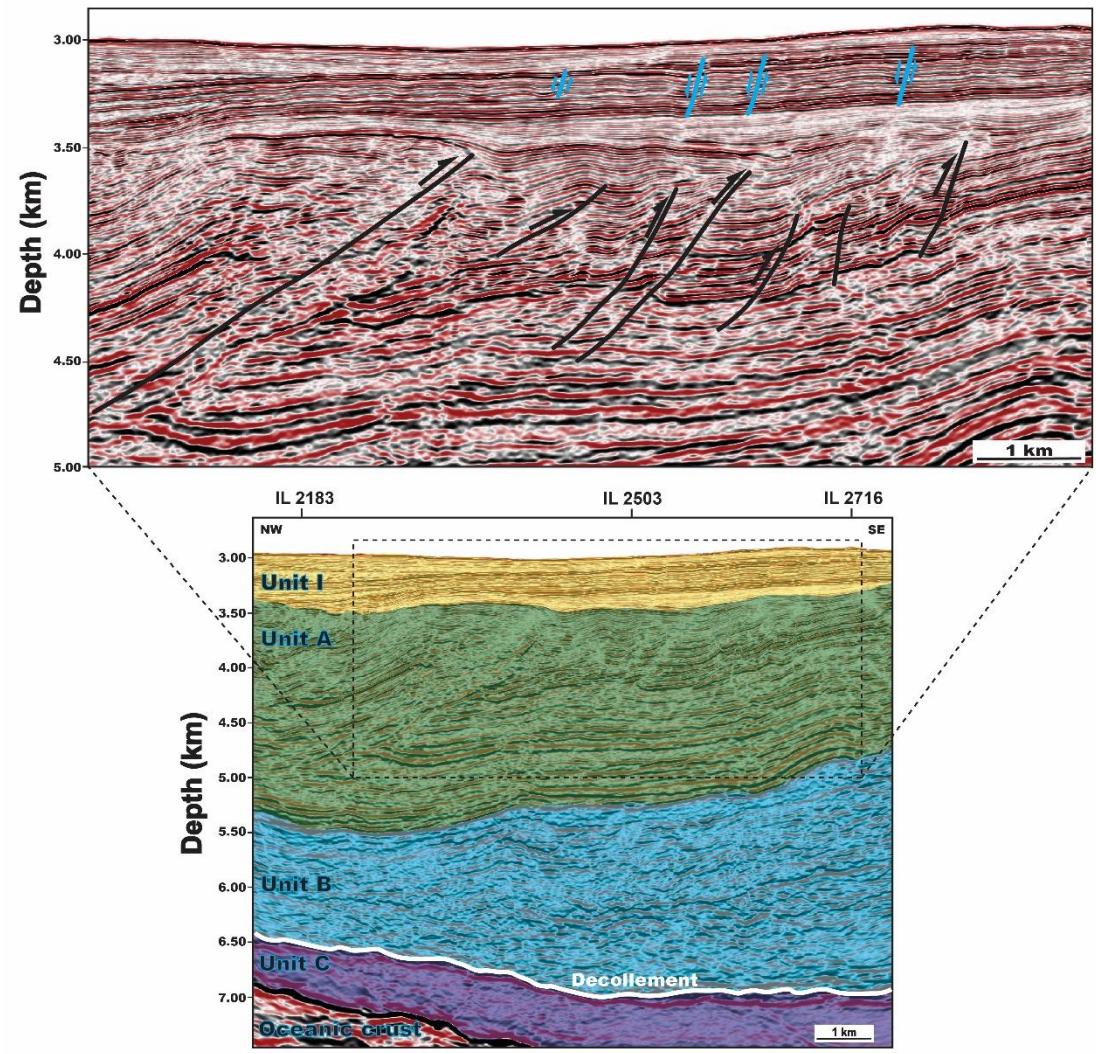

Figure 4.6 - Depth-migrated seismic crossline profile XL1920 across the landwards section of the outer wedge of the NAP showing the tectono-stratigraphic units as in Figure 2.7. The amplification shows thrust faults (black lines) within Unit A, where some reach the contact between Units I and A, and few normal faults (blue lines) within Unit I related to the gravitational collapse/adjustment that advent from uplifting caused by deeper thrust structures.

4.4.5 Deep structures

Some of the structures previously identified by Tsuji et al. (2013) as affecting the décollement or units below the Unit A were also mapped in this chapter. These structures are here referred to as 'deep' structures as opposed to the previously analysed 'shallow' structures that do not cut across lower Units B and C (including the décollement) or that do not root from/into the décollement. These deep structures normally show a larger complexity in their geometry and kinematics (Figures 2.6B, 4.7 and 4.8). According to Tsuji et al. (2013), some of the deep faults imaged on seismic data are inherited structures on the oceanic crust of the PSP. These inherited structures do not only control the thickness of the accretionary prism, but also its structural framework. These structures include active intraoceanic thrusts (Figure 2.7B) and some strike-slip faults resulting from lateral movement at the edges of the thicker parts of the NAP. In the outer wedge of the NAP, these intraoceanic thrusts will control the location of main thrust faults within the ITZ. However, in this chapter several deep-rooted faults with similar directions to the previously described strike-slip faults are identified.

Despite their larger structural complexity, deep structures show similar trends to features observed in the NAP, especially when referring to strike-slip fault families (Figure 4.7 and also referred to the next Chapter 5). It is equally important to highlight that these deep structures reach depths greater than 6

km below the sea floor, rooting at and displacing the décollement and underlying units. Some of these structures show relative displacements that do not laterally or vertically agree with a pure extensional or compressional regime of deformation (Figure 4.7). Thus, only a strike-slip or a combined regime of deformation can justify such a displacement pattern. This combined regime often generates distributed deformation zones in which strike-slip motions may not be the same as the regional strike-slip movement (McKenzie and Jackson, 1986). In addition, branching and splaying of deep structures are observed and increase upwards, resulting in a continuous decrease in the displacement of these splays/branches and, consequently, in a shallower chaotic zone of fracturing that rarely offsets the sea floor (Figure 4.7). The fact that these branched faults (and fault F1) reach the sea floor, suggests they may be active or were recently active.

As previously discussed, fault F1 is one of the few WNW-trending faults that that roots in the décollement or in deeper strata and therefore deserves to be mentioned in this section. However, the near-seafloor extension of this fault seems to vary along strike (compare Figures 4.4, 4.5 and 4.7 – remember that F1 could potentially be a seismic lineament or zone of several badly resolved WNW-trending faults). In Figure 4.4, which is located a few kilometres NW from Figures 4.5 and 4.7, a single and well-defined fault F1 is observed cutting through the outer wedge of the NAP, reaching the sea floor without any major branching or splaying. In Figure 4.7, F1 fault as it is mapped in Figure 4.2C borders a 'belt' of several closely spaced and deeply rooted WNW-trending faults

(referred to in this theses as F1 right-lateral strike-slip belt as opposed the linear right-lateral strike-slip F1 fault), creating a complex structural network badly resolved in seismic that clearly displaces the seismic reflectors within Unit A, and creates a chaotic and low seismic resolution zone in its uppermost 1km with bottom simulating reflectors (BSR) nearby, suggesting fluid movement along these faults and accumulation of gas above them. The displacement observed in the seismic reflectors do not show the same throw along dip, which seems to suggest a strike-slip component (Figure 4.7C). Such variety in the displacement of the seismic reflectors could also reflect local geometric and kinematic interactions between left-lateral NNW-trending and right-lateral WNW-trending faults in the mid NAP section.

In Figures 4.7 and 4.8 and laterally other areas of the outer wedge of NAP, the thickness of Unit C varies laterally, especially in when deeply rooted structures, such as the ones so far analysed, coexist with deep structures in the actual subducting oceanic crust. The lateral continuity and thickness of Unit B also seem to be impacted in same areas as Unit C (Figures 4.7 and 4.8). This confirms a positive correlation between local thinning of Unit C, thinning and/or disruption in the lateral continuity of Unit B and presence of deeply rooted and deep structures in the subducting oceanic plate. Tsuji et al. (2013) shows evidence of when the oceanic crust and Unit C folded and/or fractured, the Unit A usually presents a much greater deformation and structural complexity, therefore these observations are discussion worthy in terms of its impact in the décollement and the branching of deeply rooted structures.

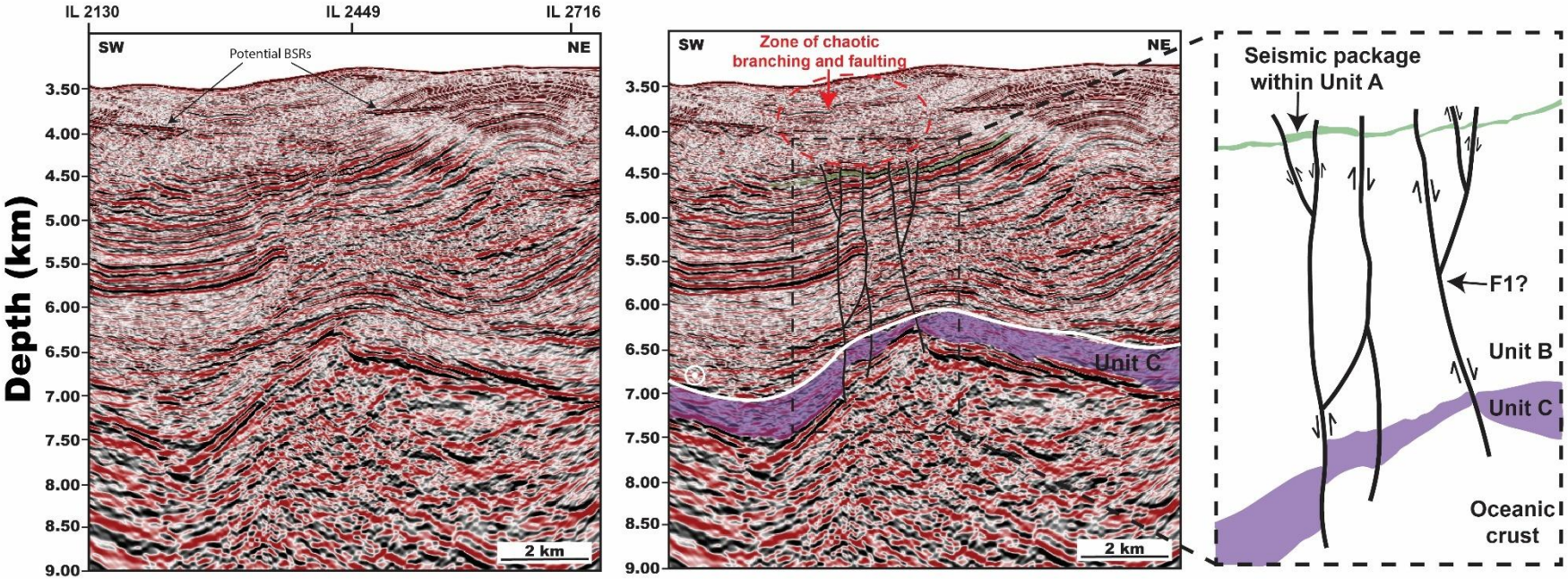

Figure 4.7 - Depth-migrated seismic crossline profile XL1320 (original on the left and interpreted on the right) showing irregular relative displacements between blocks horizontally and vertically adjacent. This non-concordance between different displacements cannot be explained through pure extensional or compressional regime. Black arrows show the relative displacement between adjacent blocks of strike-slip faults (black lines). Dashed red ellipsoid shows a shallower zone of random fractures with minor displacement(s), probably branching from the interpreted major faults. Some of these minor branches reach the seafloor slightly affecting the bathymetry. It is important to note that these seismic sections show two horizontal reflectors that are not commonly visible in this 3D seismic data and that seems to be bottom simulating reflectors (BSR). The thickness of unit C varies literally, getting thinner. This could weaken the base on which the décollement slips and may aid the décollement to migrate upward into weaker sediments, possibly facilitating shallow faulting or splay fault activity (Moore et al., 2001). Green horizon – a seismic horizon of Unit A; Purple horizon – Unit C; White line – décollement; IL - Inline

In Figure 4.8B, two scarps or faults following the same strike (and in the same position) of WNW-trending fault F1, also cause lateral variations in the thickness and continuity of both Unit C and B. Similarly to previous patterns, there is upwards branching into a chaotic deformation zone within the entire overlying Unit A. These deep structures have a throw of 500-1000 m, which is significantly larger than the throws recorded on any other thrust in the outer wedge of the NAP, and larger than the horizontal displacement of F1 fault (ca. 600 m). These thrust faults were previously interpreted as a single major intraoceanic thrust that are probably inherited from oceanic transform faults as discussed in Chapter 1, but that could be reactivated during subduction (Tsuji et al., 2008; Tsuji et al., 2013). Once more, it is possible to observe an upward decrease in their throws, probably occurring in association with splaying/branching towards shallower strata. The observed geometry suggests a variation from a deep regime where dip-slip displacement is greater than horizontal displacement, to a shallow regime where dip-slip displacement is lower than horizontal displacement.

4.4.6 Cross-cutting relationships

Unfortunately, seismic does not clearly resolve cross-cutting relationships between the families of faults studied in this chapter, but it is possible to infer the following from the seismic profiles presented in chapter:

- both NNW- and WNW-trending strike-slip displace the seismic reflectors of the synclines sitting on top of the main synthetic thrusts, so they would have to be formed after the widespread fold-and-thrust sheets. However, there is no clear evidence of these faults intersecting the main thrusts, even when they have been mapped as crossing them (e.g. F2 in Figure 4.4) as seismic does not resolve any displacement on either. This could indicate some synchronism or alternating behaviour in their slipping behaviour.
- Some deeply rooted strike-slip faults, in particular F1, F2 and F4 (in Figure 4.4 and 4.5) could potentially intersect the main synthetic thrusts as similar trends and displacements are observed above and below the thrusts.

It is also important to note that in Figures 4.3, 4.4 and 4.5 some faults, in particular WNW-trending right-lateral strike-slip F1 and NNW-trending left-lateral F2 and F3 slightly offset the seafloor, indicating their recent activity.

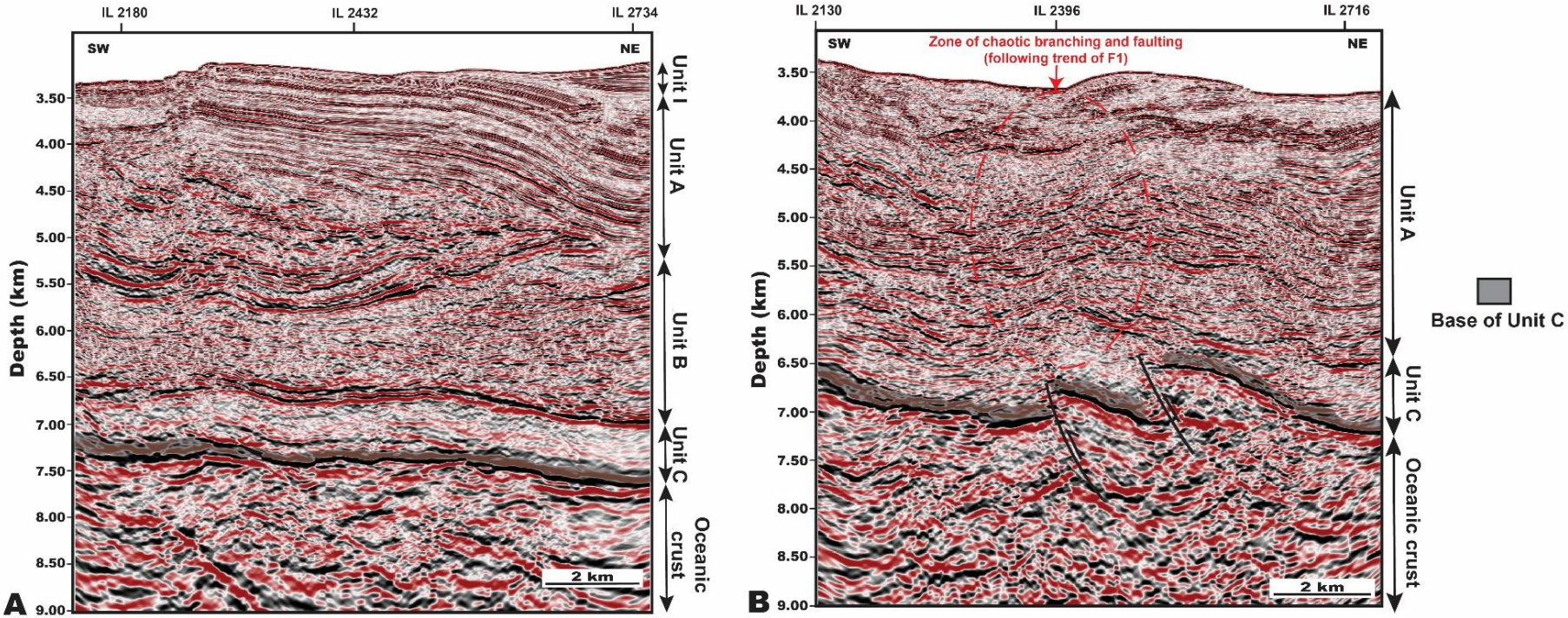

Figure 4.8 - Seismic crossline profiles XL1571 (A) and XL1139 (B) showing the main tectono-stratigraphic units as described in Figure 2.6 and the base of Unit C. A) Unit C (and décollement) presents a laterally continuous and smooth base with the overlying 'typical' fold-and-thrust Unit A. B) Unit C thickness changes laterally and both the décollement and Unit B are not as well defined in seismic. The low-velocity zone (Unit B) observed in Figure 4.8A does not seem to exist here and the overlying Unit A showcases a much larger structural complexity that seem to be similar to the belt of WNW-trending faults that are being shown in Figure 4.7.

4.5 Chapter-specific discussion

4.5.1 Significance of strike-slip faulting in the outer wedge of NAP

Despite clear evidence for primary compressional deformation across the NAP (Moore et al., 2007; Kimura et al., 2007; Kimura et al., 2011), the analysis in this chapter reveals that strain in this region is also accommodated by secondary strike-slip deformation. This observation has a significant impact in the structural framework of the NAP and the way(s) stress release and accumulation occur in the region. Therefore, the outer wedge of the NAP is being affected by two main families of strike-slip faults: WNW-trending right-lateral faults, and NNW-trending left-lateral faults. Their spatial distribution is controlled by a major F1 fault or belt (zone), which separates two different structural sectors. The fact that: (1) the horizontal displacement (120–600 m) is two or three times larger than dip-slip displacement (< 40 m), (2) fault throws are variable in both their magnitude and nature of movement, and (3) normal slip in faults does not have the same expression on the sea floor, hints towards strike-slip fault (Figure 4.2).

Figure 4.4 exhibits a likely negative flower structure with an associated normal-slip component suggesting that, within a dominant transpressional re-

gime, there could be local zones in which transtension is favoured in a distributed deformation pattern (McKenzie and Jackson, 1986). This 'flower structure' can also result from the combined effect of strike-slip and thrust movements as: (1) the structural domain to the N of F1 exhibits larger horizontal shortening and tilting than the S domain (Figure 4.10), and (2) the curved shape of the NW tip of F1 exhibits a larger throw and horizontal slip as its angle approaches a direction perpendicular to the trench. This is the first mention of flower structures in the ITZ of the NAP, although other flower structures have been identified in other parts of the Nankai Trough and associated with a lateral component of motion (Le Pichon et al., 1996; Takahashi et al., 2002).

There are several structures that follow the same orientation as these strike-slip faults, but without revealing lateral slip. These structures are relatively shallow and exhibit small normal slips to no dip-slip displacement (Figures 4.5 and 4.6). Also, they do not have any bathymetric expression. These latter structures can result from one of two scenarios: (1) blocks bordered by well-developed strike-slip faults experienced some torsion/rotation that is accommodated by extension, (2) accommodation of lateral movement in blocks bordered by strike-slip faults is no longer possible, or is significantly hindered, with new strike-slip or oblique-slip faults being newly formed as a result of a transpressive regime. It is important to mention that normal slip observed in seismic can also be interpreted as an apparent slip developed in a fold-and-thrust sequence dipping towards the NW, itself affected by strike-slip faulting with significant lateral motion (Figures 4.3, 4.4, 4.5).

The observation that deep structures within the subducting oceanic plate affecting the thickness and lateral continuity of Unit C (as well as Unit B) follow the geometry of these shallow structures (Figures 2.1, 4.7 and 4.8), highlights the fact that the uppermost strata in the outer wedge of the NAP (Unit A) is influenced by deeper structures and most importantly by faults that are deeply rooted at such structures. This is relevant for décollement mechanics as well as for the deformation of the NAP because it disrupts the well documented dynamics generally observed along the Nankai Trough, where the mechanically stronger and coupled Unit C below a weakly consolidated and over-pressurised Unit B, allows for the décollement to reliably slip on top of Unit C. However, the results from this chapter show evidence for thinning of Unit C which can have important tectonic implications (Figure 4.9) as it offers less buffering between deeper tectonic forces and overlying units, meaning that more strain is transferred upward and consequently leading to more deformation of Units A and B (Bangs et al., 2004; Saffer and Tobin, 2011), similar to what is observed in Cascadia Subduction Zone (Goldfinger et al., 1997) and Peru-Chile trench (von Huene & Suess, 1988) where limited underthrust sediment correlate with strong coupling and greater uplift of the outer wedge (von Huene & Suess, 1988). This effect could be further exacerbated by accompanied thinning of Unit B as observed in both Figures 4.7 and 4.8, where strike-slip faults deeply root into the décollement and where Unit A is severely fractured compared to areas where Unit C and décollement both remain intact. The localisation of strain more directly into overlying units could lead to more brittle deformation, in this case in

form of thrust and strike-slip faulting observed in the study area. Not only this will this cause differential compaction and/or uplift in the overlying units with effects on bathymetry and seafloor fault rupture but also could promote Unit B to become under additional increased pressure that could lead to hydrofracturing or fault reactivation that follows the trend of strike-slip faults (Saffer and Bekins, 2006). This could create pathways for fluid migration to the surface and for the occurrence of observed BSRs (Figures 4.7 and 4.8B). Additionally, faults originating in the subducting plate may propagate more easily through a thin Unit C to reach suprajacent Unit A, which could increase the likelihood of surface-breaking faults with seismic risk (Tsuji et al., 2013). Similarly, this will aid décollement to step upward into weaker layers in Unit B or A, altering the slip zone (Moore and Saffer, 2001).

The interpreted seismic volume points to a compressional accretionary prism responsible for synthetic and antithetic thrusts with a strong strike-slip faulting component that accommodates any variations in strain caused by deep structures and/or variations in the thickness of Units C and B. Both are the main structures responsible for deformation in the outer wedge of the NAP, thus providing scant evidence for extensional deformation. However, a dominant strike-slip or compressional deformation can be responsible for the formation of near-seafloor extensional structures due to gravitational collapse or through the accommodation of deformation at shallower levels of the NAP (Figure 4.5), as recorded in other compressional settings (Shelton, 1984; Burchfiel and Royden, 1985).

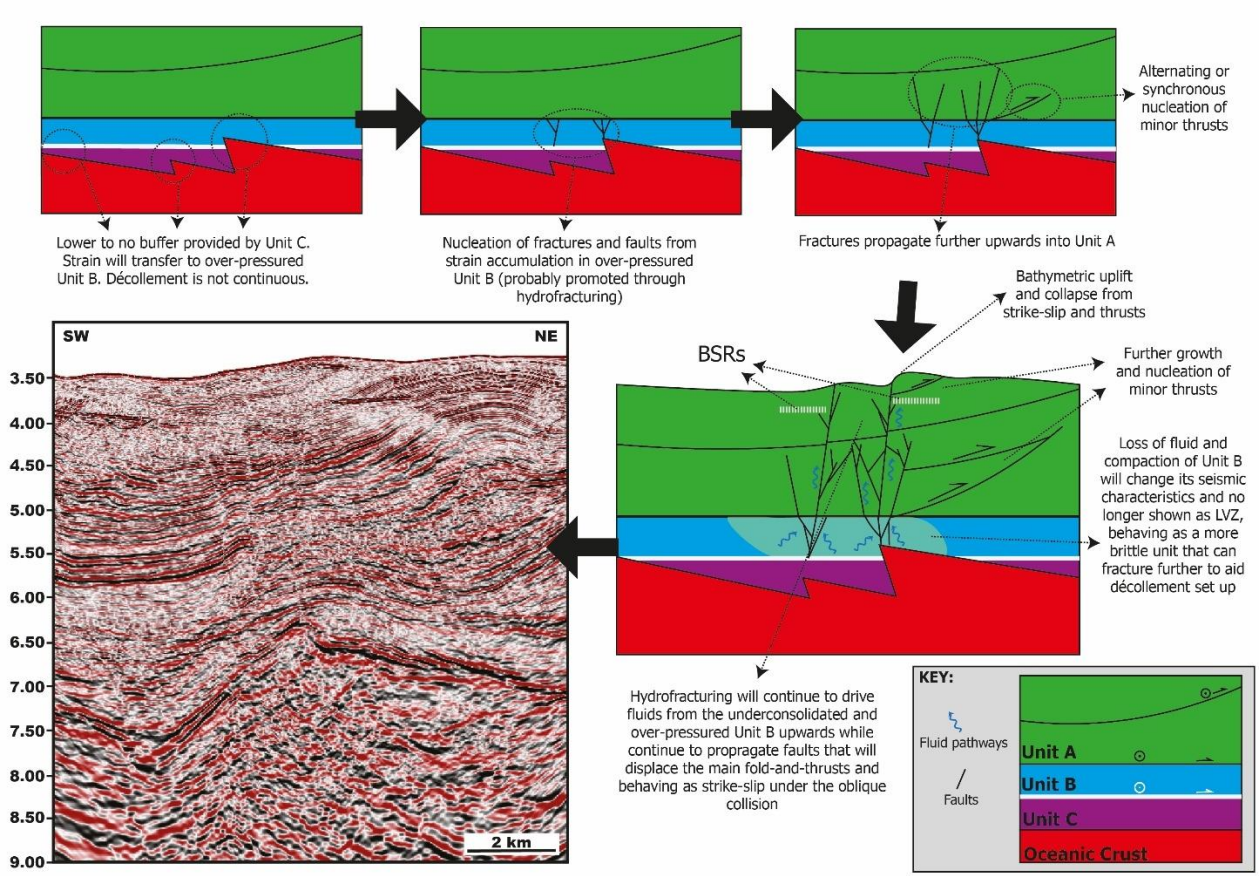

Figure 4.9 - Summary schematic diagram with the impact of deep structures in the overlying units of the NAP and their relationship with deeply rooted WNW- and NNW-trending strike slip faults identified in the study area such as a F1 and F2. Key show a schematic of the sketch block with the names of the units being represented and the kinematics of the décollement and main synthetic fold-and-thrusts.

Therefore, we corroborate the presence of a variable ECD within the NAP that is strictly associated with the thickness of the sediment cover (Van Tuyl et al., 2015). In the NAP, the dominant deformation style is not extensional, and the shallower extensional regime is just a consequence of a dominant transpressional regime.

4.5.2 Estimates of maximum horizontal stress

Thrust and strike-slip faults identified on seismic attribute maps had their strikes measured for statistical purposes, and to identify the range of strikes for each fault family (Figures 4.1 and 4.2). The measured strikes and their poles were projected to the obtain a mean vector for each family of faults. The mean vector was then used to project a new plane on the stereonet that represents the average plane for each family of faults in order to apply Andersonian theory and dihedral angle method (Hancock, 1985; Fossen et al., 2016) to interpret the maximum horizontal stress or paleo stress responsible for the structures described in this chapter as well as to confirm the conjugated nature of the strike-slip and synthetic and antithetic thrust pairs together with inferring their angles and coefficients of internal friction. This latter method is recognised to be rather simplistic but still comprising a valid approach for determining the principal stresses at the time of failure. According to Hancock (1985), an extension fracture is initiated perpendicularly to minimum stress (σ_3) in the principal stress

plane containing maximum stress (σ_1) and intermediate stress (σ_2), and conjugate hybrid or shear fractures enclose an acute bisector parallel to σ_1 (Hancock, 1985). When applying this method, we used two-dimensional strike data from attribute seismic maps and, as a result, we only estimate the maximum horizontal stress.

The mean dip azimuth of the NE-trending thrusts and back thrusts is 308°±6°. If we were to consider a pure compressional regime for the formation of the NAP, we would infer a maximum horizontal stress (σ_{Hmax}) trending perpendicularly to this fault family, i.e. 128°. This result is perpendicular to the trench and is consistent with results from borehole breakouts and drilling-induced fractures in the Nankai accretionary prism that indicate $\sigma_{Hmax} \approx 120–140°$ (Lin et al., 2010). To further enhance the discussion, the pair of synthetic and antithetic NE-trending thrusts present a dihedral angle (2θ) of 59.8° (Figure 4.10) which is very close to the ideal 60° and is typical for conjugate faults formed under Andersonian stress conditions (Anderson, 1905), meaning that they formed under the same stress regime. Additionally, the stress results suggest σ_1 and σ_2 to be close to horizontal (especially when considering the standard deviation shown in Figure 4.1) and σ_3 to be near vertical (84.2°). The values vary little from the classic Andersonian thrust faulting (Anderson, 1905) and an amended σ_1 of 138.5° still point towards a pure compressive regime where the synthetic and antithetic NE-trending thrusts accommodate coaxial shortening, especially when σ_2 is near horizontal. If we are to consider the non-horizontality

of both σ_1 and σ_2, this can still be justified by the oblique nature of the subduction, meaning that thrusts probably accommodate a slight lateral slip while thrusting.

The NAP accretionary prism is also characterised by a set of WNW-trending and another set of NNW-trending strike-slip faults regime that are likely to be arranged in a conjugate geometry as the $2\theta = 69.2°$ (Figure 4.10). This value is higher than the ideal 60° for Andersonian conjugate faults conditions (Anderson, 1905), however it is important to mention that the standard deviation of the dip azimuths for these faults vary between ±7 and ±9 (Figure 4.1), which could bring this closer to Andersonian conditions. Additionally, Anderson (1905) and Hancock (1985) postulate that in natural conditions θ should be < 40°–45°, depending on the confining pressure and resistance to failure of deformed strata, as the value $\theta = 30°$ was calculated in laboratorial conditions for isotropic and mainly non-natural material. The existence of an abnormal pore-fluid pressure, especially within Unit B of the NAP (Tsuji et al., 2008; Kodaira et al., 2004), could also justify the larger θ =34.6 calculated here, as it normally increases proportionally to the confining compressive pressure (Ramsey and Chester, 2004). Ismat (2015) defends that the dihedral angle can also increase within the hinge regions of folds, which is here most of these faults are encountered. As both sets of strike-slip faults and line of intersection present high dip, it is not possible to resolve the stress field, so stresses in Figure 4.10B are inferred from intersection with a horizontal plane, where σ_1 is provides the direction of σ_{Hmax} at 137.2°, being very close to the σ_1 obtained from thrusts, indicating the

horizontal maximum stress for both thrust and strike-slip faults with σ_1 and σ_1 swapping as they are also closely space (compare both stereonet in Figure 4.10B). The dihedral angle varies between 59.8° and 69.2° placing the maximum horizontal stress at an average azimuth of ~138°. The maximum horizontal stress here inferred from structures mapped in the NAP is very closed to the general convergence vector of azimuth 120°–130° (DeMets et al., 2010; Tsuji et al., 2014; Plata-Martinez et al., 2024), thus suggesting an oblique convergence that favours a transpressive regime with both thrusting and strike-slip faulting.

Any minor differences between the azimuths inferred from NE-trending thrusts, and the conjugate strike-slip system, could be either related to:

- a minor rotation of the stress field due to either progressive deformation or alternating seismic and inter-seismic periods, as suggested by Wang and Hu (2006).
- the existence of a pre-existing NE-trending structures in the anticlines and (deep) structures inherited from the subducting Philippines Sea Plate (Tsuji et al., 2013).

In the latter case, deep structures may have controlled the strain accommodation and stress response within the NAP, particularly when strike-slip becomes the favoured regime of deformation.

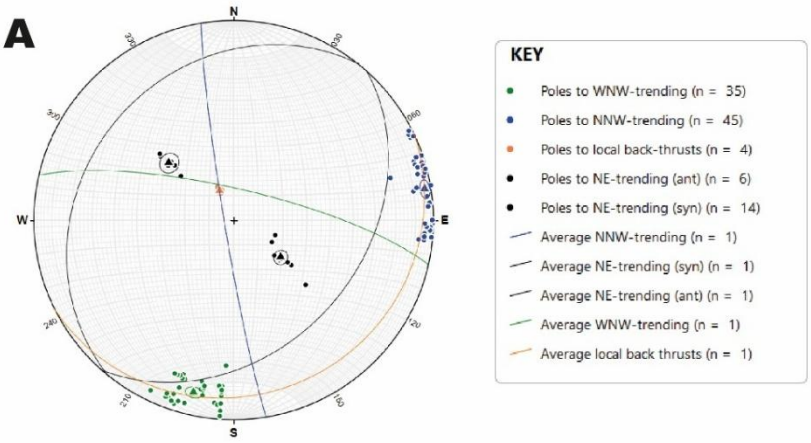

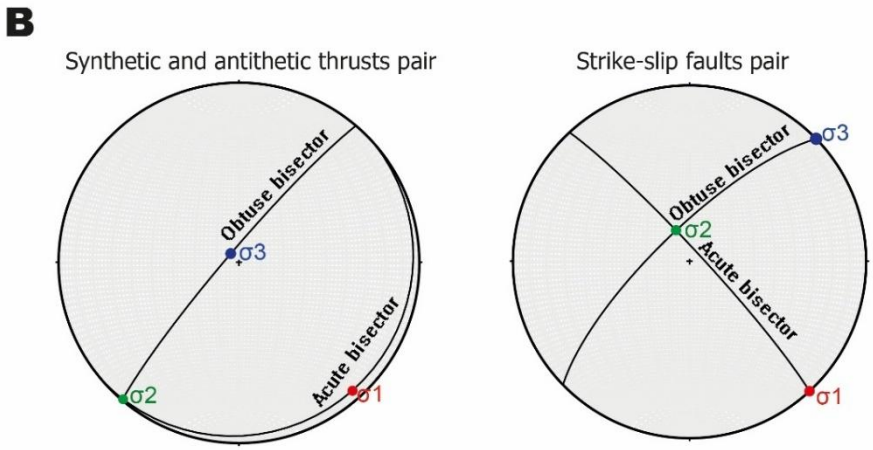

C

Set	Dihedral angle (2θ)	Angle of internal friction (ϕ)	Coefficient of internal friction (μ)	Published data
Strike-slips pair	69.2°	20.8°	0.38	ϕ: ~10°–25° μ: ~0.2–0.45 (Moore & Saffer 2001, Ikari et al. 2009)
Thrusts pair	59.8°	30.2°	0.58	

Figure 4.10 - A) Lower hemisphere stereonet with plotting of poles from Figure 4.1 and derived mean vector (triangle inside circle) and respective average plane for each family of faults. B) Lower hemisphere stereonets with inferred stress fields from each set of paired faults. C) Table showing results for angle and coefficient of internal friction based on Andersonian analysis of the dihedral angles obtained from Figures 4.10A and 4.10B.

It was not possible to calculate the exact azimuth of the convergence vector in the study area, but analysis presented in this chapter still provides a mean azimuth for the maximum horizontal stress. Despite the high probability of a σ_{Hmax} parallel to the convergence vector between the Amur Plate and the PSP, it must be assumed that they do not match. It must also be assumed that any mismatches between the calculated azimuth for maximum horizontal stress, and the azimuth for the convergence vector, may be due to structural complexity in the NAP or angular errors associated with our geometric analysis - which was purely based on the interpretation of 3D seismic data.

It is usually recognised that estimations for the stress state in the outer wedge of the NAP represent a past average stress state. However, Figures 4.3, 4.4 and 4.5 show that some faults, in particular WNW-trending right-lateral strike-slip F1 and NNW-trending left-lateral F2 and F3 seem to slightly offset the seafloor as it presents bathymetric variation in the seismic profiles, where these faults reach the seafloor. This suggests that some strike-slip faulting could still be active under the stress state previously discusses.

4.5.3 Estimates of coefficient and angle of internal friction

The coefficient (μ) and angle (ϕ) of internal friction are critical parameters (Figure 4.10C) in understanding fault mechanics within subduction zone settings. Two sets of paired faults from the NAP, one conjugated strike-slip pair

and another synthetic-antithetic thrust pair, were analysed to assess internal frictional properties using the geometrical relationship between conjugate faults and their dihedral angle (2θ), using the Mohr–Coulomb criterion (Jaeger et al., 2007), where $\phi = 90^{\circ} - 2\theta$ and $\mu = \tan(\phi)$.

For the conjugate strike-slip set, the measured 2θ is 69.2°, yielding an internal friction angle of $\phi = 20.8°$ and a coefficient of friction of $\mu = 0.384$. This value aligns well with friction coefficients commonly reported for the Nankai prism (e.g., Moore & Saffer, 2001; Ikari et al., 2009), which range between 0.2 and 0.45 due to the prevalence of clay-rich, smectite-bearing sediments and elevated pore-fluid pressures. In contrast, the thrust fault set exhibits a dihedral angle of 59.8°, corresponding to a higher internal friction angle of $\phi = 30.2°$ and a coefficient $\mu = 0.579$. This value is significantly greater than typical values for the NAP mentioned above and suggests variations in mechanical and hydrogeological conditions across structural domains, either in space or time (Moore and Saffer, 2001). Several reasons for the observed phenomena can be proposed:

- Fault kinematics and orientation: strike-slip faults generally accommodate lateral shear and tend to reactivate pre-existing weaknesses at lower frictional strength, such as those referred to as deep structures, while thrust faults tend to be capable to accommodate vertical shortening and are more likely to cut through mechanically stronger, less altered material (Sibson, 1977; 1985; 1990).

- Pore-Fluid Pressure: The thrust system may lie within a zone or time of lower pore-fluid pressure, due to its accreting nature increasing effective normal stress and hence the frictional strength, whereas strike-slip faults may result from an high pore-fluid pressure environment potentially related to hydrofracturing induced by over pressured Unit B (Figure 4.9) (Moore and Saffer, 2001; Saffer and Bekins, 2002).
- Lithological Variability: The NAP is lithologically heterogeneous, notably the sandy turbidites of Unit A and the smectite-rich hemipelagic mudstones of Unit B. Unit A, being more lithified and coarser-grained, is mechanically stronger and more likely to host higher-friction thrust faults (Ikari et al., 2009; Underwood et al., 2003). However, this would not fully justify the occurrence of strike-slip faults mainly within the anticlines of the fold-and-thrust sheet in Unit A. In contrast, Unit B's mineralogical composition and low permeability promote pore pressure buildup and fault weakening, favouring localisation of strike-slip (or splay faults), which could be related to the nucleation of deeply rooted strike-slip faults such as F1 and F2 (Moore & Saffer, 2001; Saffer et al., 2001; Moore et al., 2009).
- Deformational Timing: Strike-slip faults may represent later-stage, lower-friction deformation within actively deforming wedge structures, whereas thrusts represent earlier or deeper structural elements with higher resistance. Strike-slip faults within the NAP likely represent a later phase of deformation, often overprinting or cross-cutting

earlier thrust structures. Their development reflects localised, lower-friction deformation within a still-active accretionary wedge (von Huene & Ranero, 2004; Kimura et al., 2007). In contrast, thrust faults are typically associated with deeper or earlier stage deformation, forming the structural backbone of the accretionary complex and requiring greater frictional resistance (Lallemand et al., 1994; Moore et al., 2009).

4.5.4 Deformation styles in the outer wedge of the NAP and comparison with other accretionary prisms

In the Kumano Basin, Moore et al. (2013) identified four populations of normal faults in strata overlying the NAP. Although these faults do not fully share the trends to the faults interpreted in this chapter (Figures 4.11A–B), they still possess a valuable comparison between observations in the shallower levels of the NAP and seismic structural interpretation of the NAP. Phase 1 normal faults seem to correspond to our NE-trending thrust and back thrust faults, whereas phase 2 and phase 3 normal fault populations do not match any particular orientation from our interpreted faults sets but they could be the shallow expression of NNW-trending left-lateral strike-slip faults and WNW-trending right-lateral strike-slip faults that are geometrically different, either because they have rotated as part of their transfer into the inner wedge or because the stress field

at the time of their formation was most likely not the same. This character suggests that normal faults generated in the sediment cover of the NAP, and in Kumano Basin sediment, can be the near-surface expression of gravitational collapse or local adjustments from structures active at deeper levels, imposing anisotropic conditions in both the inner and outer wedges of the NAP. Similar syn-sedimentary normal faults have been described in the Makran accretionary prism as responding to prism overthickening caused by underplating (Platt et al., 1988).

According to Boston et al. (2016), the inner wedge of the NAP inherited a pre-existing structural framework that is chiefly composed of thrusts such as those currently interpreted in the outer wedge. Compression remains the main deformation style operating in the NAP. Considering that structural data collected by Boston et al. (2016) is obtained from the inner wedge of NAP, it is expected that the geological setting is not the same. However, three main families of fault have also been identified Boston et al. (2016) with similar angular relationships to the angular relationships that we found between out synthetic thrust and strike-slip sets. Some few deep structures identified by Boston et al. (2016) are geometrically related to some of the strike-slip fault families here identified (Figure 4.11A and C). However, no reference to strike-slip is made in their work.

Taking into consideration Moore et al. (2013) and Boston et al. (2016) interpretations, structures within the inner wedge and the Kumano Basin show

similar angular relationships to the structures identified and mapped in this chapter, and variations in strikes and faulting regimes can be entirely related to strain partitioning from the FTZ to the inner wedge or related to the MSFZ. This interpretation suggests that structures across the NAP somewhat reflect the same tectonic setting but result in different structural expressions depending on the local geologic and physical conditions. Once again, in the outer wedge, there is no evidence for a dominant extensional deformational style, especially when considering that all normal faults are small and follow the same trend of deeper strike-slip and thrust faults. Therefore, pointing towards the co-existence of both compressional and strike-slip styles of deformation, i.e. transpressional regime.

Cross-cutting relationships between strike-slip faults and thrusts are not always easy to observe due to the structural complexity of the NAP and progressively poorer seismic resolution at depth. However, structural data in this chapter together with the discussed discrepancy in the angles and coefficient of internal friction between the thrust and strike-slip sets, seems to suggest a primary fold-and-thrust framework that is later intersected by relatively recent thrust and strike-slip structures. The chronology between these latter strike-slip and thrust faults is not conclusive as they seem to have been formed simultaneously: 1) as a consequence of a transpressional regime, where both thrusting and strike-slip faulting coexist, or 2) due to alternations between co-seismic and interseismic periods favouring the generation of thrusts and strike-slip structures in discrete alternating tectonic pulses.

The results seem to favour the first hypothesis above since a transpressional regime (Figure 4.12), in which both thrusting, and strike-slip can develop, corroborates the information discussed in Chapter 4.5.2. Furthermore, the chronologic order proposed by Moore et al. (2013) for the normal fault populations in the Kumano Basin matches the postulate of an initial fold-and-thrust regime followed by a transpressional regime where thrust and strike-slip faulting coexist, like the Shumagin region of the Aleutian Trench (Lewis et al., 1988). The present-day tectonic setting in the NAP is, in fact, very similar to those of the Aleutian Trench and Makran accretionary prism, where Lewis et al. (1988) and Platt et al. (1988) proposed three evolution stages: (1) folding along an axis perpendicular to the plate convergence direction, (2) thrust faulting in the direction of plate convergence, and (3) oblique conjugate strike-slip faulting. These conjugate strike-slip faults clearly post-date the prior fold-and-thrust geometry in both the Aleutian Trench and offshore Makran but evolved simultaneously with the major thrusts in the later stages of tectonic shortening. This suggests some overlap between the stages 2 and 3 previously described.

Some of the strike-slip faults in the study area (mainly F1) are associated with deeper inherited structures affecting the décollement (Tsuji et al., 2013). Most of the left-lateral NNW- to N-trending strike-slip faults are confined within the thrust anticlines and can be associated with a flat-and-ramp setting, where the lateral component of the oblique displacement of thrusts (flat) is transferred as left-lateral displacement in strike-slip faults (ramp) (Platt et al., 1988; Cunningham, 2005).

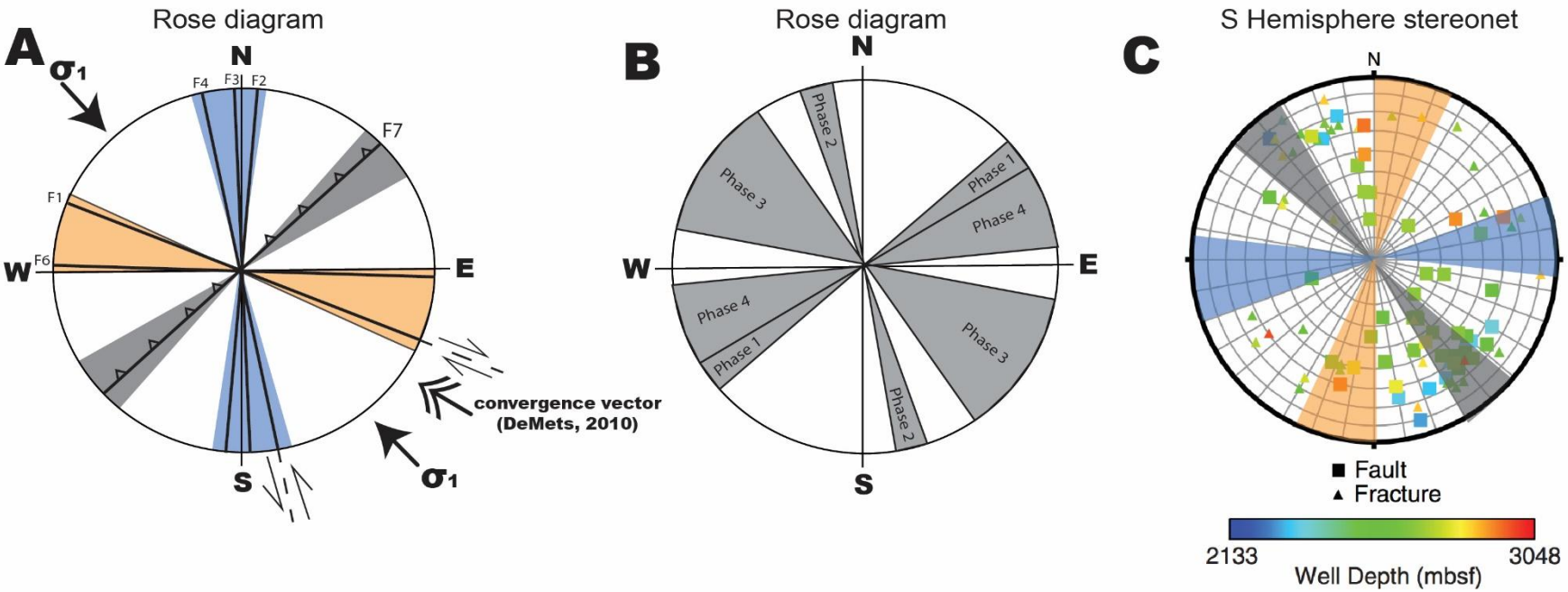

Figure 4.11 - A) Rose diagram highlighting the range of trends for fault families in the NAP. B) Rose diagram with the trend of each group of normal faults, and their chronological order, as in Moore et al. (2013). C) Lower hemisphere Schmidt Stereonet with structural data from Hole C0002P as in Boston et al. (2016) (note: rose diagrams are 90º rotated from trending readings from stereonets from Figures 4.10) and 4.). Dark grey – range of NE-trending thrust faults; Blue – range of NNW-trending left-lateral strike-slip faults. Orange – range of WNW-trending right-lateral strike-slip faults.

The presence of negative flower structures, when considered together with the branching of faults on seismic and attribute data (Figure 4.3 and 4.8), suggests the occurrence of a local transtensional regime (Sanderson and Marchini, 1984). As faults are localised, and no major normal faults are observed in the study area, transtension is interpreted because of the accommodation and partitioning of all transpressional deformation in the outer wedge of the NAP. The fact that there are no major normal faults within the outer wedge of the NAP, and that strike-slip is more common, indicates that strike-slip faulting is still accommodating the shortening of the outer wedge of the NAP, and that the maximum horizontal stress is, in fact, the direction of maximum compression (σ_1) for the study area (Figure 4.10). However, in the SW of the study area and just South of the identified negative flower structures, a localised cluster of back thrusts with different geometry from the antithetic thrusts previously discussed has been recognised (Figure 4.1). Therefore, it is possible that this cluster of back thrusts are the tectonic resolve of a local rotation of the stress field operating within the regional transpressional regime where σ_{Hmax} is 138°. These back-thrusts resolve a σ_{Hmax} is ~154°, that represents a clockwise rotation of 16° that could produce a create an extensional wedge zone between this local stress field and the regional stress field. This family of back-thrust will be later presented and discussed in Chapter 5.

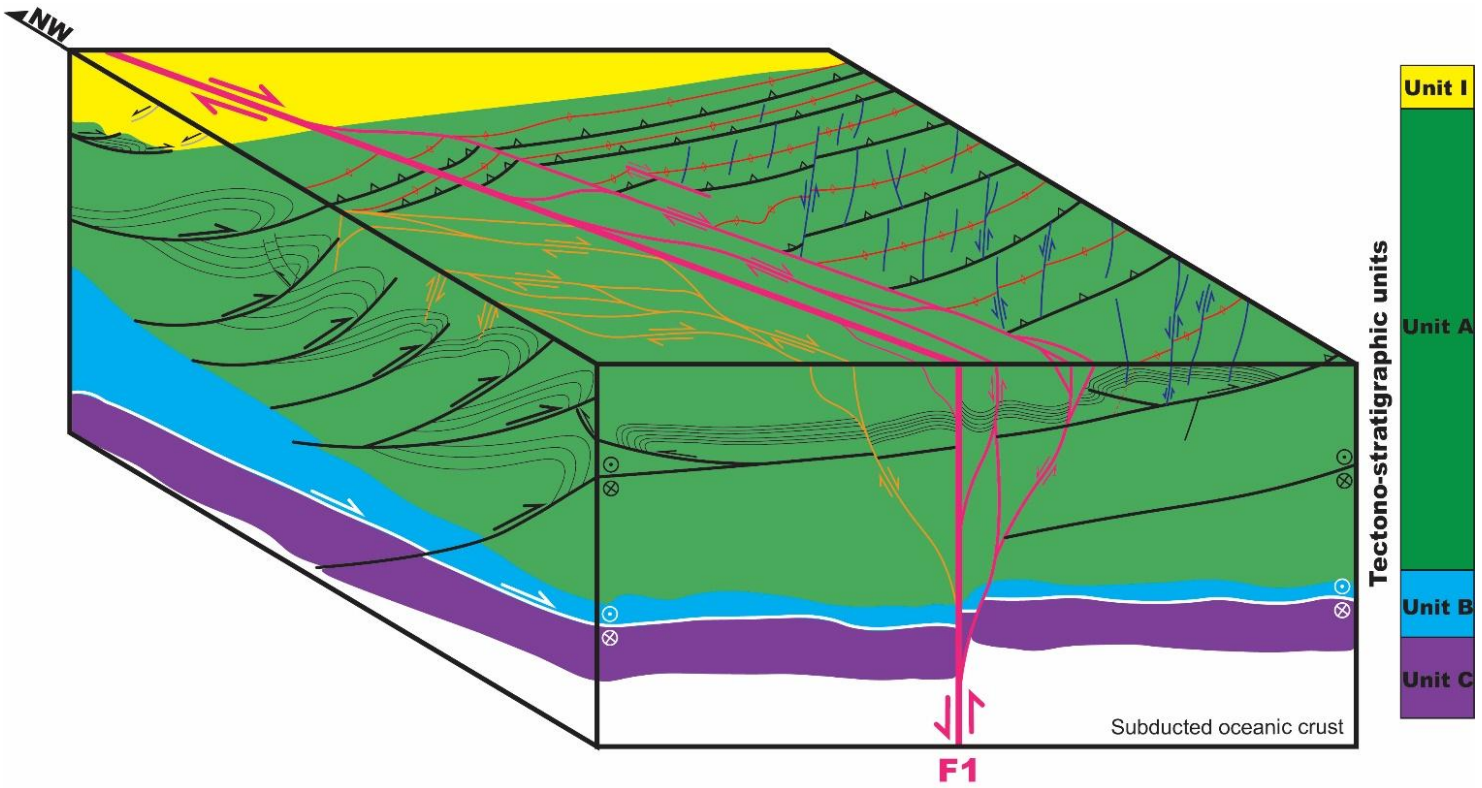

Figure 4.12 - Schematic and interpretative block diagram of the structural framework of the outer wedge of the NAP (SE of the MSFZ and NW of the FTZ) showing the branching of fault F1 as a possible 'flower structure' separating two different structural domains. The NE domain mainly characterized by well-developed thrust-and-fold structures with left-lateral strike-slip faulting within the major anticlines. The SW domain is characterized by right-lateral strike-slip faults. The relative vertical displacement is not constant in the strike-slip faults within the NAP, meaning that this is probably related to a major lateral motion. Red lines – axial planes of thrust anticlines; black lines – synthetic and antithetic thrust faults and respective anticlines; pink lines – WNW-trending right-lateral strike-slip faults; orange lines – E-W trending right-lateral faults; blue lines – NNW- to N-trending left-lateral strike-slip faults; grey lines – normal faults in Unit I; white line – décollement fault; half-arrows – relative movement of faults identified from seismic; pair of circles - relative movement of faults identified from seismic, where circle with point indicates movement of block towards the reader and circle with cross indicates movement away from the reader.

4.6 Chapter-specific conclusions

This chapter shows that the outer wedge of the NAP is a compressional region broadly affected by folding-and-thrusting and a secondary, but still important, strike-slip faulting regime. In particular, the study area is affected by three major types of structures:

- a regional fold-and-thrust setting of synthetic thrusts, antithetic thrusts, and corresponding anticlines.
- localised conjugate families of strike-slip faults comprising left-lateral NNW- to N-trending faults.
- and right-lateral WNW- to E-W trending faults. Within this latter family there is a major regional right-lateral strike-slip fault (F1) that separates two different structural domains. This strike-slip fault is associated with pre-existing structures affecting the décollement and the upper part of the outer wedge.

Maximum horizontal stress inferred from structures interpreted on seismic data is geometrically close to the convergence vector between the Amur Plate and PSP. Despite being clearly associated with past average stresses, maximum horizontal stress in the outer wedge may still represent the main direction of shortening in the NAP which is, at present, accommodated by strike-slip faults. In this rapidly evolving accretionary system, convergence was initially responsible for widespread compression in the NAP and formation of a fold-and-thrust

setting, which progressed into a transpressional regime with thrust and strike-slip faulting occurring simultaneously, or in alternation. There is no evidence for a dominant extensional regime, or a transition from a shallow extensional regime to a deeper compressional or strike-slip regime. Extensional structures and stress decoupling are only visible in regions with significant sediment cover, thus comprising the superficial expression of deeper transpressional tectonics or localized areas of larger structural complexity. The recognition of a transpressional regime operating in the outer wedge of the NAP at present has a significant impact in the stress distribution and consequent accommodation of strain offshore Nankai.

CHAPTER 5

The effect of décollement structures on horizontal shortening and structural imbrication of accretionary prisms: Nankai Through, SE Japan

A paper comprising the findings and discussion covered in this chapter is already prepared and to be submitted shortly after the submission of this thesis.

5.1 Abstract

This chapter develops a detailed mapping of the outer wedge of the Nankai Accretionary Prism (NAP), SE Japan, and reveals significant roughness in its subducting oceanic plate. A ubiquitous undulating morphology, marked by a 1.5 km high seamount and multiple fault scarps 370 m to 950 m tall, is specifically observed in the southeastern part of the study area. Thrust fault distribution and dip in the outer wedge of the NAP, linkages between deep and shallow structures, as well as the magnitude of horizontal shortening, are controlled by the basal asperities recognised in this chapter. Using an area balancing method, estimates of horizontal shortening between 29% and 32% suggest a greater structural shortening than previously suggested for the NAP. Horizontal shortening varies along and across the study area, with the presence of a subducting seamount being responsible for local shortening values of ca. 43% in the frontal part of the NAP. Seismic interpretation indicates that roughness of the décollement is critical in the spatial distribution of pore fluid pressure and variations of basal friction in the NAP, changing its critical taper conditions. These data suggests that tectonic erosion can locally override accretion within the well-known accretional-dominated Nankai margin due to increasing the mechanical coupling between the overriding NAP and the subducting oceanic crust at the outer wedge of the NAP. Such a coupling can exert an important control on the seismic slip behaviour offshore SE Japan.

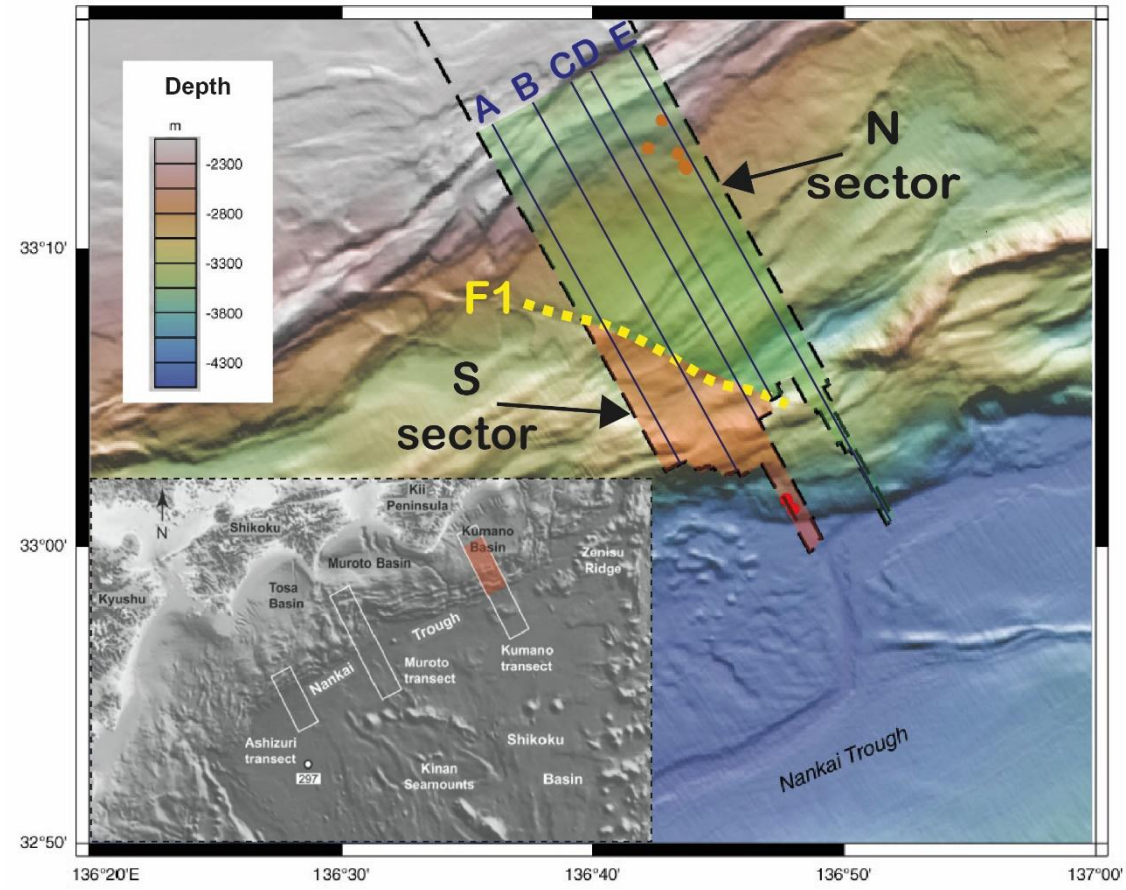

Figure 5.1 – Bathymetric map from IODP showing the study area highlighted in red in inset map from Byrne et al. (2018) with the different transects studied along the Nankai Trough. Dashed yellow line outlines the right-lateral strike-slip F1 (Azevedo et al., 2018) that separated the study area in two sectors: the N sector (green area) and the S sector (red area) as described in the Chapter 5.3. Blue lines are outlining the seismic profiles used for structural restoration: Profile A - IL2180; Profile B - IL2330; Profile C - IL2460; Profile D - IL2530; Profile E - IL2700.

5.2 Introduction

Accretionary prisms are primary structures of convergent margins formed by the scraping and accretion of sediment over a subducting oceanic plate moving at different angles and velocities (Stevenson and Turner, 1977; Schellart, 2005). The boundary between subducting and overriding plates is often interpreted in seismic data as a surface, or zone, of structural complexity and poor seismic imaging known as the décollement (Moore et al., 1990; Laubscher, 2008). Seismic slip occurs along or within this décollement, with its geometry affecting the seismic and tsunamigenic risk of accretionary prisms (Moore, 1989; Moore et al., 2013).

Convergent (or subduction) margins tend to be respectively classified as accretional or erosive depending on if they: a) accrete continental material from the subducting plate, or b) subduct trench sediment and underscrape the basement of the overlying prism (Lallemand et al., 1994; Clift and Vannucchi, 2004; Wakabayashi, 2022). It has been suggested that erosive and accretional processes may even occur at the same time in different parts of subduction zones or, instead, switch through time (Karig and Sharman, 1977; Beaumont et al., 1999; Clift and Vannucchi, 2004). The Nankai Trough, where the study area is located, has been classified as a long-term accretional subduction margin that experiences short-term events of erosion caused by the non-typical collision and subduction of seamounts (Von Huene and Lallemand, 1990; Clift and Vannucchi,

2004). Importantly, the study area is known to comprise a high density of seamounts and ridges (Figure 2.3) within the Philippines Seas Plate (PSP) (Dominguez et al., 1998; Dominguez et al., 2000). Relatively high seafloor roughness, typically observed on erosive margins, has been observed along the Nankai Trough where tectonic erosion can be caused by fluid overpressure near the décollement, in grabens within the subducted plate, or near subducted seamounts and ridges (Lallemand et al., 1994). The presence of inherited structures has been globally recognised to impact the slip behaviour along the décollement and the deformation of the overlying accretionary prisms, where regional to local strike-slip deformation and oblique shortening are common occurrences (Lewis et al., 1988; Lebrun et al., 2000; Schwarze and Kukowski, 2022). Scholz et al. (1997) found that the subduction of seamounts in the Tonga-Kermadec and Izu-Bonin Trenches have a significant impact in the mechanical deformation of subduction fronts and suprajacent accretionary prisms, as well as in the seismic-aseismic slip coupling that drives the erosive-accretional behaviour of the subduction process per se. Furthermore, Dominguez et al. (2000) interpreted that subducting seamounts and ridges form local deformation structures such as back thrusts and conjugate strike-slip faults, similar to those discussed in Chapter 4, that contrast with the regional fold-and-thrust deformation, typical of purely compressional accretionary prisms.

Seismic and borehole data from the NAP (e.g., Moore et al, 1990; Morgan et al, 1995; Ujiie et al, 2003; Ikari and Saffer, 2011) reveal a well-defined, sub-planar décollement marking the boundary between the PSP and the Amur Plate (Figures 2.1, 2.3 and 2.4). 3D PSDM seismic data acquired across the outer wedge of the NAP (Moore et al., 2001; Park et al., 2002; Tobin and Kinoshita, 2006) allow the identification of inherited structures in the subducting oceanic crust, and in the décollement (Boston et al., 2016; Azevedo et al., 2018; Shiraishi et al., 2020). Subducting seamounts and ridges are also common findings along the Nankai Trough (Yamazaki and Okamura, 1989; Park et al., 1999; Park et al., 2004; Bangs et al., 2006). As most published work mainly focuses on characterising the Megasplay Fault (MSF) and the inner wedge of the NAP, the latter of which is outside the study area of this thesis, a more detailed characterisation of the structures contributing to roughness in the décollement of the Nankai Accretionary Prism (NAP) is still needed. Shiraishi et al. (2020) made the first attempt to map the roughness of the décollement in the outer wedge of the NAP, and to relate this roughness to the seismic activity observed (Figure 5.3A). The authors also recognised a rough décollement characterised by several faults with tall bordering ridges from where complex imbricated fault systems in the overlying NAP branch from. These fault systems have been identified as inherited faults and coincide with those previously described in Chapter 4 (Azevedo et al., 2018). According to Morgan et al. (2008), any significant structure in the décollement has the potential to enhance the roughness of the subducting oceanic crust, ultimately affecting the seismicity, local geomorphology,

and subduction zone rupture dynamics along the Nankai Trough. Scant work has thus far addressed the influence of structures in the décollement in the deformation of the NAP. New data and analysis are crucial to a more complete understanding of how accretionary prisms form and grow, and the subducting crust is recycled into the upper mantle.

This chapter develops a structural restoration of five seismic profiles to quantify the horizontal shortening across the NAP. In parallel, the subducting PSP below the NAP has been mapped in detail to aid the quantification of its roughness. The mapped horizon is herein called 'Horizon NanTroR' (Figures 5.3B and 5.3C). Roughness values were compared with estimates of horizontal shortening in the overlying NAP. In summary, the key aims of this chapter are:

- To identify main structures in the subducting oceanic PSP under the NAP and estimate its roughness.
- To correlate the roughness of the PSP with the estimated horizontal shortening and interpreted deformation styles in the overlying NAP.
- To discuss how the roughness of the PSP influences the accretional-erosive behaviour of subduction margins.

5.3 Chapter-specific methodology

This chapter uses the 3D PSDM seismic volume acquired during the NanTroSEIZE as per Chapter 3, that can be characterised as a rectangular area of 2600 seismic crosslines (XL0 – XL2600, from SW to NE) by 620 seismic inlines (IL2130 to IL2750 from W to E). In this chapter, a meticulous manual picking of the top of the subducting oceanic plate was conducted every three inline seismic profiles, followed by similar procedure every five crossline seismic profiles. The mapped seismic reflector offers a very detailed structural map of the subducting plate surface, and it was named **Horizon NanTroR**. This manual picking avoided the need for considerable interpolations on Petrel® that could lead to data distortion and loss of resolution. Previous observations and studies on the 3D seismic volume from the structural analysis that is in this thesis presented in Chapter 4, allowed us to observe an almost parallel geometrical configuration of structures between the top of the oceanic crust and the décollement but due to lower seismic resolutions caused by the suprajacent high velocity Unit B which, at times, blurs the lateral continuity of the décollement, we have opt for mapping the top of the oceanic. This map will therefore be considered to represent the roughness of the subducting oceanic and by parallel, of the décollement. A descriptive analysis of the roughness observed was afterwards conducted together with quantification of the dimensions of the most relevant observed structures within the subduction plate (Figure 5.3).

Five 2D profiles of the 3D PSDM seismic data were selected based on structures identified on Horizon NanTroR (Figure 5.1):

- Profile A: in which important bathymetric relief is identified in the subducted oceanic crust.
- Profile B: with significant bathymetric relief from Profile A and scarps in the subducted oceanic crust with the same direction of strike-slip fault F1 (Azevedo et al., 2018).
- Profile C: bordering the relief observed in Profiles A and B and with visible scarps from Profile B. Also, the longest possible seismic inline mid-section within the study area.
- Profile D: imaging the scarp from Profile B.
- Profile E: an inline section with a smoother and continuous décollement, away from most structures identified in the above profiles.

Geologic structures and tectono-stratigraphic units were interpreted, using Petrel® and Move® software. An analysis of the roughness of the décollement together with a fault slip structural restoration was made using Move® software. To structurally restore and estimate the horizontal shortening caused by fault slip along the main thrust-and-folds in the compressional regime of the NAP, it is important to take into consideration the effect of compaction caused by the upmost and most recent slope sediment cover, the Unit I (check Chapter 2.5.4). In addition to influencing its own geometry, the compaction of Unit I exerts a mechanical loading effect on the underlying Unit A, contributing to its

progressive compaction over time. This vertical loading results in porosity loss and a reduction in the thickness of layers within Unit A, particularly in its upper intervals, without involving any tectonic shortening (Screaton et al., 2002). If such compaction is not accounted for during structural restoration, the resulting interpretation may erroneously attribute volume loss to tectonic processes such as thrusting or folding (Groshong, 2006). This misrepresentation can lead to an overestimation of tectonic shortening, or an incorrect distribution of fault slip within kinematic models of the restoration process (Kitajima et al., 2012). Therefore, decompaction of both Unit I and the upper portion of Unit A is essential to more accurately reconstruct the pre-deformation geometries and to quantify the true shortening associated with thrust faulting in outer wedge of the NAP (Moore et al., 2001). This Unit I is very moderately affected, if at all, by the compressive deformation identified in seismic data. Therefore, the 2D Decompaction tool in MOVE® software was applied, using an initial porosity of 0.35 and a grain density of 2650 kg/m^3 as described by Screaton et al. (2002) and Conin et al. (2011). Sedimentation and deformation occur simultaneously and sediments within the NAP experience compaction while being deformed, a phenomenon promoting vertical shortening, consolidation, and a reduction in porosity (Morgan et al., 2007; Moore et al. 2011). However, it is not possible to realistically calculate the initial porosity or dewatering rate of each tectono-stratigraphic unit because not all units have been drilled/cored by IODP, and some (especially, Unit B) are composed of scraped sediment originated from underplating of the subducted unit against the trench sediment of the NAP.

As the focus of this chapter is to estimate horizontal shortening caused by fault slip from major thrust faults within the NAP, the restoration approach assumes that slip along the décollement is the dominant mode of deformation, and that bed length is conserved, enabling the use of area balancing restoration method (Moore et al, 2011). However, in the NAP, deformation is predominantly syn-sedimentary, meaning that the above assumptions may be partially violated in detriment of simplifying the process of structural restoration. Growth strata and soft sedimentology are important parameters that will influence the bed thickness, leading to non-conservative bed lengths across folds and thrusts (Noda et al., 2020). Additionally, accommodation for shortening may occur not just by slip along the décollement but via distributed strain, minor faulting, and folding. In both previous scenarios, it is expected that restoration methods will underestimate the actual amount of horizontal shortening due to seismic not resolving minor variations in both bed thickness and/or throws along major faults. Furthermore, the assumption that the slip vector is strictly parallel to the seismic inline direction may not hold true across all profiles as it is understood, from Chapter 4, that the NAP experiences a transpressional regime with significant oblique and strike-slip motion. In areas where the structural strain or thrust transport direction is oblique to the seismic section, the 2D restoration will underestimate the actual displacement vector and associated shortening (McClay, 1990). This directional discrepancy can become a significant source of error, especially in segments where the seismic line orientation varies considerably or

where thrust systems exhibit strong along-strike curvature. Together, these assumptions introduce an uncertainty that could propagate non-linearly through the restoration, affecting both the magnitude and geometry of inferred shortening. It is expected that values presented here are consequently an underestimation of the actual shortening that NAP experienced and to minimise the impact of such assumptions in this chapter, shortening is going to be referred to as proportional to each of sectors or seismic inlines being restored rather than their absolute value.

This restoration consists of unslipping offsets on the major thrust faults and estimate the shortening by reversing fault slip while maintaining a constant area of beddings and thrust nappes (Woodward, 1989; Moore et al. 2011). This can be achieved by using the 2D Unfolding and 2D Move-on-Fault tools from MOVE®, through selection of the appropriate interpreted matching seismic horizons and kinematic indicators observable at the scale of the 3D PSDM seismic data (Figure 5.2). Although interpolation methods can lead to overestimation of horizontal shortening, the values presented here are likely underestimates. This is because fault slip along minor faults has not been accounted for, as these structures are below the resolution of the seismic data and therefore could not be mapped in this study.

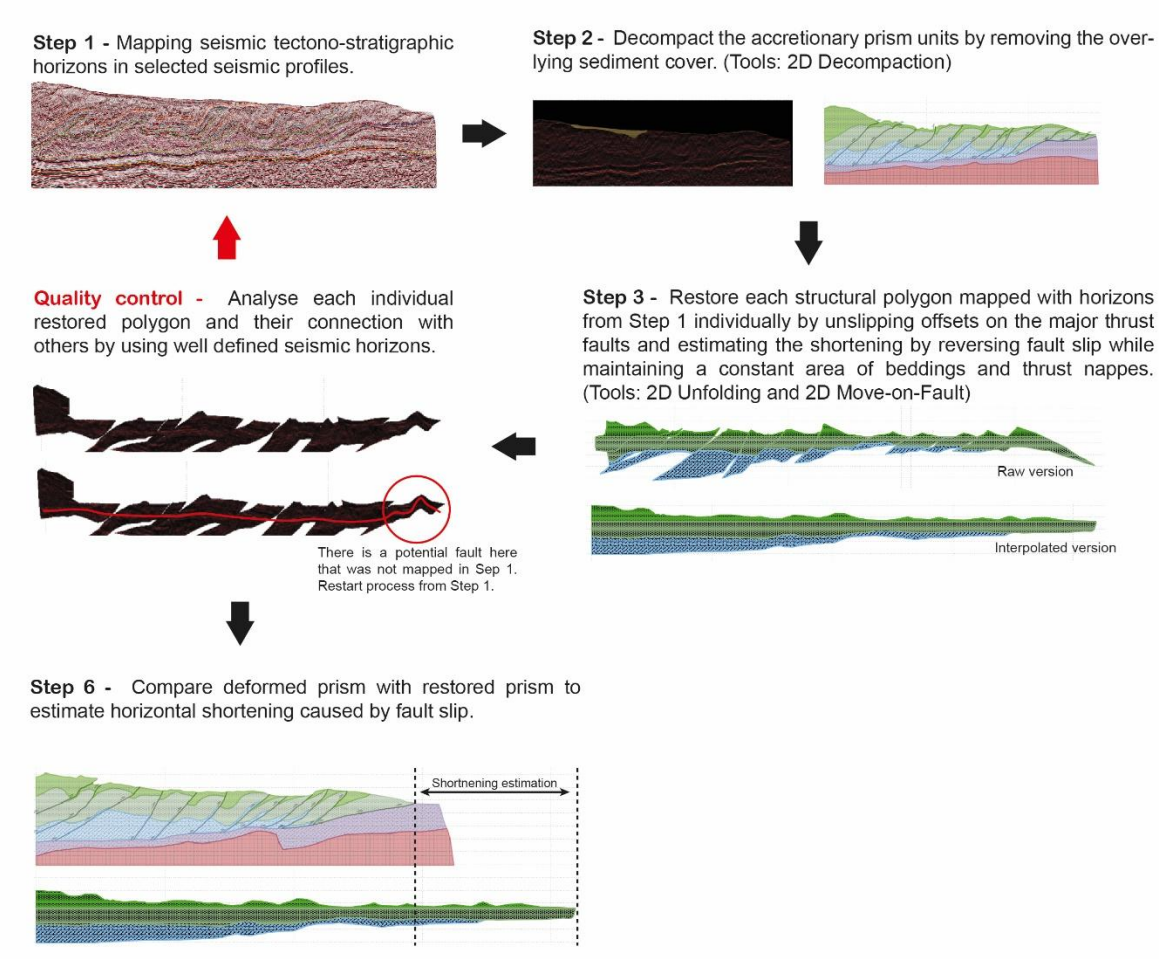

Figure 5.2 – Framework for the structural restoration of Profiles A - E (Figure 5.1) using Petrel and MOVE software. Seismic horizons were mapped with consistent detail, followed by decompaction related to overlying sediment cover and area balance restoration. Quality control before unfolding and unslipping each of the horizons relative to the thrust faults to ensure connection. Once quality control is assured, comparison between restored and original prisms is carried out to estimate horizontal shortening (similar framework to Moore et al., 2011).

After obtaining a longer and structurally restored profile for each of the seismic Profiles A to E mapped and analysed in this chapter, the percentage horizontal shortening for entire section was estimated on each selected seismic profile by comparing the length of the original 'deformed' seismic profile with the length of the final 'restored' profile. Afterwards, the horizontal shortening for the Imbricated Thrust Zone (ITZ) and the Frontal Thrust Zone (FTZ) as well as for the North and South sectors (Figure 5.1) were systematically estimated, for each of the seismic Profiles A to E. This sectioning of horizontal shortening assists in the understanding of how shortening varies within the NAP and how structures existing in the subducting oceanic crust impact the overlying deformation styles in the NAP.

Additionally, for each seismic Profile A to E, the number of thrust faults, their spacing and dips were analysed and correlated with the roughness observed in the Horizon NanTroR and horizontal shortening quantified through this methodology (Table 2).

To quantify the critical taper angle of the Nankai accretionary prism from 2D seismic profiles, surface and basal slopes were measured from interpreted seismic lines that span the entire width of the outer wedge, from the frontal thrust to the forearc high of the NAP. The surface slope was defined by fitting a straight line to the upper envelope of the seafloor, while the basal slope was extracted from the landward-dipping décollement reflector. The sum of these two slopes represents the critical taper angle (Davis et al., 1983; Dahlen, 1990).

This approach is subject to several sources of uncertainty. First, if the seismic profile is oblique to the true dip direction, taper angle estimates may be underestimated due to geometric projection effects. Second, local structures such as thrust ridges or subducted topographic highs, such as seamounts, may distort both surface and basal slopes, inflating or suppressing the calculated taper. Third, uncertainties in the imaging of the décollement, especially in deeper or poorly resolved areas, can result in misinterpretation of its true geometry. Lastly, the assumption of a planar wedge geometry inherent to the critical taper model may not fully capture along-strike variations or 3D complexities within the wedge (Saffer & Bekins, 2002; Bangs et al., 2009). Despite these limitations, this method provides a consistent first-order approximation of taper geometry, which is useful for inferring basal friction and mechanical behaviour across the margin. Considerations have been taken to minimise some of the limitations:

- For each slope, a line connecting the seafloor/décollement at the forearc high to the seafloor/décollement at frontal thrust was drawn, this was used as an average line to measure the angle of the seafloor and the décollement with the horizontal. This aims to minimise the impact of asperities that could overestimate the critical taper to unrealistic values.
- If décollement is not well resolved in seismic at one of the above ends, then the closest well-defined décollement was used to draw the line mentioned above. This reduced errors around poorly resolved image and seismic misinterpretation.

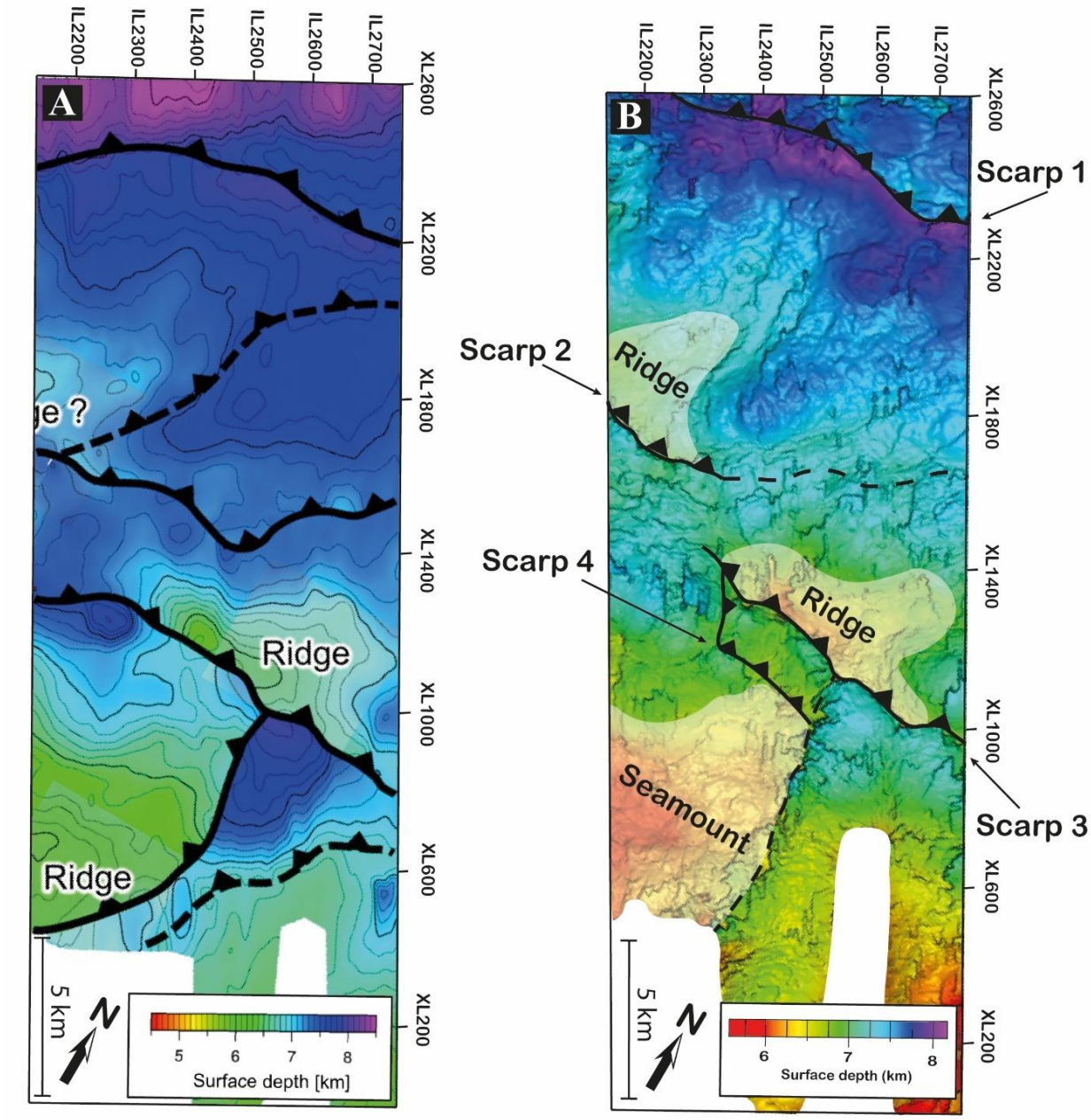

Figure 5.3 – A) Interpreted horizon of the top of the oceanic crust from Shiraishi et al. (2020), where the black lines with triangles denote reverse faults. B) Planar top view of Horizon NanTroR, representing the roughness of the décollement. Black lines with triangles delineate reverse faults where scarps and displacement are observed in the horizon and seismic data, respectively. Dashed black line delineates potential faults where scarps are visible in the horizon but displacement from seismic data is not clear. Shaded areas represent ridges or seamounts as identified.

5.4 Results

5.4.1 Roughness of subducted plate and décollement

Horizon NanTroR indicates a greater roughness of the basal décollement when compared to some of the older literature (e.g., Moore et al, 1990; Morgan et al, 1995; Ujiie et al, 2003; Ikari et al, 2011). The latter studies recognise the basal décollement as a sub-planar surface/volume below the NAP, gently dipping landwards, and showing a slight step-down near the Megasplay Fault Zone (MSFZ). In contrast, recent works by Moore et al. (2014), Boston et al. (2016), Azevedo et al. (2018) and Shiraishi et al. (2020) recognise a rougher subducting oceanic crust and corresponding basal décollement. Park et al. (1999) show evidence of a much more undulated basal décollement as a product of a rougher subducting oceanic crust, especially related to subduction of oceanic reliefs, such as seamounts. However, the latter study refers to the Muroto Transect, using 2D seismic profiles, making its comparison with our results challenging.

In this thesis, the 3D PSDM seismic interpretation shows minor, but important differences when compared to the results in Shiraishi et al. (2020), in great part due to the greater detail offered by this data (Figures 5.3A and 5.3B). Figure 5.3 reveals the morphology of the top of the subducting oceanic plate, dipping as much as 4 - 5° towards the NNW. It is possible to distinguish four WNW-trending linear structures dipping towards the N, with a 100° – 110° strike, and at least three structural highs identified as ridges or seamounts.

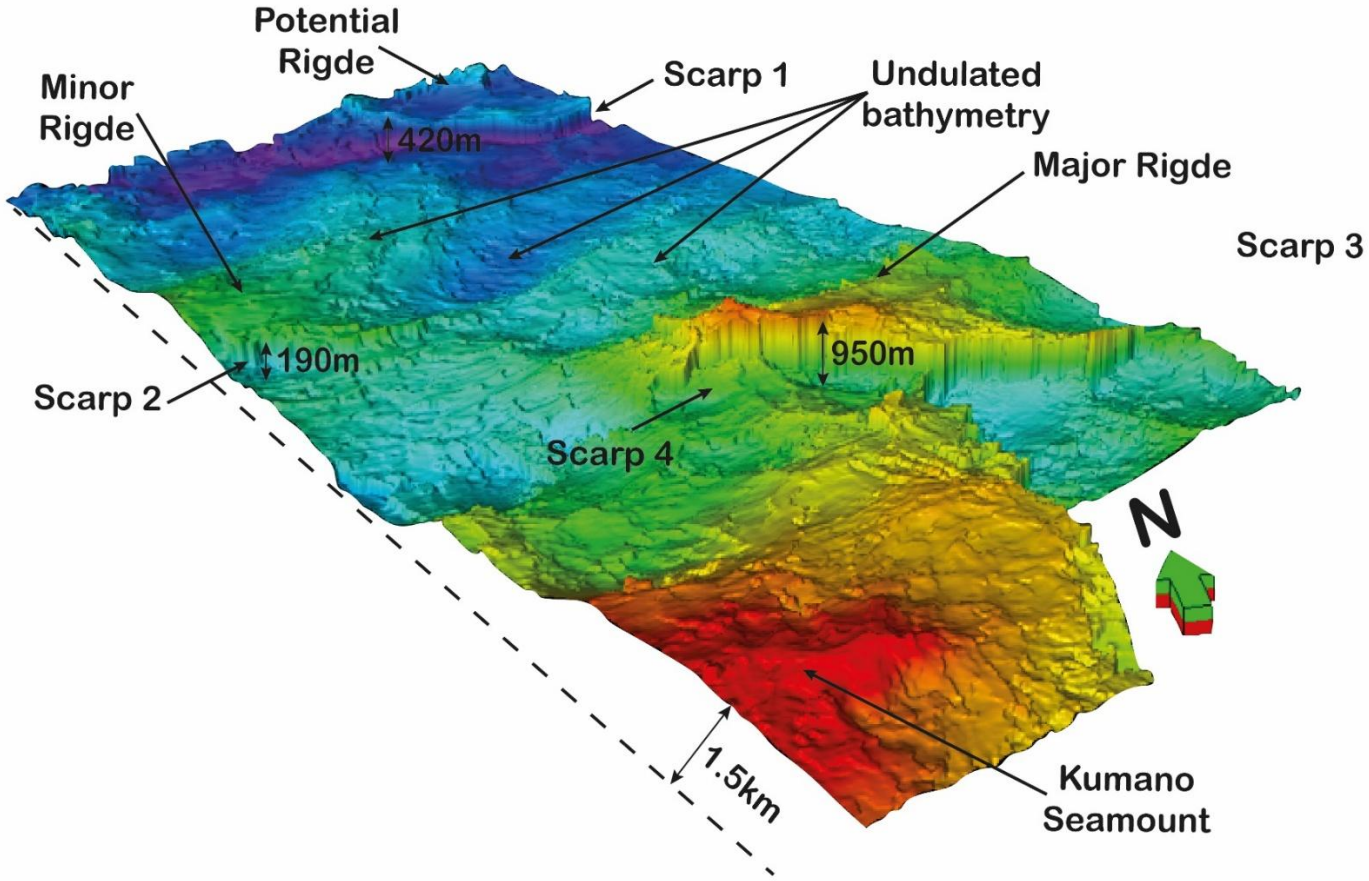

Figure 5.4 – 3D view of NanTroR, at an angle, with main bathymetrical features and quantification of their heights above the overall bathymetrical level.

The WNW-trending structure in the northmost part of the study area comprises a sub-vertical scarp with a relatively uniform displacement, revealing its upthrow side to the N and its downthrow side to the S (Scarp 1 in Figures 5.3B and 5.4). This fault scarp has a maximum height of 370 – 420 m. Further South, there another structure of similar geometry and kinematics (Scarp 3 in Figures 5.3B and 5.4) with a maximum height ranging from 850 – 950 m. Scarp 3 may continue further NW as per Shiraishi et al. (2020) but the seismic data does not show a consistent height difference in such a direction. South of Scarp 3, it is possible to observe a shorter, parallel Scarp 4 linking with the latter at its northwest end and abutting against a N-trending scarp to the SE (Figures 5.3B and 5.4). In addition, there is another fault scarp (Scarp 2 in Figures 5.3B and 5.4), which approximately follows the direction of previous scarps. Scarp 2 borders a ridge at its South side. Shiraishi et al. (2020) mapped Scarp 2 as extending further NE in the study area. Due to absence of a clear structure on Horizon NanTroR, a conservative approach was chosen as offset is not consistently observed further NE (Figure 5.3B). The N-S scarp observed in Figures 5.3B and 5.4 is in the Kumano Transect where seismic resolution is very low, and it is not possible to confirm the accuracy of the interpretation or the actual geometry responsible for this scarp.

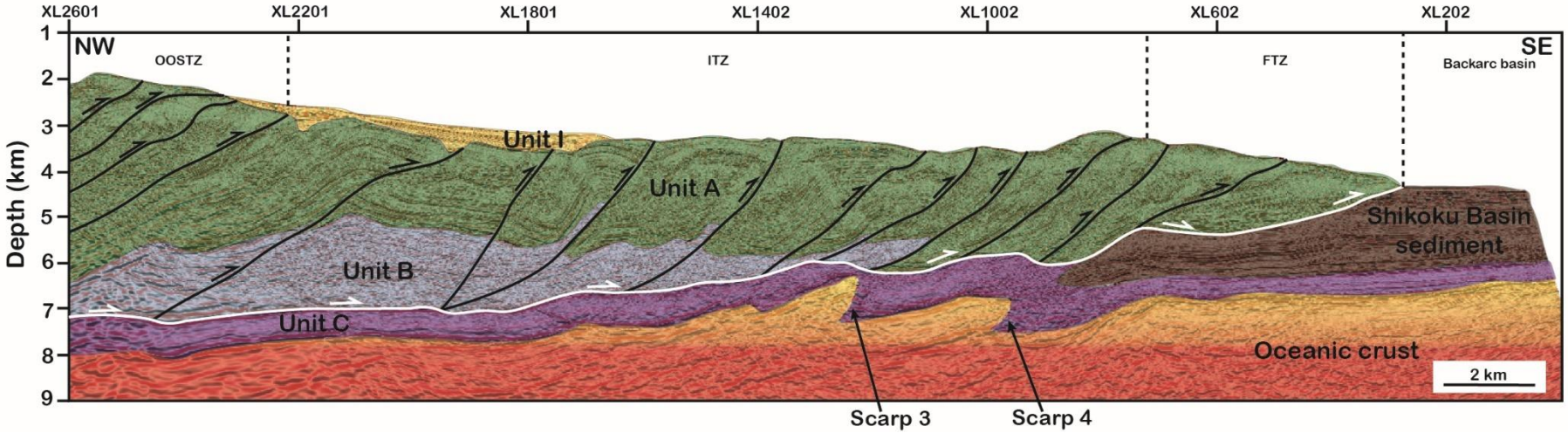

Figure 5.5 – Tectono-stratigraphic interpretation of seismic Profile C (see Azevedo et al., 2018). Black lines represent thrust faults within the NAP. White line represents the top of décollement (Unit C). The boundaries between Unit A, Unit C and Shikoku Basin sediment in the seawards part of the NAP (within the FTZ) are interpretational due to resolution of the seismic data.

Three bathymetric highs are observed in Horizon NanTroR (Figures 5.3 and 5.4) and have been identified as ridges by Shiraishi et al. (2020). The two highs to the North are limited by the WNW-trending Scarps 2 and 3 that resemble reverse faulting within the subducting oceanic plate due to their low gentle dip (Figure 5.5). In contrast, the southern 'high' comprises an irregular structure that is significantly larger than the other bathymetric highs: a 5 km wide (NE-SW), 8 km long (NW-SE) and 1.5 km high ridge (Figures 5.3B and 5.4). The southern ridge is bordered by a near vertical N-trending scarp. Due to its larger dimensions, this southern bathymetric high is identified as a seamount, herein named **Kumano Seamount** (Figure 5.3B). The remainder of the oceanic crust in the study area is depressed in relation to the structures previously described, recording a gentle WNW-trending undulation resembling an alternation between synform and antiform structures (Figure 5.4).

Detailed mapping shows that the basal décollement between Units B and C is sub-parallel to the Horizon NanTroR (Figure 5.5), following a similar morphology to this horizon, though relatively smoother. This reduced roughness of the basal décollement may be explained by (a) underplating of a weaker upper accretionary prism, masking some of the original structures on the subducting oceanic crust, or (b) the weight of the overlying sediment of the NAP compacting (i.e., smoothing) underlying structures (Morgan et al., 2004; Shiraishi et al., 2020). Additionally, the thickness of Units B (and C) increases landwards probably due to accumulation of underthrusted material (Figure 5A). The greater distance between the décollement and the top of the subducting oceanic crust

recorded landwards may explain the better "mirroring" of the structures from the subducting PSP on the décollement at its seawards section, as also suggested by Shiraishi et al. (2020) (Figures 5.6 and 5.7).

Figure 5.6 shows that the relative thickness of Unit C, and therefore the distance of the décollement above the top of the subducting oceanic crust, vary not just along the study area but also across it. There is an increase in the thickness of Unit C from SW to NE to a minimum of 12 – 17%. Moreover, the Kumano Seamount significantly impacts the thickness of Unit C. Unit C, in places, does not continue beyond the Kumano Seamount and the basal décollement possibly steps up into the FTZ (Figures 5.6 and 5.7). This phenomenon is not observed close to the northernmost highs in the study area.

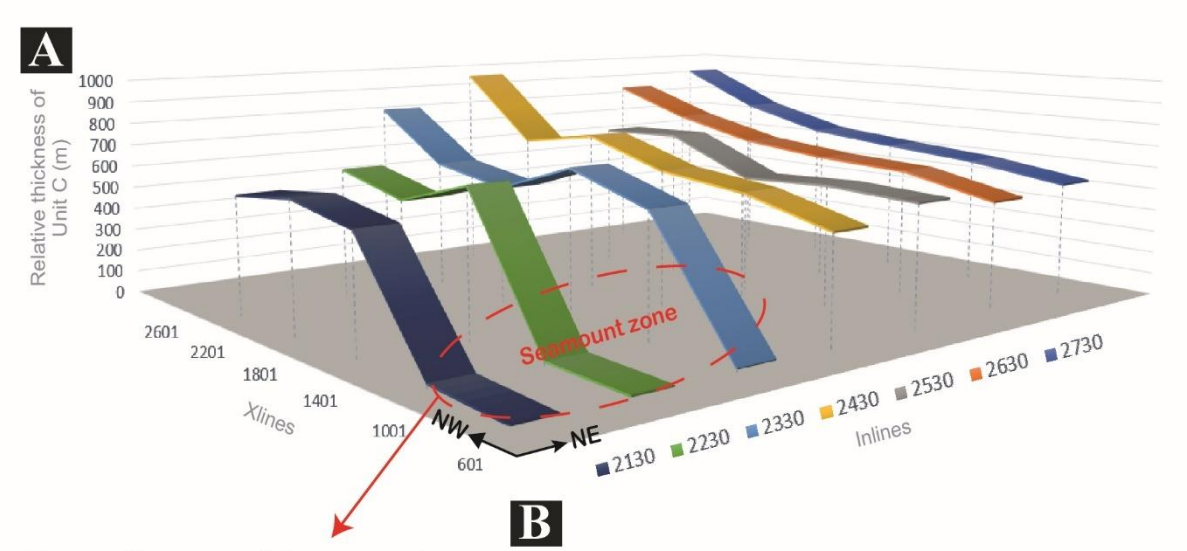

IL2130, IL2230 and IL2330 reach a minimum value of thickness for Unit C, meaning that, in theory, the décollement should be in contact (or close to) the oceanic crust. The seamount is the cause of this phenomenon, as in other ILs, away from the seamount, Unit C maintains its continuty and thickness.

B

IL \ XL	2601	2201	1801	1401	1001	601
2730	923	752	651	614	582	523
2630	847	720	632	594	577	493
2530	NR	679	694	537	556	540
2430	958	663	726	613	574	476
2330	809	586	531	670	557	12
2230	NR	602	525	643	22	5
2130	NR	534	580	523	30	2

Values in meters

Figure 5.6 – A) Graph showing the relative thickness of the tectono-stratigraphic Unit C relative to the top of the subducting oceanic crust, after being flattened on Petrel. These data were collected every 100 inline seismic profiles between inline profiles IL2130 and IL2730. This also represents the overall position of the décollement in relation to subducting oceanic plate. B) Table showing the measurements of distance décollement and the underlying oceanic plate conducted on each seismic inline. NR - No resolution for accurate measurement.

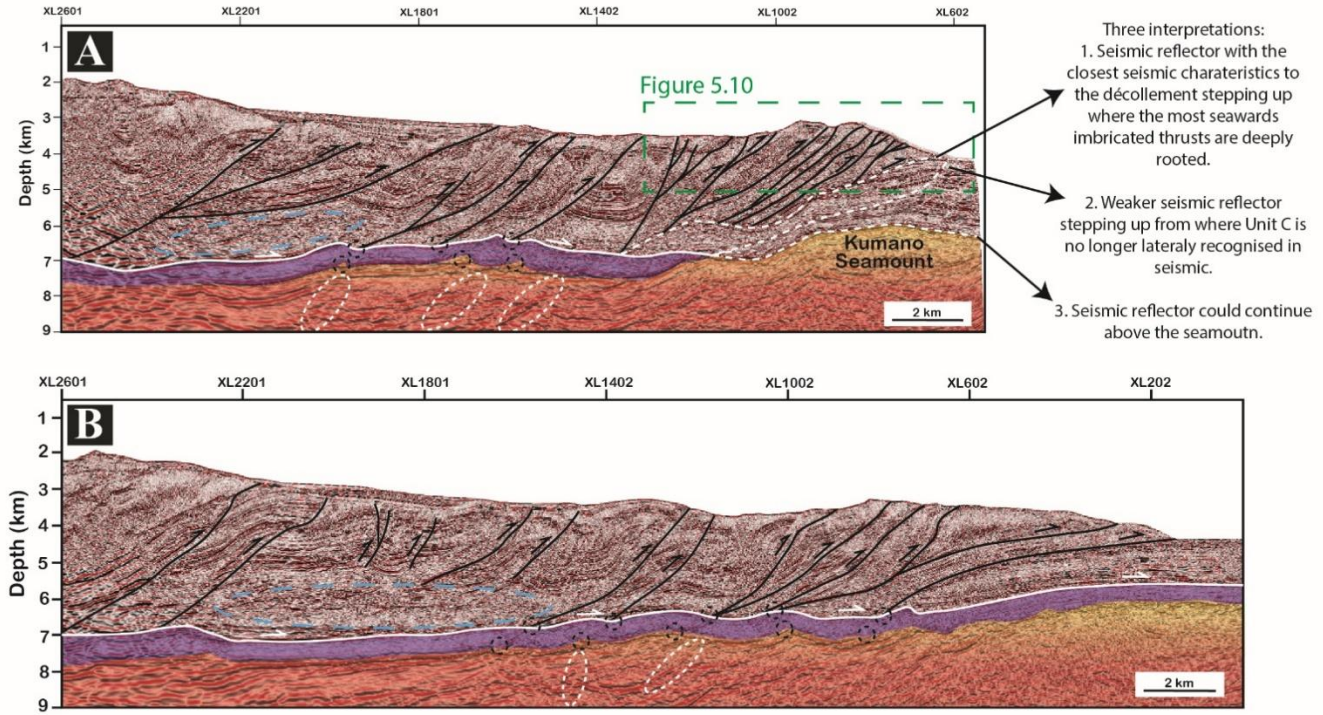

Figure 5.7 – A) Seismic inline IL2200 showing the subduction of the Kumano seamount identified in Figures 3B and 3C. There is a greater thrust fault density and dip accompanied by an uplift of the frontal part of the NAP. B) Seismic inline IL2720 showing the NAP structure in the smoother section of the subducting oceanic plate. The green rectangle delineates the close-up showed in Figure 5.10. Black lines - main thrust fault; White line - décollement; Red/Yellow area - Oceanic Plate; Purple area - Unit C; Dashed blue oval - area of Unit B is thickened and where resolution is low with several undulated seismic reflectors resembling potential shearing and ductile regime; dashed white oval – areas within the subducting oceanic crust where seismic reflectors seem to be displaced or a has strong reflector with similar direction to thrust faults; small dashed black circles – showcasing proximity of between irregularities in the oceanic crust and nucleation of faults.

5.4.2 Structural horizontal shortening

Table 1 shows an estimate of the overall horizontal shortening along NAP and in its distinct structural sectors, showing differing results from the shortening values calculated for the Muroto Transect (Moore et al., 2011). The comparison between the overall deformed and restored lengths for the entire NAP shows little variation when comparing the seismic Profiles A to E, varying between 29% and 32%, which corresponds to 10 km to 14 km of horizontal shortening, respectively. Although the overall horizontal shortening does not vary significantly between seismic Profiles A to E, the same is not observed between different structural sectors of the NAP in the studied profiles, where horizontal shortening is greater in the North sector when compared to the South sector, near the Kumano Seamount. It is also important to note that although the overall horizontal shortening does not vary significantly across the study area, Profile A images a much shorter seismic section of the NAP, which could incur in underestimations of shortening in such a profile (see Figures 5.7A and 5.7B for comparison).

Table 1 – Horizontal shortening for five seismic profiles (Figure 5.1) using the area balancing restoration framework described in Figure 5.2. The table shows the values for the difference between the deformed length (measured from seismic profiles) and the restored length (measured after area balancing restoration) for the overall NAP and individual sectors. Relative shortening proportion refers to the contribution of shortening of each named sector to the overall shortening of the NAP. * Profiles D and E barely have any S sector, so shortening along the S sector in these profiles could be ignored.

Profile	Sector	Deformed length (km) dL	Restored length (km) rL	dL - rL (km)	Relative shortening proportion	Horizontal shortening
A	NAP	24.89	35.2	10.31	N/A	29%
	FTZ	6.52	11.5	4.98	48%	43%
	ITZ	18.24	23.74	5.5	52%	23%
	North	11.52	15.11	3.59	36%	24%
	South	13.71	20.2	6.49	64%	32%
B	NAP	26.9	38.68	11.78	N/A	30%
	FTZ	6.85	9.5	2.65	22%	28%
	ITZ	19.91	29.15	9.24	78%	32%
	North	15.27	21.77	6.5	54%	30%
	South	11.46	16.9	5.44	46%	32%
C	NAP	28.9	40.9	12	N/A	29%
	FTZ	5.86	8.7	2.84	24%	33%
	ITZ	23.15	32.15	9	76%	28%
	North	18.99	28.02	9.03	76%	32%
	South	10.05	12.92	2.87	24%	22%
D	NAP	29.38	41.93	12.55	N/A	30%
	FTZ	7.53	8.37	0.84	7%	10%
	ITZ	21.65	33.57	11.92	93%	36%
	North	20.25	30.98	10.73	85%	35%
	South	9.16*	10.98*	1.82*	15%*	17%*
E	NAP	30.61	44.75	14.14	N/A	32%
	FTZ	7.61	8.28	0.67	5%	8%
	ITZ	23.16	36.35	13.19	95%	36%
	North	21.98	34.22	12.24	86%	36%
	South	8.59*	10.53*	1.94*	14%*	18%*

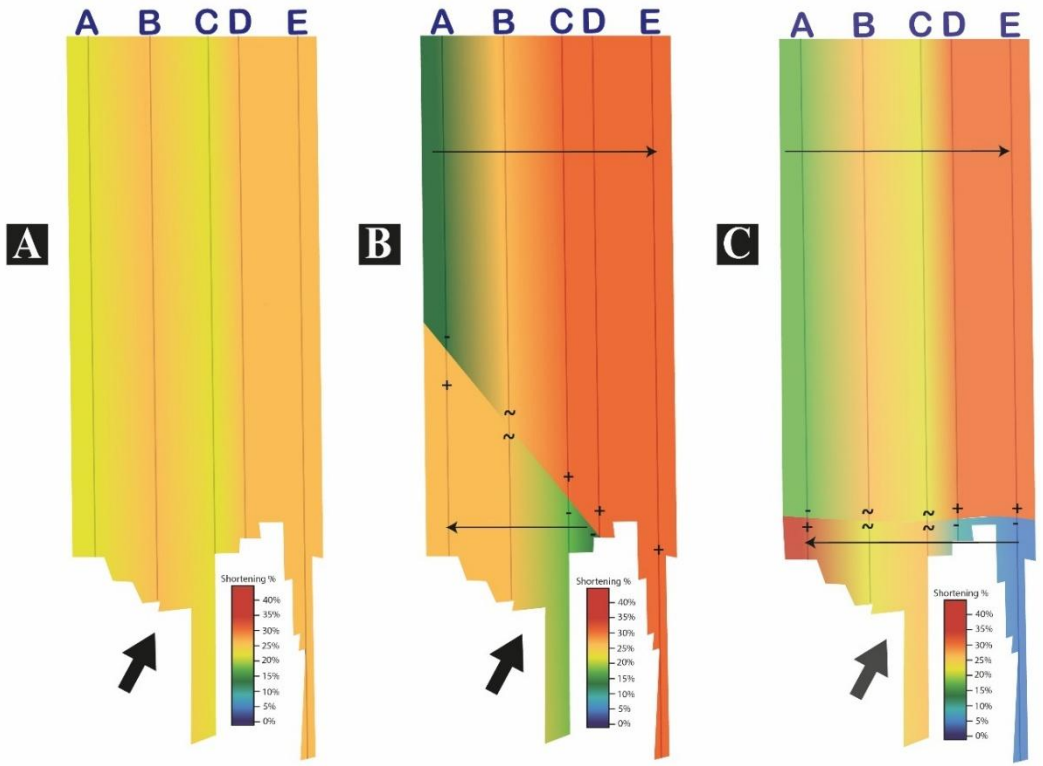

Figure 5.8 - Visual aid showing spatial variation of horizontal shortening within the study area. A) overall horizontal shortening in the NAP, showing an overall constant horizontal shortening at ~30%. B) horizontal shortening in the N and S sectors of the NAP, showing an overall increase in shortening towards the E in the N sector and towards the W in the S sector. C) horizontal shortening in the FTZ and ITZ of the NAP, show a similar trend with ITZ increasing its shortening towards the E while FTZ increases its horizontal shortening towards the W. black arrows – showing trend of increase in each section; +, - or ~ - showing the boundary difference between horizontal shortening as higher, lower or similar, respectively.

Area balancing restoration shows variations in horizontal shortening in different sectors of the NAP, in particular between the FTZ and ITZ (Figure 5.8C), and the limit between the North and South sectors. The FTZ shows broader variation in the horizontal shortening: 8% to 43%. The FTZ in profiles A, B and C present greater horizontal shortening (43%, 28% and 33%, respectively) than profiles D and E (10% and 8%, respectively). In contrast, the ITZ records a more consistent horizontal shortening ranging between 23% and 36%. The proportional contributions of the FTZ and ITZ to the overall horizontal shortening of the NAP also shows significant differences. The FTZ contributes less to the NAP's horizontal shortening than the ITZ. Horizontal shortening in the FTZ ranges from 48% to 5%, decreasing from Profile A to E, while in the ITZ varies between 52% and 95%, increasing from Profile A to E. Therefore, the study area records two distinct patterns here: (a) most of the horizontal shortening is consistently accommodated by the landward part of the outer wedge, the ITZ, compared to its seawards counterpart, the FTZ; and (b) horizontal shortening in the FTZ sharply increases towards SW, showing its greatest shortening proportion near the Kumano Seamount.

Horizontal shortening values for the North and South sectors of the NAP (Figure 5.8B) reveal more complex patterns of variation. The South sector of the NAP shows horizontal shortening varying from 22% to 32%, whereas the North sector shows shortening values varying between 24% and 36%. The data suggest that the North sector is more deformed (shortened) than the South sector, apart from Profiles A and B. When comparing the relative contribution of

each of these sectors to the overall shortening of the NAP, it is possible to also identify interesting patterns later debated in this chapter. In Profiles B, C (D and E) horizontal shortening is significantly greater in their North sector compared to their South sector: 54% vs 46% in Profile B; 76% vs 24% in Profile C (85% vs 15% in Profile D; and 86% vs 14% in Profile E). However, this pattern is not evident in Profile A, where the South sector presents a greater shortening proportion of 64%. Therefore, the data records some important aspects, such as the horizontal shortening between N and S sectors not being significantly different and could potentially be very similar when considering underestimations related to the methodology used. However, Profile A reveals an anomalous significant amount of horizontal shortening of its S sector compared to the N sector (note that this is the sector and profile closest to the Kumano Seamount). Additionally, the North sector seems to consistently accommodate a higher proportion of the overall horizontal shortening experienced by the NAP.

5.4.3 Quantitative analysis of thrust faults

The quantitative data presented in Table 2 stress the relating overall increase in the number of main thrust faults towards the SW, with the largest number of faults (16) being recorded in Profile A. However, the North and South sectors record opposing patterns, where the North sector records a gentle increase in thrust faults towards the NE (away from the Kumano Seamount)

whereas the South sector presents an increase of thrust faults towards the SW (closer to the Kumano Seamount) (Table 2). It is important to note that, due to the geometry of fault F1 (Figures 5.1), the North and South sectors are not always the same proportion in each of the seismic profiles A to E, which could lead to the difference in the number of thrust faults observed. Nevertheless, the recorded sharper increase in faults observed in the South sector would not be justified by the latter. In summary, Profile A, intersecting the Kumano Seamount, records a maximum number of thrust faults of 16, which is clearly above the average for the study area of 12.6.

To aid further discussion, it is also important to consider the spacing between thrust faults, not only in the entire NAP, but also within the North and South sectors, for each of the profiles A to E. Thrust spacing records patterns in the deformation styles of the NAP that are not influenced by the spatial dimension of the North and South sectors, but by the roughness of the subducting PSP. The data shows an increase in the number of thrust faults per km towards the SW with both the North and South sectors recording an overall decrease in thrust spacing in this same direction. However, the South sector presents closer proximity between thrust faults with an average of 0.6 thrusts every km whereas the North sector records an average thrust spacing of 0.3 thrusts/km. It is also important to note that the South sector shows a more consistent and sharper decrease in thrust spacing, where it is expected to find a main thrust fault every 1.25km in Profile A (closer to the Kumano Seamount).

Table 2 – Quantitative analysis of main thrusts from seismic data. The table shows data on number of main thrusts in the overall length of the accretionary prism, the average number of thrust faults per km and average dip of thrusts for the overall NAP and its North and South sectors for each of the five interpreted seismic profiles (Figure 5.1). S2 – Scarp 2; S3 – Scarp 3.

Profile	Structures (Roughness of décollement)	Number of main thrusts			Thrust spacing (thrusts per km)			Average dip of main thrust faults (°)		
		Overall	N sector	S sector	Overall	N sector	S sector	Overall	N sector	S sector
A	Kumano Seamount	16	5	11	0.64	0.43	0.8	41.38	43.2	43.27
B	S2+3 + Kumano Seamount	13	5	8	0.48	0.32	0.7	37.23	42.2	42.36
C	S2+3 + N-S scarp	11	5	6	0.38	0.26	0.6	39.91	43.4	35.17
D	S2+3	11	7	4	0.37	0.35	0.43	36.27	40.14	29.5
E	S2+3	12	8	4	0.39	0.36	0.46	33.92	35.13	31.5

Another important characteristic not affected by the spatial dimensions of the seismic data is the dip of the thrust faults previously identified. There is an increase in the angle of thrust faults towards the SW in both the overall NAP and both its North and South sectors for each profile A – E. Although, on average, the North sector presenting have a greater average dip of 41º compared to the South sector with an average of 36º, the South sector experiences a sharper increase (from 31.5º to 43.3º) in dip towards the SW compared to the North sector (from 35º to 43.2º). In summary, Profile A shows an average thrust-fault dip of 41.4º, which is significantly higher than the average 36.8º for the study area.

5.4.4 Seismic evidence for fluids and seismic characteristics of Unit B

Figure 5.9 focus on characterising the seismic characteristics of along three seismic crosslines and one seismic inline with the intuit of recognising and understanding how basal asperities influence fluids and gas flow, especially from the underlying tectonostratigraphic units to the overlying NAP as well as how basal asperity impacts both the seismic characteristics of Unit B (and Unit C) and the deformation of the NAP, especially in southernmost sector of higher asperity.

One striking feature observed in the 3D seismic is located along the WNW-trending left-lateral F1 fault or belt. This area consistently showcases lower seismic resolution characterised by highly chaotic and disrupted reflectors with either continuous or discontinuous bottom simulating reflectors (BSR) on top, usually sitting at 600-700m below the seafloor (Figures 5.9 and 5.11). The more displaced the oceanic crust reflectors are (e.g. Scarps 3 and 4) the more chaotic and widespread the area surrounding F1 is. It is also possible to identify several other areas of highly chaotic and disrupted reflectors:

- Along some thrusts in the ITZ cutting through Unit A and well connected to Unit B.
- Along frontal thrusts in the FTZ and especially, above the strong reflector interpreted as a potential stepped-up of the décollement as this reflector shows similar acoustic characteristics as the generally recognisable décollement in its landward limit.
- At the landward limit of the ITZ in the transition between the ITZ and the MSFZ.

Despite chaotic acoustic areas, it is also possible to observe several other variations in the acoustic amplitude of the seismic data, such as a consistent dimmed (low amplitude) band at the top of Unit A as well as BSRs, normally located in the bottom limit of these low amplitude areas (see IL2150 in Figure 5.9).

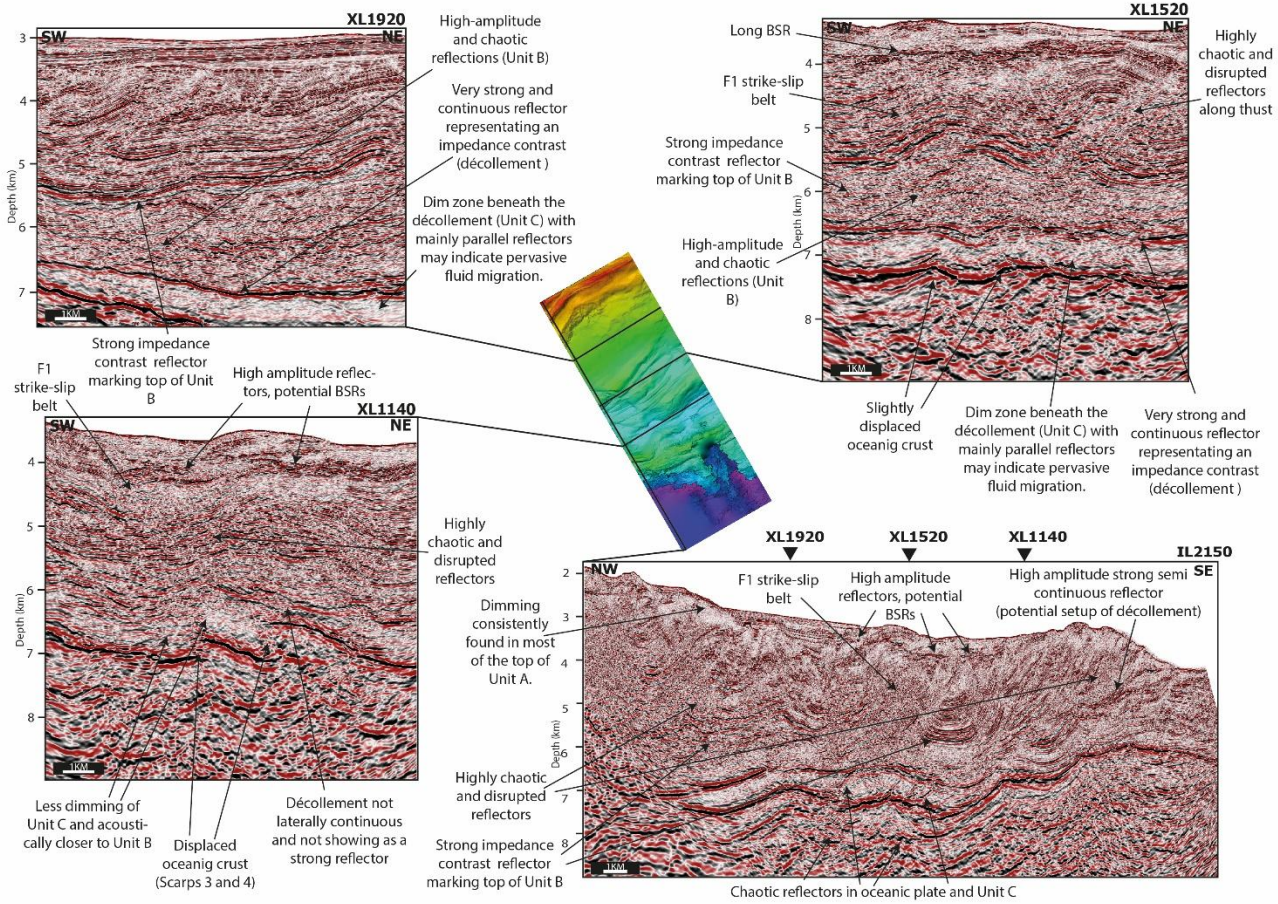

Figure 5.9 - Annotated seismic profiles with seismic characteristics of tectonostratigraphic units and key seismic indicators of fluid movement and/or accumulation.

The décollement is identified as a predominately continuous strong (high amplitude) reflector: (1) overlying a fairly consistently very dimmed (low amplitude) 500-550m thick with reflectors parallel to the strong reflectors marking the décollement (above) and the oceanic plate (below); (2) underlying a Unit B that is variable in thickness, both along and across strike, and that is represented also as chaotic area of disrupted high amplitude and curved short reflectors within a dimmed mesh. As both units are stratigraphically similar and described as Lower Shikoku sediments (see Chapter 2), the acoustic difference between the two probably relates to compaction and porosity, where Unit C undergoes longer and greater burial compaction as it subducts, reducing pore space and homogenising its physical properties which explains the more consistent dimming and parallel reflectors. Acoustically, Unit B seems to be composed of a matrix like Unit C mixed with short and curved high amplitude reflectors, which may suggest active deformation occurring here. These findings provide new insights into the origins of Unit B that deserve to be discussed later in this Chapter.

Unit C's dimness increases landwards and becomes increasingly more distinct from Unit B towards that same direction; this could be related to the increased lithostatic compaction from the growing vertical load caused by the accretion of the overlying Unit A (and B) (Tsuji et al., 2011). Although Unit B thickens towards the rear of the NAP, this tectonostratigraphic unit is not clearly recognised South of F1 strike-slip fault zone and its thickness vary along strike, being thinner in the sections overlaid by chaotic reflectors associated with either F1 or thrusts, pointing these faults towards being important venting pathways

for fluids (Taira and Pickering, 1991). Additionally, in areas above and immediately surrounding main basal asperities, such as Scarps 3 and 4 (see XL1140 in Figure 5.9) and the Kumano Seamount (see IL2150 in Figure 5.9), distinguishing Units B from C is problematic either due to Unit C becoming acoustically similar to Unit B (less dimming and more chaotic) or because one or both units are not resolved. In the sector N of F1, Unit B's across-strike continuity is better preserved with gradual thickening towards the rear of the NAP (landwards).

5.4.4 Critical taper angles and observed seismic features in the FTZ

Determining the critical taper angle (α + β) from the slope of the surface of the accretionary wedge (α) and the slope of décollement (β) is fundamental to understanding the mechanical state and evolution of accretionary wedges such as the NAP. The critical taper theory provides a framework for assessing how the prism maintains mechanical equilibrium between internal strength, basal friction, and topographic slope (Davis et al., 1983; Dahlen, 1990). By quantifying taper, it becomes possible to infer variations in basal friction and pore fluid pressure along the décollement, which directly affect the style and distribution of deformation within the wedge. A low critical taper often indicates high pore fluid pressure or low basal friction, promoting stable sliding and distributed strain, whereas a high taper suggests increased coupling and more localised thrusting. These relationships are essential for interpreting the balance between

accretion and erosion, the likelihood of slow slip events, and the spatial distribution of seismic hazard (Saffer & Tobin, 2011). Moreover, comparing taper angles across transects allows for the evaluation of how subduction inputs, such as incoming sediment thickness and basal bathymetry control wedge morphology and seismogenic behaviour.

The results show clear along-strike variability, which is interpreted considering local structural complexities, notably the presence of subducting asperities beneath profiles A and B. Across the five profiles, the total taper (α + β) of the entire outer wedge ranges from 9.53° (Profile E) to 13.01° (Profile A), indicating moderate variability (3.48°) (Table 3 and Figure 5.9). Notably, Profile E, located in a more typical accretional and sediment-dominated section without basal oceanic asperities, exhibits the lowest taper. In contrast, Profile A, which overlies a subducting seamount, has the highest total taper, consistent with localised steepening of both the surface slope and basal décollement.

The mean values for surface slope (α) and basal dip (β) across all profiles are 5.37° and 4.04°, respectively, for a mean whole-wedge taper of 9.41°. However, this average conceals significant internal variation that becomes evident upon examining sub-wedge segmentation. Given the presence of a subducting seamount in profiles A and B (Figure 5.9), the wedge displays geometric and potentially mechanical segmentation. Therefore, the 'critical taper' was assessed separately in frontal and rear domains of the outer wedge to acknowledge the impact of basal asperities on local wedge geometry and stress state.

Despite the overall south-westwards increase in the average wedge taper (from Profile E to Profiles A), Profiles A and E also exhibit pronounced differences between frontal and rear wedge taper. In Profile A, the frontal α + β reaches 26.99°, which is >2× the rear wedge value (9.18°). A similar pattern is seen in Profile B, where frontal taper is 20.8° and rear taper is 11.25° (Table 3 and Figure 5.9). This suggests frontal wedge overlying subducting seamounts is locally over steepened, likely due to uplift of the décollement, consistent with previous work (Wang & Hu, 2006), which identified that seamount subduction can cause localised thickening and steepening of the frontal wedge through underplating or toe uplift. In contrast, Profile E, which lack significant basal anomalies, show much smaller differences between frontal and rear tapers, supporting the interpretation of a more uniform wedge in these sections.

The results clearly demonstrate that a single average taper angle is insufficient to represent wedge geometry in regions affected by subducting bathymetric asperities. Instead, local critical taper conditions vary markedly along strike, particularly in response to subducting seamounts that alter both frontal wedge geometry and basal detachment geometry. These findings support a locally segmented critical taper model in Nankai, where frontal and rear domains of the outer wedge may respond differently to basal forcing and material input.

Table 3 - Values of slope of the surface of the accretionary wedge (α), the slope of décollement (β) and critical taper angle (α + β) measured from seismic profiles A – E as per Figure 5.10. Values in degrees (°)

	α	β	α + β	β Frontal section	α + β	β Rear section	α + β
Profile E	5.49	4.04	9.53	10.05	13.57	0.69	4.73
Profile D	4.68	5.69	10.37	10.88	16.06	2.71	8.4
Profile C	5.18	5.74	10.92	9.88	16.66	3.06	8.8
Profile B	4.42	8.19	12.61	18.38	20.8	3.06	11.25
Profile A	4.44	8.57	13.01	18.42	26.99	0.61	9.18

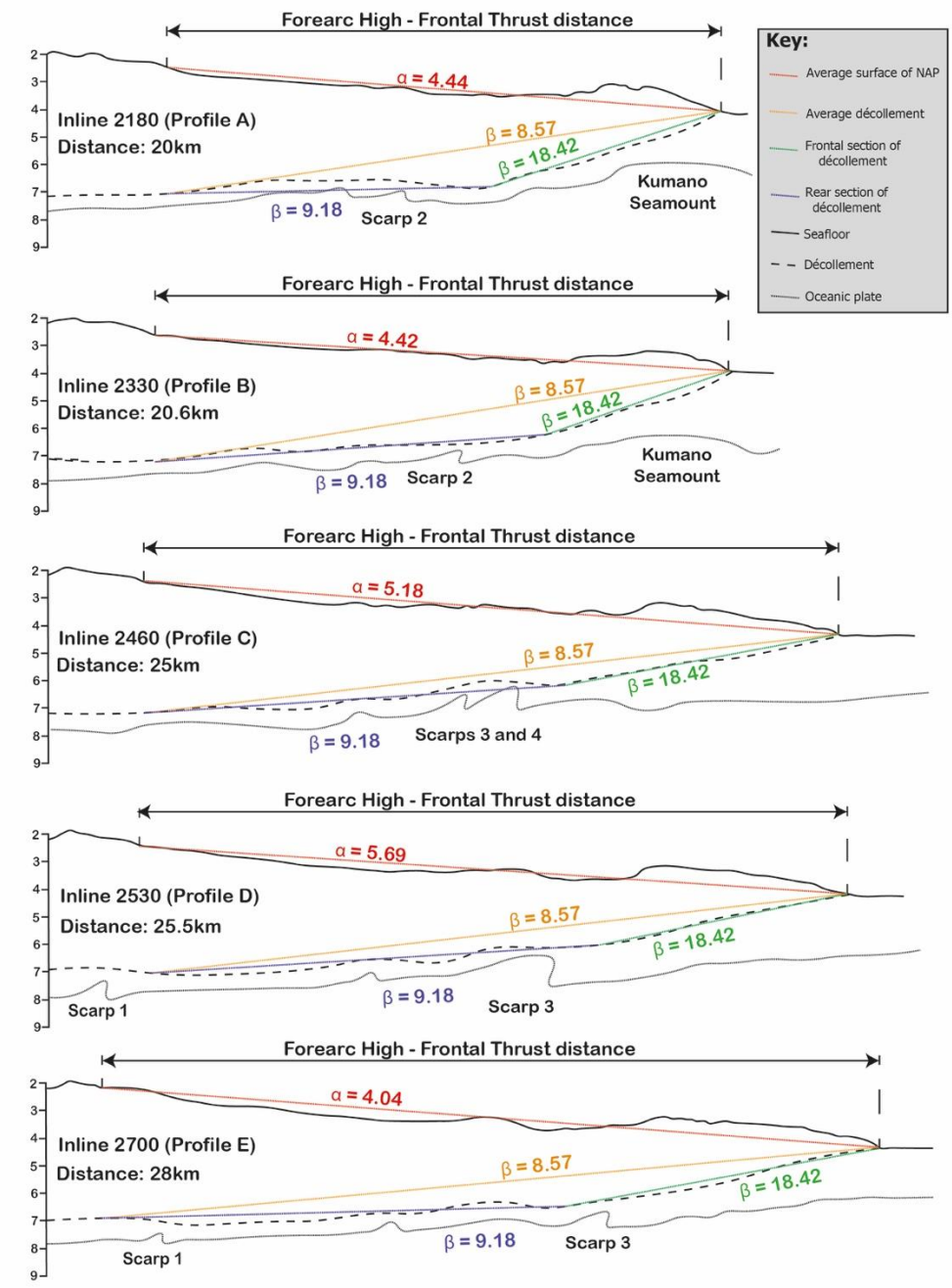

Figure 5.10 - Bathymetric tracks of the outer wedge of the NAP from seismic profiles A to E. Distance from forearc high to the frontal thrust decreases from N to S while the average slope angle does not change significantly. However, in Profile A, crossing the core of Kumano Seamount, the average slope angle is the highest. The slope angle at the FTZ seems to be more impacted by the presence of the Kumano Seamount, increasing from N to S.

5.5 Chapter-specific discussion

5.5.1 Effects on fault nucleation and stress distribution

In the study area, the Kumano Seamount is being subducted under the NAP in the southern part of the study area. This inherited structure, together with other basal asperities identified in the subducting oceanic crust and also affecting the décollement (such as scarps S1 and S2 and other undulating features) will locally increase stress coupling between the subducting and overriding plates (Park et al., 2009), affecting local seismicity (VLFE and SSE well documented in the area, especially near the South sector just north of Seamount and scarps - see Yamamoto et al, 2022; and Takemura et al., 2023) as well as the deformation of the overlying NAP. This localised increase in mechanical coupling between the subducting and overriding plates enhances interplate friction, promoting localised stress accumulation and mechanical abrasion at the plate interface (Clift and Vannucchi, 2004). These zones of elevated stress can inhibit efficient drainage of pore fluids, leading to a buildup of fluid pressure in the basal interface (Park et al., 2002). Where pore fluid pressures approach lithostatic values, the effective normal stress on the megathrust is reduced, weakening the fault zone, and potentially facilitating basal erosion (Wang et al., 2010). In this context, inherited roughness may not cause basal erosion but instead creates the mechanical and hydrological conditions that make erosional or non-

accretional subduction more likely. In accretion-dominated margins such as the Nankai Trough, unusually high pore fluid pressures are thus a necessary but not sufficient condition for erosion to occur and are closely linked to the degree of plate interface roughness. Asperities, such as the Kumano Seamount and ridges identified in the study area, although not significant enough on their own to slow down the subduction they will resist the seawards growth of the NAP. Findings from this chapter could therefore be extrapolated to other parts along the Nankai Trough or other subduction margins where roughness is significantly higher from either presence of much larger asperities or higher asperity density in subducting plate. In such scenarios, slowing subduction movement generates spatial and temporal variations in stress conditions that could relate to the variation of erosive vs accretional behaviour along the Nankai Through. On the smaller scale of our study area, where fewer and smaller basal asperities are present, features such as vertical scarps and subducting seamounts (e.g. the Kumano Seamount) can locally modify deformation patterns in the overlying accretionary prism. These subducting features can act as mechanical irregularities that generate zones of stress concentration, leading to localised thinning or thickening of tectono-stratigraphic Units B and C, particularly to the southwest of the study area (Figure 5.6). While such asperities do not significantly alter the overall subduction rate or direction (Kelleher and McCann, 1976), they can disrupt the uniformity of strain accommodation, promoting fault reactivation, strike-slip deformation, or crustal tearing in the overriding plate (Park et al., 2009). This mechanism may explain the development strike-slip F1 from Scarps

1 to 4 (Figures 5.3 and 5.4), which borders the Kumano Seamount and trend similarly.

Due to the limited geographic span of the interpreted seismic data, it is not possible to precisely characterise the mechanisms responsible for the mapped scarps 1 to 4 (Figures 5.3 and 5.4). However, it is still possible to suggest three possible causes:

- Inherited asperities originated during early tectonic phases of the Shikoku Basin's evolution, possibly during its NNW–SSE or later NW–SE opening stages (Okino et al., 1999). These inherited faults may now be reactivated due to plate bending, increased coupling at the plate interface, and interaction with basal asperities like the Kumano Seamount. Such reactivation may explain the close association between oceanic plate irregularities and the nucleation of deeply rooted structures, including both thrust and strike-slip faults (Figures 5.5 and 5.7). However, the mapped scarps (Figures 5.5 and 5.7) do not seem to fit the characteristics of any family of asperities discussed in Chapter 1 (Okino et al., 1999; Kodaira et al., 2000).
- Tear faults from regional or local segmentation of the subducting sla, possibly triggered by subducting bathymetric highs like seamounts (von Huene et al., 2004; Wang and Bilek, 2011). Scarps 1–4 fit this category, as they are near-vertical structures oblique to the trench, offsetting the NAP's fold-and-thrust structures. Notably, the strike-slip

Fault F1, which branches from Scarps 2 and 3, appears to divide the study area into two distinct structural domains (Chapter 4), and may connect with potential out-of-sequence (OOS) thrusts (Figure 5.11).

- Newly formed (or re-activated) thrusts that dip landward and branch from or merge with the décollement. They offset both the oceanic crust and the overlying NAP, similar to structures circled in Figure 5.5. These features may propagate upward into the prism or connect with established thrusts (Moore et al., 2001; Saffer and Bekins, 2002).

A combination of the last two scenarios is reasonable for the study area, where near vertical tear faults within the subducting plate develop planar weaknesses that influence the patterns of deformation on the overlying NAP while the formation of new faults or re-activation for pre-existing will displace and deform the NAP above. Altmann et al. (2014) suggested that locally enhanced stress coupling and shear stress can be significantly high values to reactivate any pre-existing inherited faults that may exist in the subducting plate and generate new faults at the border of subducting basal asperities that will deforming the overlying accretionary prism and promoting further subduction (Figure 5.11).

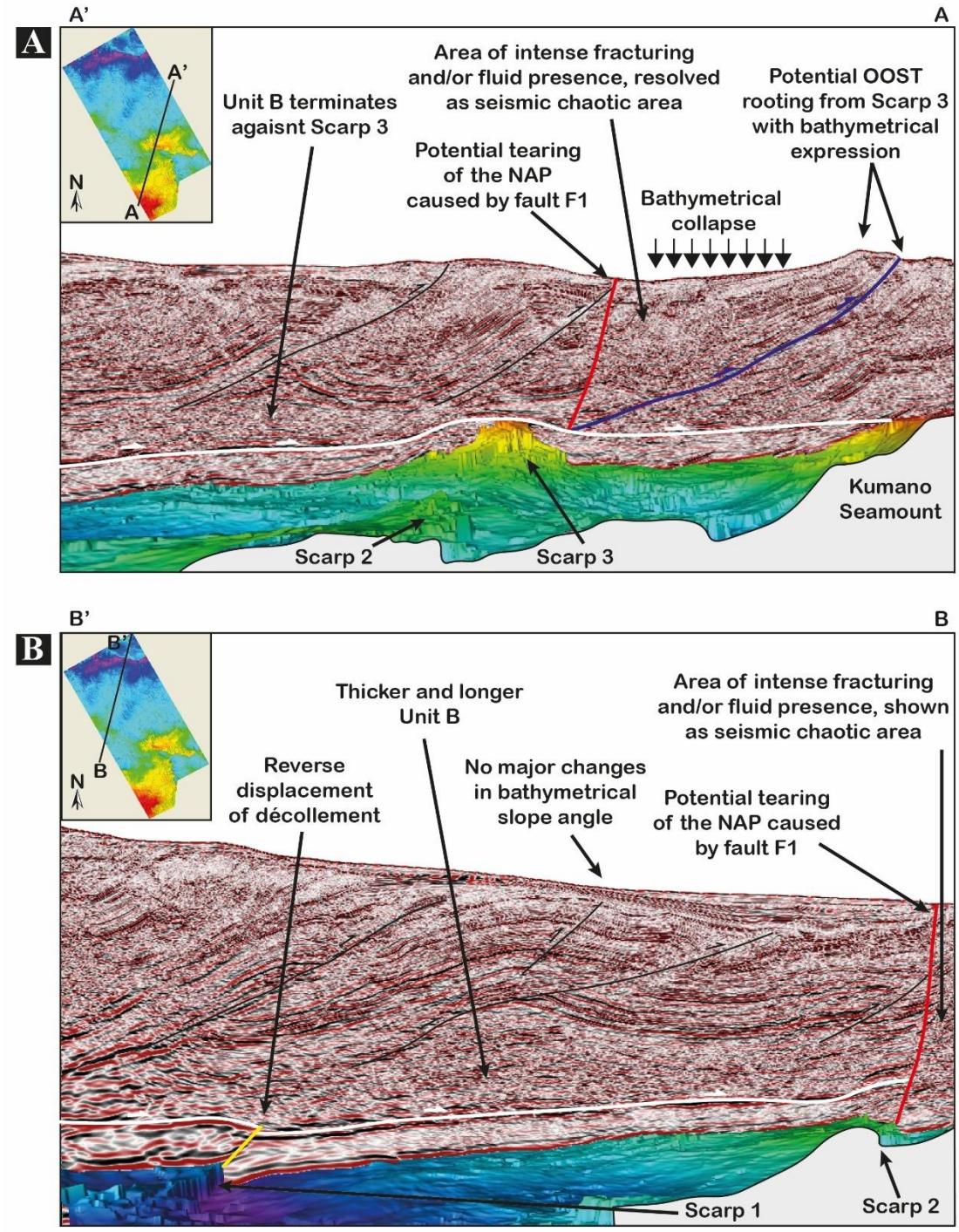

Figure 5.11 - Annotated seismic profiles with NanTroR horizon representing the roughness of the subducting plate, with inset showing the direction of profile observed. A) Seismic profile crossing rougher section of the oceanic plate with the Kumano Seamount and considerable seized ridge, Scarp 3. Scarp 3 seems to nucleate an OOOS thrust that intersects the entire NAP, with bathymetrical expression. The lower oceanic basement between Scarp 3 and Kumano Seamount is accompanied by a lower bathymetry, causing changes in slope angle. B) Smoother oceanic crust with only Scarp 1 that seems to displace the décollement. This seismic profile shows a more regular imbrication of thrust faults that seem to be coherent with ITZ described in the NAP. In both figures, the fault F1 (red) shows two very different deformation in the N (to the left of F1) and S (to the right of F1) sectors.

Although the overall subduction rate of the PSP is governed by large-scale plate motions, the presence of asperities such as the Kumano Seamount introduces mechanical heterogeneity along the plate interface. These heterogeneities do not alter the subduction rate itself but can lead to spatial variations in strain accumulation and deformation patterns within the overriding accretionary prism. As a result, segmentation of the Nankai Trough may arise, not due to changes in convergence velocity, but because of localised variations in mechanical coupling and stress transfer along the megathrust.

In this context, tearing faults may nucleate in response to the localized stress perturbations induced by subducting asperities. These structures accommodate differential deformation between regions with contrasting coupling conditions or structural architecture. Fault networks associated with slab tearing often evolve into complex systems of strike-slip structures (Bertone et al., 2020). These networks typically initiate as disconnected linear segments, which deform and propagate independently in response to stress accumulation along the subduction interface. Over time, they link and mature, resulting in the fault architecture currently observed in the NAP.

This model explains the development of Fault F1, a right-lateral strike-slip fault, and the broader partitioning of deformation observed across the study area (Azevedo et al., 2018). In particular, the inferred reactivation and upward propagation of Scarps 2 and 3 may have contributed to the initiation of Fault

F1, which appears to accommodate differences in strain localisation between the northern and southern sectors of the NAP.

Supporting evidence comes from the 2004 Kii Peninsula earthquake sequence, where epicentre clusters followed a NW–SE trend (Miyoshi and Ishibashi, 2005), consistent with the presence of deep fault zones like those proposed here. Comparable multi-segmented fault networks and tearing structures have been reported in other tectonic settings (e.g., Ambraseys and Tchalenko, 1969; Magistrale and Day, 1999; Rosenbaum et al., 2008), reinforcing this interpretation.

5.5.2 Effects on Unit B (and C) and fluids

Basal asperities being areas of elevated mechanical coupling between the subducting and the overriding plates that can affect stress distribution and strain accumulation means that they are able to locally seal or compartmentalise fluid pathways (Moore & Saffer, 2001; Saffer & Tobin, 2011). It has been recognised that Unit B (and C) is variable both along and across strike, similar to the pore-pressure spatial variation acknowledged by Kitajima and Saffer (2012) in this consistently low velocity zone (LVZ) unit whose formation in still controversial (Park at al., 2010). Therefore, it is important to discuss the mechanisms that could be involved in the formation of Units B and C in the light of the results

here presented. We propose three models to explain how Units B and C could be formed from the same lithological material and under the same regime but became acoustically different over time. These models are summarised in Figure 5.12:

- Fluid rich weak zone model: This hypothesis explains the low-velocity Units B and C as the result of differential vertical compaction and fluid pressure evolution during sediment subduction. As oceanic sediments enter the subduction zone, they undergo vertical loading. The deeper layers (Unit C) are subject to higher overburden pressure and become increasingly compacted, reducing porosity and expelling fluids upward. These expelled fluids accumulate in the overlying Unit B, where lower compaction rates allow for greater retention of pore fluids. (Figure 5.12A top). The resulting contrast in compaction and fluid content forms a mechanically decoupled shear zone, where the strength contrast between the fluid-rich Unit B and stronger, compacted Unit C allows for distributed shear and strain localisation (Figure 5.12A middle). The enhanced pore pressure in Unit B may promote hydrofracturing, leading to the upward propagation of fluids and the development of thrust faults that maintain critical taper and aid wedge growth (Figure 5.12A bottom). This model accounts for the observed low velocities and dim seismic reflectivity in both Units B and C, while highlighting how internal fluid redistribution and compaction, rather than lithological contrast or tectonic erosion,

drives structural differentiation and fault localisation within the accretionary prism (Saffer and Bekins, 2006; Moore et al., 2001).

- Erosional model: In this model, the stratigraphy and structure of Units B and C develop through progressive offscraping, shear localisation, and internal reworking during frontal accretion. As sediments are transported towards the trench on the subducting oceanic plate, the frontal thrust system first initiates offscraping of the uppermost sedimentary layers, which are less compacted and mechanically weaker. These layers are scraped off at the FTZ and incorporated into the toe of the accretionary prism, forming Unit A (Figure 5.12B top). However, not all sediment is accreted at the front. With increasing burial and slip along the décollement, shear stress becomes localized at the interface between the offscraped upper unit (A) and the more compacted and older lower sediments (Unit C), that remain below the décollement. This interface becomes the locus for formation of a basal shear zone, setting the conditions for mechanical decoupling. Over time, as convergence continues, some slices of sediment previously accreted into Unit A are tectonically removed (i.e., underscraped) and transferred into the basal shear zone. These recycled slices begin accumulating as Unit B, a stratigraphic package that records the history of erosion, underplating, and shear localisation (Figure 5.12B middle). Because these underscraped slices are less compacted than Unit C, they accommodate deformation more readily.

Duplex structures nucleate and propagate within Unit B, gradually building up a landward-thickening duplex zone. This zone is mechanically weaker, which helps maintain critical taper in the accretionary wedge by localising thrusting internally, rather than along the basal décollement. Thus, Unit B evolves into a shear zone composed of underplated, previously accreted material, now caught between the compacted and stronger Unit C and the more coherent and frontally accreted Unit A. The contrast in compaction and deformation style between Units B and C is not due to sediment type, but to their different tectonic pathways and degrees of tectonic reworking (Figure 5.12B bottom). The observed low seismic velocities in Unit B can therefore be attributed to its composite, fractured nature and relatively high porosity retained due to limited compaction during underplating. It explains the mechanical weakness of Unit B due to its relatively low consolidation and fracture susceptibility (von Huene et al., 2004, Park et al., 2010).

- Different lithological assemblage model: Here, the distinction between Units B and C is attributed to differences in lithological origin and sediment facies rather than structural processes. Unit C consists of older, fine-grained hemipelagic and pelagic oceanic sediments, compacted through time and loading, forming a relatively cohesive and strong mechanical layer (Figure 5.12C top). In contrast, Unit B is interpreted to represent coarser-grained turbidites and/or mass transport deposits (MTDs) that were deposited in the trench environment and subsequently

accreted to the wedge above the décollement. As these coarser materials are incorporated into the accretionary wedge, they retain high porosity and low seismic velocities due to their granular texture and lower degrees of diagenesis (Figure 5.12C middle). Unit B thus reflects the primary sedimentary fabric and depositional environment, rather than post-depositional fluid enrichment or tectonic erosion. The mechanical and seismic contrast between Units B and C is therefore inherent to their different sedimentary origins and compaction histories (Figure 5.12C bottom). This model provides a sedimentologically explanation for low-velocity zones within the accretionary wedge and is consistent with observations of trench fill stratigraphy and accretion processes along the Nankai margin (Strasser et al., 2011; Moore et al., 2001).

Understanding how Units B and C were formed is critical for deciphering the internal architecture of the NAP and the complex dynamics of fluid migration in subduction zones. While the models focus on different mechanisms for the formation and evolution of Unit B and its relationship to Unit C, they all highlight how variations in compaction, lithology and/or deformation styles create mechanically distinct zones that control where fluids accumulate, migrate, and are eventually expelled. These weak zones, particularly Unit B, often serve as fluids stores and hydraulic conduits that link deeper fluid sources (from Unit C) to overlying thrusts and splay faults. In tectonic settings where basal asperities exist, these internal structures can become further reactivated or reorganised

due to localised stress amplification, leading to enhanced fracturing, fluid overpressure, and possibly earthquake nucleation.

The mechanical resistance from basal asperities restricts fluid migration from overpressured sediments, particularly those in the Unit B (and C) around features like the Kumano Seamount. As a result, pore fluid pressure can rise significantly in these isolated domains (Bell et al., 2010; Shapiro et al., 2018, Cordell et al., 2019). Elevated pore pressures reduce effective stress on faults, which may in turn influence the nucleation and propagation of slow slip events and very low frequency earthquakes (VLFEs) (Kodaira et al., 2004). In this context, strike-slip faults, such as fault F1, may act as fluid conduits or pressure-release valves, redistributing both pore fluids and tectonic stress (Ikari et al., 2012). This explains the lower seismic reflectivity and resolution observed in the vicinity of F1, but also some main thrusts (Figures 5.9 and 5.11), possibly due to localised fluid overpressure. This can also lower the coefficient of internal friction estimated in Chapter 4 for the pair of strike-slip faults.

Larger asperities have the capacity to disrupt the lateral continuity of Units B and C, and consequently the décollement (Figures 5.9 and 5.11), effectively compromising the mechanical decoupling that typically exists between these units. This disruption facilitates the development of new fluid migration pathways compared to areas with fewer or smaller asperities. In some cases, large vertical scarps, whether inherited tear faults or newly formed thrusts, displace the overlying Units B and C along with the décollement. This structural

offset can allow fluids previously constrained within Unit C to more effectively migrate into Unit B, resulting in these units appearing acoustically more similar in seismic reflection data (e.g., see Line XL1140 in Figure 5.9).

Conversely, features such as the Kumano Seamount entirely truncate the seaward continuity of Units B and C, compressing and sealing fluid pathways along their leading flanks. This compression can promote steepening of frontal thrusts, which in turn channel overpressured fluids along newly formed fault surfaces and help localise the décollement. When this sealing effect intensifies due to increasing compression ahead of the seamount, fluids may instead migrate along strike-slip faults or trigger the formation of new in-sequence or out-of-sequence thrusts. Such mechanisms highlight the critical role of large asperities in reconfiguring fluid flow and fault architecture within the accretionary prism.

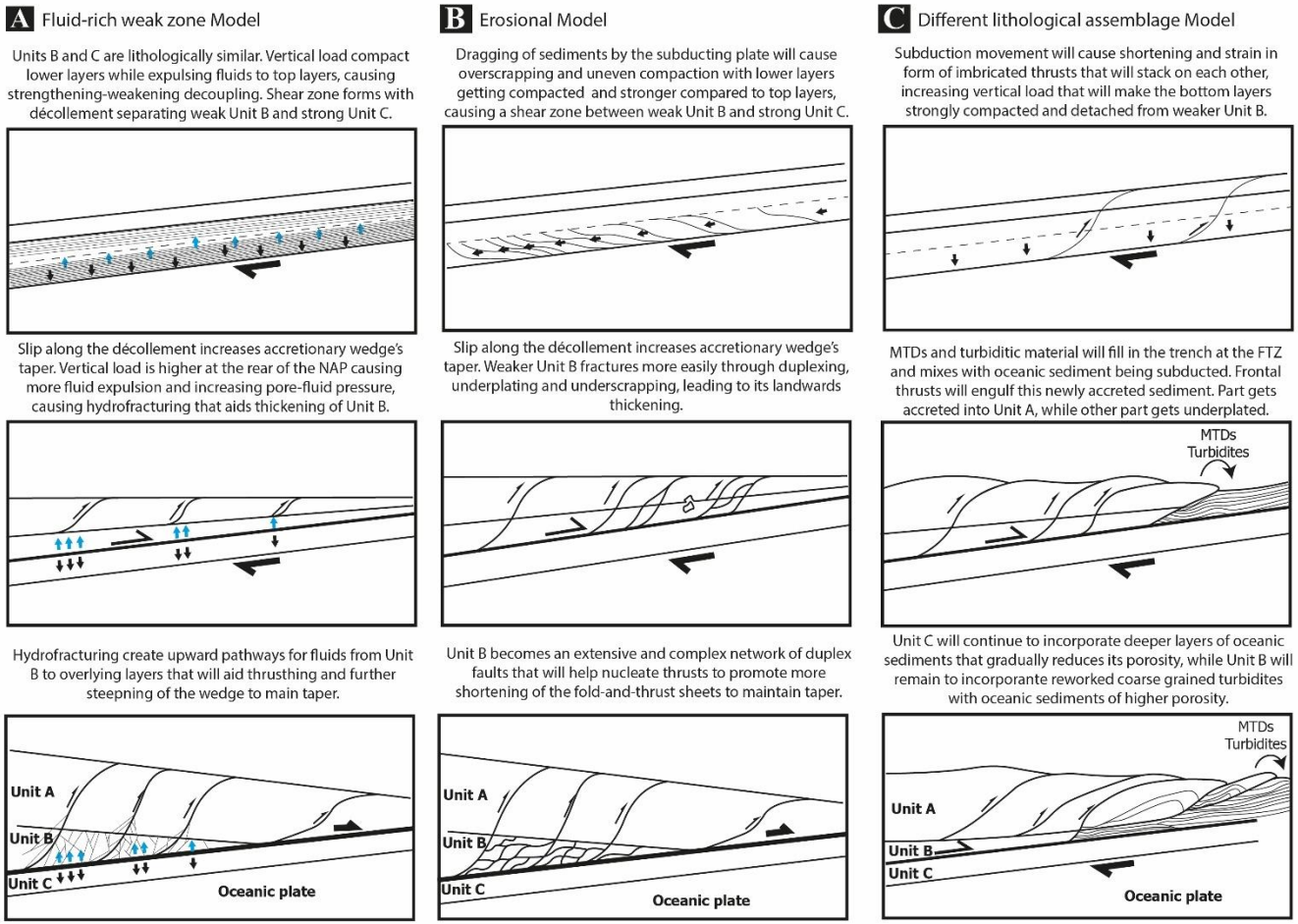

Figure 5.12 – Schematic annotated diagrams showing three proposed models for the formation of Units B and C in the NAP. MTD – mass transport deposit; blue arrows – fluid migration; black arrows – compaction.

Conversely, features such as the Kumano Seamount entirely truncate the seaward continuity of Units B and C, compressing and sealing fluid pathways along their leading flanks. This compression can promote steepening of frontal thrusts, which in turn channel overpressured fluids along newly formed fault surfaces and help localise the décollement. When this sealing effect intensifies due to increasing compression ahead of the seamount, fluids may instead migrate along strike-slip faults or trigger the formation of new in-sequence or out-of-sequence thrusts. Such mechanisms highlight the critical role of large asperities in reconfiguring fluid flow and fault architecture within the accretionary prism.

5.5.3 Effects on wedge taper

A direct effect of subducting basal asperities on convergent margins is that they change the height of the accretionary prism above them, as observed in Figures 5.7A, 5.7B, 5.9, 5.10 and 5.11, and previously identified in parts of the Nankai Through (Park et al., 1999; Bangs et al., 2006). There is also an important impact on the width of the accretionary prism, as recorded when comparing IL2200 crossing the Kumano Seamount, and IL2720 presenting a smoother section of subducting slab, far from the Kumano Seamount (Figures 5.7 and 5.10). The accretionary prism is 24.9 km and 30 km wide, respectively,

agreeing with the critical taper theory (Lallemand et al. 1994). Hence, seamounts, ridges and scarps form local basal asperities that increase the roughness of the subducting slab (Figures 5.2 and 5.4), resisting its movement and contributing to slower rates of subduction, where erosive or non-accretional behaviour could be locally favoured over accretional behaviour (Le Pichon et al., 1993). Although porosity and strength of sediments in the Nankai accretionary prism (NAP) may vary spatially and temporally due to compaction, diagenesis, and fluid flow (Saffer and Tobin, 2011), for the purposes of this discussion, they are treated as relatively uniform to isolate their effects on basal friction. This simplification allows the mechanical influence of basal asperities to be evaluated more clearly.

Data revealed significant heterogeneity in wedge geometry and internal segmentation that reflect not only geometric responses to sediment accretion and underthrusting but also the profound influence of basal topography on wedge mechanics.

The outer wedge displays a progressive increase in average taper (α + β) from Profile E (9.41°) to Profile A (18.09°). This trend mirrors the transition from structurally simpler segments (Profile E), where basal topography appears smooth and sediment input relatively continuous, to more structurally complex segments (Profile A), which overlie the Kumano Seamount. This relationship is consistent with observations from prior studies (Moore et al., 2001; Wang & Hu,

2006) showing that incoming seafloor topography strongly modulates deformation styles, basal strength, and wedge geometry. The steepening of frontal taper in the Southwestern most profiles, where α + β values exceed 20° in the frontal section, is especially notable and exceed typical critical taper estimates (~8–15°) for subduction zone wedges composed of weak, fluid-rich sediments (Davis et al., 1983; von Huene & Ranero, 2004). Such anomalously high values suggest local overcritical conditions, which may arise due to one or more of the following mechanisms:

- Uplift of the basal décollement in response to subducting seamounts, forcing overlying sediments and fold-and-thrust structures to steepen, observed in Figures 5.7 and 5.9.
- Localised strengthening of the basal interface, reducing basal decoupling and promoting internal wedge thickening through mechanisms of back-thrusting (Figure 5.13), duplexing (potentially happening in Figure 5.7A in the FTZ with closely space thrusts) and OOS thrusting (Figure 5.11).
- Enhanced tectonic underplating or buttressing, increasing taper to maintain critical conditions (Figure 5.10).

In contrast, Profiles A and C, which lack such basal irregularities, exhibit more typical and symmetric taper geometries (~9–11° total), consistent with equilibrium conditions under lower basal friction and less structural interference.

Another curious aspect of the data is related to discrepancies within the outer wedge of the NAP, between the frontal and rear sections. Profile A shows an exceptionally steep frontal taper of 26.99° but a much lower rear wedge taper (9.18°). This imbalance implies that the wedge may be internally overcritical in the frontal domain, while the rear section of the outer wedge remains at or near critical conditions. Cubas et al. (2013) also point towards critical taper conditions varying spatially within a single wedge depending on localized changes in material strength, fluid pressure, basal coupling, or input flux. Therefore, it is acceptable that accretional wedges may simultaneously contain undercritical, critical, and overcritical domains, leading to complex internal deformation styles. Such finding will be further discussed in Chapter 7.

Overall, the results support a model of the Nankai prism as a non-uniform, segmented wedge, whose geometry and stress regime vary significantly along strike in response to external controls such as subducting topographical asperities that, individually or collectively, change the interplay between material heterogeneity, basal coupling and sediment accretion rate to create a complex critical state that evolves spatially and temporally. Therefore, it is understood that asperities increase frictional resistance along the décollement, which in turn raises the critical taper angle required for wedge stability (Davis et al., 1983; Dahlen, 1990). As the wedge adjusts to maintain this higher critical taper, it accommodates more internal deformation—expressed through increased thrusting and folding within the prism itself as observed in the FTZ near the Kumano Seamount (Table 2 and Figures 5.7A and 5.13).

5.5.4 Effects on horizontal shortening

The width of the accretionary prism is often inversely related to the critical taper angle (α + β), such that wider prisms are commonly interpreted to be in subcritical states that favour horizontal shortening and internal wedge thickening (Davis et al., 1983; Dahlen, 1990). However, this relationship assumes a laterally uniform critical taper, which may not hold true in complex, heterogeneous margins like the Nankai Trough. The results demonstrate that critical taper angles vary significantly along strike (Figure 5.10), indicating that adjacent segments of the prism may reach mechanical stability at different taper values. As such, differences in prism width may reflect spatial variations in basal friction, internal strength, or loading by subducting bathymetric features, rather than simply indicating sub- or supercritical states. This highlights the importance of evaluating local taper conditions rather than assuming a globally uniform prism behaviour. The structures identified in this chapter do not seem to significantly impact the overall horizontal shortening of the overlying NAP as there is a difference of less than 3% between Profile A, where subducting plate presents greater roughness related to the Kumano Seamount, and Profile E, where the subduction slab is the smoothest. Results suggest that shortening from fault slip tends to be slightly greater in smoother subducting slabs, where seawards growth of the NAP is significant. This could be interpreted as the presence of basal asperities increasing the coupling between the subducting plate and the overlying NAP, which steepens thrusting that could diminish thrusting per se

and enhance strike-slip, thus not promoting as much growth of the frontal part of the outer wedge and decreasing the observed horizontal shortening.

Results suggest more significant differences in horizontal shortening when focusing on the different sectors of the NAP and their relationship with the interpreted structures. The ITZ consistently shows a significant greater shortening proportion than the FTZ (Figure 5.8). However, the Kumano Seamount locally contributes to a much greater proportion of shortening in the FTZ (48%), where it occurs. When a seamount is first subducted, the angle of the basal décollement landwards of the seamount suddenly changes and becomes undercritical, promoting thrusting, prism thickening and, consequently, enhancing horizontal shortening (Lallemand and Le Pichon, 1987) (Figure 5.9). This could be the reason why Profile A is the only 2D seismic section displaying greater shortening in the South sector (63%) compared to the North sector (37%) of the NAP. This is further evidence for the locking of faults in the FTZ by the Kumano Seamount, creating a barrier for fluid escape from Unit B. In this setting, shortening is accommodated by tectonically uplift of the FTZ and a 'piggyback' creep along the thrust faults in the FTZ immediately above and landwards of the Kumano Seamount. Locally, areas experiencing greater stress coupling in the vicinity of the Kumano Seamount have horizontal shortening being accommodated by back-thrusting when there are space constraints caused by asperities-related over compression (Figure 5.13).

There is evidence in the NAP for partitioning of deformation caused by Scarps 2 and 3 and suprajacent strike-slip fault F1; the North sector consistently shows greater horizontal shortening when compared to the South sector (Table 1). The North sector is much smoother and characterised by an undulated basal décollement. These undulations change the critical taper conditions within the NAP. The North sector of the NAP experiences an average shortening (31%) that is 7% greater than in the South sector (24%), confirming along-strike adjacent sections of the NAP will continue growing seawards, potentially at the regional rate of subduction, in an accretional style.

5.5.5 Smaller scale effects

The Kumano Seamount not only impedes the seaward advance of the NAP, thereby hindering its frontal growth, but also induces localised contraction within the prism. This contraction likely enhances strike-slip deformation associated with Scarps 2 and 3, as well as with fault F1. Figure 5.11 reveals considerable structural complexity in the vicinity of the seamount. Notably, evidence of back thrusting within a fold-and-thrust structure and bathymetric depression north of the seamount (interpreted as negative flower structures) suggests localised transpressional and transtensional deformations. These features, briefly discussed in Chapter 4, appear to reflect a reconfiguration of the local stress regime.

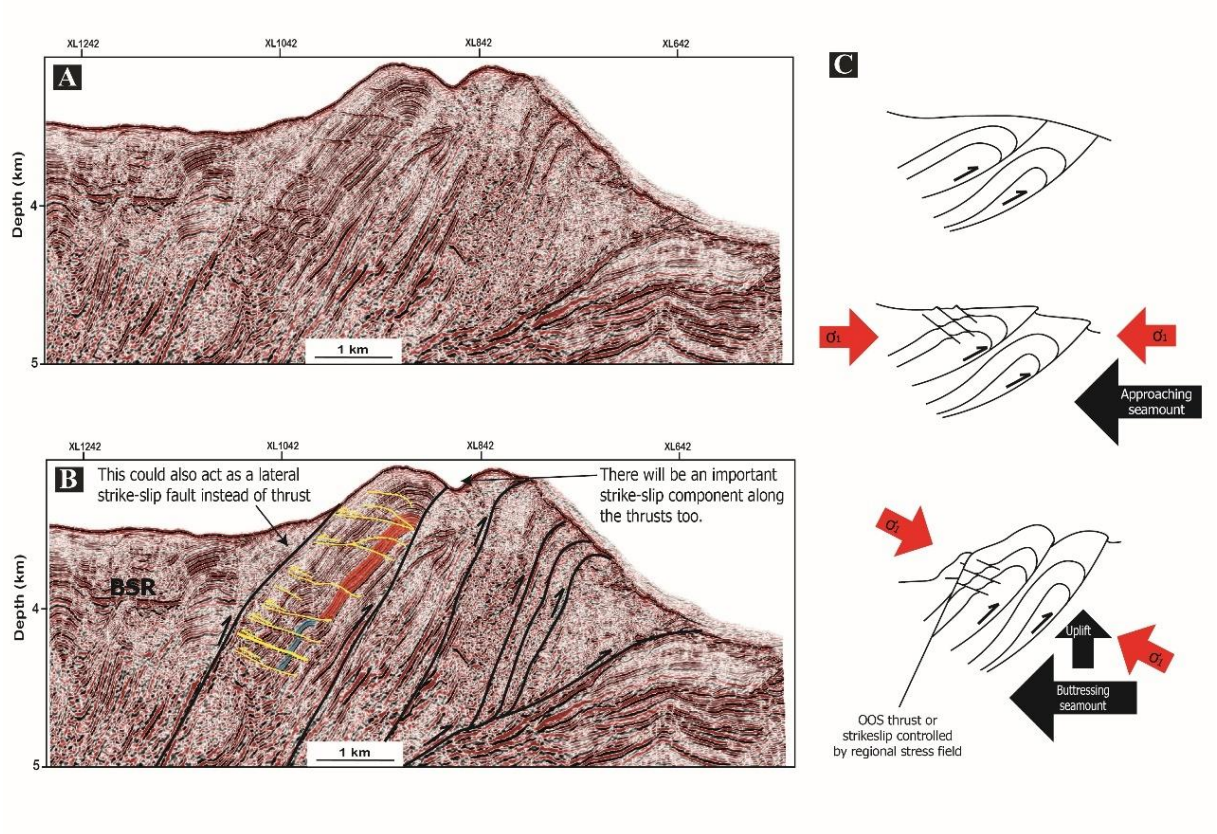

Figure 5.13 - A) Uninterpreted seismic inline IL2200. B) Interpreted seismic inline IL2200 with the yellow lines representing back-thrusting only observable in this section of the NAP just above the Kumano seamount. This pattern of back thrusts in only observable in this fold-and-thrust nappe. Black lines represent the main thrusts within Unit A. Red and blue areas show some of the seismic horizons being displaced by the identified back thrusts. C) Schematic diagram representing step-by-step formation of the observed structural arrangement observed in seismic. As the Kumano seamount approaches the FTZ it causes a rearrangement of the stress field that responds in local back-thrusting. As the Kumano seamount starts subducting the NAP it will push the above strata, which triggers a reactivation of the thrust faulting in 'piggyback' fashion that borders the back thrusts within the observed nappe while the regional stress field is still operation potentially creating OOS thrusts and/or strike-slip.

Their restriction to a zone between dominant frontal thrusts, and the absence of an associated extensional stress shadow on the seamount's leading flank, supports the interpretation that this represents an early stage of seamount subduction. In this context, the Kumano Seamount currently behaves as a tectonic buttress, locally uplifting the FTZ and accumulating compressive strain ahead of its leading flank.

This configuration likely enhances and rotates the local maximum horizontal compressive stress (SHmax) on the advancing flank (Sun et al., 2020; McNamara et al., 2021). The resulting over-compression steepens pre-existing thrusts and promotes the nucleation of new back thrusts, reflecting the modified local stress state. Furthermore, the interplay between the broader regional transpressional regime and the rotated local compressive axis may facilitate localised pull-apart deformation, producing transtensional zones. Similar structural patterns in response to subducting bathymetric highs have been observed elsewhere (Fleury et al., 2009; Mitsui et al., 2022) and replicated in analogue sandbox models (Dominguez et al., 1998; 2000), reinforcing the broader geodynamic significance of these features.

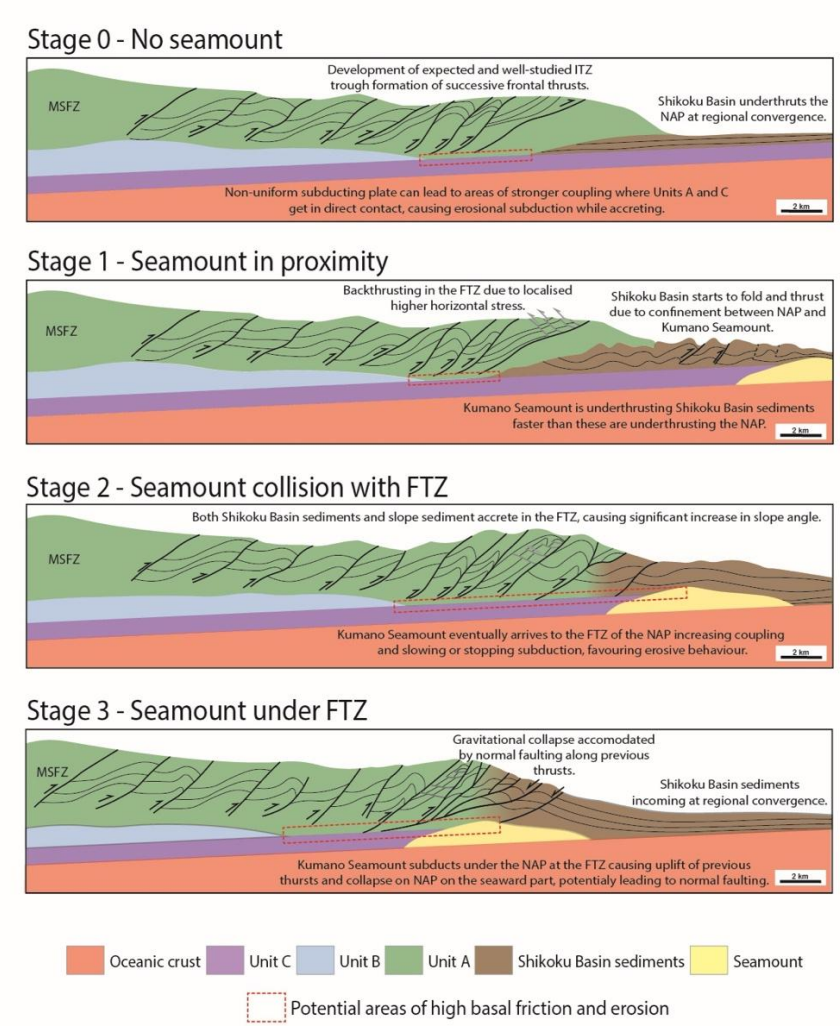

Figure 5.14 - Schematic diagram showing the influence of seamount subduction in the NAP and the mechanisms of seamount subduction in the NAP. The seamount will influence the NAP before collision by forcing early folding and proto thrusting of Shikoku Basin sediments between the more rigid accreted material from the NAP and the incoming seamount. Stress fields locally change within the FTZ, which will experience back-thrusting (Stage 1) in places of low-dip thrusts and no sediment cover. Upon initial collision of the seamount into the FTZ, some of the Shikoku Basin sediments are forced to fold-and-thrust to join the pre-accreted material from the NAP as there is spatial constraining caused by the seamount being higher than the décollement itself, which reduces the conditions favouring underthrusting and under-plating (Stage 2). The seamount will start actively eroding the bottom of the NAP and potentially some newly accreted sediment from the Shikoku Basin to continue subducting below the NAP (Stage 3). From Stage 2, the amount the area of coupling between Units A and C will increase as a response to less underscrapping, high pore fluid pressure and thickness of the NAP, leading to thinning and landwards retreat of Unit B. We propose that some of the build-up of fluid pressure is released to laterally adjacent sections of the NAP, which will continue growing in an accretional-dominated style. However, we cannot ignore the possibility that some of this fluid could potentially by forced into the inner part of the NAP and/or MSFZ, especially at later stages of seamount subduction.

5.5.6 Effects on tectonic deformation in the NAP and subduction behaviour

The results in this chapter suggest that the subduction of the Kumano Seamount and other bathymetric asperities, such as scarps, can create local conditions for the formation of new structures but most importantly enhances the structures already operating within the regional transpressional regime observed and discussed in Chapter 4. One such structure is the right-lateral strike-slip fault F1. The alignment of Scarps 2 and 3 and the positioning of the Kumano Seamount just South create the ideal geometrical anisotropy for this right-lateral to become more prominent than other strike-slip faults operating in the NAP. The interplay between transpressional regime and geometry of asperities in the subducting oceanic plate together with strike-slip faulting means that the outer wedge of the NAP will be highly compartmentalised, both across and along strike. For example, the steepening of thrust faults in the N sector, particularly towards the SW near F1 may reflect increased shortening accommodated in a piggyback thrust system rather than being a direct consequence of fault F1 itself. In this context, F1 almost function as a 'relay' fault accommodating differential displacement between adjacent thrust sheets, a phenomenon commonly seen where shortening rates vary along strike (Reading, 1980). This lateral strain partitioning between segments could explain both the observed bending and steepening of thrust faults (Table 2) and the zones of low seismic resolution

adjacent to F1 (Figures 5.9 and 5.11). Additionally, the subduction of the Kumano Seamount in the S sector likely increases basal friction, slowing wedge advance and promoting local drag and steepening of structures. However, the dominant control on thrust dip variations is more likely the differential shortening and associated 'piggyback' stacking, rather than the strike-slip kinematics along F1.

Here, key changes are proposed to the model suggested by Park et al. (1999), Park et al. (2004) and Bangs et al. (2006), as summarised in Figure 5.14. The NAP grows upwards and seawards obeying a typical accretional subduction style (Clift and Vannucchi, 2004). It accretes the trench-filled and oceanic sediments from the Shikoku Basin into the accretionary prism. However, basal asperities, such as seamounts, over compress the frontal part of the outer wedge of the NAP, even before they reach the FTZ, as the relatively shallower and less-consolidated Shikoku sediments become trapped between the FTZ and the incoming seamount. This will cause the Shikoku sediments to underthrust the FTZ, and the seamount to underthrust the Shikoku Basin sediments, as it would be expected in typical style subduction accretion. However, the lower strength and thickness of the Shikoku Basin sediments, when compared to the material accreted in the FTZ, will cause the seamount to underthrust the Shikoku Basin strata at a higher rate than that of the Shikoku Basin material underthrusting the FTZ. This leads to the setting illustrated in Figures 5.7A and 5.14. The model above stresses an important mechanism explaining how some seamounts are included within accretionary prisms without major seismogenic activity. As

the seamount top is above the basal décollement, it causes further mechanical coupling between the subducting and overriding plates (Watts et al., 2010) leading to a decrease in the subduction rate and, locally, to a temporary change to an erosive subduction style. Therefore, it is postulated that basal erosion is always present, to a variable degree, within an accretional subduction zone as the subducting oceanic crust is far from being a smooth surface. Even without any major basal asperities, the overall undulation of the incoming oceanic plate may be sufficient for localised areas of greater basal friction and consequential basal erosion to occur. In the study area, these tend to coincide with areas where Unit B is absent, and where Units A and C come into direct contact with the subducting plate, thus promoting strong mechanical coupling between the subducting and overriding plates (Bangs et al., 2006; Von Huene et al., 2009) (Figure 5.14).

Units B and C control further accretion and growth in the NAP, especially in the formation of proto thrusts (Park et al., 2010), and the expulsion of fluid from the accretionary wedge into the FTZ and upper parts of the NAP are concerned (Screaton et al., 2009). The locking of thrust faults in the FTZ, and the barriers to fluid expulsion caused by stress accumulation from the Kumano Seamount subduction may lead to an unusual increase of fluid and pore pressure, accompanied by over consolidation of sediment within the NAP at the landwards side of the seamount. These changes lead to exceptional conditions for localised tectonic erosion of the basal décollement (Wang et al., 2010; Sun et al., 2020). As the fluids are not constrained laterally, the increase in pore and fluid pressure as a function of the consolidation of sediment will promote the lateral escape of

fluids to adjacent sectors of the NAP where coupling is not as strong due to the lower roughness of the subducting plate. Strike-slip faults could prove to be important lateral pathways for fluid migration. This promotes subduction accretion and underplating, laterally thickening Unit B (Cloos and Shreve, 1996; Bangs et al., 2006).

The model above explains the retreating (and potential thinning) of Unit B observed in Figures 5.6, 5.7 and 5.12. Localised coupling-decoupling cycles between the two plates is thus responsible for the changes between typical accretional and potential erosive or non-accretional subduction styles (Wang et al., 2010). It is inferred that it is through such a mechanism that subduction zones can incorporate seamounts and other asperities in and under accretionary prisms, where:

1. Lateral adjacent areas (along the Nankai Trough) to the Kumano Seamount will experience accelerated accretion in response to fluid transfer, promoting further landward growth of Unit B in order to maintain critical taper angles.
2. The areas immediately landwards of the seamount will change into a critical compressional state caused by increasing basal friction and fluid pore pressure, promoting erosional and underplating subduction styles.

Both processes will influence Unit B (Cloos and Shreve, 1996) by either causing a step-up of the basal décollement or promoting the lateral continuation

of Unit B (and basal décollement) around the seamount. Both scenarios will eventually lead to the landwards part of the NAP reconnecting back to its seawards and frontal sectors to a more typical accretional style of subduction.

According to Shiraishi et al. (2020), the study area records a concentration of low frequency and magnitude seismic activity in the landward part of the NAP, with hypocentres near the seamount and within Unit B, that may relate to the shearing, underplating and tectonic erosion described above. The absence of seismicity near the Kumano Seamount and its surroundings suggests this area is seismically locked. However, it is not possible at this stage to determine if seamounts such as the Kumano Seamount can cause great earthquakes. It can be speculated that it will depend on the size and shape of the seamount and its effect on the stepping up of the basal décollement or formation of OOST that will be able to slip through the NAP, displacing its surface (Figure 5.8). Nevertheless, the subduction of the Kumano Seamount changes the geometry of the proto-thrusts and FTZ which, in turn, will further impact the geometry of the ITZ, enhancing the oblique nature of the subduction and the distribution of seismicity (Kimura et al., 2011). In addition, back thrusting above the seamount (Figure 5.11) can also generate isolated seismic events with tsunamigenic potential, similar to those described for the 2010 Mentawai tsunami earthquake (Hananto et al., 2020) and the 1994 Java tsunami earthquake (Xia et al., 2021).

It is important to note that although the Kumano seamount is a significant feature in the study area, it is affecting the NAP on a local to regional level

within the wider Nankai Trough. Therefore, the subduction styles will vary along the Nankai Through depending on the basal asperities present in the incoming subducting PSP, and adjacent areas along the NAP may exclusively be growing in an accretional subduction. The data in this chapter suggest that while the section of the NAP impacted by the seamount suffers a delay due to temporary stress coupling along-strike adjacent sections immediately SW and NE of the Kumano Seamount will engulf it as the NAP grows towards the SE, leading to the incorporation of the seamount and other asperities under the NAP.

5.6 Chapter-specific conclusions

This chapter shows that oceanic crust of the Shikoku Basin subducting underneath the NAP has much greater roughness than previously described. Important asperities, some inherited from processes occurring in the oceanic crust prior to its subduction, occur together with others formed at the time of subduction. This work highlights the presence of a 1.5 km high seamount below the FTZ of the NAP and several other ridges and fault scarps. The roughness of the subducting oceanic crust has a huge impact on the overlying NAP by promoting differential growth, shortening, deformation and distribution of strain, with consequences for regional seismicity. The temporary and spatial locking and coupling of sectors within the NAP may be responsible for some of the low frequency and magnitude earthquakes identified by Shiraishi et al. (2020).

Seismic interpretation of the NAP above the basal décollement shows significant differences not just in terms of the thickness and frequency of thrust faults and anticline nappes but also in their dip. Areas of subducting oceanic crust and basal décollement with inherited structures, thus record co-existing styles of deformation in the NAP that vary either in time and/or space depending on the amount of coupling created by basal asperities. The Kumano Seamount is by far the most relevant asperity in the study area and is, at present, delaying the development of frontal thrusts and the subduction movement per se. Although the amount of slip and horizontal shortening along the NAP remains the same (between 29% and 32%), horizontal shortening is accommodated in different sectors of the NAP depending on underlying asperities. In this work, the Kumano Seamount locally increases the amount of shortening in the FTZ compared to the ITZ, and in the South sector when compared to the North sector, which leads to more thrust anticlines per km, steeper thrust faults, and tighter thrust anticlines.

At the basal décollement, the pre-existing NW-striking Scarps 2 and 3 in the subducting oceanic crust and differential movement between the North and South sectors create the conditions for tearing of the NAP in the study area. Such tearing is significant enough to generate a major right-lateral strike-slip fault (F1) that becomes the main stress partitioning mechanism in the study area, separating two distinct sectors:

- a North sector where the smother basal décollement allows the NAP to extend further seawards as a product of greater prism growth promoted by increased horizontal shortening that is mainly accommodated by the ITZ.
- a South sector displaying a shorter prism with a relatively lower overall shortening caused by a shift of horizontal shortening from the larger ITZ towards the smaller FTZ, where the Kumano Seamount is located.

Roughness always impacts horizontal shortening of accretionary prisms, but the relationship is not always linear. As seen in this chapter, enhanced roughness often increases interplate coupling causing decreased shortening and growth of accretionary prisms but isolated and abnormally larger asperities, such as the Kumano Seamount, promote local increase in the shortening without much growth in the overall length of the prism, such as the one recognised in the FTZ of the South sector.

The spatial partitioning between the North and South sectors, relative to F1, suggests that although the NAP is dominated by accretional subduction, the presence of basal asperities within the incoming subducting plate can cause lateral variations in the subduction style along the Nankai Trough. Hence, some seismic profiles reveal erosive subduction. Spatial variations in the subduction style seem to influence the growth and distribution of Unit B along the Nankai Through and, consequently, the stick-slip behaviour of faults in the NAP.

The observed segmentation of the NAP caused by the Kumano Seamount is slower subduction in the South sector that experiences erosive subduction due to an increase in shear stress, thus significantly reducing the amount of fault slip in the ITZ and increasing horizontal shortening in the FTZ accommodated by the step-up of the basal décollement and nucleation of greater amount of frontal thrust faults. In contrast, the North sector, away from the Kumano Seamount and with fewer asperities, shows a greater horizontal shortening, mainly concentrated in the ITZ rather than the FTZ. There, the asperities of the subducted slab and the resistance offered to shear in the basal décollement cause the stress dissipation into distinct areas of the NAP. Strike-slip movements transfer some of the accumulated stress but can also cause other areas to remain static leading to seismic slip where stresses are accommodated away from F1. It is important to further understand the influence of roughness in the growth and development of Unit B and how this influences the seismicity, deformation of the NAP and inclusion of the asperities in convergent margins.

CHAPTER 6

Interference tectonics in the Nankai Accretionary Prism caused by asperities in the subducting Philippines Plate: Insights from sandbox modelling

A paper comprising the findings and discussion covered in this chapter is already prepared and to be submitted shortly after the submission of this thesis.

6.1 Abstract

Along the Nankai Trough, the subducting Philippines Plate contains several basal asperities that increase interplate coupling, causing along strike interferences within the Nankai Accretionary Prism (NAP). Two sandbox analogue experiments were carried out in this chapter to provide new insights on the interference of single and combined asperities in the evolution of an active accretionary prism. The experiments here considered: a) a single asperity scenario simulating the presence of a single elongated ridge, observed in the 3D seismic; b) a combined scenario simulating the presence of a major ridge and the Kumano seamount, also imaged in 3D seismic. The results obtained, when compared with seismic data from the Nankai Through, along the outer wedge of the Kumano Transect, show that deformation in the overlying accreted prism is highly controlled by subducting asperities, causing considerable variations in fluid circulation within the NAP and the thus changing the rheology of the low velocity unit (Unit B) above the décollement. Our results demonstrate that the thickness and strength of the low velocity Unit B and pore-fluid pressure are important mechanisms to fault initiation and reactivation in the NAP. Some of these faults have a significant tsunamigenic potential, particularly the Megasplay Fault Zone (MSFZ) and the Frontal Thrust Zone (FTZ).

6.2 Introduction

The way that asperities contribute to seismic activity is unclear and somehow controversial as their varying shape, geometry and kinematics make it challenging to find and pinpoint relationships between such asperities and their implications in earthquake nucleation and tectonic deformation. Asperities in oceanic basements are often referred to as seamounts, seismic or aseismic ridges or fault scarps. Wang and Bilek (2011) suggested that subducting asperities, especially seamounts, can cause the formation of a surrounding extensive fracture zone(s) that hinder rupture propagation and cause local to regional stress anomalies that have the potential to trigger slip at shallow levels and shallow seismic activity (<10 km) is considered to be responsible for more relevant near-surface seafloor displacement with greater tsunamigenic potential when compared to earthquake rupture in the regular of 10-40km (Xia et al., 2023). Not only asperities have an individual impact on a local scale but also affect subduction zones on a regional scale when considered collectively and described as roughness of the incoming subducting oceanic plate. Seismicity and the structural-mechanical evolution of the upper plate and their accretionary prisms reflects the downwards propagation of the leading edge of subducting plate roughness (Martinez-Loriente et al., 2019). Recent studies (Martinez-Loriente et al., 2019; Chow et al., 2022) seem to suggest that not only asperities cause surrounding higher pore-fluid pressure but also cause upper plate fracturing,

brittle strain, and tectonic overpressure that could nucleate seismic activity. Similarly, such fractures can also later aid the fluid escape in the wake of subducted asperities as well as the formation of normal faulting at higher depths due to bending of the subducting oceanic plate.

The offshore regions of SE Japan have historically been affected by some of the largest interplate earthquakes in the world, with the Nankai Trough experiencing large earthquakes every 100–200 years since A.D. 684. Five earthquakes of magnitude ca. 8 occurred in the last four centuries, including the most recent 1944 Tonankai and 1946 Nankaido earthquakes (Ando, 1975; Itaba et al., 2010) (Figure 6.1). The 1944 Tonankai earthquake, as many other great tsunamigenic earthquakes in the Sunda, Chilean and Alaskan subduction zones (e.g., Wang et al., 2013; Melnick et al., 2012; Chapman et al., 2014) was interpreted as a result of branching and slipping along the Megasplay Fault Zone (MSFZ) and has been the focus of recent studies (Kinoshita et al, 2018; Shiraishi et al., 2019; Roesner et al., 2022). According to Park et al. (2002), the Nankai Trough, where the oceanic PSP is subducting below the overriding Amur Plate (Figure 6.1), comprises by three distinct sectors:

1. A distinct decoupled aseismic zone, comprising the outer wedge of the NAP and considered to record and experience free slip along the décollement.
2. An intermediary zone, experiencing partitioning in slip, corresponding to the area where the décollement steps down to the branching part

of the MSFZ. Here, structural coupling between the subducting and overriding plates increases downwards, forming a transition zone between aseismic and seismic areas in the Nankai.

3. A structurally coupled seismic zone that includes the branching part of the MSFZ itself, meaning that slip is accommodated along the plate boundary, but also the MSFZ. It is important to note that the MSFZ can slip all the way to the surface with potential tsunamigenic impact.

Basal asperities in subducting crusts, such as buried seamounts, have a determinant role in the initiation of large earthquakes as often nucleate earthquakes close to seamounts and then propagate farther (Lallemand et al., 2018). Therefore, the study of subducting asperities is ultimately crucial to understand the formation and accumulation of strain leading to large earthquakes, such as those occurred along the Nankai Trough (e.g., Ruff, 1989; Scholz, 1992; Ye et al., 2018; Senatorski, 2020). The MSFZ shows lateral and temporal differences in its geometry and seismic activity that may locally be induced by the subduction of seamounts and ridges (Strasser et al., 2009; Kimura et al., 2011). Nevertheless, little work has focused on characterising the roughness of the subducting oceanic plate along the Nankai Trough, understanding its spatial influence in the seismic coupling and seismic weakness. Recent studies (Azevedo et al., 2018; Shiraishi et al., 2020) found ridges, scarps, and seamounts as forming important asperities on the subducting Philippines Sea Plate that structurally compartmentalise the outer wedge of the NAP, leading to important spatial and temporal portioning of strain. They have shown that the subducting oceanic

plate and suprajacent décollement are rougher than previously interpreted (Figure 5.3). This is important as asperities have been shown to cause high pore-fluid pressures in their surrounding areas, leading to stepping up of décollement, thus contributing to local clusters of very low frequency earthquakes (VLFEs) (Bangs et al., 2009; Tilley et al., 2021). Therefore, asperities within the subducting plate increase the degree of structural coupling between tectonic plates, potentially partitioning deformation in the overlying accretionary prisms (Azevedo et al, 2018). This means that the outer wedge zone of the NAP may not be after all as aseismic and structurally decoupled as previously described and may form regions of important seismic activity with tsunamigenic potential (Nakano et al, 2018; Takemura et al, 2019; Shiraishi et al., 2020).

This chapter presents the results of two sandbox models prepared to provide new insights on the role of discrete and combined asperities in the tectonic evolution and growth of the NAP and its tsunamigenic potential, more specifically these models will reveal the rupture patterns within the outer wedge of the NAP. The two models simulate the asperities recognised in the study area (Figure 6.1). Equally, this chapter provides a better understanding on the processes and mechanisms through which accretionary prisms incorporate asperities during their subduction as well as on the influence of asperities in the deformation and structural evolution of the overlying prism. It is worth speculating the role of these asperities in the locked MSFZ and potential initiation of great earthquakes across the outer wedge of the Nankai Accretionary Prism (NAP). Therefore, the aims of this chapter are:

1. To understand if the roughness of subducting oceanic plate and overlying décollement can influence the partitioning of stress and deformation observed in the outer wedge of the NAP.
2. To provide better insight into how asperities, with the characteristics as the ones observed in the study area are included in accretionary prisms and predict how they will impact the NAP in their wake.
3. To speculate the role of these asperities in the formation of low velocity zone Unit B and their influence in the pore-fluid pressure.
4. To attempt to predict potential areas of higher tsunamigenic risk in the study area.

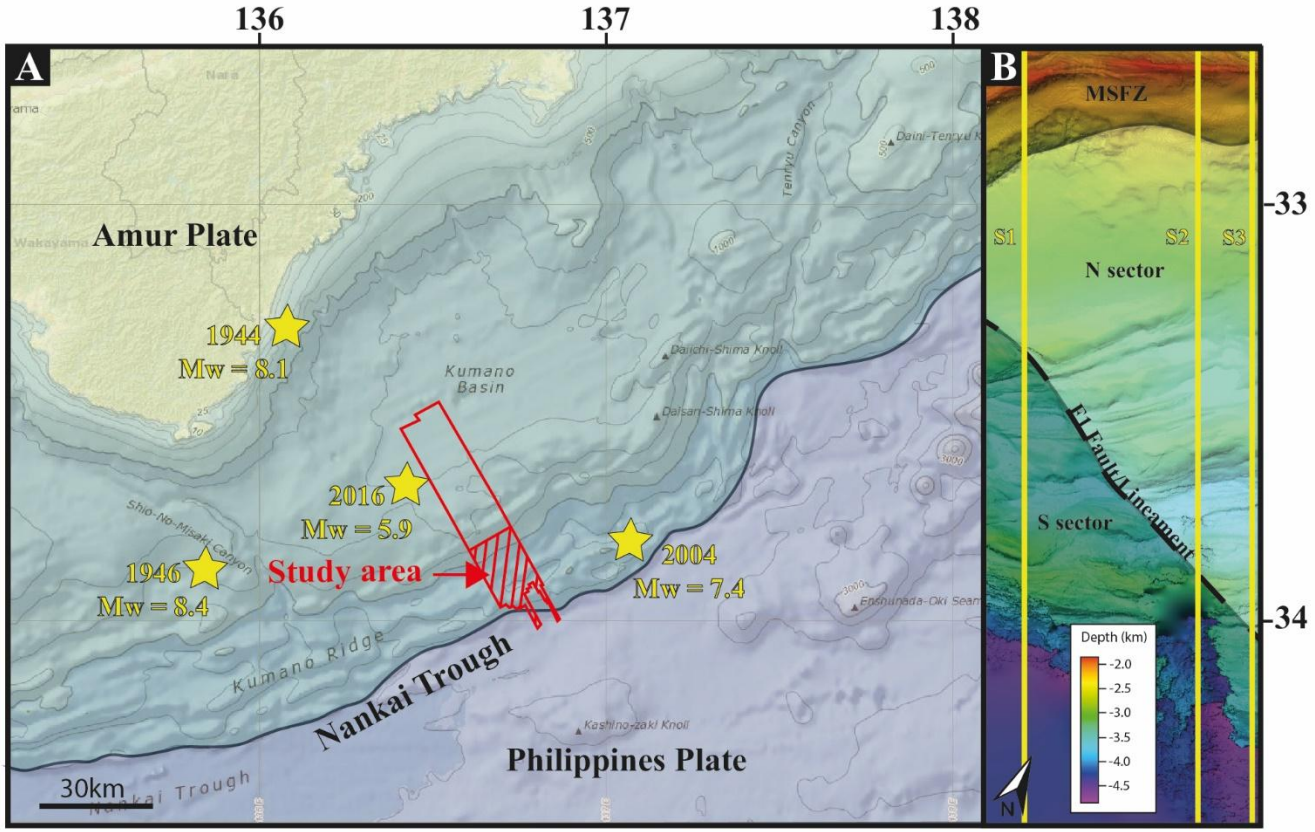

Figure 6.1 – A) Geographic location of the study area within the Kumano Transect (red area) and along the Nankai Trough with the location of major earthquakes in the surround area (Yellow stars). B) Seismic horizon of the top surface of the NAP showing the MSFZ and the partitioned N and S sectors of the study area that area separated by the lineament and fault F1. Yellow lines: seismic profiles S1, S2 and S3 from Figure 6.3.

6.3 Chapter-specific methodology

6.3.1 Experimental method

Many analogue modelling experiments have been carried out to address the influence of subducting asperities in the seismic coupling between the subducting and overlying plates along subduction zones (e.g. Dominguez et al., 1998; Dominguez et al., 2000; Van Rijsingen et al., 2019; Wang et al., 2021). However, most analogue experiments either cover a uniform roughness across the analogue subducting plate or represent one or two specific asperities, where findings cannot be directly transferred to the NAP. Additionally, only few studies (Wang et al., 2021; Furuichi et al., 2024) have focused on analogue scenarios where interference between different asperities are considered. Therefore, the present work includes two sandbox analogue experiments in which the first experiment considers a discrete asperity similar to the ridge identified in Chapter 5, just North of Scarp 3 (Figures 5.3 and 5.4) to focus on the interference caused by its collision with the NAP and to understand if elongated major ridges and related scarps of this nature can cause nucleation of tear faulting and partitioning of strain and deformation such as the one described and discussed in Chapter 4 and 5. The second experiment reflects a scenario with combined asperities, where the asperity from the first experiment is maintained, but another asperity, representing the triangular-shaped asperity of the Kumano Seamount is added.

The second experiment aims to assess the impact of the seamount and its interaction with the elongated ridge from first experiment on the strain and deformation of the NAP as well as to reveal mechanism through which this seamount can be included in the Frontal Thrust Zone (FTZ).

Both experiments have been designed by similarity scaling and created to be a close representation of the two main asperities identified from the 3D seismic data in Chapter 5 (Figure 6.2).

6.3.2 Experimental materials

Dry quartz sand was selected to simulate the brittle upper layers of the NAP, as it is a Coulomb-type granular material whose frictional behaviour mimics that of upper crustal sediments (e.g., Dominguez et al., 1998; Wang et al., 2021). Quartz sand is especially appropriate for analogue modelling of brittle wedge deformation due to its reproducible mechanical properties, including a coefficient of internal friction (μ) typically between 0.6 and 0.7, which corresponds to an internal friction angle of ~30°–35°. In our model, the measured coefficient of internal friction for the quartz sand was ~0.6, which aligns well with these published ranges (Table 4) and with the angles derived from fault geometries in Chapter 4: a coefficient of internal friction (μ) of 0.58, corresponding to an internal friction angle (ϕ) of ~30.2°, which is consistent with published values (μ ≈ 0.6–0.7; ϕ ≈ 30°–35°) (see Figure 4.9C).

The basal layer of glass microbeads was used to represent Unit B, a mechanically weak and potentially fluid-rich zone within the accretionary prism. Glass microbeads exhibit lower internal friction than dry sand ($\mu \approx 0.45$), which promotes mechanical decoupling and shear localisation. This behaviour aligns with interpretations of Unit B as an under compacted or over pressured interval prone to strain localisation. Supporting this interpretation, the dihedral angle measured from strike-slip fault pairs in Chapter 4 corresponds to an internal friction angle (ϕ) of approximately 20.8°, yielding a coefficient of internal friction (μ) of 0.38 (see Figure 4.9C). These values reinforce the mechanical appropriateness of using microbeads to simulate Unit B. The full set of measured material properties used in the experiments is summarised in Table 1.

The basal décollement in the model was simulated by a rigid, undeformable Perspex base, representing the strongly coupled Unit C and the subducting Philippine Sea Plate. Given the absence of mechanical detachment below Unit B in the analogue model (i.e., a low-permeability rigid base), this configuration assumes strong coupling at depth and no further underthrusting sediment accommodation, consistent with interpretations of limited subduction erosion or underplating beneath the study area. Additionally, Perspex wedges of fixed geometry were embedded in the base to simulate subducting bathymetric highs such as seamounts and ridges characterised in Chapter 5 (Figures 5.3 and 5.4). Their rigid nature allowed for reproducible simulation of structural buttressing and induced stress partitioning around these features.

One key limitation of the model lies in the inability to simulate high pore fluid pressures and their dynamic evolution during deformation. In natural systems like the Nankai Trough, fluids play a critical role in weakening fault zones and reducing effective normal stresses, particularly within Unit B, as discussed in Chapter 5. This implies that fault localisation and critical taper angles may differ from those observed in nature. Moreover, the lack of thermal gradients, sediment compaction, and chemical diagenesis further simplifies the physical conditions and mechanical behaviour of the subduction interface. These simplifications are acknowledged, but the primary objective of the model is to investigate large-scale mechanical responses to bathymetric asperities, not the full hydro-mechanical evolution of the subduction system.

Table 4 – Parameters and material properties used in both analogue experiments carried out as part of this chapter. Scaled fundamental units are shown in bold letter. Note: Parameter values for the natural prototype were extracted from [*1]Colin et al. (2011), [*2]Huffman and Saffer (2016) and [*3]Skarbek (2009).

Analogue tectonic unit	Materials	Parameter	Model	Prototype	Model/Prototype Ratio	
Accretionary prism (Unit A)	Dry Quartz Sand	Density (kg/m^3)	1300	2650	$\delta = 0.49$	*1
		Coefficient of internal friction, μ_c	~0.6	0.5 - 1	~1	*2
		Cohesion, c_0 (Pa)	Negligible	33×10^{-6}	-	*3
		Gravity acceleration, g (m/s^2)	9.81	9.81	$\gamma_g = 1$	
Low velocity Unit B (and décollement)	Glass Microbeads	Density (kg/m^3)	1550	2650	$\delta = 0.58$	*1
		Coefficient of internal friction, μ_c	~0.45	0.4	~1.1	*2
		Cohesion, c_0 (Pa)	Negligible	1.95×10^{-6}	-	*3
		Gravity acceleration, g (m/s^2)	9.81	9.81	$\gamma_g = 1$	
		Length, L (m)	0.06	11000	$\lambda = 5.5 \times 10^{-6}$	
		Mass, M (kg)	-	-	$\mu = 4 \times 10^{-18}$	

6.3.3 Experimental scaling

The models and natural prototypes were scaled according to the scale model theory (Hubbert, 1937), with the ratios between the model and prototype materials represented in Table 1. For proper scaling to be achieved, ration between the model and natural prototype must be independently determined for units of length (λ), time (τ) and mass (μ):

$$\lambda = \frac{L(m)}{L_{(p)}} \; ; \; \tau = \frac{T(m)}{T(p)} \; ; \; \mu = \frac{M(m)}{M(p)} \qquad \textit{Equation 1}$$

where L=length, T=time and M=mass, and (m) stands for model and (p) for natural prototype.

In terms of time (τ), the current study takes an approach of similarity scaling for horizontal shortening (Reber et al., 2020), in the τ ratio is not relevant and therefore does not need to be scaled. Equally, the use of dry quartz sand and glass microbeads as Coulomb materials for the model means that deformation of these brittle materials is time independent and yield stress is not affected by the rate of deformation, only by the amount of deformation.

In terms of length ratio (λ), the maximum length of the model apparatus was used and compared with the maximum length of the study area (see Figures 6.1 and 6.2) in order to get a scaling of $\lambda = 5.5 \times 10^{-5}$.

Although mass ratio (μ) cannot be directly inferred due to the impossibility of doing so on the prototype, it is possible to infer it from the two relevant

material properties, coefficient of internal friction (μ_c) and cohesion (c_0). As μ_c for both the model and the protype are approximately the same, their ratio is assumed to be 1. The c_0 is a dimension of stress and must be scaled as per the equation:

$$\Sigma = \frac{c_0(m)}{c_0(p)} = \frac{\mu\gamma}{\lambda^2} \qquad \textit{Equation 2}$$

As the gravity acceleration on both the model and the prototype are the same, 9.81ms^{-2}, then γ=1 as per the formula on the model/prototype gravity acceleration ratio:

$$\gamma = \gamma_g = \frac{g_{(m)}}{g(p)} = \frac{\lambda}{\tau^2} = 1 \qquad \textit{Equation 3}$$

When replacing the γ=1 on equation 2, it simplifies to:

$$\Sigma = \frac{c_0(m)}{c_0(p)} = \frac{\mu}{\lambda^2} = \frac{\mu\lambda}{\lambda^3} = \delta\lambda \qquad \textit{Equation 4}$$

Model/prototype cohesion ratio (Σ) ultimately becomes the product of correspondent density (δ) and length (λ) ratios. As the average density ratio (δ) is 0.54 and the length ratio (λ) is 5.5×10^{-5}, the strength of the materials expressed by Σ, and therefore the cohesion ratio is 2.97×10^{-5}. Equation 2 determines a mass ratio (μ) between model and prototype as reading 9×10^{-16}.

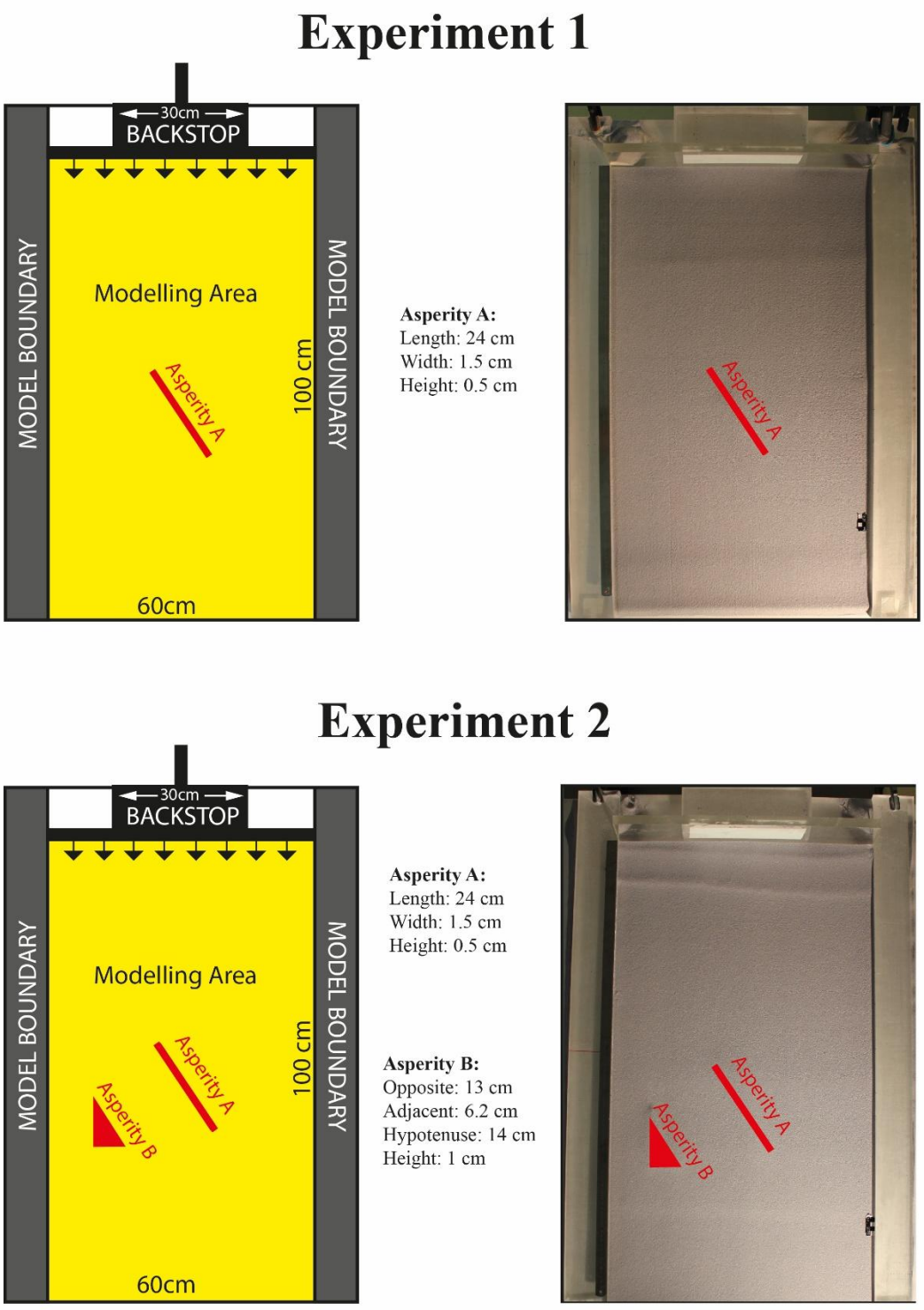

Figure 6.2 – Schematic of the sandbox model design (on the left side) and respective aerial view photo (on the right side) made on a rectangular Perspex deformation box, size 1m by 0.6m. Asperity A represents the elongated major ridge and Asperity B represents the Kumano Seamount, both identified and described in Chapter 5. The sand cake was laid out uniformly with an alternation of white and purple died dry quartz sand.

6.3.4 Apparatus and initial stage

The experiments were carried out in a rectangular 100 cm × 60 cm Perspex deformation box designed with a 100 cm x 80cm flat Perspex surface. The deformation box was bordered by two suprajacent 120 cm x 10 cm x 2.2 cm Perspex wedges on both sides and a moving backstop (Figure 6.3). For each of the experiments a 1cm thick sand cake, covering the whole 100 cm x 60cm area of the deformation box, was built using a moving elongated funnel to ensure correct flat layering between the distinct layers in the physical model. The sand cake consisted of a lowermost ca. 2 mm thick layer of clear glass microbeads representing the fluid-rich and highly brittle Unit B of the NAP. The other materials consisted of an alternation between differently coloured dry quartz sand layers, representing the overlying cover sediments (see the right end of the profiles in Figures 6.1 and 6.6). Both materials were accreted in a similar fashion to natural environment by pushing a backstop against the model sand cake. However, the backstop lacks any kind of correspondence with any natural feature and was exclusively used to produce a classical model thrust wedge. The coloured layers of dry quartz sand in the sand cake also have also no correspondence with natural stratigraphic units in Unit A of the NAP but were used as passive 3D strain markers. In both experiments, the large dimensions of the deformation box and the central placing of the obstacles, simulating the asperities, ensure that the bulk of the model was not severely affected by friction and drag near its boundaries (Figure 6.2).

Both experiments were repeated twice to ensure the reproducibility of the achieved results. Top view photographs were taken at the end of each accretion cycle, which corresponded to pushing the backstop forward by 1cm at a time. These cycles have been chosen to allow estimates of horizontal shortening in the model, and subsequent comparisons with natural shortening in the NAP. In the final stage, the model was humidified and systematically sectioned for three-dimensional analyses, as discussed later in this chapter.

6.3.5 Experimental procedure

Two main experiments were conducted to study the implications of individual and combined asperities in the deformation of the NAP:

- **Experiment 1, considering the presence of a single basal asperity:** a 10 cm x 1.5 cm x 0.5 cm block of azimuth N115° was placed to simulate a single asperity scenario representing an elongated major ridge striking in the direction of fault F1 (Figures 6.1 and 6.2), being subducted under the NAP. The reasoning behind this choice is that the ridge associated with F1 is the first major asperity being subducted in the NAP, at present.
- **Experiment 2, with two combined asperities:** the same block from the previous scenario, representing the elongated major ridge, was kept in experiment 2, with an additional 1 cm thick triangular

block (see dimensions in Figure 6.2) being added to closely simulate the Kumano Seamount identified in 3D seismic data (see Chapter 5). This scenario was focused on characterising interference between the two mentioned asperities.

6.4 Experimental results

This section of the thesis will focus on presenting and interpreting the results obtained from the sandbox Experiments 1 and 2 carried out as part of this Chapter 6.

6.4.1 Experiment 1: single asperity

Experiment 1 developed a typical accretionary prism until a horizontal shortening of 32% (Figure 6.3A). The Imbricated Thrust Zone (ITZ) and proximal Out-of-Sequence Zone (OOSZ) started forming at a horizontal shortening value of 15%. This OOSZ is bordered in its frontal part by a MSF (Figures 6.3A-C and 6.4) that overrides the backwards part of the ITZ, hiding some of the 'older' thrust nappes (Figures 6.3 and 6.4).

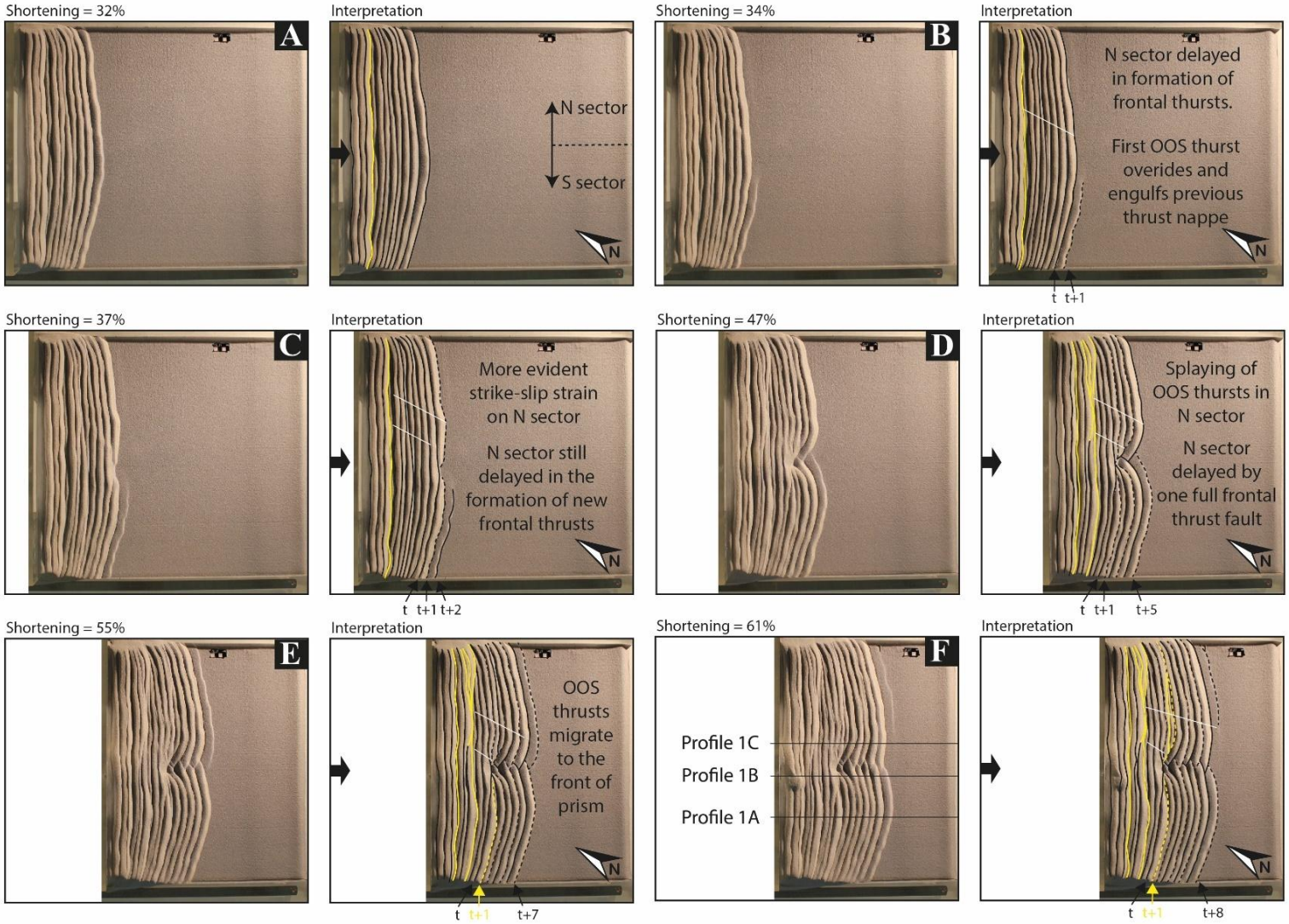
Shortening = 32%
A
Interpretation
N sector
S sector
N
Shortening = 34%
B
Interpretation
N sector delayed in formation of frontal thursts.
First OOS thurst overides and engulfs previous thrust nappe
N
t t+1
Shortening = 37%
C
Interpretation
More evident strike-slip strain on N sector
N sector still delayed in the formation of new frontal thrusts
N
t t+1 t+2
Shortening = 47%
D
Interpretation
Splaying of OOS thursts in N sector
N sector delayed by one full frontal thrust fault
N
t t+1 t+5
Shortening = 55%
E
Interpretation
OOS thrusts migrate to the front of prism
N
t t+1 t+7
Shortening = 61%
F
Profile 1C
Profile 1B
Profile 1A
Interpretation
N
t t+1 t+8

Figure 6.3 – Top view photos of Experiment 1 during its different stages of horizontal shortening (A – F). The N and S sector in A) are referenced in relation to the basal asperity but also to resemble the N and S sectors from Fault F1 as per Chapter 5. A) Horizontal shortening value of 32% reveals a fold-and-thrust geometry, typical of the ITZ, and a MSF acting an OOS fault (in yellow). B) Horizontal shortening value of 34% reveals first signs of interference of the basal asperity in the accretionary prisms. The S sector first develops new frontal thrust when compared to a delayed N sector. The N sector accommodates some strain in form of left-lateral strike-slip (in white). C) Horizontal shortening at 37% reveals a hastened S sectors in relation to the formation of frontal thrust in the ITZ, while the MSF continues to override older and more consolidated parts of the accretionary prism that are no longer visible in the top view photo. The N sector continues to develop a regime of left-lateral strike-slip faulting. D) Horizontal shortening at 47% shows the continuing delay of the N sector compared to the S sector in the formation of new frontal thrusts. There is a forward propagation of OOS thrust that seems to take advantage of previously formed imbricated thrusts. The N sector develops a splaying of OOS thrust which seems to be related to the over-compressed accretionary prisms in this sector caused by the general convergence of the model and the local convergence caused by the strike-slip faulting. E) Horizontal shortening at 55% reveals similar pattern to the one described in D) with the aspect that the N sectors is now considerable delayed, by a whole frontal thrust, in relation to the S sector. F) Horizontal shortening at 61% reveals a further forward propagation of OOS thrusts as well as the strike-slip faulting formed at earlier stages. Profiles 1A, 1B and 1C from Figure 6.4 are here represent as straight black. Yellow lines: thrusts showing OOS behaviour; Black straight and dashed lines: ITZ thrusts; White lines: potential tearing or strike-slip faulting.

At a horizontal shortening of 34%, the accretionary prism (Figure 6.3B), with a width of ~26 cm, encounters the basal asperity considered in the model, causing the new frontal thrust (t+1 in Figure 6.3B) to not develop evenly along strike, in contrast to previously developed frontal thrusts. In this case, the basal asperity is causing sediment accretion and fault rupture to first develop on the S sector of the model, to then propagate to its N sector after an increment in horizontal shortening.

Above horizontal shortening values of 37%, the previous frontal thrust (t+1 in Figure 6.3C) is entirely developed on both sectors of the basal asperity. However, an additional total horizontal shortening of ca. 3% was required for lateral continuity of the frontal thrust zone to be re-achieved and for equivalent frontal thrusts to be present on both S and N sectors of the model. An interesting point is that although the shortening seems to be delayed on the N sector, thrust faults accommodate its movement more effectively compared to the S sector (Figure 6.4C). At a horizontal shortening value of 37%, a new frontal thrust forms (t+2 in Figure 6.3C) on the S sector like the previous scenario of horizontal shortening at 34%. From this point of horizontal shortening onwards, the growth of the accretionary prism follows the same accretional pattern as previously described until the end of Experiment 1, creating an apparent strike-slip structure due to the alternating growth of prism on both sectors of the basal asperity, resembling a tear faulting system.

An interesting finding is that out-of-sequence thrusting is also affected by the basal asperity on both sectors of the accretionary prism in the model. A splaying geometry of out-of-sequence thrusts is formed on the N sector of older and most accreted part of the accretionary prism, overriding and covering part of the most recently formed thrusts at the ITZ (Figures 6.3D-F). This out-of-sequence splaying is not developed on the S sector of the model. Instead, a new out-of-sequence thrust develops on the previously imbricated thrust identified at t+1. At horizontal shortening value of 55% (Figure 6.3E), this out-of-sequence thrust no longer follows the general pattern of imbrication and starts overriding the frontal ITZ. This is evident in Figures 6.3E and 6.3F, where the t+1 thrust fault meets and almost completely overrides thrust fault t+2. A similar pattern of out-of-sequence thrusting also occurs on the N sector of the basal asperity, but only between thrusts t+2 and t+3, which also reveals a delay in the formation of the out-of-sequence thrusts.

It is important to mention that while the N sector of the accretionary prism experiences delayed accretion, when compared to the S sector, it shows larger increments in the growth of its frontal thrusts, meaning that the N sector is expected, in our model, to catch-up with the S sector, or even have a temporary stage where it slips further than the S sector, as seen in Figure 6.3F at 61% of horizontal shortening.

Profiles 1A, 1B and 1C (Figure 6.3F and Figure 6.4) also provide some important evidence in relation to the behaviour of the lowermost microbeads

layer in relation to the accretion experienced, beyond a horizontal shortening of 61%. Both Profile 1A, on the S sector, and Profile 1C, on the N sector, show similar patterns of deformation styles and geometry with the glass microbeads layer thickening towards the back of the accretionary prism and locally thickening along its width, in the areas from where major thrusts branch out (Figures 6.4A and 6.4C). Nevertheless, the out-of-sequence thrusts (yellow lines in Figures 6.3 and 6.4) coincide with the areas where microbeads layer is thicker. It is important to stress that Profile 1C reveals an overall thicker microbeads layer than Profile 1A.

Profile 1B (Figure 6.4B), crossing the basal asperity, shows a striking difference compared to the other profiles. There is a considerable thickening of the microbeads layer just behind and above the basal asperity, a character accompanied by an increase in the number of thrusts branching from this thick glass microbeads layer. The branching out of thrust faults resembles a 'flower structure', which enhances the height of the accretionary prism in this area. In front of the basal asperity, the accretion prism resumes its typical fold-and-thrust geometry observed in Profiles 1A and 1C, but also with a much thicker microbeads layer than in other profiles.

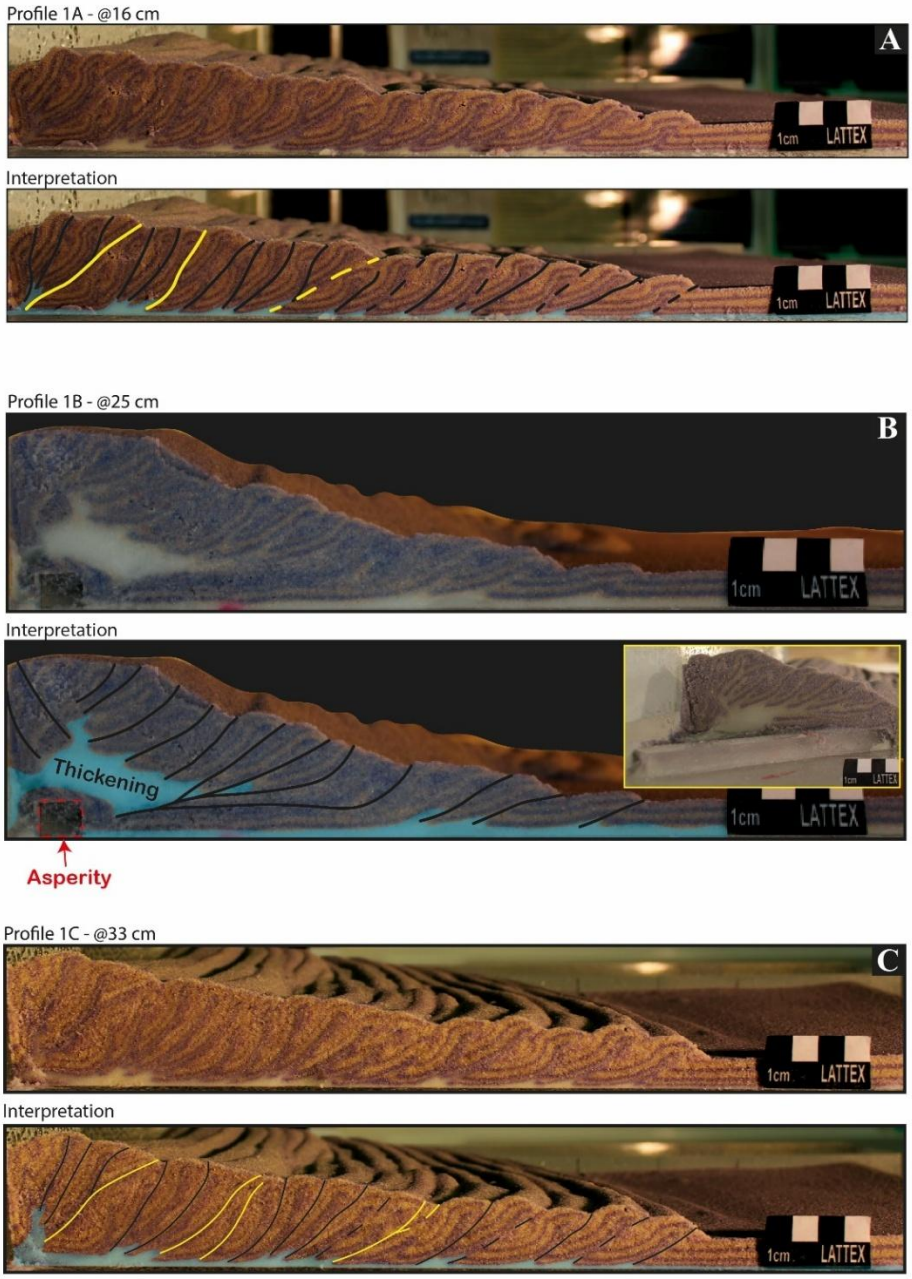

Figure 6.4 – Photos of the intersection profiles obtained from sandbox model of experiment A – Intersection profile 1A taken 16cm from the left boundary, representing the W section of the model. B – Intersection profile 1B taken 25cm from the left boundary, representing a section intersecting asperity A. An insert in yellow box showing a close-up photo at a different angle of the thickening of the glass microbeads layer. C – Intersection profile 1C taken 33cm from the left boundary, representing the E section of the model. Yellow lines: thrusts showing OOS behaviour; Black straight and dashed lines: ITZ thrusts; White lines: potential tearing or strike-slip faulting; Blue area: glass microbeads layer; Red dashed rectangle: asperity.

6.4.2 Experiment 2: combined asperities

Experiment 2 also resulted in the formation of an accretionary prism with a typical ITZ and FTZ with a fold-and-thrust geometry until a horizontal shortening value of 20% was reached (Figure 6.5A). This was followed by the formation of a proximal OOSZ, marked by the presence of a MSF. Early signs of interference from basal asperities below are revealed by the development of incipient strike-slip (or tear) faults (white lines in Figures 6.5 and 6.4) due to minor differential movement along-strike. Experiment 2 differs from the first Experiment as it required a much lower value of horizontal shortening before clear signs of differential growth were shown on the frontal part of the accretionary prism. However, it is important to stress that Experiment 2 required 12% less horizontal shortening that the first Experiment to accrete the same amount of sediment necessary to achieve an accretionary prism width of 25-26 cm, from which along-strike differential formation of new frontal thrusts is first revealed.

At a horizontal shortening value of 30% (Figure 6.5B), Experiment 2 behaves similar to Experiment 1 when considering both the alternating formation of new frontal thrusts and differential along-strike growth of the accretionary prism, where the S sector ruptures and moves before the N sector (t+1 in Figure 6.5A), as well as the formation of a lineation resembling strike-slip fault. It appears that a horizontal shortening of 30% in Experiment 2 correlates with hori-

zontal shortening values of 45 – 55% in Experiment 1, under which it was possible to observe newly formed OOS thrusts ahead of the original one (Figures 6.3E, 6.34D and 6.5B). In Experiment 2, it becomes evident that the N sector ruptures/slips further than the S sector at 30% horizontal shortening despite forming relatively later. The latter is seen in Figure 5B that shows that the newly formed frontal thrust t+4, on the S sector, is at the same level as the previously formed t+3, on the N sector.

At a horizontal shortening of 41% (Figure 6.5C), the frontal part of the accretionary prism collides with both asperities for the first time. At this stage, the width of the accretionary prism is larger on the N sector when compared to the S sector, and that the accretionary prism is now being partitioned in three sectors (Figure 6.5D). It is also important to note that at 34% horizontal shortening both N and S sectors of the accretionary prism rupture almost simultaneously at its frontal part, but the N sector is already a whole frontal thrust cycle behind, where the rupture of frontal thrust t+5 on the S sector coincides with the rupture of frontal thrust t+4 on the N sector (also t+3 and t+4 in Figure 6.5B). However, it is only at 41% horizontal shortening that the second basal asperity, representing the Kumano Seamount, seems to have a considerable impact on the along-strike rupture of the frontal thrusts, as well as on the forwards growth of the prism (Figure 6.5C).

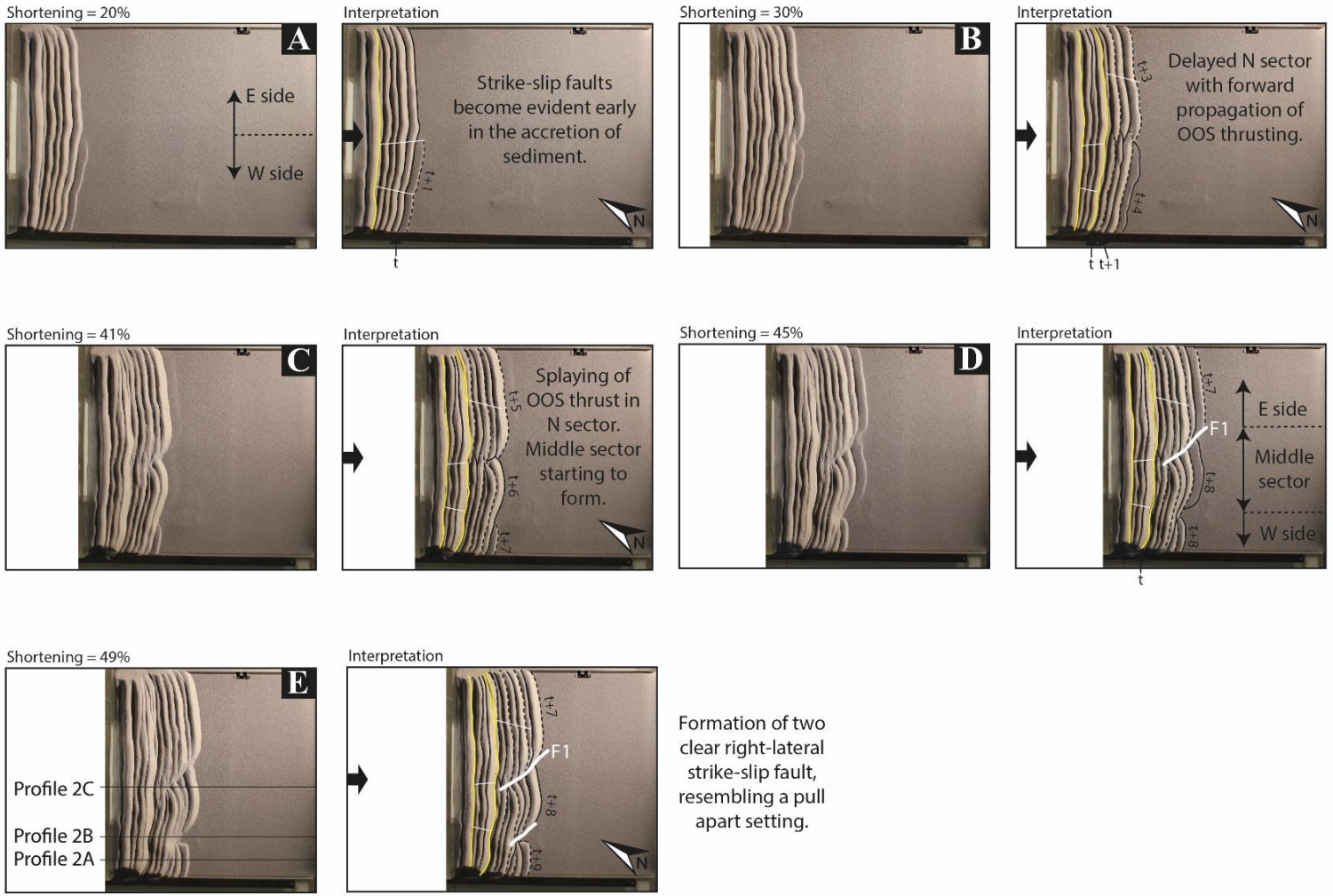
Shortening = 20%
A
E side
W side
Interpretation
Strike-slip faults become evident early in the accretion of sediment.
t+1
t
N
Shortening = 30%
B
Interpretation
Delayed N sector with forward propagation of OOS thrusting.
t+3
t+4
t t+1
N
Shortening = 41%
C
Interpretation
Splaying of OOS thrust in N sector. Middle sector starting to form.
t+5
t+6
t+7
N
Shortening = 45%
D
Interpretation
t+7
F1
t+8
t+8
E side
Middle sector
W side
t
Shortening = 49%
E
Profile 2C
Profile 2B
Profile 2A
Interpretation
t+7
F1
t+8
t+9
N
Formation of two clear right-lateral strike-slip fault, resembling a pull apart setting.

Figure 6.5 – Top view photos of Experiment 2 at different stages of horizontal shortening (A – E). The N and S sector in A) are referenced in relation to the basal asperity but also to resemble the N and S sectors from Fault F1 as per Chapter 5. The Middle sector is an additional sector included in Experiment 2 because of the formation of three distinct strain partitioned areas. A) Horizontal shortening value of 20% reveals a fold-and-thrust geometry, typical of the ITZ, and a MSF acting an OOS fault (in yellow) as well as with early signs of frontal thrust formation being delayed in the N sector Some strike-slip is left-lateral regime observed in the S sector, probably from over compression caused by two basal asperities. B) Horizontal shortening value of 30% reveals severe delay in the formation of frontal thrusts by a whole cycle and OOS thrust propagate forward through pre-existing ITZ thrusts. The propagation of OOS thrust forward seem to terminate strike-slip faults formed earlier and make them inactive. C) Horizontal shortening at 41% reveals a hastened S sectors in relation to the formation of frontal thrusts in the ITZ, but with the N sector slipping more and contribution for higher rate of frontal growth of the accretionary prism. There is a formation of right-lateral strike-slip in the N sector with early evidence on formation of third sector, the Middle sector. D) Horizontal shortening at 45% reveals clear partitioning of strain into three sectors that is responsible for the formation of the significant right-lateral strike-slip fault, resembling that of F1 in the study area. E) Horizontal shortening at 49% reveals similar pattern to the one described in D) with the aspect there are two right-lateral strike-slip faults parallel to one another and seem to border the different sectors here identified. Profiles 2A, 2B and 2C from Figure 6.6 represent as straight lines in Figure 6.5E. Yellow lines: thrusts showing OOS behaviour; Black straight and dashed lines: ITZ thrusts; White lines: potential tearing or strike-slip faulting. F) Line graph showing the number of new frontal thrust since collision with both asperities, from shortening of 20% until the end of the experiment.

Beyond a horizontal shortening value of 41% until the end of the experiment at a horizontal shortening of 49% (Figures 6.5C-E), the accretionary prism partitions itself into three sections (Figure 6.5D) as a response of the interference with the two basal asperities. The N sector shows the furthest growth in width with fewer folds and thrusts compared to the adjacent Middle and S sectors. The S sector of the accretionary prism is the shortest but possesses the greater number of thrusts (Figure 6.5F). It is important to mention that at horizontal shortening between 41% and 49%, both the N and Middle sectors have formed all their new frontal thrusts in unison and the difference in the number of thrust nappes relates to the alternating behaviour of the frontal rupture area at 20% to 32% horizontal shortening (Figure 6.5F). The difference in the number and thickness of the thrust nappes ruptured in the FTZ, due to the collision with the basal asperities, causes differential along-strike growth of the accretion prism. This discrepancy in the growth between the S, Middle and N sectors lead to tearing of the accretionary prism, partitioning the distribution of strain in the model.

Profiles 2A and 2B (Figures 6.6A and 6.6B), respectively near and at the seamount basal asperity show signs of thickening of the basal microbeads layer towards the back of the accretionary prism, with the greatest thickness recorded behind the basal asperity (Figure 6.6B). This accumulation of microbeads layer behind the basal asperity stepping up above the basal asperity, where a considerable number of low-dip thrusts branch out just above the latter. It is important

to note a considerable difference between Profile 1B (Figure 6.4B), from Experiment 1, and Profile 2B (Figure 6.6B), from Experiment 2; the sediment in front of the asperity is deformed and accreted in Experiment 1, contributing to the continuing growth of the accretionary prism, in the Experiment 2, the sediment in front of the asperity is undeformed without any evidence of accretion.

Profile 2C (Figure 6.6C) crossed the easternmost basal asperity and shows a stepping up of the basal microbeads layer and its continuation towards the other side of the asperity, leading to the further rupture and growth of the accretionary prism, as shown in Profile 1B (Figure 6.4B). Profile 2C shows a longer accretionary prism compared to the adjacent Profile 2B, with fewer thrusts and gentler dip.

Figure 6.6 – Photos of the intersection profiles obtained from sandbox model of experiment B – Intersection profile 2A taken 5cm from the left boundary, representing the W section of the model. B – Intersection profile 2B taken 12cm from the left boundary, representing a section intersecting asperity B. C – Intersection profile 2C taken 26cm from the left boundary, representing a section intersecting asperity A. Yellow lines: thrusts showing OOS behaviour; Black straight and dashed lines: ITZ thrusts; White lines: potential tearing or strike-slip faulting; Blue area: glass microbeads layer; Red dashed rectangle: asperity

6.5 Chapter-specific discussion

6.5.1 Deformation styles observed for the different modelled scenarios

The physical experiments in this chapter convey that an accretionary prism formed above a rough surface with discrete basal asperities will interfere with the fold-and-thrust process per se and with the rupture of its FTZ. Importantly, they show that the presence of basal asperities interferes with sediment accretion even before the FTZ comes into direct contact with such basal asperities. This influence is probably related to space constraints caused by the backstop behind the accretionary prism and the basal asperities in front of the upcoming prism. As a response to the increased limitation of space between the backstop and the basal asperities, the accretionary prism develops OOS thrusts along previously formed thrusts in the ITZ that will then override parts of the ITZ. This causes an increase in the height of the accretionary prism as a short-term response to accretion, as clearly shown in the two experiments, but that may be hidden in the 3D seismic data imaging the NAP due to its long-term tendency towards a uniform taper (Haq, 2012). According to the later author, the OOS thrusts normally develop along pre-existing ITZ thrusts if their orientation is favourable, as documented in this chapter (Figures 6.4 and 6.6). This is

precisely the mechanism through which an accretionary prism thickens to promote the growth of its inner and, subsequently, outer wedges. Additionally, the increased horizontal shortening experienced by an active accretionary prism forms a conjugated system of tearing faults (white lines in Figures 6.3 and 6.5) due to the presence of basal asperities as differential along-strike shortening is promoted. A slight curvature at the front of the accretionary prism develops purely as a response to the friction created between the sides of the prism and the lateral boundaries of the deformation box, which drags the lateral side of the accretion prism in relation to its central part that advances further. Although this curvature is not observed at the scale of NAP, it becomes less evident upon the collision with the basal asperities, as these become the main resistance to movement and growth of the accretionary prism.

The effect of basal asperities becomes more prominent when these collide with the front of the accretionary prism (Figures 6.3C, 6.5A and 6.5C). At this stage, the asperities behave as mechanical obstacles to the lateral and frontal propagation of the prism. In both experiments, the initial collision of the accretion prism with asperity A impacts both the frontal and inner parts of the accretionary prism. Due to further constraints in space between the backstop and the newly collided asperity, the inner part of the accretionary prism experiences thickening of the lowermost microbeads layer, aiding the formation of new out-of-sequence thrusts further ahead of the original MSF. This process increases the height of the inner part of the accretionary prism and the magnitude of horizontal shortening by overriding the outermost ITZ. In the frontal

part of the accretionary prism, the basal asperity interrupts the lateral continuity of the frontal thrust zone, creating two sectors (N and S sectors) that start growing independently from each other. The partitioning of the model into N and S sectors, when interacting with the basal asperity below, imposes new spatial constraints. The S sector experiences a scenario that changes from tightly constrained to loosely constrained as the accretionary prism grows further, while the N sectors develops in an opposite scenario, where space becomes more constrained as the accretionary prism advances. Although the lateral boundaries of the model do not represent any natural boundary from the NAP, they may resemble the presence of other neighbouring basal asperities within ridges or well-defined fault scarps and/or locked sections of the NAP that are not slipping. The starting narrow gap between the basal asperity and the lateral boundary, and the higher limitation of space experienced by the accretionary prism on the S sector creates conditions for a local increase in stress distribution, and subsequent horizontal shortening, leading to this side rupturing first. This created the apparent delayed growth of the N sector. Alternatively, the N sector of the accretionary prism may require continued sediment accretion to increase its topographic slope and basal shear stress, eventually reaching the critical taper angle required for stable wedge growth. Once this critical state is achieved, the accumulated stress exceeds the shear strength of sediments at the frontal thrust zone (FTZ), triggering rupture and the formation of a new frontal thrust, thereby promoting forward propagation and growth of the accretionary prism.

It is important to discuss the mechanisms through which the accretionary prism overcomes the basal asperities, as mechanical obstacles, and continues to grow beyond these. In other words, it is important to understand the processes that lead to the inclusion of basal asperities below the accreted sediment, and their impact on later accretion processes experienced by the active prism.

In Experiment 1, asperity A acts as a mechanical barrier to the physical rupture and growth of the accretionary prism. For the most part, horizontal shortening is accommodated a typical fold-and-thrust setting in the ITZ continues to develop due the new frontal thrusts in the FTZ. However, as inner parts of the accretionary prism become consolidated by the continuous shortening, their older inner thrusts may, at times, slip in an out-of-sequence style, causing an inner part of the accretionary prism to override its outer part. This could be the mechanism through which inner and outer wedges become distinct entities within accretionary prisms, but also a process through which the accretionary prism can maintain its critical taper condition and continue to grow (Davis et al, 1986). Nevertheless, sediment accretion in this format cannot sustain strain indefinitely due to the increasing interplate coupling upon the encounter between the accretionary prism and basal asperities. Therefore, shear stress will preferably concentrate in the flanking regions of the basal asperity, with the greatest concentration of stress occurring on the incoming (inner) side of the basal asperity. Such concentration causes the deformation of the accretionary prism that will aid the exhumation of the lowermost microbeads layer frontwards and up-

wards, towards asperity A (Baba et al, 2001). The accumulation of glass microbeads material is facilitated by development of an extensive network of thrusts that locally builds the height of the accretionary prism, helping it to reach new local critical taper conditions, from which the accretionary prism can continue to accommodate horizontal shortening. When the glass microbeads layer locally builds to or above the height of the basal asperity, it causes the step up of the detachment surface (between the microbeads and dry quartz layers) and consequently, decreasing the interplate coupling. This drop in the coupling allows the accretionary prism to resume its accretion process through branching of new frontal thrusts beyond the asperity and its further growth (Figure 6.4B). This process explains the delay observed between the N and S sectors observed in the experiments, where the time lag experienced by the N sector was related to the time taken to for the glass microbeads material to accumulate and step up the basal asperity A. Similarly, this transition between strongly coupled and decoupled boundary of the detachment surface between the microbeads and dry quartz layers may temporarily increase slip ratio along such detachment surface compared to the equivalent frontal thrusts on the S sector, thus explaining why the frontal thrusts in the N sector advance more compared to their counter parts in the S sector. Comparing Experiment 1 with the NAP shows that despite the outcome not being 100% similar to the what is currently observed in 3D seismic data, basal asperities can create differential horizontal shortening and along-strike variations in the frontal parts of an accretionary prism, thus creating tearing lineaments that resemble strike-slip faults. These lineaments

may become important pathways for stress relief, especially in terms of slow slip and associated VLFEs, and start behaving as strike-slip faults, especially under conditions of oblique subduction such as that experienced by the Nankai Through.

In Experiment 2, the existence of two basal asperities increases the complexity of the accretion process and subsequent growth of the accretionary prism. Having two coexisting asperities and particularly one of larger dimensions (Asperity B) than the other, means adding an extra and more prominent physical barrier to the propagation of the frontal thrusts, increasing the structural coupling between accreted sediments and the base over which they are being accreted. In Experiment 2, there is considerably higher spatial constraint caused by the presence of multiple basal asperities which causes earlier, and more frequent formation of Out-of-Sequence (OOS) thrusts along previously formed thrusts in the inner parts of the ITZ. In this experiment, these OOS thrusts also override outer parts of the accretionary prism, but with a greater slip movement where occasionally outer parts of the fold-and-thrust get completely overridden. Therefore, a direct relationship between number and/or size of basal asperities and strain accommodation via OOS setting is plausible. The greater dimensions of Asperity B challenge the exhumation process by the microbeads layer, as discussed for Experiment 1, causing some of this material to shift towards the inner parts of the accretionary prism, just behind the basal asperity. This promotes backwards thickening of the glass microbeads layer and subsequently helps the reactivation of previously formed imbricated thrusts as OOS thrusts

(Haq et al., 2012). Such a phenomenon is shown by the increasing number of steep thrust faults on the S sector of the accretionary prism compared to its Middle and N sectors.

Experiment 2 never achieved a condition where exhumation of microbeads layer reached the top of Asperity B. However, it is possible to see similar deformation styles to the ones observed around asperity A in both experiments. This caused the S sector to rupture more often as a response to local higher concentration of shear stress and to locally build height in order to reach a state of critical taper, while the Middle and N sectors of the accretionary prism can slip more due to the low dip, and more often, due to having gentler thrusts. This differential advancement of the frontal part of the accretionary prism promotes the formation of lineaments through tearing, similarly to Experiment 1. Comparisons with the NAP make it possible to verify similarities amongst the lineaments created in Experiment 2 and strike-slip faults described in the latter accretionary prism (compare Figure 6.1 and Figure 6.5E). This suggest that the strain partitioning and deformation in the NAP can be a product of a rough incoming Philippines Sea Plate.

6.5.2 Tectonic implications in areas of active subduction

The subducting Philippines plate under the NAP is rough and comprises several asperities (Shiraishi et al., 2020; Yamamoto et al, 2022) interpreted to

change the frictional properties and local stress fields. These changes originate clusters of VLFEs associated with release of stress, which is then transferred to the areas surrounding the asperities, locally increasing shear stress (Baba et al, 2001; Qin et al., 2021). Although there is a high concentration of VLFEs attributed to a lower slip deficit rate due to high pore-fluid pressure and the presence of complex fracture networks, particularly in areas with significant basal asperities, the study area is within a regional high slip rate area (Yokota et al., 2016). In view of these experimental results, the NAP is here interpreted to have been affected by the presence of basal asperities in the subducting plate, particularly by the subduction of the Kumano Seamount, which seems to be in its initial stages of inclusion in the NAP. Any asperity within the subducting plate will cause an increase of interplate coupling where friction is increased and movement is hindered by enhanced compressional stresses created between the basal asperities and the overlying outer wedge, which acts as a backstop. Therefore, basal asperities can create important variations in the slip rate behaviour, both along and across the Nankai Trough.

In the NAP, the initial collision with the elongated WNW major ridge (Figure 6.7C) is, by itself, able to justify the seawards growth of the accretionary prism to vary along-strike. Indeed, the NAP is characterised by alternating growth between the sectors formed on each side of the ridge. This alternating growth behaviour promotes the tearing of the overlying NAP while enhancing the dextral nature of F1's strike-slip motion (F1 in Figures 6.7B and 6.7C). While this tearing develops perpendicularly to the trough in the experiments, in the

NAP it forms at an angle to the Nankai Trough due to the oblique nature of the subduction in this region. The later collision with the Kumano Seamount (Figure 6.7C) adds to the tectonic complexity already experienced by the NAP by further enhancing the partitioning of strain and deformation. The seamount limits the growth of the NAP on its S sector relative to the N sector, similar to what is recorded in Experiment 2.

In the NAP, the low-velocity Unit B behaves similarly to the basal glass microbeads layer from the physical experiments. Figure 6.7 shows that in the presence of asperities, such as the Kumano Seamount in Figure 6.7A and elongated ridge in Figure 6.7B, the NAP records disruption in the lateral continuity of the décollement and the potential reactivation of some ITZ thrusts as OOS thrusts in association to local variations in the thickness of Unit B (Figures 6.4, 6.6 and 6.7). In 3D seismic data, the seismic signature of Unit B resembles one of a ductile shear zone, which could indicate the local presence of fluid, thus being a crucial part of how strain and deformation propagates from the décollement to Unit A in the NAP. In the light of the findings from the experiments, there are two distinct but coexisting tectonic scenarios that will impact Unit B in the NAP, both resulting from interference caused by asperities.

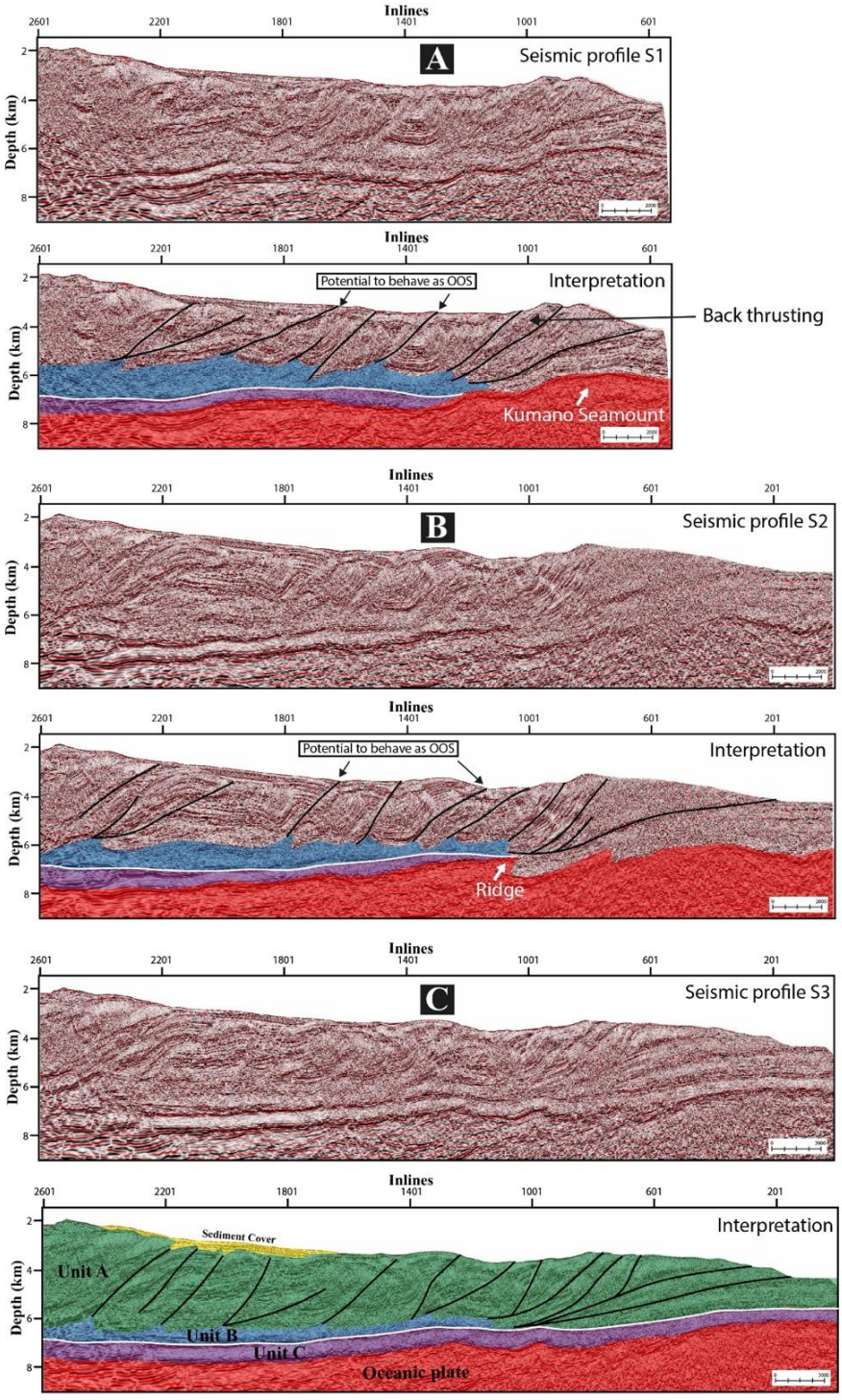

Figure 6.7 – Raw and interpreted seismic profiles from NanTroSEIZE Project. A – Seismic profile S1 taken from inline 2200, representing a section of the study area affected by the Kumano Seamount. B – Seismic profile S2 from inline 2600, representing a section of the study area affected by the elongated ridge. C – Seismic profile S3 from inline 2730, representing a section of the study area away from the influence of main asperities. The interpreted profile includes the tectonostratigraphic units as per Park et al. (2010) and Azevedo et al. (2018).

It is important to acknowledge that the sandbox experiments do not simulate fluid flow, pore pressure diffusion, or hydromechanical coupling directly. However, the choice of materials made in this modelling allows for controlled simulation of relative mechanical contrasts that, in natural systems, may arise due to high pore-fluid pressures. In this context, the glass microbeads in the model are not used to simulate fluids per se, but to represent a weak, mechanically decoupled layer (Unit B) that may behave similarly to zones affected by high fluid overpressure in the Nankai accretionary prism. Therefore, the distribution and localisation of deformation within the glass microbead layer, particularly its internal shear zones and the degree of coupling with overlying quartz sand layers, can provide indirect qualitative insight into how natural equivalents operate (e.g. zones in the model where the glass microbead layer exhibits extensive shearing or thinning beneath frontal thrusts could correlate with the locations of detachment weakening and fluid localisation in the real prism). Nevertheless, this interpretation hinges on the assumption that mechanical weakness in the natural system can arise from elevated pore-fluid pressures, and that the mechanical analogue of glass microbeads sufficiently reproduces the decoupled behaviour attributed to those zones. However, this remains a mechanical analogue, and not a direct fluid pathway simulation, and is thus limited to providing qualitative rather than quantitative insights.

The first scenario proposes that minor basal asperities in the subducting plate, such as the presence of undulating and alternating landward-dipping flat-and-ramp structures (Moore et al., 2009; Shiraishi et al., 2019) and/or lateral

variations in the diagenetic properties of sediment, affect the spatial distribution and continuity of compressional stresses in Unit B (Kitajima and Saffer, 2012). Therefore, local variations in the compaction and stacking of underscrapped material can increase the thickness of Unit B, and, consequently, pore-fluid pressure. The accreted Unit A above mostly acts as a seal for the upward movement of water from Unit B. When the thickness and pore-fluid pressure of Unit B reach critical, the water will either move seawards along the décollement, escaping in the FTZ, or may sporadically cause the hydraulic rupture to escape along pre-existing or newly formed faults. These may be responsible for the clusters of VLFEs recorded in the study area (Kamei et al., 2012; Kitajima and Saffer, 2012). This same mechanism explains the formation of OOS thrusts in the sandbox experiments, including the MSF and other potential OOS thrusts in the study area, where Unit B is the thickest (Figure 6.7). This may also be the mechanism through which the boundary between the inner and outer prism moves forward during the evolution of the NAP (Boston et al., 2016). In such a scenario, Units A and B are almost formed contemporaneously; as material gets accreted, it is underscrapped due to basal asperity differences between the subducting plate and weakly consolidated material (potential analogy with a sandpaper being pushed under a soft plastic material, which causes erosion of the bottom of that plastic material while dragging it and accreting it) – i.e. the fluid-rich and over-pressured Unit B is crucial for both the frontal growth of the NAP and thrusting in Unit A (Figure 8A).

The second scenario proposes regional variations in the distribution of stress and strain, as well as fluid pressure and fluid pathways in the NAP, due to the interference caused by the subduction of larger asperities, e.g. elongated major ridge and Kumano Seamount in the NAP. The Kumano Seamount is a physical barrier that does not only increase interplate coupling (Kodaira et al., 2000; Wang and Lin, 2022) but also blocks updip fluid migration towards the FTZ, which can be further impeded by a discontinuous or irregular décollement (Figures 6.7A, 6.7B and 6.8B). The increase in coupling promoted by the Kumano Seamount (and elongated major ridge) is accompanied by local uplift of the NAP driven by initial steep thrusts at the FTZ and, later, by back-thrusting (Figures 6.7A and 6.8B). Back-thrusts are proof of further accretion as basal asperities subduct and hardly propagate beyond the seamount (Haq et al., 2012). Equally, there is enhanced consolidation and shear strength on the landward flank of the seamount that favours strain accumulation (Sun et al., 2020). All these conditions reduce the permeability of accreted sediments and restrict fluid pathways along thrust faults (Figure 6.8B). This is particularly the case for the seaward part of the NAP, promoting a temporary increase in pore-pressure at the downdip section of Unit B. At this present-day stage of subduction of the Kumano Seamount, it could be assumed that some fluids may migrate laterally and/or landwards (downdip) and find escape pathways along the already weak MSF, helping its slip by lowering its resistance to shear deformation (Park et al., 2010). Fluids may also enhance the shear strength of the MSF through mineral precipitation, which in either case can promote tsunamigenic earthquakes.

There is also the possibility that the additional pore-pressure in Unit B downdip of the Kumano Seamount generates the necessary conditions for the formation of new OOS thrusts. These may potentially branch out from pre-existing thrusts in the ITZ of the NAP (Figure 6.8B). In both scenarios, the presence of basal asperities presents huge implications in the fluid and stress distribution within Unit B, seriously impacting the tectonic deformation of the NAP.

Comparing the experimental results with the NAP makes it acceptable to assume that changes in the thickness of Unit B in the NAP is a crucial mechanism for the inclusion of larger basal asperities into the NAP. Basal asperities in both the experiments and NAP show considerable thickening at the glass microbeads layer, and décollement and Unit B, which can potentially lead to time and spatial variations in the distribution and amount of slow slip events and occurrence of VLFEs due to shear stress build-up in Unit B, behind basal asperities. If asperity height is lower than the height of the décollement, then the asperity can be incorporate the Nankai Trough by a step up of the décollement and continuation of growth of Unit B seawards which will aid to updip fluid migration, as well as the nucleation of frontal thrusts promoting the seawards growth of the accretionary prism. If a basal asperity is considerably higher than the décollement, overcoming such barrier is considerably more challenging, causing a delay in the rupture and seawards growth of the prism as observed in both the experiments and the NAP. According to Sun et al. (2020), the landward flank of the Kumano Seamount, where décollement continuity is disrupted, is an area of tectonic instability that is prone to fault nucleation. This is observed in Figures

6.7B and 6.7C, where several thrust faults branch out from the place where Unit B and the décollement finish against the Kumano Seamount. This nucleation of thrust faults will assist the underthrusting of the seamount, creating temporary conditions for an erosive subduction style (Dominguez et al., 2000).

It is therefore postulated that future tectonic erosion will build-up underscrapped material near the seaward flank of the Kumano Seamount, which will increase the thickness and seawards growth of Unit B above the seamount, aiding the steeping-up of the décollement and nucleation of new frontal thrusts (see Figure 5.12). This process will most likely occur through repetitive creeping and slow fault slip together with the development of duplex structures and engulfing underplating, responsible for generating the observed regional cluster of VLFEs in the area surrounding the Kumano Seamount. As this process is repeated in time, it will get to a stage where both the décollement and Unit B will overstep the seamount as it gets included within Unit B. At this stage, it is expected to be a reduction of shear strength and rigidity, together with a re-establishment of updip fluid pathways that can trigger the necessary conditions for megathrust faulting and earthquakes with tsunamigenic impact (Figure 6.8B). After this stage, we propose that the seamount, now completely integrated within Unit B, will offer less resistance, and will be subducted at regional rate in a similar way to that described in Dominguez et al. (2000) (Figure 6.9).

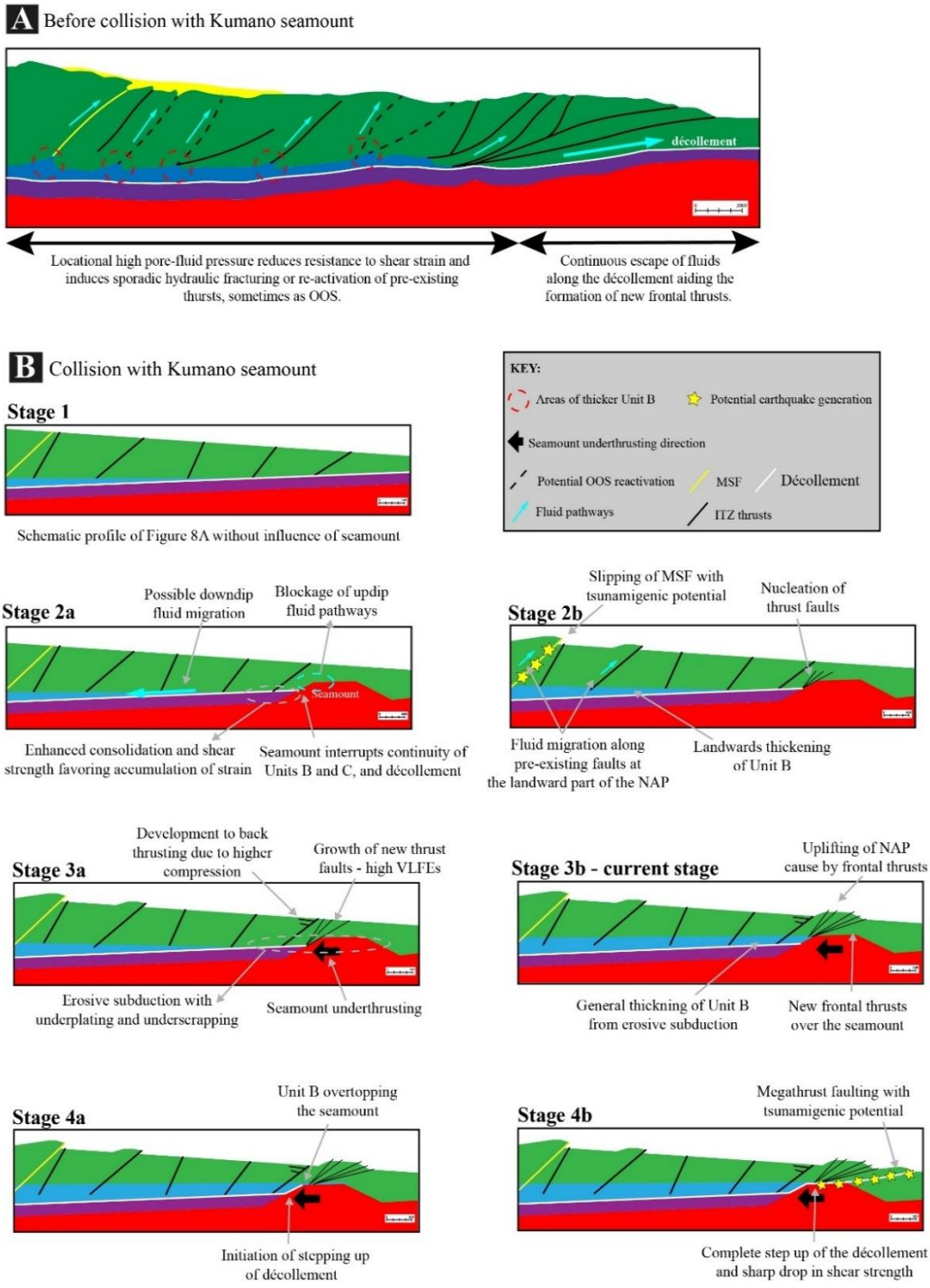

Figure 6.8 – A) Schematic tectonic framework of the NAP before collision with the Kumano seamount. B) Schematics for the tectonic implications caused by the collision of the NAP with the Kumano seamount at different stages of inclusion of the seamount in the subduction, inferred from findings from both the seismic data from the study area and sandbox model experiments.

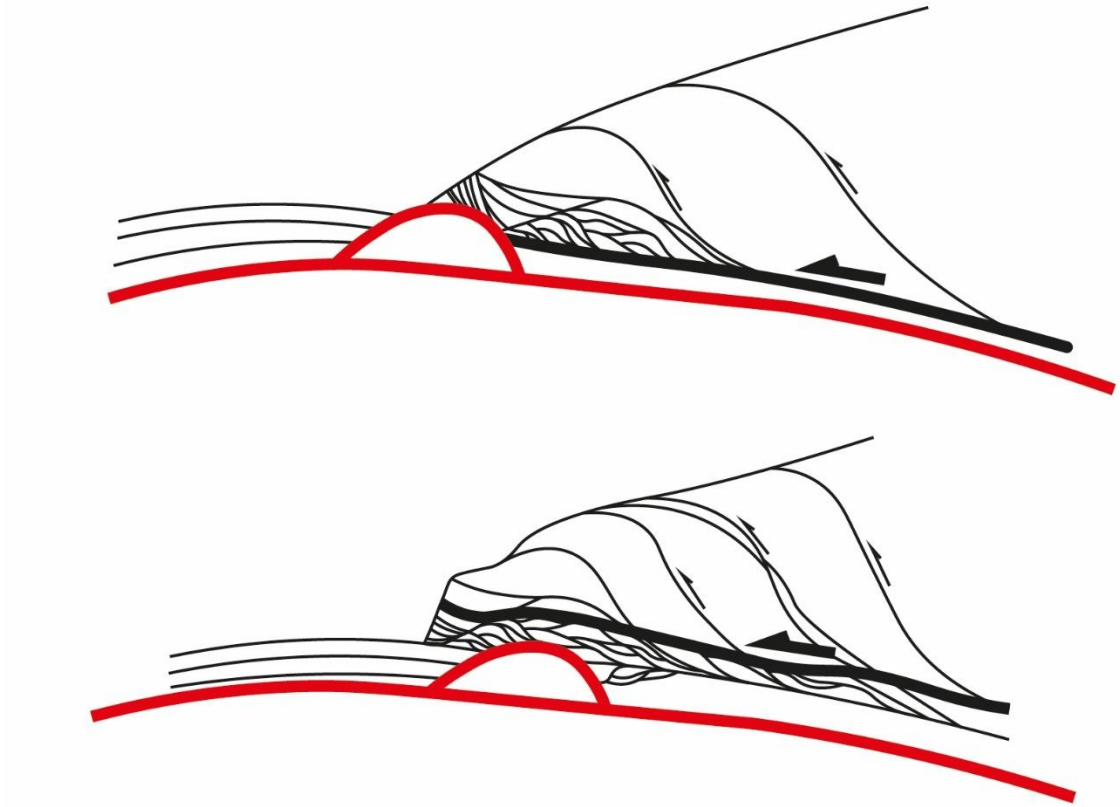

Figure 6.9 - A) Schematic showing how tectonic erosion model proposed in Figure 5.12B can be a mechanism of inclusion of seamounts into accretionary prisms through processes of underplating and duplexing that aids sleeping of frontal thrusts and steps up the basal décollement into a roof décollement.

6.6 Chapter-specific conclusions

This chapter presents sandbox experiments results that explain the formation and geometry of structures observed in 3D seismic data of the NAP. Both experiments, show that basal asperity of the subducting plate significantly influences the deformation experienced in accretionary prism. In the experiments, basal asperities cause differential growth of the accretionary prism and delays in the formation of new frontal thrusts in the FTZ, which provides an explanation for the observed uneven Nankai Trough. Similarly, the experiments reveal that as consequence of such along-strike variations in the FTZ, the accretionary prism can experience tearing and subsequent, changes in the stress field direction which is mainly accommodated by strike slip fault, similar to the observed F1 and other minor strike-slip faults in the NAP. This manifestation is interpreted as partitioning of strain in the outer wedge in both the experiments and the NAP.

In the experiments, the over consolidation and compression of accretionary prism between the backstop and the accreted sediment in its front causes some of the previously formed imbricated thrusts of the ITZ to reactivate as out-of-sequence thrust causing parts of the inner ITZ (hanging block) to overring parts of the outer ITZ (footwall block). This pattern is observed in the MSFZ with the formation of a major OOS thrust that separates the inner and outer wedges in the NAP. The results from the experiments suggest that more OOS

thrust, similar to the MSF, could form in the future evolution of the NAP causing its inner and outer wedges to migrate seawards.

Additionally, the low velocity Unit B is also influenced by basal asperity of the subducting plate as in both the experiments and the NAP, the microbeads layer and Unit B change their thickness and extent in relation to the basal asperity. Variations in their thickness cause branching of thrusts and potentially, re-activation of previously formed thrusts as OOS thrusts in the ITZ. Equally, these variations seem to be related to changes in the pore-fluid pressure of the décollement and Unit B, subsequently leading to erosive subduction and deformation of the overlying prism.

The experiments revealed that the lowermost microbeads layer is crucial in maintaining the critical taper of the accretionary prism, especially in the event of basal asperities subducting in the FTZ. One important mechanism was the deformation and potential erosion of the accretionary prism through the rooting of the thrust faults on the landwards side of basal asperities, which aided the uplift of the microbeads layer to or above the height of the basal asperity. This is so the asperity can be introduced under the FTZ of the accretionary prism and continue its subduction while the accretionary prism grows seawards. In the NAP, it is possible to observe the several gently dipped thrust faults rooting from where the décollement meets either the major elongated ridges or the Kumano Seamount. However, a thickening of the Unit B may still not be observed due to

the Kumano Seamount still being in its early stages of subduction at the Nankai Trough.

Although not fully exploited in this chapter, there are indications that basal asperities can be related to the formation of seismic activity with potential tsunamigenic risk. The experiments reveal considerable changes in the bathymetric surface of the accretionary prism which could displace the water column and form tsunami. Such changes seem to be mainly related to the OOS thrusts, where inner parts uplift over outer parts of the ITZ, or to the subduction of basal asperities in the FTZ that cause a step up of the décollement and consequential formation of a gentle thrust with long vergence. In the NAP, the formation of important seismic and tsunamigenic activity related to the MSF has been documented, however it can be speculated that new OOS thrusts within the ITZ and FTZ of the NAP could equally contribute to future formation of tsunamis.

CHAPTER 7

Summary and Discussion

7.1 Preamble

The chapters included in this thesis reveal and discuss the geometry and deformation distribution in the NAP, with particular emphasis on the influence of the subducting PSP and its roughness in the horizontal shortening and the erosive and accretional behaviour of the subduction of the NAP along the Nankai Trough. Insights on the inclusion of basal asperities and their influence in the evolution on the NAP and partitioning of the deformation is also included as part of this thesis.

The current chapter starts by providing a summary of main findings of each of the chapters covered in this thesis (Figure 7.1), followed by a holistic re-examination of the 3D seismic data, in the light of the new findings, together with review of literature to compare the NAP with other accretionary prisms and subduction settings. This will form the basis for the discussion of this thesis that will aim to cover: the influence of different characteristics within the NAP on the erosive and accretional behaviour of the subduction along the Nankai Trough; the scenarios through which basal asperities are included in the NAP; and the spatial distribution of seismic triggers and resolution stresses.

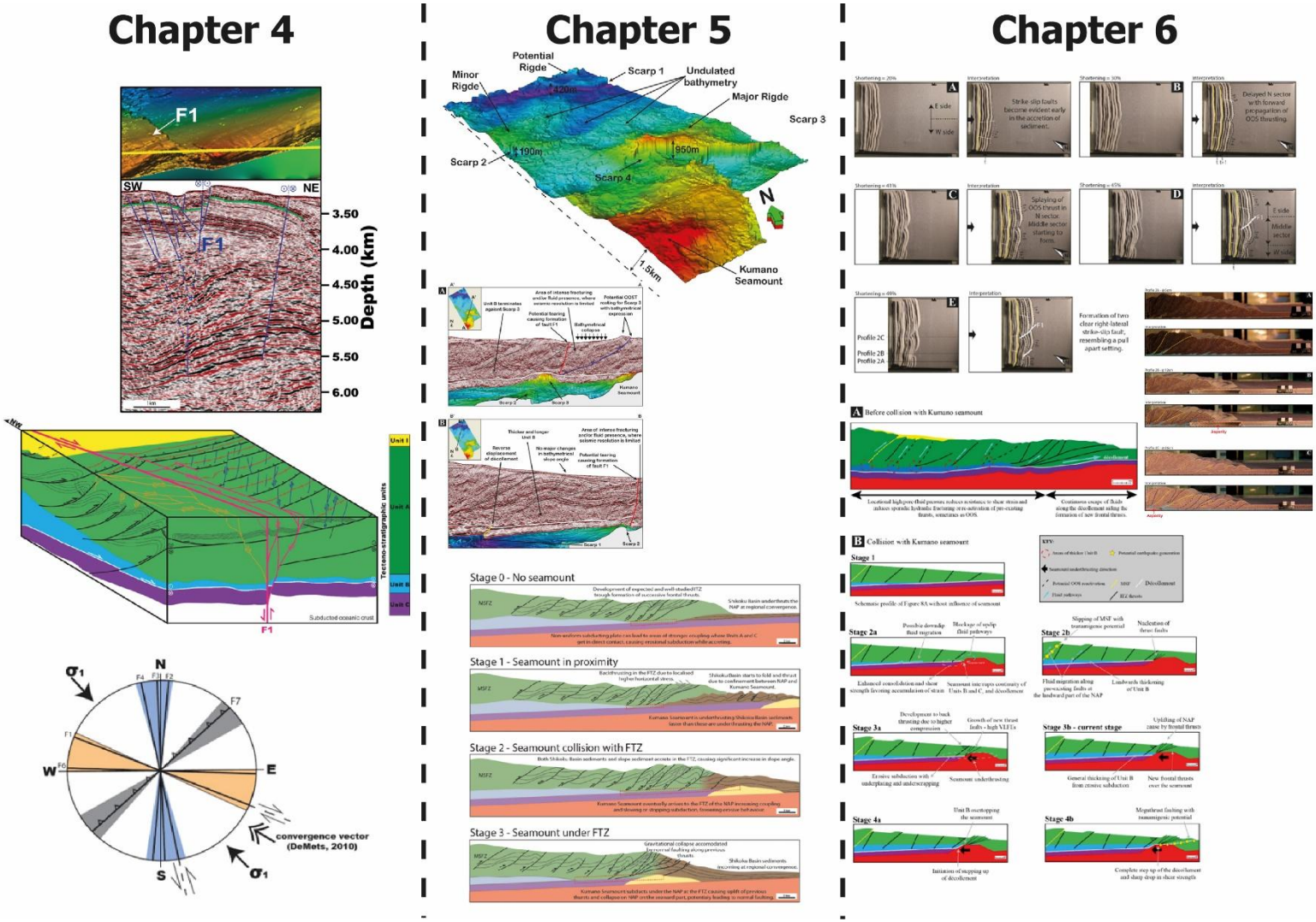
Chapter 4
F1
SW
NE
F1
3.50
4.00
4.50
5.00
5.50
6.00
Depth (km)
Tectono-stratigraphic units
Unit I
Unit A
Unit B
Unit C
Subducted oceanic crust
F1
N
E
S
W
σ1
σ1
convergence vector
(DeMets, 2010)
Chapter 5
Potential Rigde
Minor Rigde
Scarp 1
Undulated bathymetry
Major Rigde
Scarp 3
Scarp 2
Scarp 4
Kumano Seamount
1.5km
Stage 0 - No seamount
Stage 1 - Seamount in proximity
Stage 2 - Seamount collision with FTZ
Stage 3 - Seamount under FTZ
Chapter 6
Before collision with Kumano seamount
Collision with Kumano seamount
Stage 1
Stage 2a
Stage 2b
Stage 3a
Stage 3b - current stage
Stage 4a
Stage 4b

Figure 7.1 – Diagram summarising the key results presented in Chapters 4, 5 and 6 of this thesis. Chapter 4 investigates the tectonic structures and geometries in the NAP, with the identification of a major strike-slip F1 flower structure that partitions the study area into a N sector, mainly characterised by left-lateral regime, and a S sector, mainly characterised by a right-lateral regime. The study area experiences clockwise rotation of its maximum horizontal compression compared to the regional convergence rate that is concordant with the transpressional regime observed in 3D seismic. Chapter 5 investigates the roughness and main asperities in the subducting PSP under the NAP and their present-day influence in the deformation of the NAP. A major elongated ridge and Kumano Seamount have been identified as main asperities in the study area with huge influence in the erosive and accretional behaviour of the subduction zone in the Nankai Trough. Chapter 6 investigates the influence of basal asperities in the evolution and growth of accretionary prisms through sandbox models and comparison to 3D seismic data of the NAP. The sandbox experiments with similar asperities to the ones identified in Chapter 5 revealed insights on how asperities are included in accretionary prisms and on how the MSFZ and changes in Unit B can be influence by subduction of basal asperities within the PSP.

7.2 Summary of technical results

7.2.1 Chapter 4

Chapter 4 investigated the structural framework and tectonic regime currently operating in the outer wedge of the NAP using detailed faults and seismic horizons mapping and seismic attributes. An important finding from Chapter 4 was the right-lateral strike-slip fault, F1, that partitions deformation in the NAP into two distinct sectors. Both sectors are dominated by a common fold-and-thrust regime typical of accretionary prisms. However, the N sector developed a localised regime of left-lateral strike-slip faults while the S sector developed a less prominent regime of right-lateral strike-slip faults. Such strike-slip faults display a conjugate geometry that formed either after or in coexistence with the fold-and-thrust setting. Chapter 4 postulates that the outer wedge of the NAP initially developed as fold-and-thrust setting within the ITZ and FTZ because of the regional convergence between the Amur Plate and PSP, progressing later a transpressional regime with thrust and strike-slip faulting occurring simultaneously or in alternation, reflecting a slight counterclockwise rotation of the maximum compression stress in the study area.

7.2.2 Chapter 5

Chapter 5 investigated the presence of basal asperities in the subducting PSP below the NAP and its influence in the deformation and horizontal shortening of the NAP and its subduction behaviour. This chapter provided a detailed mapping and description of the roughness of the underlying PSP and identified the presence of several asperities, including a major elongated ridge bordered by a significant scarp and the 1.5km high Kumano Seamount. The Kumano Seamount delays the development of frontal thrusts and the subduction movement per se and significantly increases the amount of horizontal shortening experienced in the FTZ and South sector of the NAP, where it is recorded a great number of steeper thrusts and narrower anticlines. Strike-slip fault, F1, can be in fact a tearing fault caused by partitioning of interplate coupling between a smoother and fast moving N sector and a rougher and slow moving S sector. Chapter 5 postulates that subduction behaviour of the NAP is mainly accretional but coexistent with localised erosive behaviour, enhanced by rougher parts of the PSP being subducted under the NAP and strike-slip fault regime is a response to local accretional-erosive transitions and a mechanism to dissipate stress from mechanically strong coupled areas due to basal asperities.

7.2.3 Chapter 6

Chapter 6 investigated the influence of individual and combined basal asperities in the evolution, growth and deformation of accretionary prisms using analogue sandbox experiments simulating similar asperities to the ones identified in the NAP in Chapter 5. This chapter offered new insights into the formation of the MSFZ and other OOS thrusts within the ITZ and the local variation in thickness and length observed in Unit B, underlying the NAP. Chapter 6 confirmed right-lateral strike-slip faults, such as F1, and the different deformation observed in the N and S sectors of the NAP are compatible with partitioning of strain and tearing caused by collision of basal asperities. Basal asperities on the incoming subducting plate are a determinant factor on the physical characteristics of Unit B, such as fluid pathways and pore-fluid pressure distribution, which, subsequently, controls the deformation of the overlying NAP– the MSF, such as branching of MSF, OOS thrusts and main thrusts in the ITZ. Chapter 6 postulates that thickening of Unit B is the main mechanism of inclusion of asperities into the subduction below the NAP. When asperities surpass the height of the décollement, a thick enough Unit B, that must overcome the asperity, may take longer than other basal asperities, thus delaying the frontal growth of the NAP or it may be that such thickness may never be achieved before the MSF or a new OOS thrusts are used as a pathway of stress relief, thus having consequential tsunamigenic impact.

7.3 The role of asperities in the PSP on the tectonic evolution of the NAP

Throughout this thesis, the outer wedge of the NAP shown to be an area of significant tectonic and structural complexity that seems to be influenced by several factors both within the overlying accretionary prism and the underlying PSP, as summarised in Section 7.2 (Figure 7.1). However, the latter seems to be a notably determinant factor as commonly suggested in literature (Kirkpatrick et al., 2020; Okuma et al., 2022). This section presents an evaluation of the impact of roughness of the subducting PSP in the spatial distribution of stress fields and related strain accommodation as well as in the subduction rate and behaviour and their influence their influence in fluid pathways within the NAP.

7.3.1 Implications to the movement and spatial distribution of stresses in subduction zones

The results presented in this thesis support the view that the Nankai Trough experiences spatial variations in the subduction movement and accretionary prism growth. Chapters 4 and 5 revealed that the Nankai Trough is far from being a straight through, reflecting along-strike variations in the frontal accretion of sediment and in the seaward propagation of thrusts in the FTZ of

the NAP, similar to what is observed in the Hikurangi margin, in New Zealand (Gase et al., 2021).

Chapter 5 showed that rougher sectors of the Nankai Trough possess shorter accretionary prisms when compared to smoother sectors. The presence of elongated major ridges and, more importantly, the Kumano Seamount, as basal asperities significantly higher than the décollement, act as physical and buoyant barriers that will resist subduction, increasing the mechanical coupling (Dominguez et al., 2000) between the overlying accretionary prism and the underlying PSP. In Chapter 6, sandbox experiments showed that such differential frontal growth of accretionary prism can occur before the actual encounter between basal asperities and the FTZ, where rougher sectors promote earlier rupture of frontal thrust zones in the FTZ than smoother sectors of the subducting plate. However, not necessarily promoting further seaward growth of the accretionary prism. Chapters 5 and 6 suggest a reverse relationship between roughness of the subducting plate and seawards growth of the accretionary prism but a positive relationship between roughness and number of steep thrusts. The horizontal shortening estimations carried out in Chapter 5 justify such complex relationships with the roughness of the PSP.

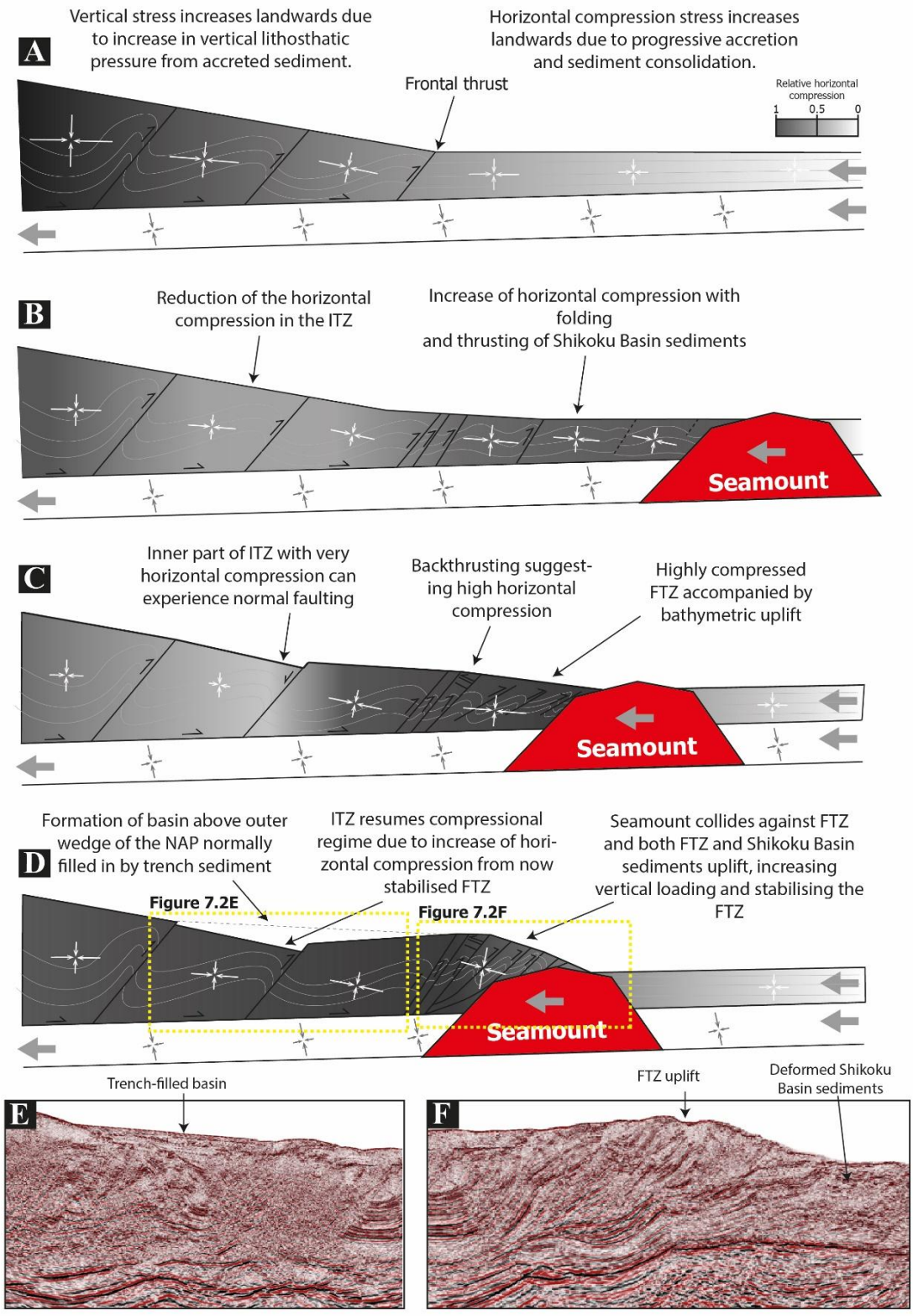
A
Vertical stress increases landwards due to increase in vertical lithosthatic pressure from accreted sediment.
Horizontal compression stress increases landwards due to progressive accretion and sediment consolidation.
Frontal thrust
Relative horizontal compression
1 0,5 0
B
Reduction of the horizontal compression in the ITZ
Increase of horizontal compression with folding and thrusting of Shikoku Basin sediments
Seamount
C
Inner part of ITZ with very horizontal compression can experience normal faulting
Backthrusting suggesting high horizontal compression
Highly compressed FTZ accompanied by bathymetric uplift
Seamount
D
Formation of basin above outer wedge of the NAP normally filled in by trench sediment
ITZ resumes compressional regime due to increase of horizontal compression from now stabilised FTZ
Seamount collides against FTZ and both FTZ and Shikoku Basin sediments uplift, increasing vertical loading and stabilising the FTZ
Figure 7.2E
Figure 7.2F
Seamount
Trench-filled basin
FTZ uplift
Deformed Shikoku Basin sediments
E
F

Figure 7.2 – Schematic diagram showing the change in the stress fields and relative horizontal compression in different sections of the NAP and Shikoku Basin at different stages of incoming seamount. A) Diagram adapted from Flemings and Saffer (2018) with stress field distribution in the NAP, assuming no changes in the subduction channel (Unit C) for simplification. B) Incoming seamount will start deforming the Shikoku Basin sediments as horizontal compression concentrates between the seamount and the FTZ, causing folding and thrusting of the hemipelagic sediments. C) Seamount continues being pushed towards the Nankai Trough by regional convergence rate, causing further consolidation, thrusting, and shortening of the FTZ of the NA, thus allowing horizontal compression to migrate to outer parts of the ITZ. However, inner parts of the ITZ will be relaxing and potentially experiencing a reduction in horizontal stress that may lead to normal faulting. D) Seamount finally collides with the NAP compressing the entire Shikoku Basin and accreted trench sediments, causing the FTZ to significantly uplift. This uplift will increase the vertical loading and vertical stress can be close or above horizontal stress which stabilises the FTZ and allows the rest of the ITZ to resume its compressional state.

The overall regional convergence rate of the PSP against the Amur Plate plays the dominant factor in the horizontal shortening and deformation along the Nankai Trough, which results in the overall horizontal shortening experienced by the NAP to not change significantly along-strike (between 29% and 32%). However, horizontal shortening is not evenly distributed within the NAP and along-strike as asperities induce spatial variations on how and where such horizontal shortening is mainly accommodated. Therefore, rougher sectors tend to not only concentrate the slightly lower horizontal shortening than adjacent smoother sectors (N vs S sectors) but tend to, conversely, mainly concentrate shortening in their FTZ while smoother sectors tend to distribute strain and horizontal shortening more evenly between the FTZ and ITZ. This concentration of horizontal shortening in the frontal part of the accretionary prism indicates a spatial change in the overall stress field of the NAP (Flemmings and Saffer, 2018), especially when a basal asperity, such as the Kumano Seamount, collides against its FTZ. Before colliding against the FTZ of the NAP, the Kumano Seamount and other basal asperities will start progressively changing the stress field while approaching the Nankai Trough at the regional convergence rate.

As the Kumano Seamount approaches the Nankai Trough, it is going to cause an increase in the horizontal compression experienced by the less consolidated Shikoku Basin sediments between the more consolidated NAP and the rigid Kumano Seamount. The increase in the horizontal stress, where $\sigma_1 = \sigma_{Hmax,}$ causes the Shikoku Basin sediments to experience early consolidation and sub-

sequent early nucleation of thrusts in the proto-FTZ, which explains the observed early formation of the frontal thrusts in the S sector of sandbox experiments in Chapter 6. As the Shikoku Basin sediments become further consolidated, the progressively increased horizontal compression caused by the incoming seamount will be able to migrate further landwards to cause amplified horizontal shortening in the FTZ. It is possible that this phenomenon could also impact the outermost parts of the ITZ in the NAP. This means that the inner parts of the ITZ could temporarily suffer relaxation in its horizontal compression that is now concentrated in the frontal part of the accretionary prism. Such a condition may cause the NAP to experience periods of tectonic extension due to the stress caused by vertical lithostatic pressure being temporarily greater than the reduced horizontal compression. Therefore, when $\sigma_1 = \sigma_v$, some thrusts may re-activate as normal faults during this extensional period, which could form the trench-filled basin (Unit I) observed above the ITZ of the outer wedge of the NAP.

As discussed in Chapter 5, the Kumano Seamount being a rigid asperity in the subducting plate will be able to accrete and underthrust the weakly consolidated Shikoku Sediments while the later will equally start underthrust the NAP at the FTZ. However, due to rigidity/consolidation differences, the seamount will underthrust the Shikoku Basin sediments faster that the later can underthrust the NAP because the hemipelagic Shikoku Basin sediments will need to accrete and consolidate before being able to rupture and being included in the front of the NAP (Clarke et al., 2018). This will cause a considerable uplift

of the FTZ and its slope angle (Lallemand et al., 1990; Von Huene, 2008) when the Kumano Seamount finally collides with the NAP, thus increasing the vertical lithostatic pressure in relation to the already enhanced horizontal compression. As the vertical stress approaches the horizontal stress ($\sigma_{Hmax} \sim \sigma_v$), the FTZ of the NAP stabilises, allowing strain and compression to migrate back the inner parts of the ITZ, where it resumes the overall compressional regime driven by the regional convergence rate (Figure 7.2).

The 3D seismic data does not possess the resolution to observe geometries in the deeper parts of the NAP, so stress field distribution in the subduction channel (Unit C) was considered constant for simplification. However, according to Von Huene (2008), sliding over seamounts tend to be stable while in the subduction channel in front of seamount tends to be intermittent. Therefore, it can be assumed that the subduction channel must suffer changes in the stress fields as a consequence of basal asperities, especially those higher than the décollement.

Despite the localised and temporary resistance to subduction by basal asperities, the overall regional convergence rate will prevail as slab pull of PSP will continue to drive the subduction movement (Kimura et al., 2021; Moreno et al., 2023). As a result, basal asperities temporarily and locally slow the downwards movement of the subduction channel, but such movement would gradually resume to its regional rate as you go downdip. This postulate leads to believe that changes in the stress field also must occur in the lowermost layers of

the NAP, potentially characterised by a decrease in horizontal compression due to the pull apart occurring between a landwards subduction channel being slab pulled and the seawards subduction channel being held by basal asperities. This decrease in horizontal compression in relation to the vertical stress cause by the overlying NAP, could promote flexural bending and normal faulting of the subducting channel and possibly the subducting plate with important consequences for fluid migration and pore-pressure, which will be discussed in more detail in the next section (Figure 7.3). This can also aid the normal faulting and collapse of the overlying NAP as previously described.

Distribution of stress fields and strain accumulation present to be far more complicated than it has been discussed so far. Chapter 6 indicates that the ITZ of the NAP can be intersected by other OOS thrusts besides the well-studied MSF, during its growth and evolution. The results presented in this thesis suggest that the occurrence of such OOS thrusts is related to over-consolidation and therefore, over-compression within the ITZ of the NAP, which seems to be accommodated by inner parts overriding outer parts of the ITZ.

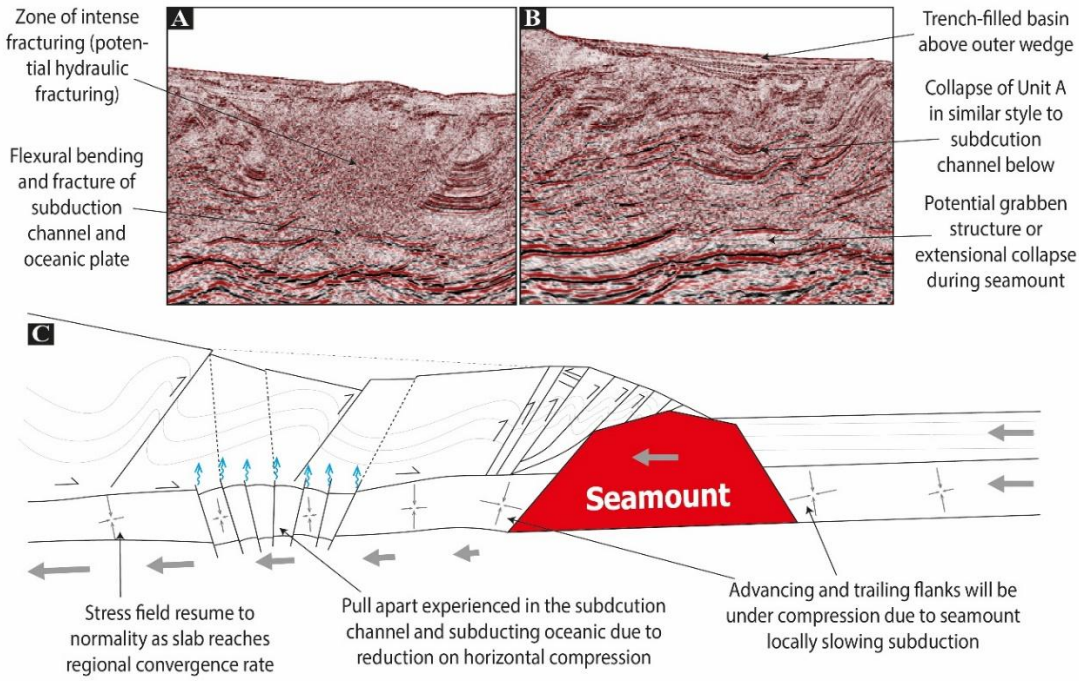

Figure 7.3 – Seismic profiles with evidence of deformation in the subduction channel and subducting oceanic with schematic diagram showing changes in the stress fields along the subduction channel during collision with seamount at the FTZ of the NAP. A) Seismic inline profile 2130, showing low seismic resolution in Unit A of the NAP due to intense fracturing which could be related to the flexural bending and faulting in the lowermost Unit C. B) Extensional collapse in graben style of both Units A and C with branching of normal faults from the subducting oceanic crust. C) Schematic diagram showing the changed in the stress fields along the Unit C. In the areas flanking the seamount, the horizontal compression with be at its maximum due local shortening and slower subduction rate caused by the seamount. Further downdip from the seamount the slab will be resuming its regional subduction rate due to the slab pull of the PSP, which causes pull apart between this faster part of the subduction and a slower seawards part of the subduction., thus triggering extensional tectonics that will impact the NAP above. Grey arrow – subduction rate; blue arrows – fluid escape pathways; dashed black line – probable normal faults; black lines – faults.

There seems to be a link between variations in the underlying Unit B and potential formation of OOS thrusts in the Unit A of the NAP, which will be discussed in more detail in another section. However, it is relevant to discuss here that these OOS thrusts seem to be mainly related to gradual landwards increase of consolidation and compression caused by the progressive accretion of sediment in the FTZ. In other words, as horizontal compression in the outer wedge increases towards the inner wedge, that acts as a backstop (Tsuji et al., 2015) (Figure 7.2A), some of the previously formed imbricated thrusts within the inner and more consolidated part of the ITZ will be re-activated as OOS thrusts. This overriding phenomenon will uplift the NAP which subsequently increases the vertical stress due to lithostatic overloading, thus causing vertical and horizontal stresses to be similar ($\sigma_{Hmax} \sim \sigma_v$), as previously discussed for thickening of the FTZ during seamount collision. This seems to be the mechanism through which the MSF was formed and explains how outer and inner prisms of the NAP may migrate seawards. It can be postulated that OOS thrusts are the mechanism through which inner parts of the ITZ, in the outer wedge, are transferred to the inner wedge as they become stable and locked, and behaving as a new backstop. The results in Chapter 6 support this postulate because these OOS thrust tend to form at equivalent scenarios of horizontal shortening in both N and S sectors of the NAP. Additionally, when a new OOS thrust ruptures landward of the previous one, such as the MSF, the entire section of the NAP seawards of the new OOS thrust becomes locked, as previous OOS thrusts, strike-slip faults and imbricated thrusts no longer slip or creep or no longer extent beyond the

new OOS thrust. Therefore, it is possible that the MSFZ will continue to grow seawards with the formation of the MSFs in the future tectonic development of the NAP.

3D seismic data seems to reveal few individual imbricated thrusts that may have been behaving as OOS thrusts which could be explained by the accommodation of spatial variations in the horizontal compressional stress in the Unit A of the NAP that can locally rupture in an OOS style while that section of the NAP is still not consolidated enough to become part of the inner wedge.

Chapter 6 also reveals that basal asperities in the subducting plate also influence the formation of the OOS thrusts previously discussed. Data from the analogue sandbox experiments suggest that increased roughness of the subducting plate and/or presence of bathymetrically higher asperities, such as the Kumano Seamount, promotes earlier formation of the MSF and other OOS thrusts due to increased shortening caused in such scenarios.

The results discussed so far in this thesis clearly point out that subduction of basal asperities will cause time and spatial variations in the rate of subduction, both along and across the Nankai Trough. The factors affecting subduction rate so far discussed include: the consolidation of the FTZ, caused by concentration of horizontal compression and shortening; the extension of the subduction channel and potentially the subducting oceanic crust, caused by pull apart; and potential along-strike variations of the inner-outer wedge transfer. These factors

are determinant on the tectonic evolution and growth of the NAP and other accretionary prisms.

Variations in the stress fields along the Nankai Trough are consequently expected to happen, causing the observed deformation and tectonic settings observed and described in Chapters 4 and 5. As the S sector of the NAP presents a rougher subducting PSP, characterised by the presence of Kumano Seamount, when compared to the N sector that is smoother, the subduction rate of the S sector will be significantly reduced in relation to the N sector due to the acting factors enumerated and discussed previously. This justifies the higher horizontal shortening and narrower accretionary prism observed in the FTZ of the S sector in the NAP. Chapter 6 provides evidence for an independent growth of both sectors of the NAP. The higher asperity of the S sector causes prior rupture of new frontal thrusts in the FTZ compared to the N sector, where this delay leads to the number of imbricated thrusts and fold nappes to be lower than the S sector over time. However, the N sector reveals a much wider spacing between thrusts as well as gentle thrust dip, which assists slipping along these thrusts and, consequently, the greater seawards growth of the NAP. Therefore, basal asperities are the main reason for the observed partitioning of strain in the study area, where the N and S sectors develop as distinct sectors of the NAP with individual stress field within the general convergence rate and associated stress field.

The partitioning is triggered by the presence and specific geometries of basal asperities in the subducting PSP, which in 3D seismic data is interpreted as a right-lateral strike-slip fault, F1, similar to what has been recorded in Alaska and Aleutian subduction that also suffers from oblique subduction (Kharizi et al., 2024). While the Kumano Seamount is responsible for the strain partitioning into the N and S sectors, it is the geometry of the elongated ridges and related scarps described in Chapter 5 that are responsible for the geometry of the strain partitioning. The geometry of the fault F1 follows very closely the geometries of the Scarps 2, 3 and 4, and related ridges (Figure 7.4). These basal asperities in the subducting PSP are connected to suprajacent areas characterised by intense fracturing and faulting in the overlying NAP. Such areas are normally not well resolved in 3D seismic, which may suggest fluid migration, but it is possible to recognise several structural alignments that probably nucleated from these basal asperities, propagating and linking together to form the observed strike-slip fault F1, as a response to the overall oblique convergence and strain partitioning between the N and S sectors (Barnhart et al., 2015; Maunde et al., 2021).

The study area of this thesis is of small scale when compared to the overall scale of the Nankai Trough. However, the results here discussed could be extrapolated to other larger adjacent areas along the Nankai Trough with contrasting roughness and asperities within the subducting PSP.

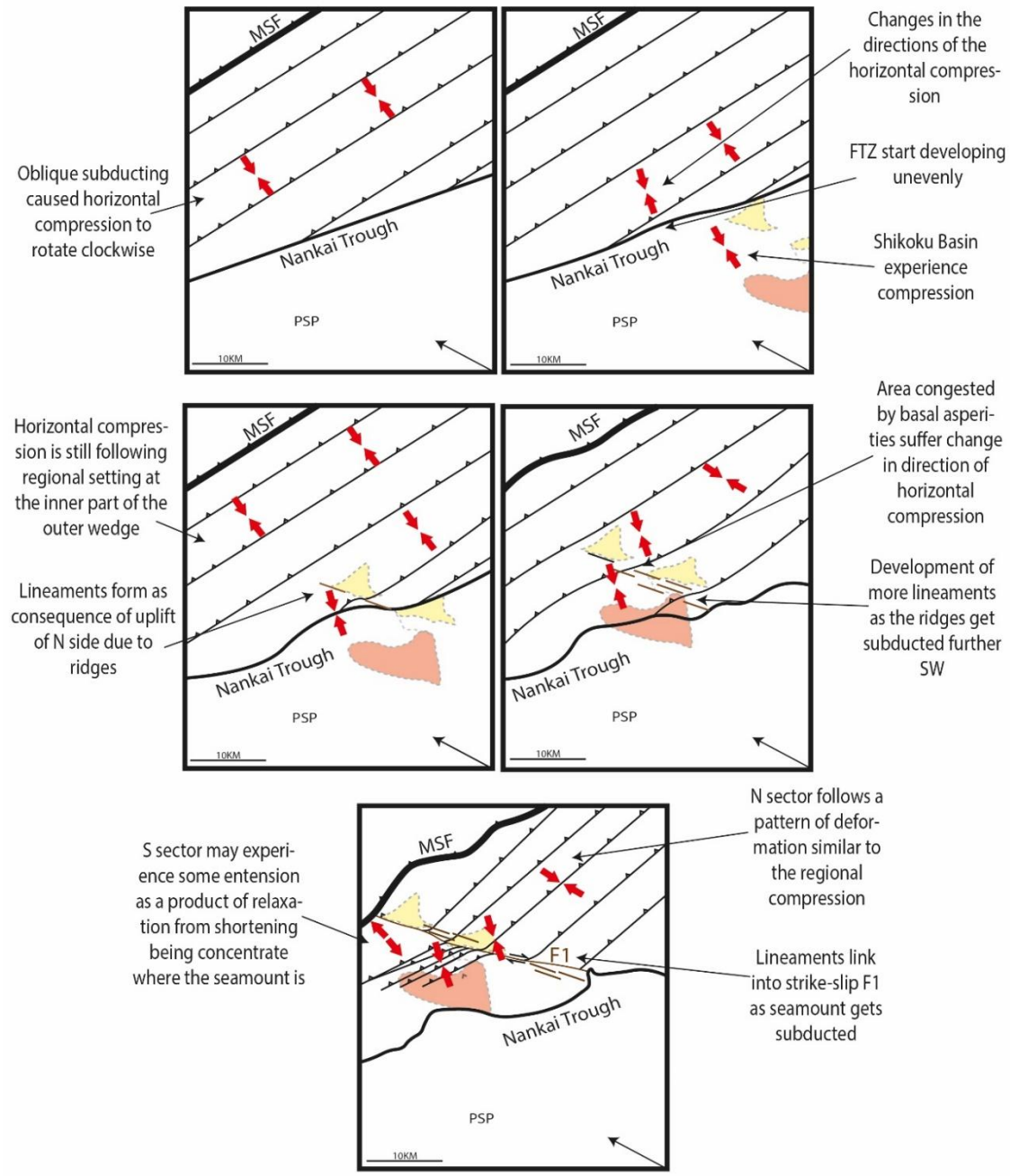

Figure 7.4 – Schematic diagram showing the development of strain partitioning of the NAO into the N and S sectors. Ridges (pale yellow) control the geometry of the lineaments that separate the N and S sectors, while the Kumano Seamount (pale red) mainly controls the different stress fields experienced in the N and S sectors and may also be responsible for linking these different lineaments. Red arrows = maximum horizontal stress (compression or extension), Black arrow = regional convergence

7.3.2 Implications to fluid migration and pore-pressure distribution in Unit B

Data presented in this thesis reveal clear occurrence of variations in the thickness and extent of the low velocity Unit B and Chapters 5 and 6 recognise that such variations could be related to basal asperities on the subducting oceanic crust. As this Unit B is described as a fluid-rich layer resulting from the understhrusting Unit C (Park et al., 2010), it would be expected that this tectono-stratigraphic unit will have a significant impact on of the fluid and pore-pressure distribution in the outer wedge of the NAP.

It is not clear whether the presence of basal asperities, such as the Kumano Seamount, will increase or decrease the thickness of Unit B as the 3D seismic data does not always resolve this area with clarity. However, it is possible to recognise that basal asperities affect this Unit B somehow. One interesting finding from combining the results from Chapters 4, 5 and 6 is that this Unit B seems to be mainly confined to the N sector of the NAP. Additionally, there is a negative relationship between the roughness of the subducting oceanic crust and the extent of Unit B, where rougher PSP with high basal asperities present a shorter Unit B. This relationship complements well with the finding that the Unit B is mainly confined within the N sector of the NAP as the N sector in the smoother section of the NAP. Such observation seems to be concordant with

Park et al. (2010) that interprets this unit as an underthrust package underplated in response to the lateral growth of the accretionary prism.

The partitioning of strain, caused by the subduction of the Kumano Basin and elongated major ridges and manifested as a right-lateral strike-slip fault F1 separating the N and S sectors of the NAP, could also be responsible for the observations previously discussed about Unit B. As Unit B is a fluid-rich unit interpreted as an over pressured zone of the footwall of the MSF (Tsuji et al., 2014), then it can be assumed that local variations in the consolidation and compressional states caused by the basal asperities subducting under the NAP may equally cause changes in the fluid pathways and migration in the NAP.

One important fluid pathway that could be severely impacted by the subduction of the Kumano Seamount is that occurring in the FTZ. Not only the FTZ presents a pathways for fluid escape from deeper and inner parts of the NAP, especially within the fluid-rich subduction channel (Unit C), but it is also the greatest source of fluids from expulsion of seawater by consolidation and porosity reduction (Langseth and Moore, 1990; Ellis et al., 2015). As previously discussed, the approach of the Kumano Seamount and, ultimately, its collision in the FTZ of the NAP will cause a spatial over consolidation of the sediment in the advancing flank of the seamount. This phenomenon causes an early expulsion of fluids, especially of those in the hemipelagic sediment of the Shikoku Basin, and it will produce a more consolidated and lower porosity FTZ compared to adjacent areas along the Nankai Trough. Additionally, the over compressed

FTZ, evidenced by the presence of local back thrusting, will cause most (if not all) faults in the advancing flank of the Kumano Seamount to resist migration of fluids. These two combined effects will therefore promote impediment of fluid migration along the FTZ in the S sector of the NAP:

- Fluid will not be able to migrate across the NAP, from downdip to the toe of the accretionary prism.
- Fluid will not be able to migrate laterally from adjacent areas along the Nankai Trough.

The disconnected fractures and lineaments formed in the NAP by the subduction of the elongated ridges (Figure 7.4) may have opened and ruptured to connect both horizontally and vertically into the present-day right-lateral strike-slip fault F1, displaying a flower structure style (Tsuji et al., 2018). The oblique subduction of PSP under the Amur Plate and the Kumano Seamount subduction could also influence spatial and time variations in the behaviour of the strike-slip fault F1 as a fluid pathway. 3D seismic data show areas of intense hydraulic fracturing in fault F1 or its vicinity, while other areas, particularly bordering the Kumano Seamount or major ridges seem to be spatially constrained with little evidence of hydraulic fracturing (Figures 7.3A and 7.3B). This suggest that the Kumano Seamount and oblique convergence can close or open fractures along the strike-slip fault zone F1, which can further restrain fluid escape from the NAP at different times and spaces.

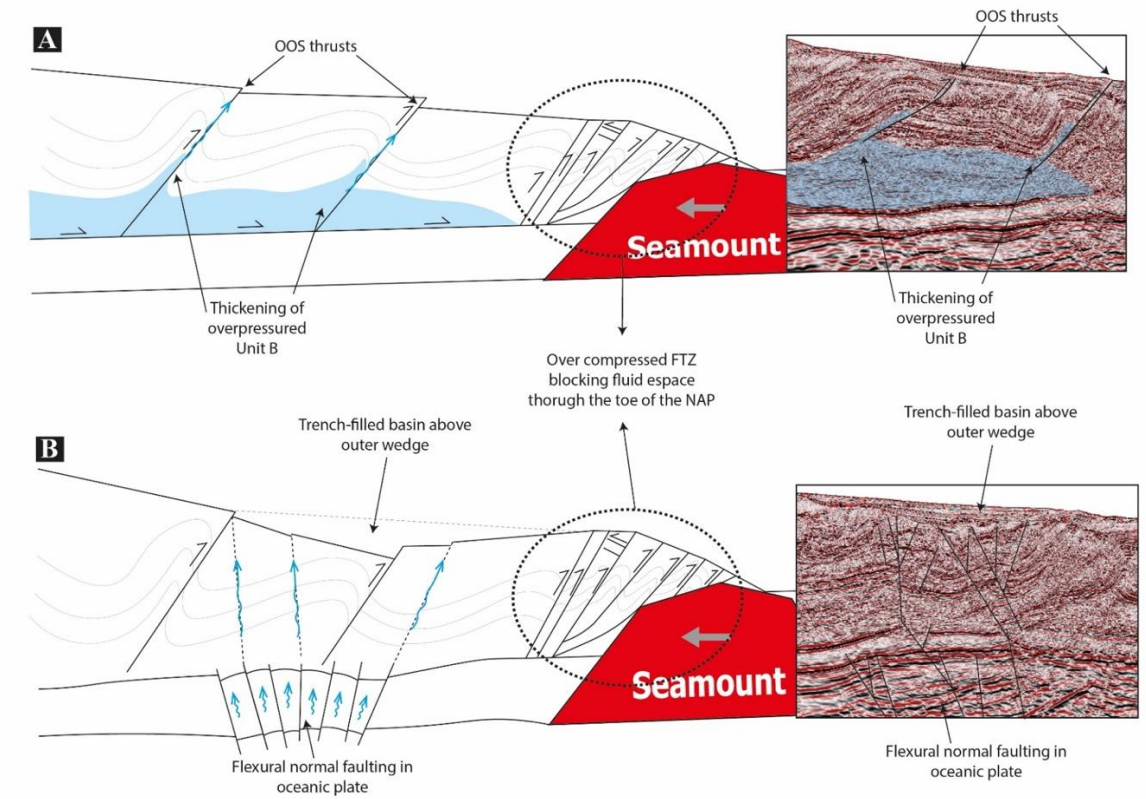

Figure 7.5 – Schematic diagram of two possible fluid pathways in the NAP in the event of the of blockage of fluid escape at the FTZ due to over-consolidation and over-compression caused by the collision of the Kumano Seamount at the toe of the NAP as well as laterally A) Thickening of over pressured Unit B will induce re-activation of some imbricated thrusts in sections of the NAP that are better consolidated. B) Flexural bending with accompanying normal faulting of the subducting oceanic crust caused by pull apart of the subduction channel, which developed an extensive network of fracturing and normal faulting in the overlying NAP, offering escape pathways for fluids.

The 3D seismic data reveals two different mechanisms for the fluid escape pathway in case of fluid migration being blocked both at the FTZ due to over consolidation and over compression caused by the subduction of the Kumano Seamount in the S sector of the NAP and laterally, along the strike-slip fault zone F1. These mechanisms are shown in Figure 7.5 and briefly mentioned in Chapters 5 and 6:

- The restricted fluid escape pathways in the NAP transfer the already over pressured Unit B to a super-critical state that causes localised uplift and thickening of the Unit B and subsequently, re-activation of pre-existing imbricated thrusts in form of out-of-sequence thrusting. This OOS re-activation is potentially occurring along the most consolidated parts of the ITZ or most over compressed thrust nappes. The mechanisms through which Unit B thickens will be further discussed in the next section. This mechanism is more commonly observed in the smoother N sector of the NAP.
- The delaying in the subduction rate caused by the Kumano Seamount collision against the NAP and related differential subduction rate between the subducting plate just landwards of the seamount and the subducting PSP further downdip causes the subducting oceanic PSP to suffer flexural bending and normal faulting responsible for branching an extensive network of fractures and normal faults upwards in the NAP. This structural network displaces the NAP, at times until the bathymetric surface, and could open fractures that will act as fluid

escape pathways. The mechanism is more commonly observed in the rougher S sector of the NAP.

7.3.3 Implications to the flipping between accretional and erosive tectonics in subduction zones

Although the NAP is believed to be an accretional-dominated margin, this thesis proposes that even accretional-dominated margins may exhibit complex subduction dynamics that include spatial and temporal transitions into regimes of reduced accretion or even mild tectonic erosion. Therefore, the NAP may experience erosive or non-accretional subduction under certain transient or localised conditions similar to what Wakabayashi (2022) describes for the Franciscan subduction.

According to Clift and Vannucchi (2004), a stronger mechanical interplate coupling caused by both high friction abrasion and high fluid pressure are the main conditions for subduction erosion to occur. The data here discussed reveals that the NAP can contain both high friction abrasion caused by the rough subducting PSP and high basal asperities (Liu et al., 2024), especially in the S sector of the NAP, and high fluid pressure due to blocked fluid escape pathways and presence of overpressured Unit B. Additionally, faster rates of subduction lead to steeper forearc slope angles which result in increased basal friction, thus

making it more likely to experience localised erosive tectonics (Clift and Vannucchi, 2004). However, it is important to acknowledge that such interpretations are indirect and depend on features that could also arise from other processes such as internal wedge deformation or mechanical partitioning. As a result, the faster and smoother N sector of the NAP could also be experiencing either erosive or non-accretionary subduction.

The 3D seismic and horizontal shortening data from Chapters 5 and 6 suggest that the S sector experiences an early increase in accretion, mainly at the FTZ, which may start before the Kumano Seamount collides against the NAP, as previously reported. This accretional process will accrete sediments from both the trench and the incoming Shikoku Basin, well revealed in 3D seismic by an increase in concentration of imbricated and frontal thrust faults and considerably narrow fold-and-thrust sheets. However, in the present-day scenario, where the Kumano Seamount is colliding and underthrusting the FTZ, the S sector of the NAP also reveals features that might be interpreted as consistent with erosive tectonics, such as having a shorter accretionary prism compared to adjacent sections due to steeper imbricated and frontal thrusts that do not slip as much. Yet, such features might also align with a non-accretionary regime, characterised by suppressed frontal accretion without clear removal of material from the overriding plate (Shreve and Cloos, 1986; Clift and Vannucchi, 2004). This setting will mechanically increase the coupling between the overlying NAP and underlying PSP with the seamount, slowing down or stopping the subduction, thus

causing temporary thinning of the inner part of the ITZ. Thinning of the overriding plate is considered another important feature of subduction erosion (Murauchi, 1980; Kopp et al., 2006), and Liu et al. (2024) refers to the fact that reasons for such thinning of the overriding plate remain unsolved. Therefore, there is a possibility that when accretional-dominant margins temporarily stop accreting due to asperities, they may locally thin due to localised changes in stress distribution without erosion. It is important to mention that a potential mechanism of thinning of the overriding plate was explained in the previous section of this discussion and could represent an important process of inclusion of basal asperities into accretionary prisms, which will be discussed in more detail in the following section of this chapter (Figures 7.5B and 7.6). Moreover, certain seismic inline profiles in the S sector of NAP reveal taper angles between 8° and 10°, thus being very close to those of typical erosive tectonics, such as the Tonga margin with a taper angle value of 11° (Clift and Vannucchi, 2004). However, reduced taper angles alone do not necessarily confirm erosion and could reflect other factors such as low basal friction or high fluid overpressures without net material loss, characteristic of low-efficiency accretional systems or non-accretional settings (e.g., Wang and Hu, 2006).

Another feature observed in the 3D seismic data and mentioned in Chapters 4, 5 and 6 of this thesis is the step-up of the décollement near the toe of the accretionary prism (Figure 7.6). The stepping-up presents another erosive mechanism through which basal parts of the NAP are transferred and included

into the subduction channel by underplating and underthrusting. Therefore, basal asperities increase both accretional and erosive behaviour of the subduction in the S sector of the NAP (Safonova and Khanchuk, 2021). Additionally, depressed areas in the subducting oceanic plate between basal asperities, especially such as those observed between Scarps 3 and 4, and these scarps and the Kumano Seamount also offer conditions for collapse of the overlying NAP and inclusion of weakly consolidated sediment into the subduction channel as the décollement overrides these smaller basal asperities. Similar settings are observed in the Java margin (Kopp et al., 2006) and Peruvian margin (Hampel et al., 2004). Nevertheless, such processes may operate without the net loss of upper plate material, aligning more closely with a non-accretionary model where sediment bypass or internal recycling dominates (von Huene and Suess, 1988).

The N sector of the NAP equally displays features of both accretional and erosive behaviour with some being considerably distinct from the ones discussed for the S sector. Similar to the S sector, there is also evidence of décollement step-up at the FTZ (Figure 7.6) as a mechanism of tectonic erosion to separate and transport sediments of the upper plate into the subduction channel (Safonova and Khanchuk, 2021). However, the step-up of the décollement in the N sector seems to be somehow related to the extent of Unit B, rather than the Kumano Seamount or any basal asperities. 3D seismic data reveal that Unit B thins seawards and, shortly seawards of Unit B disappearing, several low-angled thrust faults branch out from the décollement, which could lead to its potential step-up.

The Unit B, that seems to almost only exist or form in the N sector of the NAP (Figure 7.6), is another feature of the erosive tectonics operating within the NAP as this unit is an overpressured zone interpreted as a shear zone that may be currently forming a mélange or antiformal stacking (Park et al., 2010), a mechanism through which basal erosion of the overlying Unit A intensifies landwards and causes Unit B to thicken towards the same direction. Alternatively, this thickening and structural development may be a manifestation of internal wedge dynamics under a non-accretionary regime, particularly under high pore pressure and low effective stress conditions (Saffer and Tobin, 2011). The faster subduction rate of the N sector of the NAP together with a regionally younger and buoyant incoming PSP along the Nankai Trough create the ideal conditions for basal erosion below the entire section of the NAP where elevated pore pressure at the FTZ reduces the décollement friction, allowing the décollement and frontal thrusts to advance further into the proto-FTZ and underthrust larger amounts of trench and hemipelagic sediment. As these fluid-rich sediments subduct under the NAP, fluid will migrate to the upper NAP, increasing the pore pressure in the basal section of the accreted but weakly consolidated Unit A which will result in intense hydrofracturing. This network of hydrofracturing, observed in both N and S sectors, separates fractured blocks of sediment and rocks from the upper part of the NAP into the subduction channel, where they get subducted further downdip. This mechanism proposed by Von Huene et al. (2004) explains the landward growth of Unit B, observed in the N

sector, and the hydrofracturing network, occasionally observed in both sectors (Figure 7.6).

Although the NAP is mainly characterised by accretional tectonics, evidence discussed in this section indicates that this accretionary prism is far from being an end member of erosive–accretional subduction type as suggested by some authors (Moore et al., 2001; Kopf et al. 2013). Instead, it is here proposed that the NAP is dominated by accretional tectonics, mainly concentrated in the uppermost Unit A, with either:

- Periods of erosive tectonics triggered by the subduction of greater basal asperities that are normally above the décollement and resist subduction, such as the Kumano Seamount.
- Spatial variations where accretional and erosive tectonics can switch in response to smaller basal asperities, such as scarps and ridges, or general roughness of the incoming oceanic plate, especially at the lower levels of the accretionary prism where fluid pressure is a determinant factor.
- Zones or intervals of reduced accretion or tectonic quiescence, potentially representing non-accretionary regimes where incoming sediments are neither fully accreted nor removed from the overriding plate, but are instead underthrust, bypassed, or recycled within the subduction system (Shreve and Cloos, 1986; von Huene and Scholl, 1991; Wang and Hu, 2006).

Recognising these three possible tectonic behaviours—accretion, erosion, and non-accretion—is critical to understanding how even dominantly accretionary systems like the NAP may dynamically evolve in response to changes in basal topography, fluid pressure, and convergence rate.

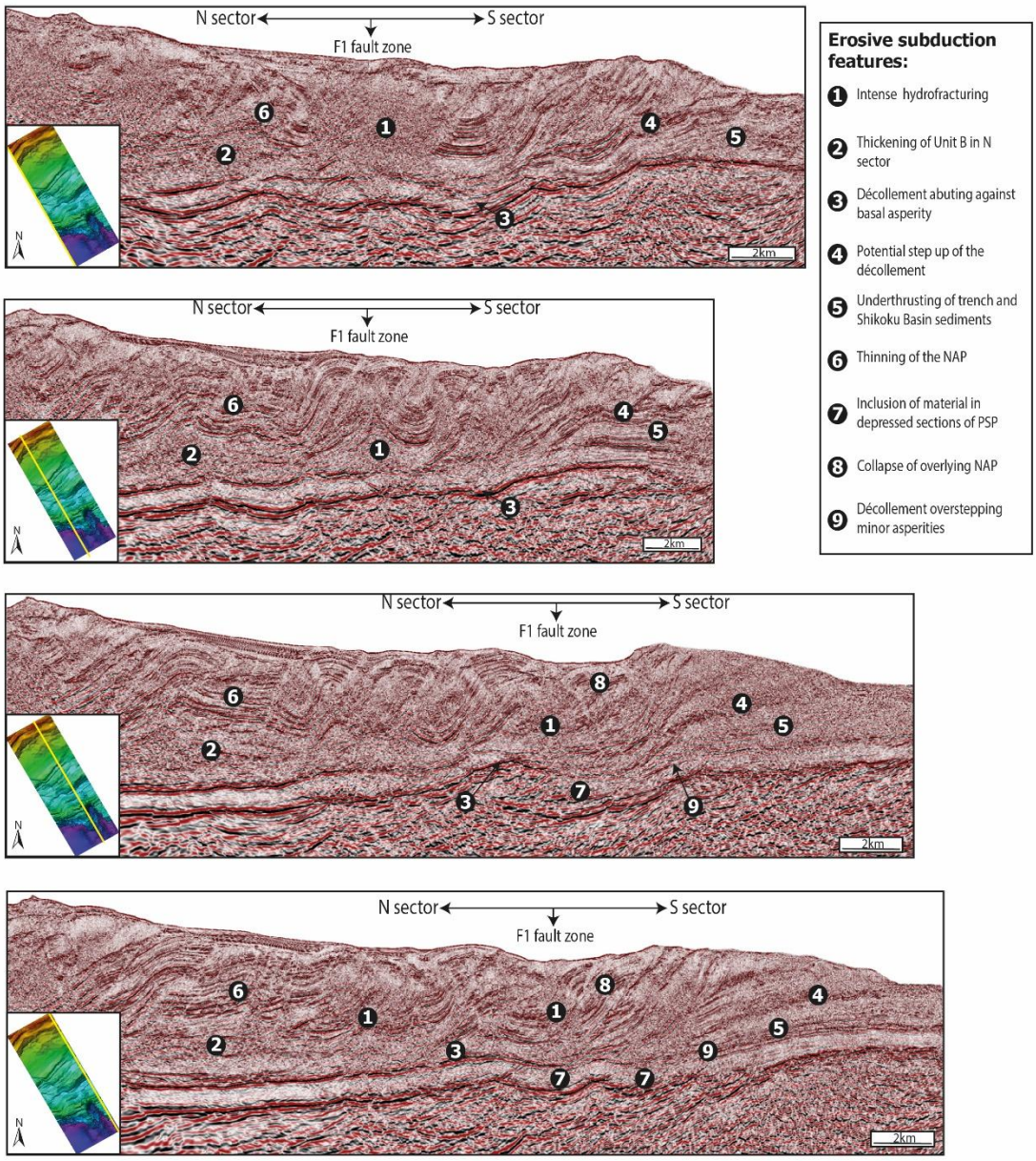

Figure 7.6 – Review of seismic inline profiles IL2130, IL2330, IL2530 and IL2730 (from top to bottom) to identify evidence of erosive tectonics in the accretional-dominated NAP. Insights mainly collected from Chapters 5 and 6.

7.4 Inclusion of asperities in the NAP

This section does not intend to provide mechanisms that will in fact happen in the future inclusion of the Kumano Seamount under the NAP. Instead, it aims to discuss and evaluate potential scenarios of inclusion of basal asperities under the NAP and other accretionary prisms by taking a predictive approach in the light of all the evidence gathered and discussed so far in this thesis.

7.4.1 Décollement step-up – duplex structures

Stepping up of the basal décollement is widely covered in literature (Wang et al., 2021) as a mechanism to include and subduct seamounts. This mechanism is well observed in the 3D seismic data and seems to be present in the analogue sandbox experiments covered in Chapters 5 and 6, respectively. It seems that the best way to overcome resistance offered by incoming asperities at toe of the NAP is to promote stepping up of the décollement to create a higher and smoother interplate surface above such basal asperities. In this scenario, the NAP initiates a phase of erosive tectonics that will underplate and underthrust sections of Unit A into the subduction channel (Units B and/or C). This mechanism seems plausible for smaller asperities that are within or slightly higher than the décollement, such as the scarps and ridges identified in the NAP

(Figure 7.6). However, for basal asperities significantly higher than the décollement, such as the Kumano Seamount, a potential step up of the décollement is observed in 3D seismic but not always connected. Moreover, the prior décollement abuts against the Kumano Seamount accompanied by seaward thinning of Unit C (Figure 7.6). Therefore, this potential step up of the décollement could just be interpreted as apparent or actual thrust faults developed at the toe of the NAP due to the collision of the Kumano Seamount into the FTZ of the NAP and subsequent, accretion and uplift of the previously accreted trench and Shikoku Basin sediments. It is also difficult to reason how this significant stepping up of the décollement alone can introduce the Kumano Seamount under the NAP and help its continuing subduction.

One such mechanism could be that described by Wang et al. (2021) for the Costa Rica margin where seamount subduction significantly hinders the seaward propagation causing the accretionary wedge to become narrower and steeper. This uplift and steepening of FTZ helps the formation of duplex structures in the advancing flank of the seamount that will transport deep subducted sediments into the shallow part of the wedge, which could re-join the prior landwards décollement with the newly stepped-up décollement. However, the formation of these duplex structures is intrinsically related to the presence of basement ramps/relief within the subducting plate prior to these main basal asperities.

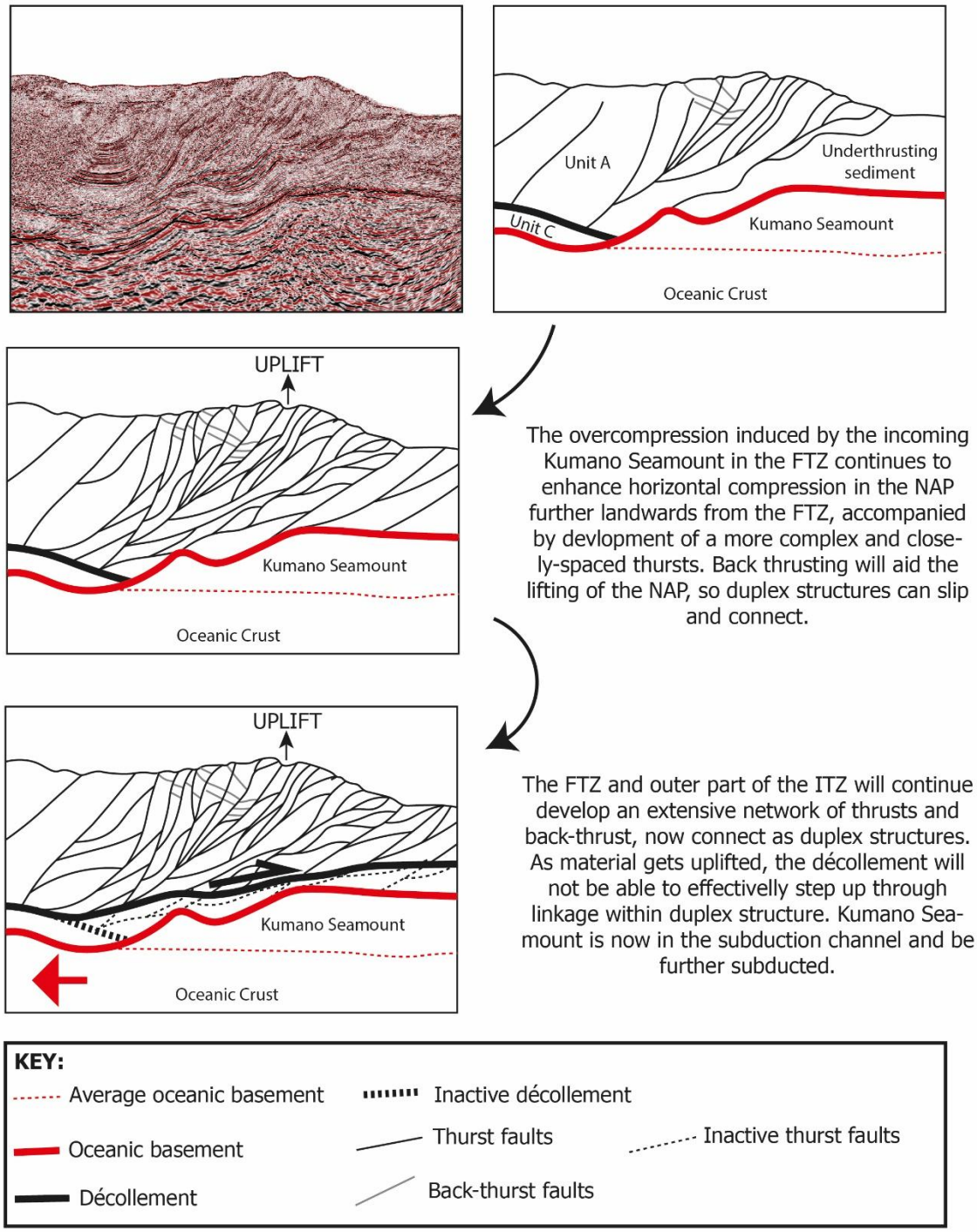

Figure 7.7 – Schematic interpretation of how the Kumano Seamount can underthrust the NAP and continue subduction through a mechanism of décollement step up.

3D seismic data does not clearly show such settings as the décollement abruptly abuts against the Kumano Seamount. Moreover, evidence of such duplex structures has not been recognised on the 3D seismic used in this thesis, especially in the advancing flank of the Kumano Seamount. Instead, a series of thrusts branching out from the 'new stepped-up décollement' is observed. There is a possibility that such branching is the process prior to the formation of duplex structures and that the Kumano Seamount is still in its initial phase of collision that this still have not developed enough to be resolved by 3D seismic (Figure 7.7).

7.4.2 Décollement step-up – spill point model

Another possible scenario for the inclusion and further subduction of basal asperities, especially of the dimensions of the Kumano Seamount is the 'spill point' scenario that considers insights revealed by both 3D seismic and analogue sandbox experiments in Chapters 5 and 6, respectively.

This scenario is discussed and summarised in Figure 6.8 of Chapter 6 and involves a seawards growth of the over pressured Unit B during erosive periods experienced in the NAP and enhanced by the subduction of the Kumano Basin. This could be related to the over compression at the FTZ, caused by the Kumano

Seamount, that blocks the typical fluid escape pathway at the toe of an accretionary prism. This setting causes excess pore fluid pressures along and above the subduction interface, where the Unit B lays (Ellis et al., 2015). Such a condition could be determinant to the upwards and seawards growth of the over pressured Unit B.

3D seismic and sandbox experiments are concordant in the fact that changes in thickness and pore-pressure in Unit B have significant impacts in the branching of new imbricated and OOS thrusts. Therefore, as Unit B thickens and expands further landwards, it will eventually meet the Kumano Seamount and build up to achieve the top of the seamount. When this occurs, the fluid within the over pressured Unit B will encounter the extensive network of thrust faults above the seamount, where it will 'spill' (escape) along these faults that will slip, promoting underthrusting and frontal growth of the NAP, as observed in the sandbox experiments in Chapter 6. This combined effect may aid the further subduction of the Kumano Seamount while also helping with the branching of new thrusts in the FTZ and outer parts of the ITZ that could link to the décollement to promote its stepping up in a similar fashion to the duplex structure previously discussed.

Although the 'duplex structure' and 'spill point' scenarios are here discussed separately, it could be that they are coexisting in aiding the décollement to step up. However, there is no consistent evidence from 3D seismic that indicates if one is more dominant over the other.

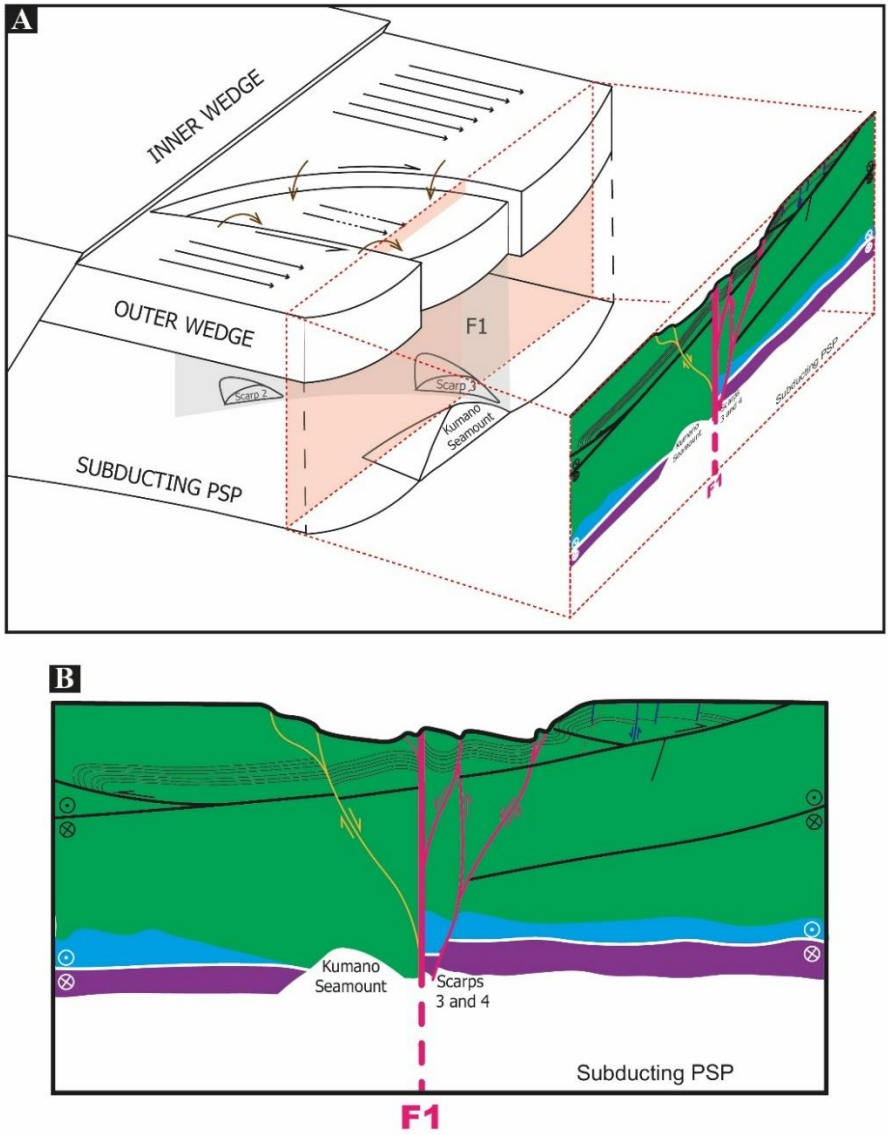

Figure 7.8 – Schematic diagrams and profiles showing how pull apart basin can exist in the NAP. A) Schematic 3D diagram (not at scale) showing the pull apart basin formed by localised transtensional regime caused by the collision of the Kumano Seamount with the NAP. This basin is filled in with sediment sources from higher adjacent areas of the NAP (brown arrows). The adjacent sectors are moving at stable regional rate (low black arrow) leading to progressive deformation of their respective accretionary prisms while the sector affected by the Kumano Seamount show a stick-slip behaviour (alternating full and dashed black arrows). Fault F1 represented by grey plane. Red plane shows the cross section showed in B). B) An adaptation from figure in Chapter 4 (Azevedo et al., 2018), showing F1 as a strike-slip negative structure typical of transtensional regimes.

7.4.3 Lateral by-pass model

The evidence discussed across Chapters 4, 5 and 6 suggest that the strike-slip fault F1 is not a single fault but a strike-slip zone (Figure 7.8B) rooting deep in the NAP as response to the along-strike differential subduction rate and varying growth rate of the accretionary prism induced by basal asperities, such as the Kumano Seamount. Chapter 4 discusses the S sector of the NAP displaying settings similar to those of pull-apart basins (Figure 7.8). This setting could reasonably be created by a localised transtensional regime created by the oblique subduction of the PSP under the Amur Plate (Dewey et al., 1998).

Another proposed scenario through which the Kumano Seamount may be included and subducted under the NAP is here discussed and named as 'lateral by-pass'. In this scenario, the collision of the Kumano Seamount at the toe of the NAP causes the subduction rate to significantly decrease or stop at a local level, especially after uplift and stabilisation of the FTZ of the NAP, as previously discussed. Contrastingly, adjacent sectors of the NAP along the Nankai Trough, including the N sector and another further south from the S sector, will progressively accrete and override a potentially smoother PSP that will subduct at or close to the regional convergence rate, causing these adjacent accretionary sections to growth further seawards and faster. This along-strike variation in the subduction rate is accommodated by a strike-slip motion in the zone landwards

of and around the Kumano Seamount, at the S sector of the NAP (Figures 7.8 and 7.9).

From the discussion in section 7.3.1, it is plausible that the slab pull from subduction movement will create tension in the PSP just under the outer wedge of the NAP due to the locking effect from the Kumano Seamount at the toe of the NAP. This local extensional setting in the subduction channel induces hydraulic fracturing of the overlying NAP due to the upwards fluid escape which, consequently, thins Unit A and aids normal faulting and collapse of the NAP (Figure 7.9A). This phenomenon together with the strike-slip zone previously described develops a depressed pull-apart wedge. This wedge is visible in 3D seismic as a bathymetric basin above the outer wedge of the NAP that is filled by trench sediment, probably sourced from laterally higher adjacent sectors along the Nankai Trough and the seawards FTZ (Figure 7.8 and 7.9).

The weakly consolidated trench sediment deposited in this new forearc basin together with weakened underlying Unit A by hydrofracturing (von Huene et al., 2004) may create a situation where the FTZ and outer parts of the ITZ are stronger and more consolidated than inner parts of the ITZ. This internal difference in consolidation and strength could resolve in internal parts of the NAP now being able to accommodate renewed strain, accompanied by further landwards movement of the Kumano Seamount into the NAP (Figure 7.9B). This process is concordant to that modelled by Sun et al. (2020) where force imbal-

ance caused by the increase in effective fault-normal stress from incoming seamount leads to slip acceleration and unstable stick-slip. Moreover, Sun et al. (2020) suggest that enhanced lithification and consolidation also caused by incoming seamount creates transition from rate strengthening to rate weakening frictional behaviour, crucial to nucleation of unstable slip (Figure 7.9B).

A cyclic repetition of periods of hydrofracturing and thinning of the NAP followed by periods of renewed compression and subduction could present a process through which seamounts move further downdip. However, there are a few issues with this mechanism as the sole process through which basal asperities effectively subduct:

- Although it explains how seamounts and other basal asperities can continue moving landwards under a situation of over-consolidation and stabilisation at the FTZ, it does not explain how such basal asperities get embedded into either the subduction channel or the overlying accretionary prism.
- Despite explaining how the subduction can restart or regain its motion, this section would still move at slower rate than adjacent sectors. Punctual basal asperities, such as the Kumano Seamount, do not have the ability to permanently change the rate of subduction. Normally, individual asperities will get included and the FTZ will resume its regional convergent.

- In this process, sediment would indefinitely accrete and pile up in the advancing flank and above the seamount, which is not concordant with the critical taper theory.

This is where the lateral by-pass scenario will come into play and where Unit B in the N sector of the NAP could become a determinant factor in the inclusion of a basal asperity, such as the Kumano Seamount, in the subduction channel. As the smoother N sector of the NAP moves and grows at a faster rate it will eventually overrun the delayed rougher S sector to a point that the prior will be significantly seawards than the later (Figure 7.9B). However, that mechanism alone is also not enough to completely engulf the Kumano Seamount in the subduction channel. Such situation will be achieved with the lateral thickening of Unit B and OOS thrusting within the ITZ of the N sector and lateral thinning of the S sectors. This combined effect will create a condition where the décollement will be able to either laterally ramp up from the N sector to the S sector, above the Kumano Seamount, or Unit B from the N sector will expand in the S sector producing a lateral spill point mechanism where a new higher décollement can replace the prior one (Figure 7.9C).

It is important to mention that this lateral by-pass scenario can happen in both laterally adjacent sectors to the basal asperity. However, the 3D seismic volume only covers the two sectors mentioned in the discussion above, but Figure 7.9 shows a bilateral by-pass scenario.

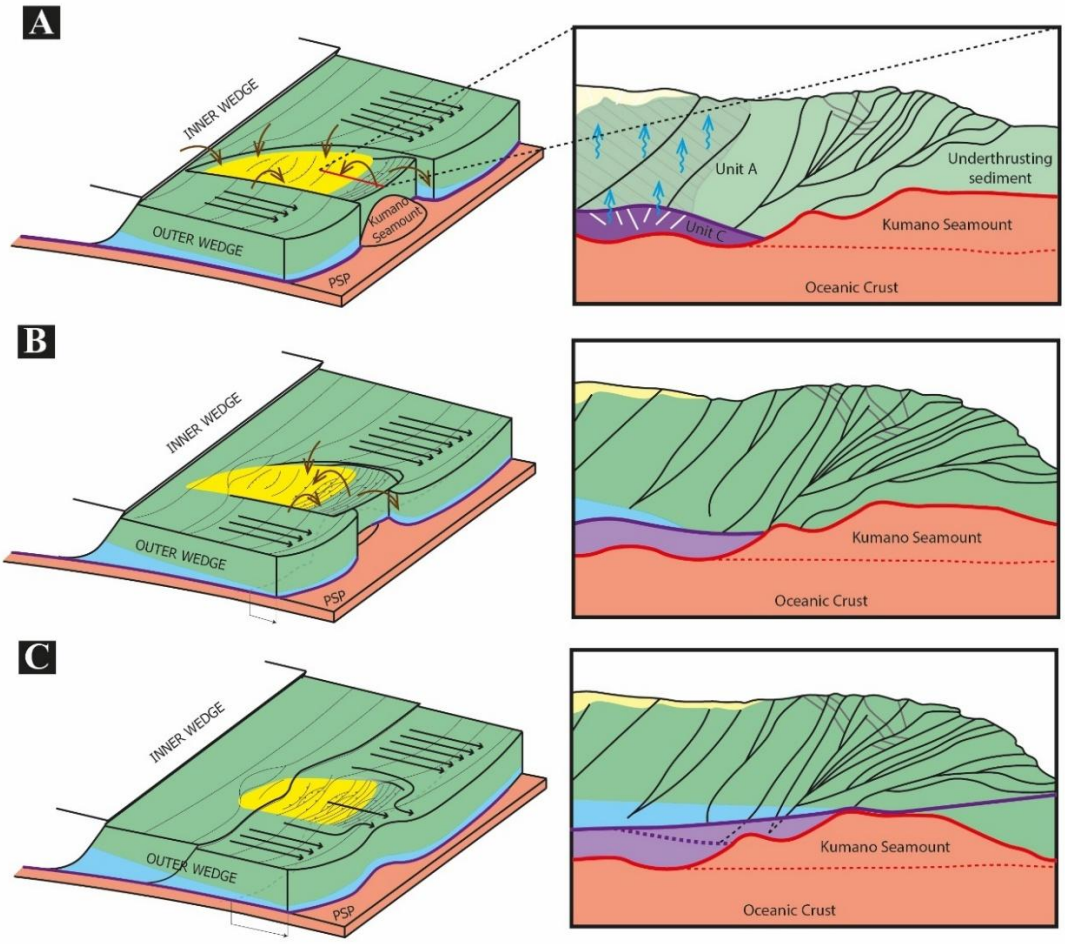

Figure 7.9 – Schematic 3D and 2D diagrams showing a 'bilateral by-pass' scenario to subduct the Kumano Seamount. A) Adaptation of Figure 7.8 with Kumano Seamount over compression and consolidating the FTZ of the NAP, stabilising section. As a result of the slab pull, subducting PSP and suprajacent Unit C suffer extensional strain, releasing fluids in Unit A that will promote its thinning and extension through hydraulic fracturing. This creates a pull apart basin in the middle of the outer wedge of the NAP that will be filled in by sediment by all the adjacent higher sectors, including the raised FTZ (brown arrows). The sectors immediately adjacent to the Kumano Seamount will progressively accrete and growth at regional convergence rate, therefore growing further seawards. B) The inner parts of the NAP, just landwards of the Kumano Seamount, is weak due to the hydraulic fracturing and newly added trench sediment. Thus, will be able to accommodate compressional strain from the Kumano Seamount at the FTZ, allowing the seamount to move further downdip. This will cause consolidation and compression of the internal part of the NAP, create conditions for basal erosion that will reform Unit B. C) Seaward growth of over pressure Unit B will enhance formation of new thrusts that will facilitate the step up of the décollement through either duplex and/or spill point mechanism. The migration of compression into inner parts of the NAP, caused by the Kumano Seamount, together with growth of the Unit B can create conditions for formation of OOS thrusts in the inner parts of the ITZ.

7.4.4 Other possible mechanisms

The scenarios discussed so far only consider mechanisms through which the Kumano Seamount is included within the subduction channel below the décollement. These mechanisms seem to be more probable due to role that subduction channel, décollement and Unit B have in the subduction operating in the NAP along the Nankai Trough. However, there is always the possibility that basal asperities are instead accreted and included in the NAP rather than being further subducted. Tetreault and Buiter (2014) identify decapitation as the most common process of accreting seamounts. In this section, two models are suggested based on isolated evidence collected from the 3D seismic data, but they are unlikely to happen on an overall weakly consolidated accretionary prism such as the NAP.

Despite lower resolutions at depth, 3D seismic of the subducting PSP and Unit C images what appears to be extensional faulting in areas surrounding the Kumano Seamount, especially at its advancing flank. Such extensional settings in the subducting oceanic plate, either pre-existing or newly formed, can also occur in the Kumano Seamount as it bends and gets further subducted (Masson et al., 1990). As previously discussed, such extensional settings generate conditions for upward fluid escape that will weaken the upper NAP through hydrofracturing while strengthening the lower plate (von Huene et al., 2004). This

coupled with the enhanced consolidation and rigidity of the NAP at the advancing flank of the Kumano Seamount increases shear strength of the megathrust and favours storage of elastic strain, leading to fault instability (Sun et al., 2020). Such mechanisms could promote the following scenarios, yet unlikely to happen:

- **Truncation scenario:** as the subduction channel and underlying oceanic plates increase their shear strength from fluid escape to the suprajacent layers, the seamount is probably going to experience a concentration of horizontal compression stress in its advancing flank which will be accommodated in form of elastic strain. This is more significant when considering that Kumano Seamount is higher that the décollement and that the décollement is currently abutting against the seamount instead of stepping up. The accumulation of elastic strain in the Kumano Seamount could lead to it being truncated or decapitated at the current level of the décollement, which would allow the décollement to link back to the FTZ and continued the growth of the NAP while accreting the top part of the Kumano Seamount (Figure 7.10A).
- '**Step down' scenario:** 3D seismic data around the elongated major ridges identified in this thesis reveals that the décollement, at times, also seem to be abutting against theses basal asperities. This could create a similar mechanism to the truncation scenario

where the décollement on the seawards side of the basal asperities will rupture through the scarp to join the décollement on the landwards side of the scarp (Figure 7.10B).

7.5 Implications to the seismicity and tsunamigenic potential of subduction zones around the world

Wang and Bilek (2011) and Menichelli et al. (2023) state that although seamount subduction occasionally can generate large earthquakes, normally, most seamounts and other basal asperities subduct aseismically through a process of creeping that is possible due to the complex network of fractures and faults created by the subduction of those same basal asperities. The data interpreted and discussed in this thesis reveal that the NAP has that sort of complex network of fractures and faults that will create a variety of stress fields within the accretionary prism. This stress field conditions will dissipate stress and accommodate strain in heterogeneous ways that, ultimately, will normally not be favourable for the generation of great ruptures.

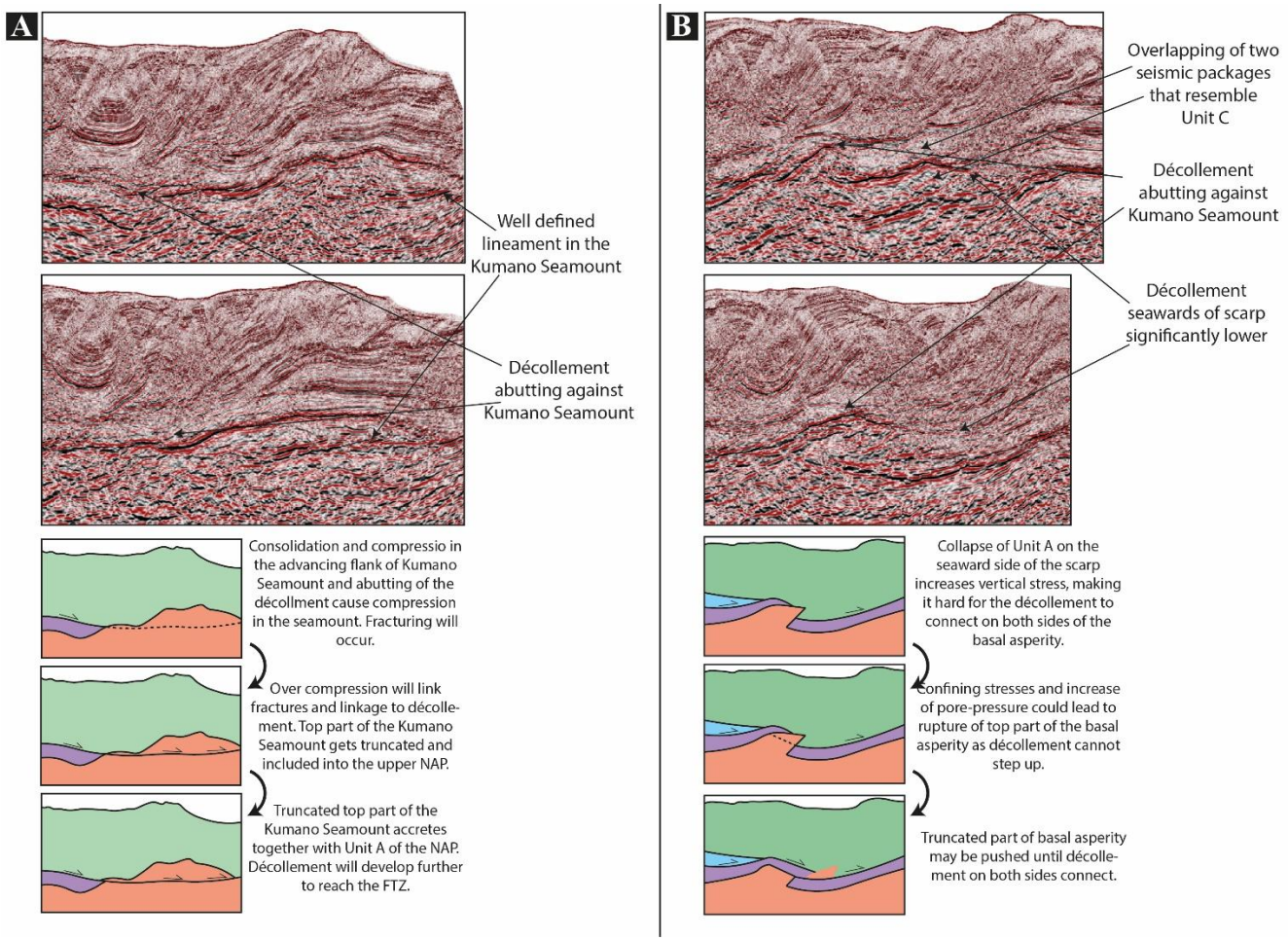

Figure 7.10 – Seismic profiles showing evidence from 3D seismic that may suggest other forms of subduction of asperities with schematic diagrams explaining the mechanism involved in each of the scenarios. A) Truncation scenario showing some evidence from seismic inline profiles IL2230 and IL2330. B) 'Step down' scenario showing some evidence from seismic inline profiles IL2460 and IL2530.

In the NAP, the strike-slip fault zone F1 showcases one mechanism described above that promotes changes in the stress field and accommodate strain in complex ways. Another feature that may contribute to the complex dissipation of stress in the NAP is the thinning of Unit A caused by either thickening on Unit B or extensional stress in the subducting PSP and lowermost subduction channel (Unit C). Both features seem to contribute to the VLFEs and SSEs recorded in several recent studies (Tamaribuchi et al., 2019; Takemura et al., 2022; Yamamoto et al, 2022; Flores et al., 2023). Regardless of being able to generate great earthquakes or not, these findings are still important as they could impact propagation of rupture in the event of great earthquakes outside of the study area. Menichelli et al. (2023) mentions that seamounts reduce seismic coupling and acts as a barrier to rupture propagation as seamount-induced fractures and fluid release are important mechanisms that prevent rupture propagation. Taking this into consideration, the strike-slip fault zone F1 created by the interaction of the NAP with the Kumano Seamount and other basal asperities that partitions stress and strain between the S and N sector of the NAP could present a significant barrier to rupture propagation during a great earthquake event in such way that the smoother N sector presents a great potential for propagation than the rougher S sector.

The analysis of the seismic data carried out in this thesis alone does not allow to quantify the movement of some of the events discussed in this section, such as the formation of OOS thrusts and mechanism of inclusion of the Kumano Seamount as most of these processes are still not occurring at present-day and

therefore not registered in seismic data, but it is possible to predict what sort of events can have the potential to generate displacements on the bathymetric surface. Such predictions are useful to understand the tsunamigenic potential of the certain structures and processes operating in the NAP.

Uplift of the FTZ during coseismic rupture is an important mechanism to generate tsunamis and has been identified as the cause of the tsunamis of the 2011 Tohoku and the 1944 Tonankai earthquakes (Park et al., 2010; Tsuji et al., 2018). The uplift of the FTZ of the NAP caused by the Kumano Seamount and observed in the S sector is probably not going to be a significant contributor to the tsunamigenic risk on its own as most of the uplift has occurred through a process of SSEs and creeping, which does not allow enough elastic strain to be accumulated for large ruptures. However, there are three implications that cannot be ignored due to this uplift causing the FTZ to become consolidated and over compressed:

- The localised compaction of the accreted sedimentary material in the FTZ of the NAP, will increase pore pressures. The over compression from the convergence will cause stress and strain to accumulate in this FTZ, potentially leading to fault reactivation and seismic slip (Moore et al., 2007) with minor displacements of the bathymetric surface that can trigger large-scale submarine landslides and, subsequently, tsunamis due to unstable FTZ (Zhang et al., 2016).

- The over compression locally experienced in the FTZ of the S sector can lead to redistribution of fluids and increased pore pressure that could leads to the Kumano Seamount or décollement to rupture if shear strength is overcome. Mechanisms of décollement step up and truncation of seamount are processes to aid the seawards continuation of the interplate surface so that frontal growth of the accretionary prism can progress. These mechanisms can be triggered during great earthquakes events and displace the bathymetry at the toe of the NAP.
- The partitioning of stress and strain between the N and S sectors in the NAP could reveal to have a great tsunamigenic risk as during great earthquakes, rupture propagation would mainly concentrate in the smoother N sector, which could be accompanied by rapid formation of frontal thrusts in the proto-FTZ.

Another important factor to consider is the combination of the stress distribution caused by the Kumano Seamount and the growth of the Unit B. These processes cause even more complex scenarios within the NAP. The first is related to the redistribution of fluids in sections of the NAP where hydrofracturing is not occurring and where fluid is not able to escape due to the over compressed FTZ induced by the Kumano Seamount. This could lead to fluid pressure to migrate towards the MSF and cause its reactivation (Moore et al., 2007). The second scenario could be related the branching and reactivation of imbricated

thrusts as newly formed OOS thrusts that will be able to displace the surface of the NAP and consequently, generate tsunamis.

Basal asperities present to be significant factors in both the seismic activity and tsunamigenic risk as asperities such as the Kumano Seamount have the capacity to change the stress distribution and fluid pathways, which will dictate how the NAP will deform and evolve.

7.6 Limitations of this research

The main limitations in this thesis relate mainly to the analysis and interpretation carried on the 3D seismic data and the analogue sandbox experiments.

In relation to the 3D seismic data used to map and analyse the structural framework and tectonics operating in the NAP, the main limitations are related to the vertical and horizontal (both across and along) resolution and extent of the 3D PSDM seismic data used. As most of the work carried out in this thesis relates to the deeper layers and subducting oceanic PSP, especially in Chapters 5 and 6, the progressively poorer seismic resolution at depth proved to be a challenge in terms of mapping continuous seismic horizons and structures and therefore, to make interpretations with confidence on its accuracy. This was also the case for the SE-limit of the 3D seismic volume that does not only show poor

seismic quality but also did not uniformly extend to the limit of the seismic volume, therefore missing some important images of the FTZ and proto-FTZ of the NAP. The irregular boundaries in the SE-limit of the 3D seismic data were caused by the high-speed Kuroshio current that produced difficulties during the acquisition of the seismic data. These resolution issues also created constraints in the study of horizontal shortening in the NAP as it made challenging to map seismic horizons within the smaller and more fractured seismic packages of the Unit A.

The horizontal extent of the 3D seismic volume, both across and along, also offered some challenges to this thesis. This is because it is clear there is another sector south of the S sector of the NAP, identified in this thesis, which would have been important to study and understand how it interacts with the basal asperities identified in the S sector and the oblique subduction. Additionally, the real dimensions and extend of the Kumano Seamount were not possible to be accurately assessed as the seismic volume only images what we predict to be around half of the seamount. The 3D seismic data of NAP that the Cardiff University have access to only covers the outer wedge of the NAP, which diverted the focus of this thesis to the outer wedge of the NAP, but it could have been useful to have access to the inner wedge to see if asperities in the outer wedge somehow influence the inner wedge.

The lack of well and borehole data on the deeper layers of the NAP present to be a limitation as such information would help our structural and fault analysis, especially in terms of the strike-slip fault zone F1 and their influence in

fluid pathways and stress distribution as it would made it possible to carry out correlations between fault segmentation and growth and lithology and its consolidation.

Ultimately, the analogue sandbox models were very useful to visualise how certain structures have developed during the evolution of the NAP and to understand how basal asperities are introduced in accretionary prisms and get further subducted into the subduction channel. However, it is recognised that these sandbox experiments can have spatial constraints issues that will cause dragging and changes of stress fields in the borders of the deformation box. Additionally, the asperities simulated in both experiments in Chapter 6 are far from representing the real roughness of the subducting PSP, so results here interpreted could be an underestimation of the actual impacts the basal asperities on the overlying NAP.

7.7 Future work

Although the NAP is one of the most heavily studied subduction zones on Earth, it would be useful to do a detailed structural and tectonics analysis, similar to the one carried out in this thesis, on the inner wedge of the NAP and correlate new findings to the ones in the here addressed. Most studies either cover the outer wedge and inner edge as independent units but it is suspected that a lot

of links can be made between these two areas in such way that settings and structures on one will undoubtedly affect the other.

For future work, it would be promising to integrate the findings of this thesis with existing and future well and borehole data in order to test the accuracy of interpretations made of areas in the 3D seismic were the resolution is limited. Similarly, studying well and borehole data from other similar accretionary prisms and where they reach deeper layers also offer great spectrum for future work.

Ultimately, a revision of erosive vs accretional end-members in the light of new and future seismic acquisitions could also be valuable future work as this thesis revealed that the NAP is far from being an end-member type of accretional margin with some potential non-accretional regime operating. Such future study may show that both subduction regimes may actually coexist in different space and/or time.

CHAPTER 8

Conclusions

At the beginning of the Chapter 1, a rationale and aims for this thesis were proposed, which will now be reviewed in the light of the discussion and evaluation carried throughout:

Hypothesis 1: ***Stress and strain distribution in the NAP accretionary prism is partitioned***. *If correct, one should expect to discover a complex structural framework in the study area, and one that changes either spatially or temporally with clear difference in the deformation styles. If incorrect, then the NAP be-haves as a typical, structurally homogeneous accretionary prism*.

Chapters 4, 5 and 6 showed that the NAP is far from being a typical compressional accretionary prism characterised only or mainly by a fold-and-thrust tectonic setting. Chapter 4 revealed that the NAP is actually partitioned into a S and N sectors with separate regimes. While both show evidence of the expected fold-and-thrust settings, each of these sectors also show an important strike-slip component that resemble a conjugate setting. Chapters 4 and 5 discussed that in fact such partitioning is reigned by an important right-lateral strike slip fault that roots deep in the NAP and Chapter 6 demonstrated how such setting can be formed by basal asperities being subducted under the NAP.

Hypothesis 2: ***The roughness of the subducting Philippines Plate is rougher than previously described***. *If correct, detailed 3D seismic mapping will show evidence of asperities within the incoming subducting plate. If incorrect, the subducting plate will be smooth*.

This thesis provides the most detailed seismic mapping of the subducting PSP done to date, in Chapter 5, and it reveals that in fact the oceanic crust subducting beneath the NAP is rougher than previously described. However, this roughness is varying across the area as it is characterised by a rougher S sector compared to a smoother N sector with important implications in the overlying NAP. The area of the NAP studied in this thesis show an important seamount, the Kumano Seamount, in its early stages of collision with the FTZ, and several minor and major elongated ridges.

Hypothesis 3: ***Horizontal shortening and frontal growth of the NAP is affected by the roughness of the subducting Philippines Plate.*** *If correct, estimations of horizontal shortening, the length of the accretionary prism, and structures in the overlying NAP will all show evidence of some sort of physical or structural relationship. If incorrect, no correlation is found*.

The horizontal shortening and frontal growth discussed in Chapters 5 and 6 are significantly affected by the roughness of the subducting PSP. The roughness of the incoming oceanic plate unexpectedly affects the horizontal shorten-

ing of the NAP in the way that is does not significantly changes its overall shortening, but it significantly impacts the distribution and concentration of that shortening within the NAP. Basal asperities increase local horizontal shortening of the NAP in the areas immediately surrounding them, while stopping or slowing shortening in other areas away from their influence. However, the overall horizontal shortening is still achieved as a consequence of the regional convergence. The frontal growth of the NAP is the most impacted by the collision and subduction of basal asperities, with the S sector, affected by the Kumano Seamount, experiencing retreat of the trench as reported in many erosive margins.

Hypothesis 4: ***The roughness of the subducting Philippines Plate will affect interplate coupling and can initiate earthquakes***. *If correct, there will be evidence in both the 3D seismic dataset and sandbox analogue models for asperities affecting stress and strain distribution, as well as fluid pathways within the NAP. If incorrect, then any asperities on the subducting plate will not show sign of interference with the overlying NAP*.

This thesis shows that roughness of the subducting PSP definitely interferes with stress and strain distribution as well as fluid and pore-pressure along and across the NAP, as stated in Chapters 4 and 5. These findings do not really show if great earthquakes will be initiated or not, but allows to predict scenarios in which distributions of stresses and slip may occurs, especially in relation to earthquakes or tremors that can generate tsunamis.

CHAPTER 9

References

Ambraseys, N. N., Tchalenko, J. S. (1969). The Dasht-e Bayāz (Iran) earthquake of August 31, 1968: A field report. Bulletin of the Seismological Society of America, 59(5), 1751-1792. https://doi.org/10.1785/BSSA0590051751

Alaei, B. (2012). Seismic modeling of complex geological structures. Seismic Waves-Research and Analysis, 11, 528-529.

Altmann, J. B., Müller, B. I. R., Müller, T. M., Heidbach, O., Tingay, M. R. P., Weißhardt, A. (2014). Pore pressure stress coupling in 3D and consequences for reservoir stress states and fault reactivation. Geothermics, 52, 195-205. https://doi.org/10.1016/j.geothermics.2014.01.004

Alves, T. M., Strasser, M., Moore, G. F. (2014). Erosional features as indicators of thrust fault activity (Nankai Trough, Japan). Marine Geology, 356, 5-18. https://doi.org/10.1016/j.margeo.2013.07.011

Akuhara, T., Tsuji, T., Tonegawa, T. (2020). Overpressured underthrust sediment in the Nankai Trough forearc inferred from transdimensional inversion of high-frequency teleseismic waveforms. Geophysical Research Letters, 47(15), e2020GL088280. https://doi.org/10.1029/2020GL088280

Anderson, E. M. (1905). The dynamics of faulting: Transactions of the Edinburgh Geological Society, v.8 (3), p. 387-402, https://doi.org/10.1144/transed.8.3.387

Ando, M. (1975). Source mechanisms and tectonic significance of historical earthquakes along the Nankai Trough, Japan. Tectonophysics, 27(2), 119-140. https://doi.org/10.1016/0040-1951(75)90102-X

Arai, R., Iwasaki, T., Sato, H., Abe, S., Hirata, N. (2013). Crustal structure of the Izu collision zone in central Japan from seismic refraction data. Journal of Geophysical Research: Solid Earth, 118(12), 6258-6268. https://doi.org/10.1002/2013JB010532

Arjmandzadeh, R., Karimpour, M. H., Mazaheri, S. A., Santos, J. F., Medina, J. M., Homam, S. M. (2011). Two-sided asymmetric subduction; implications for tectonomagmatic and metallogenic evolution of the Lut Block, eastern Iran.

Azevedo, M. C., Alves, T. M., Fonseca, P. E., Moore, G. F. (2018). Strike-slip deformation reflects complex partitioning of strain in the Nankai Accretionary Prism (SE Japan). Tectonophysics, 723, 81-94. https://doi.org/10.1016/j.tecto.2017.11.023

Azuma, S., Yamamoto, S., Ichikawa, H., Maruyama, S. (2017). Why primordial continents were recycled to the deep: Role of subduction erosion. Geoscience Frontiers, 8(2), 337-346. https://doi.org/10.1016/j.earscirev.2012.11.003

Deformation of a seamount subducting beneath an accretionary prism: Constraints from numerical simulation. Geophysical Research Letters, 28(9), 1827-1830. https://doi.org/10.1029/2000GL012266

Baba, K., Yamada, Y. (2004). BSRs and associated reflections as an indicator of gas hydrate and free gas accumulation: An example of accretionary prism and forearc basin system along the Nankai Trough, off central Japan. Resource Geology, 54(1), 11-24. https://doi.org/10.1111/j.1751-3928.2004.tb00183.x

Bacon, M., Simm, R., Redshaw, T. (2007). 3-D seismic interpretation. Cambridge University Press.

Bangs, N. L., Shipley, T. H., Gulick, S. P., Moore, G. F., Kuromoto, S., Nakamura, Y. (2004). Evolution of the Nankai Trough décollement from the trench into the seismogenic zone: Inferences from three-dimensional seismic reflection imaging. Geology, 32(4), 273-276. https://doi.org/10.1130/G20211.2

Bangs, N.L.B., Gulick, S.P.S., Shipley, T.H., (2006). Seamount subduction in the erosion in the Nankai Trough and its potential impact on the seismogenic zone. Geology 34 (8), 701–704. https://doi.org/10.1130/G22451.1

Bangs, N. L. B., Moore, G. F., Gulick, S. P. S., Pangborn, E. M., Tobin, H. J., Kuramoto, S., Taira, A. (2009). Broad, weak regions of the Nankai megathrust and implications for shallow coseismic slip. Earth and Planetary Science Letters, 284(1-2), 44–44, 49. https://doi.org/10.1016/j.epsl.2009.04.026

Barnhart, W. D., Briggs, R. W., Reitman, N. G., Gold, R. D., Hayes, G. P. (2015). Evidence for slip partitioning and bimodal slip behavior on a single fault: Surface slip characteristics of the 2013 Mw7. 7 Balochistan, Pakistan earthquake. Earth and Planetary Science Letters, 420, 1-11. https://doi.org/10.1016/j.epsl.2015.03.027

Bassett, D., Arnulf, A., Kodaira, S., Nakanishi, A., Harding, A., Moore, G. (2022). Crustal structure of the Nankai subduction zone revealed by two decades of onshore-offshore and ocean-bottom seismic data: Implications for the dimensions and slip behavior of the seismogenic zone. Journal of Geophysical Research: Solid Earth, 127, e2022JB024992. https://doi.org/10.1029/2022JB024992

Beaumont, C., Ellis, S., Pfiffner, A. (1999). Dynamics of sediment subduction-accretion at convergent margins: Short-term modes, long-term deformation, and tectonic implications. Journal of Geophysical Research: Solid Earth, 104(B8), 17573-17601. https://doi.org/10.1029/1999JB900136

Behr, W. M., Becker, T. W. (2018). Sediment control on subduction plate speeds. Earth and Planetary Science Letters, 502, 166-173. https://doi.org/10.1016/j.epsl.2018.08.057

Bell, R., Sutherland, R., Barker, D. H., Henrys, S., Bannister, S., Wallace, L., Beavan, J. (2010). Seismic reflection character of the Hikurangi subduction interface, New Zealand, in the region of repeated Gisborne slow slip events.

Geophysical Journal International, 180(1), 34-48. https://doi.org/10.1111/j.1365-246X.2009.04401.x

Bertone, N., Bonini, L., Basili, R., Del Ben, A., Maesano, F. E., Tiberti, M. M., Pini, G. A. (2020). Evolution of tear faults in subduction zones: an analogue modelling perspective. In EGU General Assembly Conference Abstracts (p. 7608). https://doi.org/10.5194/egusphere-egu2020-7608

Boston, B., Moore, G. F., Jurado, M. J., and Sone, H. (2016). Deformation of the Nankai Trough inner accretionary prism: the role of inherited structures: Geochemistry Geophysics Geosystem, v. 17, p. 485-500, https://doi.org/10.1002/2015GC006185

Bourlange, S., Henry, P., Moore, J. C., Mikada, H., Klaus, A. (2003). Fracture porosity in the décollement zone of Nankai accretionary wedge using Logging While Drilling resistivity data. Earth and Planetary Science Letters, 209(1-2), 103-112. https://doi.org/10.1016/S0012-821X(03)00082-7

Brizzi, S., van Zelst, I., Funiciello, F., Corbi, F., van Dinther, Y. (2020). How sediment thickness influences subduction dynamics and seismicity. Journal of Geophysical Research: Solid Earth, 125, e2019JB018964. https://doi.org/10.1029/2019JB018964

Burchfiel, B. C., Royden, L. H. (1985). North-south extension within the convergent Himalayan region: Geology, v. 13.10, p. 679-682, https://doi.org/10.1130/0091-7613(1985)13%3C679:NEWTCH%3E2.0.CO;2

Byrne, D.E., Wang, W.H., Davis, D.M. (1993). Mechanical role of back-stops in the growth of forearcs. Tectonics 12 (1), 123–144. http://dx.doi.org/10.1029/92TC00618

Byrne, T.B., Lin, W., Tsutsumi, A., Yamamoto, Y., Lewis, J.C., Kanagawa, K., Kitamura, Y., Carson, B., Screaton, E. J. (1998). Fluid flow in accretionary prisms: Evidence for focused, time-variable discharge. Reviews of Geophysics, 36(3), 329-351. https://doi.org/10.1029/97RG03633

Byrne, T. B., Lin, W., Tsutsumi, A., Yamamoto, Y., Lewis, J. C., Kanagawa, K., Kitamura, Y., Yamaguchi, A., Kimura, G. (2009) Anelastic strain recovery reveals extension across SW Japan subduction zone: Geophysical research letters, v. 36(23). https://doi.org/10.1029/2009GL040749

Cartwright, J., Huuse, M. (2005). 3D seismic technology: the geological 'Hubble'. Basin Research, 17(1), 1-20. https://doi.org/10.1111/j.1365-2117.2005.00252.x

Cartwright, J., Santamarina, C. (2015). Seismic characteristics of fluid escape pipes in sedimentary basins: Implications for pipe genesis. Marine and Petroleum Geology, 65, 126-140. https://doi.org/10.1016/j.marpetgeo.2015.03.023

Chang, C., I. Song (2016). Present-day stress states underneath the Kumano basin to 2 km below seafloor based on borehole wall failures at IODP site

C0002, Nankai accretionary wedge: Geochem. Geophys. Geosyst., v. 17, https://doi.org/10.1002/2016GC006562

Chapman, J. B., Elliott, J., Doser, D. I., Pavlis, T. L. (2014). Slip on the Suckling Hills splay fault during the 1964 Alaska earthquake. Tectonophysics, 637, 191-197. https://doi.org/10.1016/j.tecto.2014.10.007

Chen, S. S., Hou, T., Liu, J. Q., Zhang, Z. C. (2020). Geochemical variation of Miocene basalts within Shikoku Basin: Magma source compositions and geo-dynamic implications. Minerals, 11(1), 25. https://doi.org/10.3390/min11010025

Chopra, S., Marfurt, K. J. (2005). Seismic attributes—A historical perspec-tive. Geophysics, v. 70 (5), p. 3SO-28SO. https://doi.org/10.1190/1.2098670

Chopra, S., Marfurt, K. (2007a). Curvature attribute applications to 3D surface seismic data: The Leading Edge, v. 26(4), p. 404-414. https://doi.org/10.1190/1.2723201

Chopra, S., Marfurt, K. J. (2007b). Volumetric curvature attributes for fault/fracture characterization: First break, v. 25(7), p. 35-46. https://doi.org/10.3997/1365-2397.2007019

Chow, B., Kaneko, Y., Townend, J. (2022). Evidence for deeply subducted lower-plate seamounts at the Hikurangi subduction margin: Implications for seismic and aseismic behavior. Journal of Geophysical Research: Solid Earth, 127, e2021JB022866. https://doi.org/10.1029/2021JB022866

Clarke, A. P., Vannucchi, P., Morgan, J. (2018). Seamount chain–subduction zone interactions: Implications for accretionary and erosive subduction zone behavior. Geology, 46(4), 367-370. https://doi.org/10.1130/G40063.1

Clift, P., Vannucchi, P. (2004). Controls on tectonic accretion versus erosion in subduction zones: Implications for the origin and recycling of the continental crust. Reviews of Geophysics, 42(2). https://doi.org/10.1029/2003RG000127

Cloos, M. 1993. Lithospheric buoyancy and collisional orogenesis: Subduction of oceanic plateaus, continental margins, island arcs, spreading ridges, and seamounts. Geological Society of America Bulletin 105:715–737. https://doi.org/10.1130/0016-7606(1993)105%3C0715:LBACOS%3E2.3.CO;2

Cloos, M., R.L. Shreve (1996). Shear-zone thickness and the seismicity of Chilean- and Marianas-type subduction zones. Geology 24:107–110. https://doi.org/10.1130/0091-7613(1996)024%3C0107:SZTATS%3E2.3.CO;2

Conin, M., Henry, P., Bourlange, S., Raimbourg, H., Reuschlé, T. (2011). Interpretation of porosity and LWD resistivity from the Nankai accretionary wedge in light of clay physicochemical properties: Evidence for erosion and local overpressuring. Geochemistry, Geophysics, Geosystems, 12(3). https://doi.org/10.1029/2010GC003381

Cordell, D., Unsworth, M. J., Diaz, D., Reyes-Wagner, V., Currie, C. A., Hicks, S. P. (2019). Fluid and melt pathways in the central Chilean subduction

zone near the 2010 Maule earthquake (35–36 S) as inferred from magnetotelluric data. Geochemistry, Geophysics, Geosystems, 20(4), 1818-1835. https://doi.org/10.1029/2018GC008167

Couzens, B. A., Wiltschko, D. V. (1996). The control of mechanical stratigraphy on the formation of triangle zones. Bulletin of Canadian Petroleum Geology, 44(2), 165-179. https://doi.org/10.35767/gscpgbull.44.2.165

Cowan, D. S., Silling, R. M. (1978). A dynamic, scaled model of accretion at trenches and its implications for the tectonic evolution of subduction complexes. Journal of Geophysical Research: Solid Earth, 83(B11), 5389-5396. https://doi.org/10.1029/JB083iB11p05389

Cubas, N., Avouac, J. P., Souloumiac, P., & Leroy, Y. (2013). Megathrust friction determined from mechanical analysis of the forearc in the Maule earthquake area. Earth and Planetary Science Letters, 381, 92-103. https://doi.org/10.1016/j.epsl.2013.07.037

Cunningham, D. (2005). Active intracontinental transpressional mountain building in the Mongolian Altai: defining a new class of orogeny: Earth and Planetary Science Letters, v. 240(2), p. 436-444. https://doi.org/10.1016/j.epsl.2005.09.013

Dahlen, F. A., Suppe, J., Davis, D. (1984). Mechanics of fold-and-thrust belts and accretionary wedges: Cohesive Coulomb theory. Journal of Geophysical Research: Solid Earth, 89(B12), 10087-10101. https://doi.org/10.1029/JB089iB12p10087

Davis, D., Suppe, J., Dahlen, F. A. (1983). Mechanics of fold-and-thrust belts and accretionary wedges. Journal of Geophysical Research: Solid Earth, 88(B2), 1153-1172. https://doi.org/10.1029/JB088iB02p01153

De Franco, R., Govers, R., Wortel, R. (2008). Nature of the plate contact and subduction zones diversity. Earth and Planetary Science Letters, 271(1-4), 245-253. https://doi.org/10.1016/j.epsl.2008.04.019

DeMets, C., Gordon, R.G., Argus, D.F. (2010). Geologically current plate motions. Geophys. J. Int. 181 (1), 1–80. http://dx.doi.org/10.1111/j.1365-246X.2009.04491.x

Dewey, J.F., Bird, J.M. (1970). Mountain belts and the global tectonics. Journal of Geophysical Research 75, 2625–2647. https://doi.org/10.1029/JB075i014p02625

Dewey, J. F., Holdsworth, R. E., Strachan, R. A. (1998). Transpression and transtension zones. Geological Society, London, Special Publications, 135(1), 1-14. https://doi.org/10.1144/GSL.SP.1998.135.01.01

Dickinson, W. R., Seely, D. R. (1979). Structure and stratigraphy of fore-arc regions. AAPG Bulletin, 63(1), 2-31. https://doi.org/10.1306/C1EA55AD-16C9-11D7-8645000102C1865D

Dominguez, S., Lallemand, S. E., Malavieille, J., von Huene, R. (1998). Upper plate deformation associated with seamount subduction. Tectonophysics, 293(3-4), 207-224. https://doi.org/10.1016/S0040-1951(98)00086-9

Dominguez, S., Malavieille, J., Lallemand, S. E. (2000). Deformation of accretionary wedges in response to seamount subduction: Insights from sand-box experiments. Tectonics, 19(1), 182-196. https://doi.org/10.1029/1999TC90005

Doo, W. B., Hsu, S. K., Yeh, Y. C., Tsai, C. H., Chang, C. M. (2015). Age and tectonic evolution of the northwest corner of the West Philippine Basin. Marine Geophysical Research, 36, 113-125. https://doi.org/10.1007/s11001-014-9234-8

Draut, A. E., Clift, P. D. (2013). Differential preservation in the geologic record of intraoceanic arc sedimentary and tectonic processes. Earth-Science Reviews, 116, 57-84. https://doi.org/10.1016/j.earscirev.2012.11.003

Egawa, K., Furukawa, T., Saeki, T., Suzuki, K., Narita, H. (2013). Three-dimensional paleomorphologic reconstruction and turbidite distribution predic-tion revealing a Pleistocene confined basin system in the northeast Nankai

Trough area. AAPG bulletin, 97(5), 781-798. https://doi.org/10.1306/10161212014

Ellis, S., Fagereng, Å., Barker, D., Henrys, S., Saffer, D., Wallace, L., Williams, C., Harris, R. (2015). Fluid budgets along the northern Hikurangi subduction margin, New Zealand: The effect of a subducting seamount on fluid pressure. Geophysical Journal International, 202(1), 277-297. https://doi.org/10.1093/gji/ggv127

Expedition 315 Scientists (2009). Expedition 315 Site C0001: Proceedings of the Integrated Ocean Drilling Program, v. 314/315/316, doi: 10.2204/iodp.proc.314315316.123.2009

Expedition 316 Scientists (2009). Expedition 316 Site C0006. In: Kinoshita, M., Tobin, H., Ashi, J., Kimura, G., Lallemant, S., Screaton, E.J., Curewitz, D., Masago, H., Moe, K.T. (Eds.), The Expedition 314/315/316 Scientists, Proc. IODP, 314/315/316. http://dx.doi.org/10.2204/iodp.proc.314315316.134.2009

Expedition 333 Scientists (2012). Site C0018. In: Henry, P., Kanamatsu, T., Moe, K. (Eds.), The Expedition 333 Scientists, Proc. IODP, 333. Integrated Ocean Drilling Program Management International, Inc., Tokyo. http://dx.doi.org/10.2204/iodp.proc.333.103.2012

Faleide, T. S., Braathen, A., Lecomte, I., Mulrooney, M. J., Midtkandal, I., Bugge, A. J., Planke, S. (2021). Impacts of seismic resolution on fault interpretation: Insights from seismic modelling. Tectonophysics, 816, 229008. https://doi.org/10.1016/j.tecto.2021.229008

Fischer, K. M., Rychert, C. A., Dalton, C. A., Miller, M. S., Beghein, C., Schutt, D. L. (2020). A comparison of oceanic and continental mantle lithosphere. Physics of the Earth and Planetary Interiors, 309, 106600. https://doi.org/10.1016/j.pepi.2020.106600

Flemings, P. B., Saffer, D. M. (2018). Pressure and stress prediction in the Nankai accretionary prism: A critical state soil mechanics porosity-based approach. Journal of Geophysical Research: Solid Earth, 123(2), 1089-1115. https://doi.org/10.1002/2017JB015025

Fleury, J. M., Pubellier, M., de Urreiztieta, M. (2009). Structural expression of forearc crust uplift due to subducting asperity. Lithos, 113(1-2), 318-330. https://doi.org/10.1016/j.lithos.2009.07.007

Flores, P. C. M., Kodaira, S., Kimura, G., Shiraishi, K., Nakamura, Y., Fujie, G., No, T., Kaiho, Y. (2023). Link between geometrical and physical property changes along Nankai Trough with slow earthquake activity revealed by dense reflection survey. Authorea Preprints. https://doi.org/10.22541/essoar.169686248.89201128/v1

Fossen, H. (2016). Structural geology. Cambridge university press.

Foucher, J. P., Henry, P., Le Pichon, X., Kobayashi, K. (1992). Time-variations of fluid expulsion velocities at the toe of the eastern Nankai accretionary complex. Earth and planetary science letters, 109(3-4), 373-382. https://doi.org/10.1016/0012-821X(92)90099-H

Furuichi, M., Chen, J., Nishiura, D., Arai, R., Yamamoto, Y., Ide, S. (2024). Virtual earthquakes in a numerical granular rock box experiment. Tectonophysics, 874, 230230. https://doi.org/10.1016/j.tecto.2024.230230

Gao, X., Wang, K. (2017). Rheological separation of the megathrust seismogenic zone and episodic tremor and slip. Nature, 543(7645), 416-419. https://doi.org/10.1038/nature21389

Gase, A. C., Van Avendonk, H. J., Bangs, N. L., Bassett, D., Henrys, S. A., Barker, D. H., Kodaira, S., Jacobs, K.M., Luckie, T.W., Okaya, D.A., Fujie, G., Yamamoto, Y., Arnulf, A.F., Arai, R. (2021). Crustal structure of the northern Hikurangi margin, New Zealand: variable accretion and overthrusting plate strength influenced by rough subduction. Journal of Geophysical Research: Solid Earth, 126(5), e2020JB021176. https://doi.org/10.1029/2020JB021176

Gerya, T. V., Meilick, F. I. (2011). Geodynamic regimes of subduction under an active margin: effects of rheological weakening by fluids and melts. Journal of Metamorphic Geology, 29(1), 7-31. https://doi.org/10.1111/j.1525-1314.2010.00904.x

Goldfinger, C., Nelson, C.H., Johnson, J.E. (1997). Holocene earthquake records from the Cascadia subduction zone and northern San Andreas fault based on precise dating of offshore turbidites. Annual Review of Earth and Planetary Sciences, 25, 403–434. https://doi.org/10.1146/annurev.earth.31.100901.141246

Groshong, R.H. Jr. (2006). 3D Structural Geology: A Practical Guide to Quantitative Surface and Subsurface Map Interpretation. http://dx.doi.org/10.1007/978-3-540-31055-6

Gulick, S.P.S., Bangs, N.L.B., Shipley, T.H., Nakamura, Y., Moore, G., Kuramoto, S. (2004). Three-dimensional architecture of the Nankai accretionary prism's imbricate thrust zone off Cape Muroto, Japan: prism reconstruction via en echelon thrust propagation. J. Geophys. Res. Solid Earth 109 (B2), 1978–2012. http://dx.doi.org/10.1029/2003JB002654

Hamada, Y., Hirose, T., Ijiri, A., Yamada, Y., Sanada, Y., Saito, S., Sakurai, N., Sugihara, T., Yokoyama, T., Saruhashi, T., Hoshino, T., Kamiya, N., Bowden, S., Cramm, M., Henkel, S., Homola, K., Imachi, H., Kaneko, M., Lagostina, L., Manners, H., McClelland, H-L., Metcalfe, K., Okutsu, N., Pan, D., Raudsepp, M.J., Sauvage, J., Schubotz, F., Spivack, A., Tonai, S., Treude, T., Tsang, M-Y., Viehweger, D., Wang., D.T., Whitaker, E., Yamamoto, Y., Yang, K., Kinoshite, M., Maeda, L., Kubo, Y., Morono, Y., Inagaki, F., Heuer, V. B. (2018). In-situ mechanical weakness of subducting sediments beneath a plate

boundary décollement in the Nankai Trough. Progress in Earth and Planetary Science, 5(1), 1-10. https://doi.org/10.1186/s40645-018-0228-z

Hamilton, W. (1977). Subduction in the Indonesion Region. Island Arcs, Deep Sea Trenches and Back-Arc Basins, 1, 15-31. https://doi.org/10.1029/ME001p0015

Hampel, A., Kukowski, N., Bialas, J., Huebscher, C., Heinbockel, R. (2004). Ridge subduction at an erosive margin: The collision zone of the Nazca Ridge in southern Peru. Journal of Geophysical Research: Solid Earth, 109(B2). https://doi.org/10.1029/2003JB002593

Hananto, N. D., Leclerc, F., Li, L., Etchebes, M., Carton, H., Tapponnier, P., Qin, Y., Avianto, P., Singh, S.C., Wei, S. (2020). Tsunami earthquakes: Vertical pop-up expulsion at the forefront of subduction megathrust. Earth and Planetary Science Letters, 538, 116197. https://doi.org/10.1016/j.epsl.2020.116197

Hancock, P. L. (1985). Brittle microtectonics: principles and practice: Journal of structural geology, v.7 (3), p. 437-457. https://doi.org/10.1016/0191-8141(85)90048-3

Haq, S. S. (2012). Out-of-sequence thrusting in experimental Coulomb wedges: Implications for the structural development of mega-splay faults and forearc basins. Geophysical research letters, 39(20). https://doi.org/10.1029/2012GL053176

Harding, T. P. (1985). Seismic characteristics and identification of negative flower structures, positive flower structures, and positive structural inversion: AAPG Bulletin, v. 69(4), p. 582–600. https://doi.org/10.1306/AD462538-16F7-11D7-8645000102C1865D

Hayman, N. W., Toshiya, K. (2012). Structural evolution of an inner accretionary wedge and forearc basin initiation, Nankai margin, Japan. Earth and Planetary Science Letters, 353, 163-172. https://doi.org/10.1016/j.epsl.2012.07.040

Huene, R., Culotta, R. (1989). Tectonic erosion at the front of the Japan Trench convergent margin. Tectonophysics, 160(1-4), 75-90. https://doi.org/10.1016/0040-1951(89)90385-5

Huene, R., Lallemand, S. (1990). Tectonic erosion along the Japan and Peru convergent margins. Geological Society of America Bulletin, 102(6), 704-720. https://doi.org/10.1130/00167606(1990)102%3C0704:TEATJA%3E2.3.CO;2

Huffman, K. A., D. M. Saffer (2016). In situ stress magnitudes at the toe of the Nankai Trough Accretionary Prism, offshore Shikoku Island, Japan: J. Geophys. Res. Solid Earth, v. 121, p. 1202–1217. https://doi.org/10.1002/2015JB012415

Hyndman, R. D., Yamano, M., Oleskevich, D. A. (1997). The seismogenic zone of subduction thrust faults. Island Arc, 6(3), 244-260. https://doi.org/10.1111/j.1440-1738.1997.tb00175.x

Ikari, M. J., Saffer, D. M. (2011). Comparison of frictional strength and velocity dependence between fault zones in the Nankai accretionary complex. Geochemistry, Geophysics, Geosystems, 12(4). https://doi.org/10.1029/2010GC003442

Ikari, M. J., Saffer, D. M. (2012). Permeability contrasts between sheared and normally consolidated sediments in the Nankai accretionary prism. Marine Geology, 295, 1-13. https://doi.org/10.1016/j.margeo.2011.11.006

Ismat, Z. (2015). What can the dihedral angle of conjugate-faults tell us?. Journal of Structural Geology, v.73, p. 97-113. https://doi.org/10.1016/j.jsg.2015.02.008

Itaba, S., Koizumi, N., Matsumoto, N., Ohtani, R. (2010). Continuous observation of groundwater and crustal deformation for forecasting Tonankai and Nankai earthquakes in Japan. In Seismogenesis and Earthquake Forecasting: The Frank Evison Volume II (pp. 251-260). Springer, Basel. https://doi.org/10.1007/s00024-010-0095-z

Jaeger, J.C., Cook, N.G.W., & Zimmerman, R. (2007). Fundamentals of Rock Mechanics (4th ed.). Wiley-Blackwell.

Kahrizi, A., Delescluse, M., Chamot-Rooke, N., Pubellier, M., Bécel, A., Shillington, D., Nedimovic, M., Bulois, C. (2024). Extensional forearc structures at the transition from Alaska to Aleutian Subduction Zone: slip partitioning, terranes and large earthquakes. Comptes Rendus. Géoscience, 356(S2), 1-25. https://doi.org/10.5802/crgeos.225

Kamei, R., Pratt, R.G., Tsuji, T. (2012). Waveform tomography imaging of a megasplay fault system in the seismogenic Nankai subduction zone. Earth Planet. Sci. Lett. 317, 343–353. http://dx.doi.org/10.1016/j.epsl.2011.10.042

Karig, D. E., Sharman, G. F. (1975). Subduction and accretion in trenches. Geological Society of America Bulletin, 86(3), 377-389. https://doi.org/10.1130/0016-7606(1975)86%3C377:SAAIT%3E2.0.CO;2

Karig, D.E. (1986). The framework of deformation in the Nankai Trough, Initial Reports Deep Sea Drilling Projects. U.S. Government Printing Office, Washington, pp. 927-940. https://10.1126/science.289.5476.10

Kawamura, K., Ogawa, Y., Anma, R., Yokoyama, S., Kawakami, S., Dilek, Y., Moore, G. F., Hirano, S., Yamaguchi, A., Sasaki, T., YK05-08 Leg 2 and YK06-02 Shipboard Scientific Parties. (2009). Structural architecture and active deformation of the Nankai Accretionary Prism, Japan: submersible survey results from the Tenryu Submarine Canyon. Geological Society of America Bulletin, 121(11-12), 1629-1646. https://doi.org/10.1130/B26219.1

Kelleher, J., McCann, W. (1976). Buoyant zones, great earthquakes, and unstable boundaries of subduction. Journal of Geophysical Research, 81(26), 4885-4896. https://doi.org/10.1029/JB081i026p04885

Keim, M. E. (2006). Cyclones, tsunamis and human health. Oceanography, 19(2), 40-49.

Kimura, G., Kitamura, Y., Hashimoto, Y., Yamaguchi, A., Shibata, T., Ujiie, K., and Okamoto, S. Y. (2007). Transition of accretionary wedge structures around the up-dip limit of the seismogenic subduction zone: Earth and Planetary Science Letters, v. 255(3), p. 471-484, https://doi.org/10.1016/j.epsl.2007.01.005

Kimura, G., Moore, G.F., Strasser, M., Screaton, E., Curewitz, D., Streiff, C., Tobin, H. (2011). Spatial and temporal evolution of the megasplay fault in the Nankai Trough. Geochem. Geophys. Geosyst. 12 (3). http://dx.doi.org/10.1029/2010GC003335

Kimura, G., Koge, H., Tsuji, T. (2018). Punctuated growth of an accretionary prism and the onset of a seismogenic megathrust in the Nankai Trough. Progress in Earth and Planetary Science, 5(1), 1-12. https://doi.org/10.1186/s40645-018-0234-1

Kimura, G., Nakamura, Y., Shiraishi, K., Fujie, G., Kodaira, S., Yamaguchi, A., Fukuchi, R., Hashimoto, Y. (2021). Rejuvenated extension of the Philippine

Sea plate and its effect on subduction dynamics in the Nankai Trough. Island Arc, 30(1), e12402. https://doi.org/10.1111/iar.12402

Kinoshita, C., Saffer, D., Kopf, A., Roesner, A., Wallace, L. M., Araki, E., Kimura, T., Machida, Y., Kobayashi, R., Davis, E, Carr, S (2018). Changes in physical properties of the Nankai Trough Megasplay Fault induced by earthquakes, detected by continuous pressure monitoring. Journal of Geophysical Research: Solid Earth, 123(2), 1072-1088. https://doi.org/10.1002/2017JB014924

Kirkpatrick, J. D., Edwards, J. H., Verdecchia, A., Kluesner, J. W., Harrington, R. M., Silver, E. A. (2020). Subduction megathrust heterogeneity characterized from 3D seismic data. Nature Geoscience, 13(5), 369-374. https://doi.org/10.1038/s41561-020-0562-9

Kitajima, H., Saffer, D. M. (2012). Elevated pore pressure and anomalously low stress in regions of low frequency earthquakes along the Nankai Trough subduction megathrust. Geophysical Research Letters, 39(23). https://doi.org/10.1029/2012GL053793

Kobayashi, K., Nakada, M. (1978). Magnetic anomalies and tectonic evolution of the Shikoku inter-arc basin. Journal of Physics of the Earth, 26(Supplement), S391-S402. https://doi.org/10.4294/jpe1952.26.Supplement_S391

Kobayashi, K. (1984). Subsidence of the Shikoku back-arc basin. Tectonophysics, 102(1-4), 105-117. https://doi.org/10.1016/0040-1951(84)90010-6

Kobayashi, K., Kasuga, S., Okino, K. (1995). Shikoku Basin and its margins. In Backarc Basins: Tectonics and Magmatism (pp. 381-405). Boston, MA: Springer US. https://doi.org/10.1007/978-1-4615-1843-3_10

Kodaira, S., Takahashi, N., Nakanishi, A., Miura, S., Kaneda, Y. (2000). Subducted seamount imaged in the rupture zone of the 1946 Nankaido earthquake. Science, 289(5476), 104-106. https://doi.org/10.1126/science.289.5476.104

Kodaira, S., Iidaka, T., Kato, A., Park, J. O., Iwasaki, T., and Kaneda, Y. (2004). High pore fluid pressure may cause silent slip in the Nankai Trough. Science, v. 304 (5675), p. 1295-1298. https://doi.org/10.1126/science.1096535

Kodaira, S., Hori, T., Ito, A., Miura, S., Fujie, G., Park, J. O., ... & Kaneda, Y. (2006). A cause of rupture segmentation and synchronization in the Nankai trough revealed by seismic imaging and numerical simulation. Journal of Geophysical Research: Solid Earth, 111(B9). https://doi.org/10.1029/2005JB004030

Kopf, A. (2013). Effective strength of incoming sediments and its implications for plate boundary propagation: Nankai and Costa Rica as type examples of accreting vs. erosive convergent margins. Tectonophysics, 608, 958-969. https://doi.org/10.1016/j.tecto.2013.07.023

Kopp, H., Flueh, E. R., Petersen, C. J., Weinrebe, W., Wittwer, A., Scientists, M. (2006). The Java margin revisited: Evidence for subduction erosion off

Java. Earth and Planetary Science Letters, 242(1-2), 130-142. https://doi.org/10.1016/j.epsl.2005.11.036

Lackey, J. K., Regalla, C. A., Moore, G. F. (2020). Tectonic influences on trench slope basin development via structural restoration along the outer Nankai accretionary prism, southwest Japan. Geochemistry, Geophysics, Geosystems, 21(8), e2020GC009038. https://doi.org/10.1029/2020GC009038

Langseth, M. G., Casey Moore, J. (1990). Fluids in accretionary prisms. https://doi.org/10.1029/90EO00031

Lallemand, S., Collot, J. Y., Pelletier, B., Rangin, C., Cadet, J. P. (1990). Impact of oceanic asperities on the tectogenesis of modern convergent margins. Oceanologica Acta, Special issue.

Lallemand, S. E., Schnürle, P., Malavieille, J. (1994). Coulomb theory applied to accretionary and nonaccretionary wedges: Possible causes for tectonic erosion and/or frontal accretion. Journal of Geophysical Research: Solid Earth, 99: B6, 12033-12055. https://doi.org/10.1029/94JB00124

Lallemand, S., Peyret, M., van Rijsingen, E., Arcay, D., Heuret, A. (2018). Roughness characteristics of oceanic seafloor prior to subduction in relation to the seismogenic potential of subduction zones. Geochemistry, Geophysics, Geosystems, 19, 2121–2146. https://doi.org/10.1029/2018GC007434

Laubscher, H. (2008). The Grenchenberg conundrum in the Swiss Jura: a case for the centenary of the thin-skin décollement nappe model (Buxtorf 1907).

Swiss Journal of Geosciences 101.1, 41-60. https://doi.org/10.1007/s00015-008-1248-2

Lebrun, J. F., Lamarche, G., Collot, J. Y., Delteil, J. (2000). Abrupt strike-slip fault to subduction transition: The Alpine fault-Puysegur trench connection, New Zealand. Tectonics, 19(4), 688-706. https://doi.org/10.1029/2000TC900008

Le Pichon, X., Iiyama, T., Boulègue, J., Charvet, J., Faure, M., Kano, K., Lallemant, S., Okada, H., Rangin, C., Taira, A., Urabe., T., Uyeda, S. (1987). Nankai Trough and Zenisu Ridge: a deep-sea submersible survey. Earth and Planetary Science Letters, 83(1-4), 285-299. https://doi.org/10.1016/0012-821X(87)90072-0

Lewis, S. D., Ladd, J. W., and Bruns, T. R. (1988). Structural development of an accretionary prism by thrust and strike-slip faulting: Shumagin region, Aleutian Trench. Geological Society of America Bulletin, v. 100, p. 767–782. https://doi.org/10.1130/0016-7606(1988)100%3C0767:SDOAAP%3E2.3.CO;2

Le Pichon, X. L., Henry, P., Lallemant, S. (1993). Accretion and erosion in subduction zones: The role of fluids. Annual Review of Earth and Planetary Sciences, 21(1), 307-331. https://doi.org/10.1146/annurev.ea.21.050193.001515

Le Pichon, X., Wmant, S., Tokuyama, H., Thoue, F., Huchon, P., and Henry, P. (1996). Structure and evolution of the backstop in the eastern Nankai

trough area (Japan): Implications for the soon-to-come Tokai earthquake. Island Arc, v. 5(4), p. 440–454. https://doi.org/10.1111/j.1440-1738.1996.tb00164.x

Leng, W., Mao, W. (2015). Geodynamic modeling of thermal structure of subduction zones. Science China Earth Sciences, 58, 1070-1083. https://doi.org/10.1007/s11430-015-5107-5

Lewis, J. C., Byrne, T. B., Kanagawa, K. (2013). Evidence for mechanical decoupling of the upper plate at the Nankai subduction zone: Constraints from core-scale faults at NantroSEIZE Sites C0001 and C0002. Geochemistry, Geophysics, Geosystems, v. 14(3), pp. 620-633. https://doi.org/10.1029/2012GC004406

Li, X., Guo, X., Tian, F., Fang, X. (2024). The Effects of Controlling Gas Escape and Bottom Current Activity on the Evolution of Pockmarks in the Northwest of the Xisha Uplift, South China Sea. Journal of Marine Science and Engineering, 12(9), 1505. https://doi.org/10.3390/jmse12091505

Liu, X., Zhao, D., Li, S. (2013). Seismic imaging of the Southwest Japan arc from the Nankai trough to the Japan Sea. Physics of the Earth and Planetary Interiors, 216, 59-73. http://dx.doi.org/10.1016/j.pepi.2013.01.003

Lin, W., et al. (2010). "Present-day principal horizontal stress orientations in the Kumano forearc basin of the southwest Japan plate convergent margin."

Journal of Geophysical Research: Solid Earth, 115(B11), B11403. https://doi.org/10.1029/2010GL043158

Lin, W., Doan, M. L., Moore, J. C., McNeill, L., Byrne, T. B., Ito, T., and Moe, K. T. (2015). Present-day principal horizontal stress orientations in the Kumano forearc basin of the southwest Japan subduction zone determined from IODP NanTroSEIZE drilling Site C0009. Geophysical research letters, 37(13). https://doi.org/10.1029/2010GL043158

Liu, Y., Wu, Z., Le Pourhiet, L., Coltice, N., Li, C. F., Shang, J., Zhao, D., Zhou, J., Wang, M. (2024). Geomorphology and mechanisms of subduction erosion in the sediment-starved Mariana convergent margin. Geomorphology, 109161. https://doi.org/10.1016/j.geomorph.2024.109161

Loreto, M. F., Tinivella, U., Ranero, C. R. (2007). Evidence for fluid circulation, overpressure and tectonic style along the Southern Chilean margin. Tectonophysics, 429(3-4), 183-200. https://doi.org/10.1016/j.tecto.2006.09.016

MacKay, M.E., Moore, G.F., Cochrane, G.R., Casey Moore, J. and Kulm, LaVerne D. (1992) Landward vergence and oblique structural trends in the Oregon margin accretionary prism: Implications and effect on fluid flow. Earth and Planetary Science Letters, v. 109(3-4), p. 477-491. https://doi.org/10.1016/0012-821X(92)90108-8

Magistrale, H., Day, S. (1999). 3D simulations of multi-segment thrust fault rupture. Geophysical Research Letters, 26(14), 2093-2096. https://doi.org/10.1029/1999GL900401

Mai, H. T., Marfurt, K. J., Chávez-Pérez, S. (2009). Coherence and volumetric curvatures and their spatial relationship to faults and folds, an example from Chicontepec basin, Mexico. In SEG Technical Program Expanded Abstracts 2009 (pp. 1063-1067). Society of Exploration Geophysicists. https://doi.org/10.1190/1.3255033

Martin, K.M., Gulick, S.P.S., Bangs, N.L.B., Moore, G.F., Ashi, J., Park, J.-O., Kuramoto, S., Taira, A. (2010). Possible strain partitioning structure between the Kumano fore-arc basin and the slope of the Nankai Trough accretionary prism. Geochem. Geophys. Geosyst. 11 https://doi.org/10.1029/2009GC002668

Martínez-Loriente, S., Sallarès, V., R. Ranero, C., B. Ruh, J., Barckhausen, U., Grevemeyer, I., Bangs, N. (2019). Influence of incoming plate relief on overriding plate deformation and earthquake nucleation: Cocos Ridge subduction (Costa Rica). Tectonics, 38(12), 4360-4377. https://doi.org/10.1029/2019TC005586

Masson, D. G., Parson, L. M., Milsom, J., Nichols, G., Sikumbang, N., Dwiyanto, B., Kallagher, H. (1990). Subduction of seamounts at the Java Trench: a view with long-range sidescan sonar. Tectonophysics, 185(1-2), 51-65. https://doi.org/10.1016/0040-1951(90)90404-V

Matsumoto, H., Mikada, H. (2005). Fault geometry of the 2004 off the Kii peninsula earthquake inferred from offshore pressure waveforms. Earth, Planets and Space, 57(3), 161–166. https://doi.org/10.1186/BF03351809

Maunde, A., Alves, T. M., Moore, G. F. (2021). Shallow fault systems of thrust anticlines responding to changes in accretionary prism lithology (Nankai, SE Japan). Tectonophysics, 812, 228888. https://doi.org/10.1016/j.tecto.2021.228888

Mazzotti, S., Lallemant, S. J., Henry, P., Le Pichon, X., Tokuyama, H., Takahashi, N. (2002). Intraplate shortening and underthrusting of a large basement ridge in the eastern Nankai subduction zone. Marine geology, 187(1-2), 63-88. https://doi.org/10.1016/S0025-3227(02)00245-1

McClay, K.R. (1990). Extensional fault systems in sedimentary basins: a review of analogue model studies. Marine and Petroleum Geology, 7(3), 206–233. https://doi.org/10.1016/0264-8172(90)90001-W

McKenzie, D. and Jackson, J. (1986). A block model of distributed deformation by faulting. Journal of the Geological Society, v. 143(2), p.349-353. https://doi.org/10.1144/gsjgs.143.2.0349

McNamara, D. D., Behboudi, E., Wallace, L., Saffer, D., Cook, A. E., Fagereng, A., Oaganoni, M., Kim, G., Lee, H., Savage, H. M., Barnes, P., Pecher, I., LeVay, L. J., Petronotis, K. E. (2021). Variable in situ stress orientations

across the Northern Hikurangi Subduction Margin. Geophysical Research Letters, 48(5). https://doi.org/10.1029/2020GL091707

Melnick, D., Moreno, M., Motagh, M., Cisternas, M., Wesson, R. L. (2012). Splay fault slip during the Mw 8.8 2010 Maule Chile earthquake. Geology, 40(3), 251-254. https://doi.org/10.1130/G32712.1

Menichelli, I., Corbi, F., Brizzi, S., van Rijsingen, E., Lallemand, S., Funiciello, F. (2023). Seamount subduction and megathrust seismicity: The interplay between geometry and friction. Geophysical Research Letters, 50, e2022GL102191. https://doi.org/10.1029/2022GL102191

Mitsui, Y., Uehara, K., Kosugi, I., Matsuo, K. (2022). Along-strike distribution of seismicity and large slow slip correlated with gravity at the Nankai Trough. Earth and Planetary Science Letters, 598, 117824. https://doi.org/10.1016/j.epsl.2022.117824

Miyazaki, S. I., Heki, K. (2001). Crustal velocity field of southwest Japan: Subduction and arc-arc collision. Journal of Geophysical Research: Solid Earth, 106(B3), 4305-4326. https://doi.org/10.1029/2000JB900312

Miyoshi, T., Ishibashi, K. (2005). A tectonic interpretation of NW-SE strike-slip faulting during the 2004 off the Kii peninsula earthquakes, Japan: Probable tear of the Philippine Sea plate. Earth, planets and space, 57, 1115-1120. https://doi.org/10.1186/BF03351891

Moreno, E. J., Manea, V. C., Manea, M., Yoshioka, S., Suenaga, N., Bayona, A. (2023). Numerical modeling of subduction and evaluation of Philippine Sea Plate tectonic history along the Nankai Trough. Scientific Reports, 13(1), 18313. https://doi.org/10.1038/s41598-023-45370-2

Morgan, J. K., Karig, D. E. (1995). Décollement processes at the Nankai accretionary margin, southeast Japan: Propagation, deformation, and dewatering. Journal of Geophysical Research: Solid Earth, 100(B8), 15221-15231. https://doi.org/10.1029/95JB00675

Morgan, J. K., Ask, M. V. (2004). Consolidation state and strength of underthrust sediments and evolution of the décollement at the Nankai accretionary margin: Results of uniaxial reconsolidation experiments. Journal of Geophysical Research: Solid Earth, 109(B3). https://doi.org/10.1029/2002JB002335

Morgan, J. K., Ramsey, E. B., Ask, M. V. (2007). Deformation and mechanical strength of sediments at the Nankai subduction zone: Implications for prism evolution and décollement initiation and propagation. In The seismogenic zone of subduction thrust faults (pp. 210-256). Columbia University Press. https://doi.org/10.7312/dixo13866-008

Morgan, E.C., McAdoo, B.G, Baise, L. (2008). Quantifying geomorphology associated with large subduction zone earthquakes. Basin Research 20, 531 – 542. https://doi.org/10.1111/j.1365-2117.2008.00368.x

Moore, J. C., Silver, E. A. (1987). Continental margin tectonics: submarine accretionary prisms. Reviews of Geophysics, 25(6), 1305-1312. https://doi.org/10.1029/RG025i006p01305

Moore, J. C. (1989). Tectonics and hydrogeology of accretionary prisms: role of the décollement zone. Journal of Structural Geology, 11(1-2), 95-106. https://doi.org/10.1016/0191-8141(89)90037-0

Moore, G. F., Shipley, T. H., Stoffa, P. L., Karig, D. E., Taira, A., Kuramoto, S., Tokuyama, H., Suyehiro, K. (1990). Structure of the Nankai Trough accretionary zone from multichannel seismic reflection data. Journal of Geophysical Research: Solid Earth 95.B6, 8753-8765. https://doi.org/10.1029/JB095iB06p08753

Moore, J. C., Vrolijk, P. (1992). Fluids in accretionary prisms. Reviews of Geophysics, 30(2), 113-135. https://doi.org/10.1029/92RG00201

Moore, G. F., Taira, A., Klaus, A., Becker, L., Boeckel, B., Cragg, B. A., Dean, A., Fergusson, C. L., Henry, P., Hirano, S., Hisamitsu, T., Hunze, S., Kastner, M., Maltman, A. J., Morgan, J. K., Murakami, Y., Saffer, D. M., Sanchez-Gomez, M., Screaton, E. J., Smith, D. C., Spivack, A. J., Steurer, J., Tobin, H. J., Ujiie, L., Underwood., M. B., Wilson, M. (2001). New insights into deformation and fluid flow processes in the Nankai Trough accretionary prism: Results of Ocean Drilling Program Leg 190. Geochemistry, Geophysics, Geosystems, 2(10). https://doi.org/10.1029/2001GC000166

Moore, J. C., Rowe, C., Meneghini, F. (2007). 10. How Accretionary Prisms Elucidate Seismogenesis in Subduction Zones. In The seismogenic zone of subduction thrust faults (pp. 288-315). Columbia University Press. https://doi.org/10.7312/dixo13866-010

Moore, G.F., Park, J.-O., Bangs, N.L., Gulick, S.P., Tobin, H.J., Nakamura, Y., Saito, S., Tsuji, T., Yoro, T., Tanaka, H., Uraki, S., Kido, Y., Sanada, Y., Kuramoto, S., Taira, A. (2009). Structural and seismic stratigraphic framework of the NanTroSEIZE Stage 1 transect, in: Kinoshita, M., Tobin, H., Ashi, J., Kimura, G., Lallemant, S., Screaton, E.J., Curewitz, D., Masago, H., Moe, K.T., and the Expedition 314/315/316 Scientists (Eds.), NanTroSEIZE Stage 1: investigations of seismogenesis, Nankai Trough, Japan. Integrated Ocean Drilling Program, Washington, D.C. https://doi.org/10.2204/iodp.proc.314315316.102.2009

Moore, G. F., Saffer, D., Studer, M., Costa Pisani, P. (2011). Structural restoration of thrusts at the toe of the Nankai Trough accretionary prism off Shikoku Island, Japan: Implications for dewatering processes. Geochemistry, Geophysics, Geosystems, 12(5). https://doi.org/10.1029/2010GC003453

Moore, G. F., Boston, B. B., Sacks, A. F., and Saffer, D. M. (2013). Analysis of normal fault populations in the Kumano Forearc Basin, Nankai Trough, Japan: 1. Multiple orientations and generations of faults from 3-D coherency mapping. Geochemistry, Geophysics, Geosystems, v. 14(6), p. 1989–2002. https://doi.org/10.1002/ggge.20119

Moore, G. F., Kanagawa, K., Strasser, M., Dugan, B., Maeda, L., Toczko, S. (2014). IODP Expedition 338: NanTroSEIZE Stage 3: NanTroSEIZE plate boundary deep riser 2. Scientific Drilling, 17, 1-12. https://doi.org/10.5194/sd-17-1-2014

Moore, G.F., Boston, B.B., Strasser, M., Underwood, M.B., Ratliff, R.A. (2015). Evolution of tectono-sedimentary systems in the Kumano Basin, Nankai Trough forearc. Marine and Petroleum Geology 67, 604–616. https://doi.org/10.1016/j.marpetgeo.2015.05.032

Moore, J. C., Saffer, D. (2001). Updip limit of the seismogenic zone beneath the accretionary prism of southwest Japan: An effect of diagenetic to low-grade metamorphic processes and increasing effective stress. Geology, 29(2), 183-186. https://doi.org/10.1130/0091-7613(2001)029%3C0183:ULOTSZ%3E2.0.CO;2

Morton, E. A., Bilek, S. L., & Rowe, C. A. (2018). Newly detected earthquakes in the Cascadia subduction zone linked to seamount subduction and deformed upper plate. Geology, 46(11), 943-946. https://doi.org/10.1130/G45354.1

Munoz-Montecinos, J., Cambeses, A., & Angiboust, S. (2024). Accretion and subduction mass transfer processes: Zircon SHRIMP and geochemical insights from the Carboniferous Western Series, Central Chile. International Geology Review, 66(1), 54-80. https://doi.org/10.1080/00206814.2023.2185822

Murauchi, S. (1980). Crustal structure of the japan trench: the effect of subduction of ocean crust. Notes, 144, 27.

Nakano, M., Hyodo, M., Nakanishi, A., Yamashita, M., Hori, T., Kamiya, S. I., Suzuki, K., Tonegawa, T., Kodaira, S., Takahashi, N., Kaneda, Y. (2018). The 2016 Mw 5.9 earthquake off the southeastern coast of Mie Prefecture as an indicator of preparatory processes of the next Nankai Trough megathrust earthquake. Progress in Earth and Planetary Science, 5(1), 1-17. https://doi.org/10.1186/s40645-018-0188-3

Nishizawa, A., Kaneda, K., Oikawa, M. (2011). Backarc basin oceanic crust and uppermost mantle seismic velocity structure of the Shikoku Basin, south of Japan. Earth, planets and space, 63(2), 151-155. https://doi.org/10.5047/eps.2010.12.003

Noda, A., Koge, H., Yamada, Y., Miyakawa, A., Ashi, J. (2020). Forearc basin stratigraphy resulting from syntectonic sedimentation during accretionary wedge growth: Insights from sandbox analog experiments. Tectonics, 39(3). https://doi.org/10.1029/2019TC006033

Noda, A., Graveleau, F., Witt, C., Chanier, F., Vendeville, B. (2023). Accretion cycles, structural evolution, and thrust activity in accretionary wedges with various décollement configurations: Insights from sandbox analog modeling. Journal of Geophysical Research: Solid Earth, 128(12), e2023JB027131. https://doi.org/10.1029/2023JB027131

Okino, K., Shimakawa, Y., Nagaoka, S. (1994). Evolution of the Shikoku basin. Journal of geomagnetism and geoelectricity, 46(6), 463-479. https://doi.org/10.5636/jgg.46.463

Okino, K., Y. Ohara, S. Kasuga, Y. Kato (1999), The Philippine Sea: New survey results reveal the structure and the history of the marginal basins. Geophys. Res. Lett., 26, 2287–2290. https://doi.org/10.1029/1999GL900537

Oakley, A. J., Taylor, B., Moore, G. F. (2008). Pacific Plate subduction beneath the central Mariana and Izu-Bonin fore arcs: New insights from an old margin. Geochemistry, Geophysics, Geosystems, 9(6). https://doi.org/10.1029/2007GC001820

Obana, K., Kodaira, S., Kaneda, Y. (2005). Seismicity in the incoming/subducting Philippine Sea plate off the Kii Peninsula, central Nankai trough. Journal of Geophysical Research: Solid Earth, 110(B11). https://doi.org/10.1029/2004JB003487

Okino, K., Ohara, Y., Kasuga, S., Kato, Y. (1999). The Philippine Sea: New survey results reveal the structure and the history of the marginal basins. Geophysical Research Letters, 26(15), 2287-2290. https://doi.org/10.1029/1999GL900537

Okino, K., Ohara, Y., Fujiwara, T., Lee, S. M., Nakamura, Y., Wu, S. (2009). Tectonics of the southern tip of the Parece Vela Basin, Philippine Sea

Plate. Tectonophysics, 466(3-4), 213-228. https://doi.org/10.1016/j.tecto.2007.11.017

Okuma, Y., Noda, A., Koge, H., Yamada, Y., Yamaguchi, A., Ashi, J. (2022). Surface friction of subducting seamounts influences deformation of the accretionary wedge. Tectonophysics, 845, 229644. https://doi.org/10.1016/j.tecto.2022.229644

Park, J. O., Tsuru, T., Kaneda, Y., Kono, Y., Kodaira, S., Takahashi, N., and Kinoshita, H. (1999). A subducting seamount beneath the Nankai accretionary prism off Shikoku, southwestern Japan. Geophysical Research Letters, v. 26(7), pp. 931-934. https://doi.org/10.1029/1999GL900134

Park, J. O., Tsuru, T., Kodaira, S., Cummins, P. R., Kaneda, Y. (2002). Splay fault branching along the Nankai subduction zone. Science, 297(5584), 1157-1160. https://doi.org/10.1126/science.1074111

Park, J.O., Moore, G.F., Tsuru, T., Kodaira, S., Kaneda, Y. (2004). A subducted oceanic ridge influencing the Nankai megathrust earthquake rupture. Earth and Planetary Science Letters 217 (1-2), 77-84. https://doi.org/10.1016/S0012-821X(03)00553-3

Park, J. O., Hori, T., Kaneda, Y. (2009). Seismotectonic implications of the Kyushu-Palau ridge subducting beneath the westernmost Nankai forearc. Earth, planets and space, 61, 1013-1018. https://doi.org/10.1186/BF03352951

Park, J-O., Fujie, G., Wijerathne, L., Hori, T., Kodaira, S., Fukao, Y., Moore, G. F., Bangs, N. L., Kuramoto, S. and Taira, A. (2010). A low-velocity zone with weak reflectivity along the Nankai subduction zone. Geology, v. 38 (3), p. 283-286. https://doi.org/10.1130/G30205.1

Plata-Martinez, R., Iinuma, T., Tomita, F., Nakamura, Y., Nishimura, T., Hori, T. (2024). Revisiting slip deficit rates and its insights into large and slow earthquakes at the Nankai subduction zone. Journal of Geophysical Research: Solid Earth, 129(12), e2023JB027942. https://doi.org/10.1029/2023JB027942

Platt, J. P., Leggett, J. K., Alam, S. (1988). Slip vectors and fault mechanics in the Makran accretionary wedge, southwest Pakistan. Journal of Geophysical Research: Solid Earth, v. 93(B7), p. 7955-7973. https://doi.org/10.1029/JB093iB07p07955

Polet, J., & Kanamori, H. (2022). Tsunami earthquakes. Complexity in Tsunamis, Volcanoes, and their Hazards, 3-23. https://doi.org/10.1007/978-3-642-27737-5_567-3

Qin, Y., Fujie, G., Kodaira, S., Nakamura, Y., Kaiho, Y., No, T., Obana, K., Miura, S. (2021). High-density seismic refraction imaging of plate-boundary structures in the slow earthquake gap zone off western Kii Peninsula, Nankai Trough. Geophysical Research Letters, 48, e2020GL089132. https://doi.org/10.1029/2020GL089132

Raimbourg, H., S. Tadahiro, Y. Asuka, Y. Haruka, G. Kimura (2009), Horizontal shortening versus vertical loading inaccretionary prisms,Geochem. Geophys. Geosyst.,10, Q04007. https://doi.org/10.1029/2008GC002279

Ramsey, J. M., Chester, F. M. (2004). Hybrid fracture and the transition from extension fracture to shear fracture. Nature, v.428 (6978), p.63-66. https://doi.org/10.1038/nature02333

Räss, L., Simon, N. S., Podladchikov, Y. Y. (2018). Spontaneous formation of fluid escape pipes from subsurface reservoirs. Scientific reports, 8(1), 11116.

Reading, H. G. (1980). Characteristics and recognition of strike-slip fault systems. Sedimentation in oblique-slip mobile zones, 7-26. https://doi.org/10.1002/9781444303735.ch2

Reber, J. E., Cooke, M. L., & Dooley, T. P. (2020). What model material to use? A Review on rock analogs for structural geology and tectonics. Earth-Science Reviews, 202, 103107. https://doi.org/10.1016/j.earscirev.2020.103107

Roberts, A. (2001). Curvature attributes and their application to 3 D interpreted horizons. First break, v. 19(2), p. 85-100. https://doi.org/10.1046/j.0263-5046.2001.00142.x

Roesner, A., Ikari, M. J., Hüpers, A., Kopf, A. J. (2022). Weakening behavior of the shallow megasplay fault in the Nankai subduction zone. Earth, Planets and Space, 74(1), 1-15. https://doi.org/10.1186/s40623-022-01728-w

Rosenbaum, G., Gasparon, M., Lucente, F. P., Peccerillo, A., Miller, M. S. (2008). Kinematics of slab tear faults during subduction segmentation and implications for Italian magmatism. Tectonics, 27(2). https://doi.org/10.1029/2007TC002143

Rowe, K. T., Screaton, E. J., Ge, S. (2012). Coupled fluid flow and deformation modeling of the frontal thrust region of the Kumano Basin transect, Japan: Implications for fluid pressures and decollement downstepping. Geochemistry, Geophysics, Geosystems, 13(3). https://doi.org/10.1029/2011GC003861

Ruff, L. J. (1992). Asperity distributions and large earthquake occurrence in subduction zones. Tectonophysics, 211(1-4), 61-83. https://doi.org/10.1016/0040-1951(92)90051-7

Ruff, L. J., Tichelaar, B. W. (1996). What controls the seismogenic plate interface in subduction zones?. Washington DC American Geophysical Union Geophysical Monograph Series, 96, 105-111. https://doi.org/10.1029/GM096p0105

Ruh, J. B., Sallarès, V., Ranero, C. R., Gerya, T. (2016). Crustal deformation dynamics and stress evolution during seamount subduction: High-resolution 3-D numerical modeling. Journal of Geophysical Research: Solid Earth, 121(9), 6880-6902. https://doi.org/10.1002/2016JB013250

Safonova, I. Y., Khanchuk, A. I. (2021). Subduction erosion at Pacific-type convergent margins. Russian Journal of Pacific Geology, 15, 495-509. https://doi.org/10.1134/S1819714021060087

Saito, T., Noda, A. (2022). Mechanically coupled areas on the plate interface in the Nankai trough, Japan and a possible seismic and aseismic rupture scenario for megathrust earthquakes. Journal of Geophysical Research: Solid Earth, 127(8), e2022JB023992. https://doi.org/10.1029/2022JB023992

Sato, H., Machida, S., Kanayama, S., Taniguchi, H., Ishii, T. (2002). Geochemical and isotopic characteristics of the Kinan Seamount Chain in the Shikoku Basin. Geochemical Journal, 36(5), 519-526. https://doi.org/10.2343/geochemj.36.519

Saffer, D. M., Bekins, B. A. (2006). An evaluation of factors influencing pore pressure in accretionary complexes: Implications for taper angle and wedge mechanics. Journal of Geophysical Research: Solid Earth, 111(B4). https://doi.org/10.1029/2005JB003990

Saffer, D. M., Tobin, H. J. (2011). Hydrogeology and mechanics of subduction zone forearcs: Fluid flow and pore pressure. Annual Review of Earth and Planetary Sciences, 39, 157-186. https://doi.org/10.1146/annurev-earth-040610-133408

Sanderson, D. J., Marchini, W.R.D. (1984). Transpression. Journal of structural Geology v.6.5, p. 449–458. https://doi.org/10.1016/0191-8141(84)90058-0

Schellart, W. P. (2005). Influence of the subducting plate velocity on the geometry of the slab and migration of the subduction hinge. Earth and Planetary Science Letters 231.3-4, 197-219. https://doi.org/10.1016/j.epsl.2004.12.019

Schellart, W. P., Rawlinson, N. (2010). Convergent plate margin dynamics: New perspectives from structural geology, geophysics and geodynamic modelling. Tectonophysics, 483(1-2), 4-19. https://doi.org/10.1016/j.tecto.2009.08.030

Scholz, C. H. (1992). Paradigms or small change in earthquake mechanics. In International Geophysics (Vol. 51, pp. 505-517). Academic Press. https://doi.org/10.1016/S0074-6142(08)62836-3

Scholz, C. H., Small, C. (1997). The effect of seamount subduction on seismic coupling. Geology, 25(6), 487-490. https://doi.org/10.1130/0091-7613(1997)025%3C0487:TEOSSO%3E2.3.CO;2

Schwarze, C. O., Kukowski, N. (2022). Décollement strength and mechanical segmentation along the frontal wedge of the Hikurangi convergent margin (New Zealand): Insights from critical taper analysis. Tectonophysics, 844, 229622. https://doi.org/10.1016/j.tecto.2022.229622

Scudder, R. P., Murray, R. W., Kutterolf, S., Schindlbeck, J. C., Underwood, M. B., Wang, K. L. (2018). Sedimentary inputs to the Nankai subduction zone: The importance of dispersed ash. Geosphere, 14(4), 1451-1467. https://doi.org/10.1130/GES01558.1

Screaton, E., Saffer, D., Henry, P., Hunze, S. (2002). Porosity loss within the underthrust sediments of the Nankai accretionary complex: Implications for overpressures. Geology, 30(1), 19-22. https://doi.org/10.1130/0091-7613(2002)030%3C0019:PLWTUS%3E2.0.CO;2

Screaton, E., Kimura, G., Curewitz, D., Moore, G., Chester, F., Fabbri, O., Fergusson, C., Girault, F., Goldsby, D., Harris, R., Inagaki, F., Jiang, T., Kitamura, Y., Knuth, M., Li, C-F., Liljedahl, L., Louis, L., Milliken, K., Nicholson, U., Riedinger, N., Sakaguchi, A., Solomon, E., Strasser, M., Su, X., Tsutsumi, A., Yamaguchi, A., Ujiee, K., Zhao, X. (2009). Interactions between deformation and fluids in the frontal thrust region of the NanTroSEIZE transect offshore the Kii Peninsula, Japan: Results from IODP Expedition 316 Sites C0006 and C0007. Geochemistry, Geophysics, Geosystems, 10(12). https://doi.org/10.1029/2009GC002713

Senatorski, P. (2020). Gutenberg–Richter'sb value and earthquake asperity models. Pure and Applied Geophysics, 177(5), 1891-1905. https://doi.org/10.1007/s00024-019-02385-z

Shapiro, N. M., Campillo, M., Kaminski, E., Vilotte, J. P., Jaupart, C. (2018). Low-frequency earthquakes and pore pressure transients in subduction

zones. Geophysical Research Letters, 45(20), 11-083. https://doi.org/10.1029/2018GL079893

Shelton, J. W. (1984). Listric normal faults: an illustrated summary. AAPG Bulletin, v. 68 (7), p. 801-815. https://doi.org/10.1306/AD461426-16F7-11D7-8645000102C1865D

Shiraishi, K., Moore, G. F., Yamada, Y., Kinoshita, M., Sanada, Y., Kimura, G. (2019). Seismogenic zone structures revealed by improved 3-D seismic images in the Nankai Trough off Kumano. Geochemistry, Geophysics, Geosystems, 20, 2252–2271. https://doi.org/10.1029/2018GC008173

Shiraishi, K., Yamada, Y., Nakano, M., Kinoshita, M., Kimura, G. (2020). Three-dimensional topographic relief of the oceanic crust may control the occurrence of shallow very-low-frequency earthquakes in the Nankai Trough off Kumano. earth, planets and space, 72(1), 1-14. https://doi.org/10.1186/s40623-020-01204-3v

Shreve, R. L., Cloos, M. (1986). Dynamics of sediment subduction, melange formation, and prism accretion. Journal of Geophysical Research: Solid Earth, 91(B10), 10229-10245. https://doi.org/10.1029/JB091iB10p10229

Sibson, R. H. (1977). Fault rocks and fault mechanisms. Journal of the Geological Society, 133(3), 191–213. https://doi.org/10.1144/gsjgs.133.3.0191

Sibson, R. H. (1985). A note on fault reactivation. Journal of Structural Geology, 7(6), 751–754. https://doi.org/10.1016/0191-8141(85)90150-6

Sibson, R. H. (1990). Conditions for fault-valve behavior. Geological Society, London, Special Publications, 54(1), 15–28. https://doi.org/10.1144/GSL.SP.1990.054.01.02

Smith, G. L., McNeill, L. C., Wang, K., He, J., Henstock, T. J. (2013). Thermal structure and megathrust seismogenic potential of the Makran subduction zone. Geophysical Research Letters, 40(8), 1528-1533. https://doi.org/10.1002/grl.50374

Spandler, C., Pirard, C. (2013). Element recycling from subducting slabs to arc crust: A review. Lithos, 170, 208-223. http://dx.doi.org/10.1016/j.lithos.2013.02.016

Stein, C. A., Stein, S. (1992). A model for the global variation in oceanic depth and heat flow with lithospheric age. Nature, 359(6391), 123-129. https://doi.org/10.1038/359123a0

Stern, R. J. (2002). Subduction zones. Reviews of geophysics, 40(4), 3-1. https://doi.org/10.1029/2001RG000108

Stevenson, D. J., J. S. Turner (1977). Angle of subduction. Nature 270.5635, 334-336. https://doi.org/10.1038/270334a0

Strasser, M., Moore, G. F., Kimura, G., Kitamura, Y., Kopf, A. J., Lallemant, S., Park, J-O., Screaton, E., Su, X., Underwood, M., Zhao, X. (2009). Origin and evolution of a splay fault in the Nankai accretionary wedge. Nature Geoscience, 2(9), 648-652. http://www.nature.com/doifinder/10.1038/ngeo609

Strasser, M., Moore, G.F., Kimura, G., Kopf, A.J., Underwood, M.B., Guo, J., Screaton, E.J. (2011). Slumping and mass transport deposition in the Nankai fore arc: evidence from IODP drilling and 3-D reflection seismic data. Geochem. Geophys. Geosyst. 12 (5). http://dx.doi.org/10.1029/2010GC003431

Strasser, M., Dugan, B., Kanagawa, K., Moore, G.F., Toczko, S., Maeda, L., and the Expedition 338 Scientists (2014). Site C0018: Proceedings of the Integrated Ocean Drilling Program, v. 338, p. 2. http://dx.doi.org/10.2204/iodp.proc.338.105.2014

Sun, T., Saffer, D., Ellis, S. (2020). Mechanical and hydrological effects of seamount subduction on megathrust stress and slip. Nat. Geosci. 13, 249–255. https://doi.org/10.1038/s41561-020-0542-0

Taira, A., Pickering, K. T. (1991). Sediment deformation and fluid activity in the Nankai, Izu-Bonin and Japan forearc slopes and trenches. Philosophical Transactions of the Royal Society of London. Series A: Physical and Engineering Sciences, 335(1638), 289-313. https://doi.org/10.1098/rsta.1991.0048

Takahashi, N., Kodaira, S., Nakanishi, A., Park, J. O., Miura, S., Tsuru, T., Kaneda, Y., Kinoshita, H., Hirata, N., and Iwasaki, T. (2002). Seismic structure of western end of the Nankai trough seismogenic zone. Journal of Geophysical Research: Solid Earth (1978–2012), v. 107(B10), p. ESE 2-1–ESE 2-19. http://dx.doi.org/10.1029/2000JB000121

Takemura, S., Matsuzawa, T., Noda, A.,Tonegawa, T., Asano, Y., Kimura, T., Shiomi, K. (2019). Structuralcharacteristics of the Nankai Troughshallow plate boundary inferred fromshallow very low frequencyearthquakes.Geophysical ResearchLetters,46, 4192–4201. https://doi.org/10.1029/2019GL082448

Takemura, S., Obara, K., Shiomi, K., Baba, S. (2022). Spatiotemporal variations of shallow very low frequency earthquake activity southeast off the Kii Peninsula, along the Nankai Trough, Japan. Journal of Geophysical Research: Solid Earth, 127(3), e2021JB023073. https://doi.org/10.1029/2021JB023073

Takemura, S., Hamada, Y., Okuda, H., Okada, Y., Okubo, K., Akuhara, T., Noda, A., Tonegawa, T. (2023). A review of shallow slow earthquakes along the Nankai Trough. Earth, Planets and Space, 75(1), 1-22. https://doi.org/10.1186/s40623-023-01920-6

Tamaribuchi, K., Kobayashi, A., Nishimiya, T., Hirose, F., & Annoura, S. (2019). Characteristics of shallow low-frequency earthquakes off the Kii Peninsula, Japan, in 2004 revealed by ocean bottom seismometers. Geophysical Research Letters, 46, 13,737–13,745. https://doi.org/10.1029/2019GL085158

Teichert, B. M. A., Torres, M. E., Bohrmann, G., Eisenhauer, A. (2005). Fluid sources, fluid pathways and diagenetic reactions across an accretionary prism revealed by Sr and B geochemistry. Earth and Planetary Science Letters, 239(1-2), 106-121. https://doi.org/10.1016/j.epsl.2005.08.002

Tetreault, J. L., Buiter, S. J. H. (2014). Future accreted terranes: a compilation of island arcs, oceanic plateaus, submarine ridges, seamounts, and continental fragments. Solid Earth, 5(2), 1243-1275. https://doi.org/10.5194/se-5-1243-2014

Tilley, H., Moore, G. F., Underwood, M. B., Hernández-Molina, F. J., Yamashita, M., Kodaira, S., Nakanishi, A. (2021). Heterogeneous sediment input at the Nankai Trough subduction zone: Implications for shallow slow earthquake localization. Geochemistry, Geophysics, Geosystems, 22(10), e2021GC009965. https://doi.org/10.1029/2021GC009965

Tobin, H. J., Kinoshita, M. (2006). NanTroSEIZE: the IODP Nankai Trough seismogenic zone experiment. Scientific Drilling, 2, 23-27. http://dx.doi.org/10.2204/iodp.sd.2.06.2006

Tobin, H., Kinoshita, M. (2007). The IODP Nankai Trough seismogenic zone experiment. Scientific Drilling, 39-41. https://doi.org/10.2204/iodp.sd.s01.30.2007

Tobin, H., Hirose, T., Ikari, M., Kanagawa, K., Kimura, G., Kinoshita, M., Kitajima, H., Saffer, D., Yamaguchi, A. Egu-chi, N., Maeda, L., Toczko, S., and the Expedition 358 Scientists (2019). Expedition 358 Preliminary Report: NanTroSEIZE Plate Boundary Deep Riser 4: Nankai Seismogenic/Slow Slip Megathrust. International Ocean Discovery Program. https://doi.org/10.14379/iodp.pr.358.2019

Tsuji, T., Dvorkin, J., Mavko, G., Nakata, N., Matsuoka, T., Nakanishi, A.,, Kodaira, S., Nishizawa, O. (2011). VP/VS ratio and shear-wave splitting in the Nankai Trough seismogenic zone: Insights into effective stress, pore pressure, and sediment consolidation. Geophysics, 76(3), WA71-WA82. https://doi.org/10.1190/1.3560018

Tsuji, T., Tokuyama, H., Costa Pisani, P., Moore, G. (2008). Effective stress and pore pressure in the Nankai accretionary prism off the Muroto Peninsula, southwestern Japan. Journal of Geophysical Research: Solid Earth, v.113 (B11). https://doi.org/10.1029/2007JB005002

Tsuji, T., Kodaira, S., Ashi, J., Park, J. O. (2013). Widely distributed thrust and strike-slip faults within subducting oceanic crust in the Nankai Trough off the Kii Peninsula, Japan. Tectonophysics, v. 600, p. 52-62. https://doi.org/10.1016/j.tecto.2013.03.014

Tsuji, T., Ashi, J., & Ikeda, Y. (2014). Strike-slip motion of a mega-splay fault system in the Nankai oblique subduction zone. Earth, Planets and Space, 66, 1-14. https://doi.org/10.1186/1880-5981-66-120

Tsuji, T., Kamei, R., Pratt, R. G. (2014). Pore pressure distribution of a mega-splay fault system in the Nankai Trough subduction zone: Insight into up-dip extent of the seismogenic zone. Earth and Planetary Science Letters, 396, 165-178. https://doi.org/10.1016/j.epsl.2014.04.011

Tsuji, T., Ashi, J., Strasser, M., Kimura, G. (2015). Identification of the static backstop and its influence on the evolution of the accretionary prism in the Nankai Trough. Earth and Planetary Science Letters, 431, 15-25. https://doi.org/10.1016/j.epsl.2015.09.011

Ujiie, K., Hisamitsu, T., Taira, A. (2003). Deformation and fluid pressure variation during initiation and evolution of the plate boundary décollement zone in the Nankai accretionary prism. Journal of Geophysical Research: Solid Earth, 108(B8). https://doi.org/10.1029/2002JB002314

Uyeda, S. (1982). Subduction zones: an introduction to comparative subductology. Tectonophysics, 81(3-4), 133-159. https://doi.org/10.1016/0040-1951(82)90126-3

Uyeda, S. (1987). Chilean vs. Mariana type subduction zones with remarks on arc volcanism and collision tectonics. Circum-Pacific orogenic belts and evolution of the Pacific Ocean basin, 18, 1-7. https://doi.org/10.1029/GD018p0001

van Keken, P. E. (2003). The structure and dynamics of the mantle wedge. Earth and planetary science letters, 215(3-4), 323-338. https://doi.org/10.1016/S0012-821X(03)00460-6

Van Tuyl, J., Alves, T. M., Moore, G. F. (2015). Strain decoupling reveals variable seismogenic risk in SE Japan (Nankai Trough). Geochemistry, Geophysics, Geosystems, v. 16(7), p. 2025–2037. https://doi.org/10.1002/2015GC005778

Von Huene, R., Lallemand, S. (1990). Tectonic erosion along the Japan and Peru convergent margins. Geological Society of America Bulletin, 102(6), 704-720. https://doi.org/10.1130/00167606(1990)102%3C0704:TEATJA%3E2.3.CO;2

Von Huene, R., Scholl, D. W. (1991). Observations at convergent margins concerning sediment subduction, subduction erosion, and the growth of continental crust. Reviews of Geophysics, 29(3), 279-316. https://doi.org/10.1029/91RG00969

Von Huene, R., Reston, T., Kukwski, N., Dehghani, G. A., Weinrebe, W., IMERSE Working Group. (1997). A subducting seamount beneath the Mediterranean Ridge. Tectonophysics, 271(3-4), 249-261. https://doi.org/10.1016/S0040-1951(96)00241-7

von Huene, R., Suess, E. (1988). Ocean drilling detects subduction erosion. Geology, 16(3), 196–199. https://doi.org/10.1130/0016-7606(1990)102%3C0704:TEATJA%3E2.3.CO;2

von Huene, R., Ranero, C. R., Vannucchi, P. (2004). Generic model of subduction erosion. Geology, 32(10), 913-916. https://doi.org/10.1130/G20563.1

von Huene, R. (2008). When seamounts subduct. Science, 321(5893), 1165-1166. https://doi.org/10.1126/science.1162868

Wakabayashi, J. (2022). Along-Strike Variation in Accretion, Non-accretion, and Subduction Erosion Recorded in Rocks of the Jurassic-Neogene Convergent Plate Margin of California. Frontiers in Earth Science, 10, 818171. https://doi.org/10.3389/feart.2022.818171

Wallace, L.M., M.J. Ikari, D.M. Saffer, H. Kitajima. (2019). Slow motion earthquakes: Taking the pulse of slow slip with scientific ocean drilling. Oceanography 32(1):106–118. https://doi.org/10.5670/oceanog.2019.131

Watts, A. B., Koppers, A. A. P., Robinson, D. P. (2010). Seamount subduction and earthquakes. Oceanography, 23, 166–173.

Wang, K., Hu, Y. (2006). Accretionary prisms in subduction earthquake cycles: The theory of dynamic Coulomb wedge. Journal of Geophysical Research: Solid Earth, 111(B6). https://doi.org/10.1029/2005JB004094

Wang, K., Hu, Y., Von Huene, R., Kukowski, N. (2010). Interplate earthquakes as a driver of shallow subduction erosion. Geology, 38(5), 431-434. https://doi.org/10.1130/G30597.1

Wang, K., Bilek, S. L. (2011). Do subducting seamounts generate or stop large earthquakes?. Geology, 39(9), 819-822. https://doi.org/10.1130/G31856.1

Wang, C.Y., Chen, H.L., Cheng, X.G., Li, K. (2013). Evaluating the role of syn-thrusting sedimentation and interaction with frictional detachment in the structural evolution of the SW Tarim basin, NW China: insights from analogue

modelling. Tectonophysics 608, 642–652. https://doi.org/10.1016/j.tecto.2013.08.016

Wang, C., Ding, W., Schellart, W. P., Li, J., Dong, C., Fang, Y., Hao, T., Tong, Z. (2021). Effects of multi-seamount subduction on accretionary wedge deformation: Insights from analogue modelling. Journal of Geodynamics, 145, 101842. https://doi.org/10.1016/j.jog.2021.101842

Wang, Z., Lin, J. (2022). Role of fluids and seamount subduction in interplate coupling and the mechanism of the 2021 Mw 7.1 Fukushima-Oki earthquake, Japan. Earth and Planetary Science Letters, 584, 117439. https://doi.org/10.1016/j.epsl.2022.117439

Willett, S. D. (1992). Dynamic and kinematic growth and change of a Coulomb wedge. In Thrust tectonics (pp. 19-31). Dordrecht: Springer Netherlands. https://doi.org/10.1007/978-94-011-3066-0_2

Woodward, N. B., Boyer, S. E., Suppe, J. (1989). Balanced geological cross-sections. Short course in geology, 6, 132.

Wu, H. Y., Chan, C. H., Kinoshita, M., Saito, S. (2013). Stress field observation and modeling from the NanTroSEIZE scientific drillings in the Nankai Trough system, SW Japan. Tectonophysics, v. 600, p. 99-107, https://doi.org/10.1016/j.tecto.2013.04.009

Xia, Y., Geersen, J., Klaeschen, D., Ma, B., Lange, D., Riedel, M., Schnabel, M., Kopp, H. (2021). Marine forearc structure of eastern Java and its role

in the 1994 Java tsunami earthquake. Solid Earth, 12(11), 2467-2477. https://doi.org/10.5194/se-12-2467-2021

Xia, Y., Kopp, H., Klaeschen, D., Geersen, J., Ma, B., Schnabel, M. (2023). Seamount and ridge subduction at the Java margin, Indonesia: Effects on structural geology and seismogenesis. Journal of Geophysical Research: Solid Earth, 128, e2022JB026272. https://doi.org/10.1029/2022JB026272

Yamada, Y., Baba, K., Matsuoka, T. (2006). Analogue and numerical modelling of accretionary prisms with a decollement in sediments. Geological Society, London, Special Publications, 253(1), 169-183. https://doi.org/10.1144/GSL.SP.2006.253.01.09

Yamamoto, Y., Ariyoshi, K., Yada, S., Nakano, M., Hori, T. (2022). Spatiotemporal distribution of shallow very-low-frequency earthquakes between December 2020 and January 2021 in Kumano-nada, Nankai subduction zone, detected by a permanent seafloor seismic network. Earth Planets Space 74, 14. https://doi.org/10.1186/s40623-022-01573-x

Yamazaki, T., Okamura, Y. (1989). Subducting seamounts and deformation of overriding forearc wedges around Japan. In: J.P. Cadet and S. Uyeda (Editors), Subduction Zones: the Kaiko Project. Tectonophysics, 160: 207-229. https://doi.org/10.1016/0040-1951(89)90392-2

Yan, Q., Shi, X., Yuan, L., Yan, S., Liu, Z. (2022). Tectono-magmatic evolution of the Philippine Sea Plate: A review. Geosystems and Geoenvironment, 1(2), 100018. https://doi.org/10.1016/j.geogeo.2021.100018

Yang, G., Si, G., Tong, L., Li, H., Lindagato, P., Zeng, R. (2022). The effect of seamount chain subduction and accretion. Geological Journal, 57(7), 2712-2734. https://doi.org/10.1002/gj.4435

Yokota, Y., Ishikawa, T., Watanabe, S. I., Tashiro, T., Asada, A. (2016). Seafloor geodetic constraints on interplate coupling of the Nankai Trough megathrust zone. Nature, 534(7607), 374-377. https://doi.org/10.1038/nature17632

Yoshida, M. (2017). Trench dynamics: Effects of dynamically migrating trench on subducting slab morphology and characteristics of subduction zones systems. Physics of the Earth and Planetary Interiors, 268, 35-53. https://doi.org/10.1016/j.pepi.2017.05.004

Zhang, J., Chen, L., Cheng, Z., Tang, L. (2020). Geological characteristics of the Nankai Trough subduction zone and their tectonic significances. Acta Oceanologica Sinica, 39, 81-95. https://doi.org/10.1007/s13131-020-1663-4

Zhang, T. Y., Li, P. F., Shang, L. N., Cong, J. Y., Li, X., Yao, Y. J., Zhang, Y. (2022). Identification and evolution of tectonic units in the Philippine Sea Plate. China Geology, 5(1), 96-109. https://doi.org/10.1016/S2096-5192(22)00089-1

Zhao, Z., Moore, G. F., Shipley, T. H. (1998). Deformation and dewatering of the subducting plate beneath the lower slope of the northern Barbados accretionary prism. Journal of Geophysical Research: Solid Earth, 103(B12), 30431-30449. https://doi.org/10.1029/1998JB900012

Zhang, M., Huang, Y., Bao, Y. (2016). The mechanism of shallow submarine landslides triggered by storm surge. Natural Hazards, 81, 1373-1383. https://doi.org/10.1007/s11069-015-2112-0

Zheng, Y. F., Zhao, Z. F. (2017). Introduction to the structures and processes of subduction zones. Journal of Asian Earth Sciences, 145, 1-15. https://doi.org/10.1016/j.jseaes.2017.06.034

Zheng, Y., Chen, Y., Chen, R., Dai, L. (2022). Tectonic evolution of convergent plate margins and its geological effects. Science China Earth Sciences, 65(7), 1247-1276. https://doi.org/10.1007/s11430-022-9947-6